Development and engineering of optogenetic systems and reconstruction of light signaling pathways

Inaugural-Dissertation

zur Erlangung des Doktorgrades
der Mathematisch-Naturwissenschaftlichen Fakultät
der Heinrich-Heine-Universität Düsseldorf

vorgelegt von

Patrick Fischbach
aus Wuppertal

Düsseldorf, Dezember 2019

aus dem Institut für Synthetische Biologie
der Heinrich-Heine-Universität Düsseldorf

Gedruckt mit der Genehmigung der
Mathematisch-Naturwissenschaftlichen Fakultät der
Heinrich-Heine-Universität Düsseldorf

Berichterstatter:

1. Prof. Dr. Matias D. Zurbriggen

2. Prof. Dr. Andreas Möglich

Tag der mündlichen Prüfung: 17.02.2020

Erklärung

Ich versichere an Eides Statt, dass die Dissertation von mir selbständig und ohne unzulässige fremde Hilfe unter Beachtung der „Grundsätze zur Sicherung guter wissenschaftlicher Praxis an der Heinrich-Heine-Universität Düsseldorf“ erstellt worden ist.

_____ _____

Datum Unterschrift

Table of Contents

Danksagung

An dieser Stelle möchte ich mich bei Prof. Dr. Matias D. Zurbriggen bedanken, der mir nicht nur die Möglichkeit gab meine Doktorarbeit in einem interessanten und zukunftsrelevanten Forschungsgebiet durchzuführen, sondern auch stets mit kreativer Kritik, Kompetenz und Inspiration meine wissenschaftliche Entwicklung, Selbständigkeit und Organisationsfähigkeit förderte. Er erkannte bereits frühzeitig meine weiteren Fähigkeiten in der Administration, Lehre und Projektdesign und Management und förderte diese. Weiterhin danke ich Prof. Dr. Andreas Möglich für die Übernahme der Mentorenrolle. Die Diskussionen, Betreuung und Unterstützung unteranderem auf Konferenzen, verbesserten meine Arbeit enorm und resultierten in einer erfolgreichen Zusammenarbeit.

Außerdem möchte ich meinen Kollaborationspartnern für die gute Zusammenarbeit danken. Im speziellen, Prof. Dr. Andreas Hiltbrunner für den guten Datenaustausch und Diskussionen über verschiedene Projekte sowie Prof. Dr. Jorge Casal für die einmalige Gelegenheit neue Erfahrungen in seinem Institut in Buenos Aires zu machen.

Ganz besonderen Dank möchte ich meiner besten Freundin und Kollegin Jennifer Andres aussprechen. Durch Ihre Unterstützung und Zusammenarbeit wurde nicht nur die gesamte Doktorandenzeit wesentlich schöner, erträglicher und produktiver, sondern auch persönlich, wissenschaftlich und sprachlich half sie mir stets über mich hinauszuwachsen und das nun schon seit 8 Jahren. Gerade in schwierigen Zeiten sowohl privat wie auch in der Arbeit konnte ich immer auf ihr Verständnis, ihren Rat und ihre Hilfe bauen und sie schaffte es, dass ich der Schreibphase doch etwas Gutes abgewinnen konnte. Großer Dank gilt auch Tim Blomeier und Leonie-Alexa Koch, die über die letzten Jahre von Kollegen zu Freunden wurden und gemeinsam mit Jennifer zu einem sehr guten und freundlichen Arbeitsklima beigetragen haben. Auch sie standen mir immer mit Rat und Tat zur Seite und ermöglichten überhaupt erst viele Dinge während meiner Zeit in diesem Labor.

Des Weiteren danke ich meinem ehemaligen Masterstudenten Sergey Fedotov für seine gute Arbeit und Hilfe während seiner Masterarbeit.

Ich danke der gesamten AG Zurbriggen für die gute Zusammenarbeit. Besonders hervorheben möchte ich Reinhild Wurm, die mir während der gesamten Zeit immer mit fachlicher Kompetenz zur Seite stand und ohne die eigentlich keines meiner Experimente möglich gewesen wäre.

Anschließend danke ich meiner gesamten Familie und meiner Freundin für die Unterstützung und das Verständnis das sie auch in schwierigen Zeiten aufbrachten, sowie die Tatsache das genau diese Unterstützung mein gesamtes Studium samt Ph.D. überhaupt erst ermöglicht haben. Ich danke ihnen, dass sie meine Launen in stressigen Phasen ausgehalten haben und mir in allen Lebenslagen immer zu Seite standen.

Abschließend möchte Ich noch allen meinen Freunden danken. Im besonderen Natascha Künzel, die mich bereits seit meiner Bachelorarbeit nicht nur fachlich, sondern auch persönlich stets mit einem Bier und einem offenen Ohr unterstützt hat. Außerdem danke Ich Fabian Dolch, Steffen Schindler und Nils Kapust einfach dafür das sie als Freunde immer für mich da waren und für die unterstützenden Kommentare, wenn Ich mal wieder nur gemeckert habe.

Gerade für Familie und Freunde ist es schwer die richtigen Worte der Dankbarkeit zu finden, deshalb hoffe Ich das jedem in meiner Familie und meinem Freundeskreis meine Dankbarkeit bewusst ist, auch wenn sie nicht namentlich und Ihnen nicht im gebührenden Umfang hier gedankt wurde. Dieser Titel ist auch ein Stück weit euer Verdienst.

Vielen Dank!

Figures

Abbreviations

ABA	Abscisic acid
AD	Activation domain
ADA	Adenosin deaminase
APA	Active phytochrome binding A
APB	Active phytochrome binding B
BLUF	Blue light-using FAD
bPAC	Photoactivated adenylyl cyclase
cAMP	Cyclic adenosine monophosphate
Cas	CRISPR-associated protein
CCA	Circadian clock associated
ChR2	Channel rhodopsin
CIB	Calcium and integrin-binding protein
CMV	Cytomegalovirus promoter
COP1	Constitutive photomorphogenic 1
CRISPR	Clustered regularly interspaced short palindromic repeats
Cry	cryptochrome
DBD	DNA-binding domain
DNA	Deoxyribonucleic acid
E.coli	*Escherichia coli*
EL222	*Erythrobacter litoralis* protein 222
ELF3	E74-like transcription factor 3
ERF	Ethylene response factor
FAD	Flavin-adenine dinucleotide
FKF	Flavin-binding, Kelch, F-box
GA	Gibberellin acid
GAF	cGMP-stimulated phosphodiesterase, adenylyl cyclase, FhlA
GAL	Galactose
GFP	Green fluorescent protein
GI	Gigantea
goi	Gene of interest
GPCRs	G-protein coupled receptor
HFR1	Long hypocotyl in far-red

HLH	Helix-loop-helix
HTH	Helix-turn-helix
IPTG	Isopropyl-β-D-thiogalactopyranoside
IRES	Internal ribosomal entry site
JA	Jasmonic acid
JAZ	Jasmonate ZIM-domain
KRAB	Krüppel-associated box protein
LKP	Lov kelch protein
LOV	Light-oxygen-voltage
mRNA	Messenger ribonucleic acid
NES	Nuclear export signal
NpHR	Halorhodopsin
NLS	Nuclear localization signal
NTE	N-terminal extension
OPA	Only with phytochrome A
OPM	Output module
PAS	Per-Arndt-Sim domain
PCB	phycocyanobilin
PCM	Photosensory core module
Phy	phytochrome
PIF	Phytochrome interaction factor
POI	Protein of interest
SEAP	Human secreted alkaline phosphatase
SPA1	Suppressor of phytochrome A
SV40	Simian virus 40 promoter
TA	Poly-A terminator
TALE	Transcription activator-like effector
TCR	T-cell receptor
Tet	tetracycline
TF	Transcription factor
TIR	Transport inhibitor response
TOC	Timing of CAB expression protein
TPL	topless
UTR	Untranslated region
UV	Ultra-violet
UVR	UV-response
VP16	Virus protein 16

VVD	vivid
YFP	Yellow fluorescence protein
ZTL	zeitlupe

Summary

To reconstruct and understand complex regulatory networks and signaling pathways, the field of synthetic biology evolved from synthetic gene circuits to the construction of toggles switches and complex molecular tools. Within those tools, new synthetic approaches such as the relatively new field of optogenetics arose and showed increased applicability in bacteria, plants and mammalian cells.
Since the first optogenetic tool based on the light-dependent ion-channel channelrhodopsin was developed, various light-activatable systems to control and study cellular processes with a high spatiotemporal resolution were engineered. Those studies and the deciphering of complex pathways is particularly difficult in many organisms, because of genetic redundancy, interconnectivity and component number. To gain better understanding of light signaling pathways, a synthetic, optogenetic approach to screen, analyze and reconstruct complex plant signaling pathways in an orthogonal mammalian cell-based platform is one part of this work. Furthermore, an optogenetic tool for *in vivo* applications was generated since the control of gene expression in a non-invasive manner by light in *in vivo* situations with high precision and a deep tissue penetration still lags behind.

A phytochrome B-based toggle switch was re-engineered for a highly customizable and easily exchangeable modular structure. This optimized toggle switch has been used i) to study the light-dependent interaction with truncated versions of PIF1,3 and 6 in detail, ii) as a screening platform for light-dependent interactions of various plant transcription factors and phytochromes in an orthogonal platform, iii) to engineer a novel red light-inducible phytochrome A-based split transcription factor system and iv) in a developed lentiviral delivery system in neuronal-like cells in view of future *in vivo* applications.

Optogenetic tools based on different photoreceptors to target transcriptional inhibition, protein stability and mRNA levels simultaneously, were designed, characterized and combined for a complete light-induced protein knockout in mammalian cells. These approaches or switches were used for i) quantitative analysis, ii) control of programmed cell death and iii) control of cell cycle progression by endogenous protein knockout.

The demonstration of the comprehensive applicability of optogenetic tools designed in this work exemplifies the possibilities and perspectives in various research fields and the importance of synthetic biology to answer today´s fundamental scientific questions. Furthermore, this work illustrates the transmission from the reconstruction of plant light-signaling pathways to the design and construction of novel optogenetic tools based on this knowledge.

1 Introduction

The fundamentals of synthetic biology and the resulting optogenetic tools are the basic of the work done in this thesis. This introductory part describes relevant synthetic biology principles, the advantage of CRISPR/Cas9 in synthetic biology and detailed background information about plant transcription factors and optogenetic light-switches.

1.1 Introduction in synthetic biology

During the last 20 years, synthetic biology has developed from simply engineering approaches to complex engineered gene circuits. This fast growing field of study is motivated by the need of a molecular toolbox based on Boolean logic gates (Jewett, 2017). The roots of synthetic biology were described in 1961 by Jacob and Monod (MONOD and JACOB, 1961). By showing the existence of a regulatory circuit in *E. coli* they pined the response of a cell to its environment. From this timepoint the assembly of new regulatory systems in bacteria started. Throughout the years, a lot of different circuits and systems were established in bacteria (**Fig. 1 A**) (Liu et al., 2017; Andres et al., 2019). For example, in the early 2000s the first genetic toggle switch with expressing inhibitory repressors was engineered (**Fig. 1 B**) (Gardner et al., 2000). Additionally, an oscillatory circuit consisting of a triple negative-feedback loop (Elowitz and Leibler, 2000) and even more advanced circuits like light-sensing bacteria (Levskaya et al., 2005) or combinatorial genetic circuits (Guet et al., 2002) were developed (**Fig. 1 C**). During the last years, the achievements in synthetic biology have been more advanced, complex and they also include different organisms and combinations with other tools like CRISPR/Cas9. For instance, RNA-based Boolean logic gates (Win and Smolke, 2008), edge detectors (Tabor et al., 2009) , microbial kill switches (Callura et al., 2010), transcriptional regulatory circuits in animal cells (Lutz and Bujard, 1997; Weber and Fussenegger, 2006) and activation as well as repression of gene expression using CRISPR/Cas (Bikard et al., 2013). Those synthetic tools allowed profound advances in cancer research (Anderson et al., 2006), immunology (Geering and Fussenegger, 2015), protein expression (Gardner et al., 2000) and genome analysis (Gibson et al., 2010; Doudna and Charpentier, 2014). Taken together, the synthetic toolbox, inspired by nature, allows the control of gene expression, interrogation of gene networks and customization of cellular devices. Nevertheless, one of the goals of synthetic biology is to further develop novel molecular and cellular systems with desired properties and biological functionalities that are not present in nature (Andres et al., 2019).

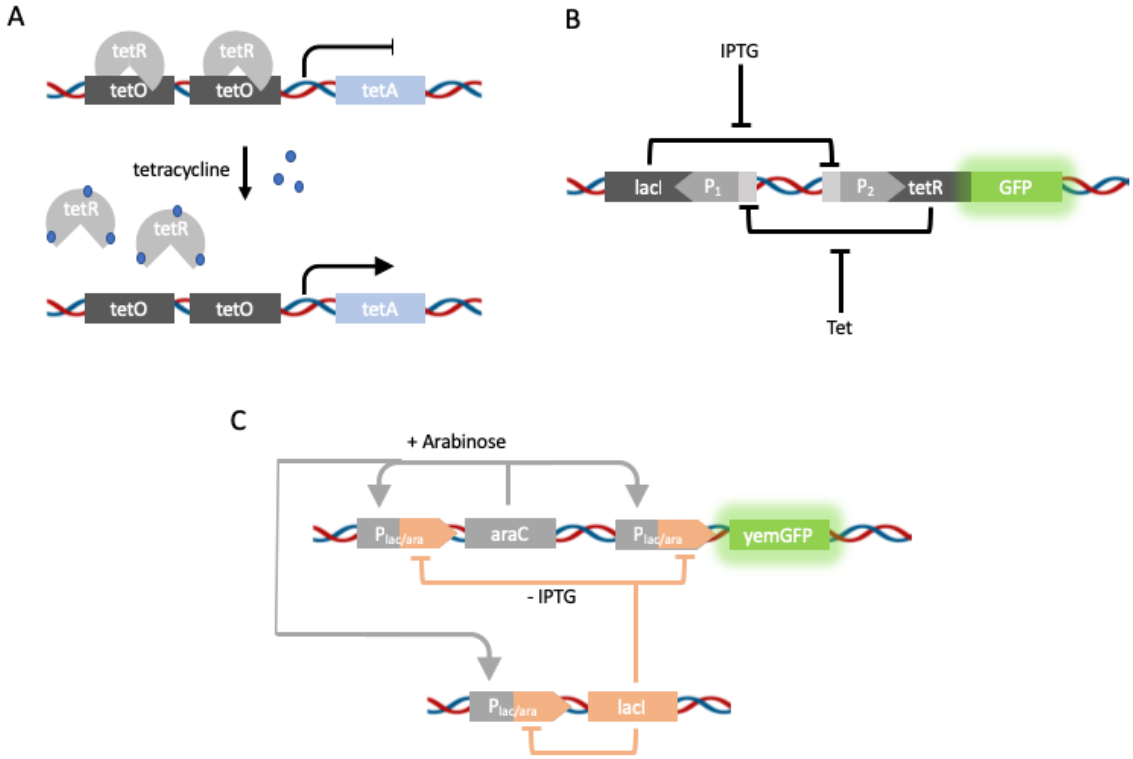

Fig. 1: Examples of regulatory circuits. A) Natural tetracycline switch. The tet repressor (tetR) is bound to its cognate tet operator (tetO) DNA-binding motif in the absence of tetracycline and represses the expression of the tet resistance-mediating tetA gene. When cellular levels of tetracycline increase, it binds to tetR and induces a conformational change resulting in the dissociation from the tetO sequence which provides expression of tetA (Adapted from Andres, Blomeier and Zurbriggen, 2019). **B**) An early engineered toggle switch. Two promoters each controlling expression of one repressor encoding gene (tetR, lacI). Each of the repressors regulates the promoter of the counterpart repressor antagonistically. This results in a bistable circuit, additionally controllable by supplementation with inducers such as isopropyl-β-1-thiogalactopyranoside (IPTG) or tetracycline (Tet). Addition of one of the inducers provides a stable state over a longer time period without further inducer addition which can be visualized by co-expression of GFP with one repressor (Adapted from Gardner, Cantor and Collins, 2000). **C**) Scheme of a synthetic oscillator (Stricker et al., 2008). All genes (araC, lacI and yemGFP) are under the control of a synthetic hybrid promoter $P_{lac/ara-1}$, consisting out of the activation operator site from the araBAD promoter and the repression site from the lacZYA promoter (Lutz and Bujard, 1997). The araC protein, in presence of arabinose, activates the hybrid promoter and thereby the gene expression of all three genes, which results in two feedback loops. The positive feedback loop gets activated by the hybrid promoter through the production of araC, and the negative feedback loop is based on the repression via the production of the lacI protein. LacI negatively regulates the expression of all three genes in the absence of IPTG. In summary, both feedback loops together constitute the synthetic oscillator (Adapted from Andres, Blomeier and Zurbriggen, 2019).

1.1.1 Synthetic biology in mammalian cells

Since the field of synthetic biology in microbial systems was growing fast, it was no surprise that these concepts were adopted by researchers working in mammalian cells or other eukaryotes. Transcriptional circuits, in an orthogonal manner were constructed to control cellular processes in other cell types (Weber et al., 2006). To date the largest number of mammalian synthetic circuits, consist of transcription factor circuits because they are intuitive to design and implement and they allow a high temporal control of expression of the protein of interest (Lienert et al., 2014). Those transcription factors usually contain a DNA binding domain and transcriptional-activation or -repression domains for positive or negative regulation of target genes (Lienert et al., 2014). Utilizing the ability of transcription factors to recognize their cognate DNA binding domain on specific DNA sequences makes it possible to engineer synthetic promoters (Gossen and Bujard, 1992). The first generation of synthetic gene circuits was based on naturally existing transcription factors, such as LacI, TetR and GAL4, or PIP or E (Folcher et al., 2001; Weber et al., 2002). Since then they were continuously replaced by programmable transcription factors such as zinc-finger-containing factors (Laity et al., 2001), transcription activator-like effectors (TALE) (Moore et al., 2014) and clustered regularly interspaced short palindromic repeats (CRISPR)- based regulators (Sander and Joung, 2014) (**Fig. 2 A**). Each of them can be engineered to bind desired DNA sequences. The fact that synthetic circuits and tools are not limited to transcriptional regulation allows their applicability on additional cellular hierarchy levels. During the last decade translational or posttranslational switches and regulators got more prominent in mammalian synthetic biology (Liang et al., 2011). For instance, RNA-based approaches like RNAi (Fire et al., 1998), microRNAs (Lagos-Quintana et al., 2001), aptamers and ribozymes (Etzel and Mörl, 2017) were developed to control translational or post-transcriptional processes. While RNAi, miRNAs and ribozymes lead to cleavage or splicing of the target mRNA, aptamers bind to specific targets like metal ions, small molecules, DNA or proteins (Xiao et al., 2008; Andres et al., 2019). Aptamers are structured, noncoding RNAs, which can interfere via ribosomes with mRNA leading to transcriptional control (Andres et al., 2019). One example, of RNA-based regulation for aptamers was shown by the workgroup of Ausländer et al. (Ausländer et al., 2011). They placed aptamers that sense the presence of specific proteins in the 5´-untranslated region (UTR) of transcripts, resulting in translational inhibition in the presence of the sensed protein (Ausländer et al., 2011; Lienert et al., 2014) (**Fig. 2 B**). Furthermore, siRNAs and miRNAs-based regulators have been shown as viable options for Boolean logic computing frameworks (Rinaudo et al., 2007; Lienert et al., 2014). Those RNA-based systems are relatively fast-acting, as they do not require translation. Moreover, RNA-targeted systems are very effective when combined with transcriptional regulation (Lienert et al., 2014). Additionally, RNA-based parts and devices hold many advantages but also trade-offs, such as off-targets not-related to

the gene of interest, compared with other types of regulators (Lienert et al., 2014). The combination of Inhibitory RNA and a transcriptional repressor can lead to a nearly complete repression of gene activity (Deans et al., 2007; Garg et al., 2012).

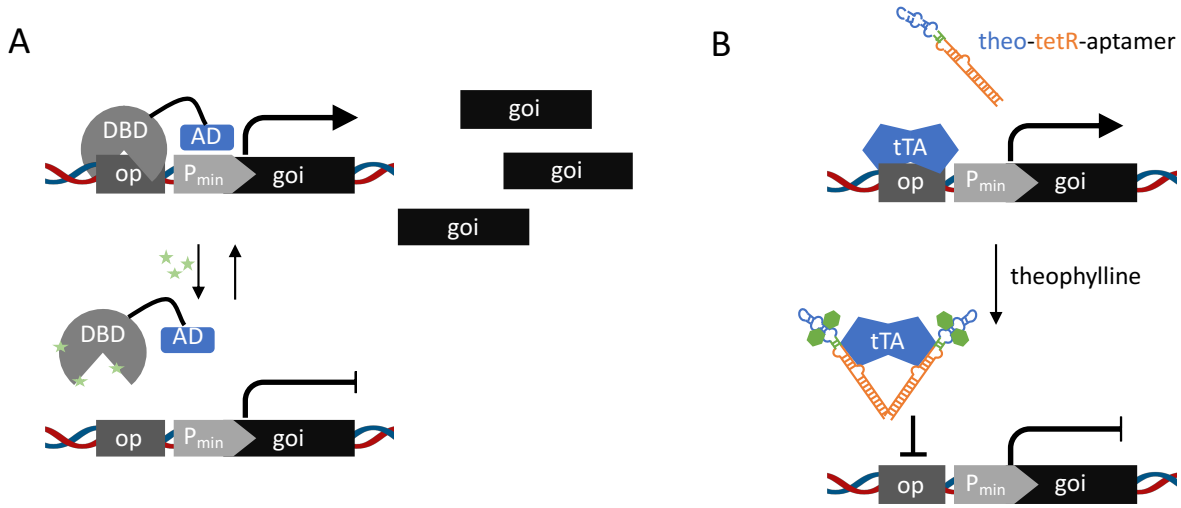

Fig. 2: Scheme of transcriptional regulators in mammalian cells. A) Transcriptional chimeric regulator. A DNA binding domain (DBD, e.g. tetR, E, Pip) is fused to an activation domain (AD, e.g. VP16, VP64). In absence of the inhibitory molecule, the DBD binds to its cognate operator site (op, e.g. tetO, etr8), the fused activation domain gets in close proximity to the minimal promoter and induces transcription of the gene of interest (goi). Addition of the inhibitory molecule leads to a conformational change of the DBD-AD fusion protein, releases the operator and terminates transcription (adapted from Hannes Beyer PhD Thesis, 2015). **B)** Mechanism of the theophylline-responsive tetR aptamer. The DNA-binding domain tetR is fused to the virus-derived trans activator VP16 (tTA) which binds to its specific DNA operator sequence (op) and activates transcription of the gene of interest (goi). In presence of theophylline, the structure of the theo-tetR-aptamer is restored. This allows specific binding to tTA and therefore inhibition of the transcriptional activity (adapted from Ausländer et al., 2011).

In contrast to the transcriptional and translational control of a protein, the protein stability itself offers a powerful application to rapidly and post-translationally control protein activity. Protein stability depends on several factors such as length of the peptide sequence, occurrence of specific amino acids that can be phosphorylated or other post-translational modifications, such as SUMOylation (Yen et al., 2008; Lienert et al., 2014; Park et al., 2016). However, the stability of proteins can be actively regulated for instance by adding a glycine to the N-terminus of the protein or by actively inducing degradation via the ubiquitylation pathway. The E3 ubiquitin ligase recognizes proteins that harbor a specific domain and catalysis the transfer of ubiquitin to this target protein, leading to recognition and degradation by the 26S proteasome (Hershko and Ciechanover, 1998; Lienert et al., 2014). For example, the *A. thaliana* F-box protein TRANSPORT INHIBITOR RESPONSE 1 (TIR1) has been shown to form an active E3 ubiquitin ligase complex in mammalian cells together with the SCF-complex. Upon binding to the SCF-complex it can bind auxins, which are plant hormones that are involved in many signaling pathways *in planta*, but also in gene expression (Calderón Villalobos et al., 2012; Lienert et

al., 2014). With this system, GFP was engineered to contain a recognition site for TIR1, for a auxin-dependent degradation of the protein of interest (Nishimura et al., 2009; Wend et al., 2013). Studies of cellular signaling and signaling pathways in mammalian cells are another important field. To introduce novel control schemes or to reroute information flow in signaling networks and pathways, they were synthetically engineered (Archer and Süel, 2013). For instance, G protein coupled receptors (GPCRs) which are activated by specific ligands to induce downstream pathways, were modified to detect synthetic small molecules for orthogonal external control (Barnea et al., 2008). Another essential part of synthetic biology in mammalian cells is the reconstruction of complex signaling pathways to define essential components of those or use the mammalian system as an orthogonal platform to study plant signaling pathways. Such an approach was used to express proteins involved in the B-cell receptor (BCR) signaling pathway and T cell receptor (TCR) signaling pathway in non-immune cells (Yang and Reth, 2010; Lienert et al., 2014). By expressing 10 or more heterologous proteins, James and Vale were able to recapitulate TCR signaling (James and Vale, 2012). Another approach to reconstruct plant signaling pathways in mammalian cells was to analyze the translocation into the nucleus of *A. thaliana* phytochrome B (PhyB) via phytochrome interacting factor 3 (PIF3). Two hypotheses existed: i) an endogenous NLS sequence of PhyB which is exposed upon illumination with red light and ii) an NLS sequence of PIF3 which can interact with PhyB upon red light-illumination and transport PhyB into the nucleus to induce light-signaling (Chen et al., 2005; Pfeiffer et al., 2012). Using an orthogonal mammalian system and with a synthetic approach Beyer et al. could proof the second hypothesis by reconstructing this minimal pathway with fluorescent tagged proteins and analyzing the light-dependent translocation to the nucleus (Beyer et al., 2015b) (**Fig. 3**).

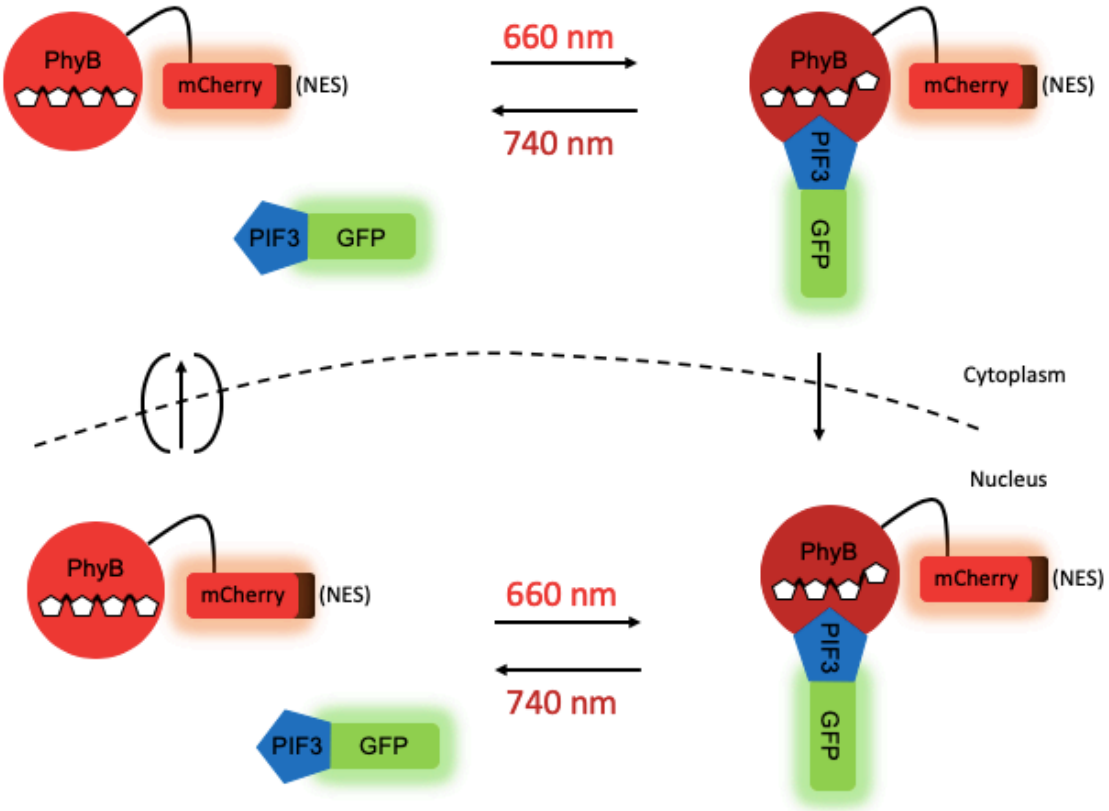

Fig. 3: Reconstruction of PIF mediated phytochrome B nuclear transport. Design of the red light-controlled nuclear localization system. *Arabidopsis thaliana* phytochrome B (PhyB) is fused to mCherry and PHYTOCHROME INTERACTION FACTOR 3 (PIF3) is fused to GFP. Optionally a nuclear export signal (NES) can be added. Upon illumination with red light (660 nm) and in presence of the chromophore Phycocyanobilin (PCB), PhyB changes its conformation to its active state (Pfr) and directly binds to PIF3. PIF3 contains an intrinsic nuclear localization sequence (NLS) and provides the nuclear transport of the heteromeric complex. Illumination with far-red light (740 nm) leads to conversion of PhyB to its inactive state (Pr) followed by the dissociation of PIF3. In presence of a NES sequence, PhyB shuttles back to the cytoplasm (Adapted from Beyer et al., 2015).

Today synthetic biology aims to develop new therapeutic applications. Therefore, synthetic approaches are used for instance to express therapeutic genes from promoter elements that are only active in certain cell types to provoke cell-type specific activity (Whitfield et al., 2012). Moreover, synthetic biology improves combined therapeutics, such as direct fusion of antibodies to a therapeutic protein (Ortiz-Sánchez et al., 2008), building chimeric activators (Cironi et al., 2008), influence the protein delivery in mammalian cells by liposomes (Akinc et al., 2010), nano-particles (Hasadsri et al., 2009) and receptor-ligand fusions (Rizk et al., 2009; Cameron et al., 2014).

To construct all of these synthetic tools, fast and cheap cloning approaches are needed. Over the years different techniques were published. One of the oldest synthetic cloning techniques

was shown by Gibson et al. to clone the whole genome of *Mycoplasma genitalium* (Gibson et al., 2008). In addition, methods like golden gate and enzyme free cloning were developed during the last years (Engler and Marillonnet, 2014; Beyer et al., 2015a).

1.1.2 CRISPR/Cas in synthetic biology

The immunological memory in bacteria of prior infections by bacteriophages and mobile genetic elements is provided by using CRISPR/Cas (clustered regularly interspaced short palindromic repeats/CRISPR-associated) (Marraffini, 2015; Hille and Charpentier, 2016; Mekler et al., 2019). They store the genetic information of viruses in their CRISPR arrays for a rapid immunological response upon invader infection (Barrangou and Doudna, 2016). Those foreign guide sequences are processed and part of the CRISPR RNAs (crRNAs) which are necessary for the binding of Cas effector proteins to the matching region of the invaders DNA (Jackson and Wiedenheft, 2015). Through the endonuclease activity of the Cas effector protein, the target is cleaved and a subsequent infection is avoided (Marraffini, 2015; Hille and Charpentier, 2016; Mekler et al., 2019). Recently the CRISPR/Cas system reached a huge popularity as a new, powerful method for precise genome editing and genome engineering (Marchisio and Huang, 2017). Since the programming of Cas is very easy by simply customizing the sequence of the guide RNA to match the target DNA, it is used extensively for genome editing (Doudna and Charpentier, 2014). The most prominent CRISPR Class 2 system is based on the Type II Cas9 from *Streptococcus pyogenes* (Jiang and Doudna, 2017). These Cas9 effector requires an additional trans-acting crRNA (tracrRNA) (Deltcheva et al., 2011) and a protospacer adjacent motif (PAM) to be activated and to find and cleave the target dsDNA (Mojica et al., 2009; Sternberg et al., 2014). Both RNAs and the PAM motif were combined into a single-guide RNA (sgRNA) to make the system more suitable for biotechnology and synthetic biology (Jinek et al., 2012). So far the main application is DNA editing (Marchisio and Huang, 2017). CRISPR/Cas9 was used for knock out (Cho et al., 2013) or knock in (Wang et al., 2013) mutants in several model organisms by using their own homology directed repair (HDR) or non-homologous end joining (NHEJ) systems. Furthermore, the CRISPR/Cas system was successfully used for therapeutically purposes as for instance to correct the CYSTIC FIBROSIS (CTFR) locus via homologous recombination in cultured intestinal stem cells of patients with cystic fibrosis (Schwank et al., 2013; Pellagatti et al., 2015).

Also, a catalytically inactive Cas9 variant (dCas9) is a key element for the construction of new transcription factors in synthetic biology (Marchisio and Huang, 2017). This new and powerful way of engineering orthogonal transcription factors gave researchers the possibility to regulate promoter sequences in a highly customizable manner (Marchisio and Huang, 2017). To that end, dCas9 is fused to activation or repressor domains such as VP64 (Gilbert et al., 2013) or

KRAB (Beerli et al., 2000), thereby allowing regulation of protein expression via customized gRNAs. Those gRNAs usually are synthesized by RNA polymerase III promoters such as the murine U6 or yeast SNR52 promoters (DiCarlo et al., 2013; Gilbert et al., 2013). An advantage of the Cas-based systems is their usage as a scaffold (Konermann et al., 2015) or as an inducible system (Zetsche et al., 2015). Within the different Cas types there is only one (Type VI), beside Class I Type III, that is able to recognize RNA instead of DNA as a target. The best characterized member of this family so far is Cas13a (formerly C2c2). Liu et al. could determine the function of the cleavage mechanism of Cas13a on ssRNA and show that protospacer flanking sites (PFS) influence the efficiency of the Cas13 effector (Liu et al., 2018). Interestingly the Cas13 effector does not depend on a PAM sequence, since it is necessary for the unwinding process of the DNA (Murugan et al., 2017). After a screening of a family subset of Cas13 enzymes it was discovered that Cas13b from *Prevotella sp* (PspCas13b) has the highest mRNA cleavage efficiency (Cox et al., 2017). Additionally, PspCas13b showed the highest specificity in cleavage with a strongly decreased number of off-targets. To give the system also the ability to be an editing tool, a deaminase (ADA2) was fused to a catalytically inactive variant of PspCas13b (dCas13b). This deaminase is able to change an adenosine to an inosine directly in the RNA. Ribosomes are recognizing this inosine as a guanine which leads to a mutation in the protein. With this tool (Cas13b-REPAIR) Cox et al. were able to modify mRNAs of interest with an efficiency up to 50% depending on the mRNA sequence (Cox et al., 2017).

1.1.3 Optogenetic tools in synthetic biology

Light is one of the most important abiotic environmental stimuli. In nature, a range of photoreceptors exist sensing light in the entire visible spectrum. In *planta*, light is essential for development, growth and photosynthetic energy production (Ni et al., 2014). In mammalian cells and higher eukaryotes, light influences cellular processes and the circadian clock via retinal absorption (Hattar et al., 2002). In fungi, like *Neurospora*, light plays a critical role in the circadian rhythm (Schafmeier and Diernfellner, 2011). In contrast to chemicals, light has numerous advantages. For instance, it allows, depending on the wavelength, deep tissue penetration with minimized invasiveness. Additionally, light as an application enables high spatiotemporal resolution, while chemical inducers suffer from toxicity, tissue diffusion and non-reversibility. By taking advantage of these unique features, light is used as an inducer for several approaches. Since Oesterhelt and Stoeckenius found in 1971 a light-dependent proton pump, bacteriorhodopsin (OESTERHELT and STOECKENIUS, 1971), several other opsin proteins were discovered. The use and introduction of opsins in neuroscience and animal cells allowed to selectively change neuronal membrane potentials by regulating micro bacterial ion pumps or channels via light. The term “optogenetics” was more and more established in the

growing research field using those opsins to study neuroscience in animal cells. Especially, established neuronal activators like channelrhodopsin (ChR2) or inhibitors like halorhodopsin (NpHR) were used as optogenetic tools and set the start to develop better or different variants as well as novel and more complex tools (Nagel et al., 2003; Adamantidis et al., 2007; Arenkiel et al., 2007; Hegemann and Möglich, 2011). In the last ten years a second wave of optogenetic tools, based on plant and bacterial photoreceptors, were developed to construct synthetic signaling pathways in *E. coli* and yeast (Shimizu-Sato et al., 2002; Levskaya et al., 2005). More recently, optogenetic light-switches based on photoreceptors from all living organisms were engineered for use in mammalian cells to control cellular processes, signaling pathways as well as protein localization and stability (Levskaya et al., 2009; Wu et al., 2009; Yazawa et al., 2009; Müller et al., 2013a; Motta-Mena et al., 2014; Beyer et al., 2015b; Kaberniuk et al., 2016; Baaske et al., 2018; Chatelle et al., 2018).

1.2 Optogenetic light-switches

In the last years several optogenetic light-switches based on photoreceptors from all kingdoms of life and covering the whole visible light-spectra were developed. An overview and description of these non-neuronal optogenetic switches are following starting with UV-light switches.

1.2.1 Photoreceptors and their application in light-switches

UV-light

UV-light is toxic at high intensities not only for humans but also for plants. As an inducible protection mechanism, plants like *A. thaliana*, contain a seven bladed β-propeller photoreceptor UV resistance 8 (UVR8). In the absence of ultraviolet-B light the UVR8 photoreceptor forms a dimer (Rizzini et al., 2011; Christie et al., 2012; Di Wu et al., 2012; Crefcoeur et al., 2013). Upon UV-B light illumination at 280 nm, the UVR8 dimer dissociates into monomers which can interact with the constitutively photomorphogenic 1 (COP1) protein, which is an important part of the UVB-signaling pathway (Yin et al., 2015). Based on this UV-B light induced interaction and on the heterodimerization, optogenetic switches for transcriptional control were developed (Crefcoeur et al., 2013; Müller et al., 2013b)(**Fig. 4**). Additionally, the homodimerization of UVR8 was used to engineer cytokinin release switches and inducible protein secretion (Chen et al., 2013; Sarris et al., 2016).

Fig. 4: UVR8 based optogenetic switch. UVR8 is present as a dimer in darkness. Upon illumination with UV-B light the homodimer dissociates and interacts with COP1. In darkness the heteromeric complex dissociates, leading to homodimerization of UVR8.

Blue-light

Several optogenetic switches based on blue light-responsive receptors and proteins exist, such as Dronpa, light-oxygen-voltage (LOV), EL222, bPAC, cryptochrome 2 (CRY2), gigantea (GI), VVD and Melanopsin.

Dronpa is a fluorescent protein from the *Pectiniidae* family which was discovered by a cDNA screening (Habuchi et al., 2006). The engineered variant of Dronpa, 145N, can be switched off by illumination with cyan light at ~500 nm and switched on with violet light (~400 nm). The fluorescent tetramer of Dronpa monomerizes when excited at ~500 nm and loses the fluorescence while it tetramerizes upon excitation with ~400 nm (Zhou et al., 2012; Beyer et al., 2015c) (**Fig. 5**).

Light-oxygen-voltage (LOV) domains are the key flavin-containing domains of most of the blue light photoreceptor families, such as phototropin, zeitlupe (ZTL), flavin binding kelch repeat F-box 1 (FKF1), LOV kelch protein 2 (LKP2), neochrome and aureochrome (Kong and Okajima, 2016). Those photoreceptor families can be separated into two different groups, the ones forming dimers (hetero- or homodimers), and the ones which cage a part of the photoreceptor. For instance, the LOV2 domain of *Avena sativa* contains a carboxy-terminal α-helix (Jα-helix) which is bound to the core domain of LOV2. Upon photon absorption a cysteine-flavin bond is established between a conserved cysteine and the flavin mononucleotide (FMN) chromophore. This leads to structural changes and unwinding of the Jα-helix. In optogenetic approaches, for instance the fusion of a specific protein-tag to the Jα-helix leads to the blue light-induced exposure of this tag and therefore to interaction with the corresponding protein. The additional fusion of a DNA-binding domain to LOV2 and the fusion of a VP16 transactivator domain to the other protein allows blue light dependent transcriptional control (Müller et al., 2013b). Depending on the used LOV domain the recovery time back to the dark state takes

seconds to days (Harper et al., 2004; Nakasone et al., 2010; Strickland et al., 2010; Müller et al., 2014) (**Fig. 5**).

Homodimerizing examples of blue light photoreceptors are EL222 or VVD. EL222 is a photosensitive transcription factor from the bacterium *Erythrobacter litoralis* (Baaske et al., 2018). This transcription factor contains a LOV domain with a helix-turn-helix (HTH) DNA-binding domain. In the dark, LOV binds with the HTH domain, circumventing HTH induced dimerization. Upon blue light illumination the interaction of LOV and HTH is disrupted and the transcription factor homodimerizes and can bind at its specific cognate DNA-sequence. This dimerization is spontaneously interrupted in dark deactivating DNA-binding (Baaske et al., 2018). For instance, in one optogenetic approach the homodimerization of EL222 was used to inhibit transcriptional activity. Therefore, EL222 was fused to a human-derived repressor domain and the cognate DNA-binding sequence of EL222 was placed in front of the regulated gene (Nash et al., 2011; Zoltowski and Gardner, 2011; Rivera-Cancel et al., 2012; Motta-Mena et al., 2014; Baaske et al., 2018). VVD from *Neurospora crassa* is also a homodimerizing blue light photoreceptor. Quite similar to EL222, VVD homodimerizes upon blue light illumination. A site-directed mutagenesis of residues in the homodimer interface increased the dimerization efficiency for the applicability in synthetic approaches (Nihongaki et al., 2014; Salinas et al., 2018) (**Fig. 5**).

FKF1 is an example of a LOV-domain containing photoreceptor that heterodimerizes. In *planta*, FKF1 is involved in the day-regulation of a flowering locus. It can interact upon blue light illumination with several interaction partners such as gigantea (GI) or zeitlupe (ZTL) to regulate gene expression. The fusion of FKF1 to a DNA-binding domain and the fusion of a transactivator to GI, gives the possibility to regulate transcriptional activity by blue light, which is an example of the engineering of this photoreceptor as an optogenetic tool (Song et al., 2014; Quejada et al., 2017) (**Fig. 5**).

Another blue light induced photoreceptor that heterodimerizes is cryptochrome 2 (Cry2) from *A. thaliana.* Cry2 can interact upon blue light illumination with the cryptochrome-interacting bHLH 1 protein (CIB1). Similar to other blue light photoreceptors that heterodimerizes, the interaction of Cry2 and CIB was utilized in an optogenetic approach for light-induced transcriptional regulation. The half-life time of Cry2 in the dark is ~12 min (Liu et al., 2008; Kennedy et al., 2010; Pathak et al., 2014). Additionally, Cry2 clusters in nuclear bodies in nature (Yu et al., 2009). This blue light-induced oligomerization of Cry2 opened an additional application possibility of this switch (Taslimi et al., 2014; Hörner et al., 2018) (**Fig. 5**).

Photoactivated adenylyl cyclases (PACs) are natural blue light-regulated enzymes. PACs like euPAC from *Euglena gracilis* consist of subunits containing repeats of BLUF (blue light receptor using FAD) and two adenylyl cyclase-domains. The workgroup of Stierl et al. found a much smaller variant of dimeric PAC in *Beggiatoa* (bPAC) consisting of a single BLUF- and an

adenylyl cyclase-domain (Schröder-Lang et al., 2007; Stierl et al., 2011). Upon photon absorption by BLUF, the adenylyl cyclase is activated and generates cAMP and is therefore an important tool for signal activation for example in neuroscience (Zhang and Tzanakakis, 2017) (**Fig. 5**).

One opsin that occurs in mammalian cells is Melanopsin. Melanopsin is a member of the G protein-coupled receptor superfamily and a blue light-activatable transmembrane photoreceptor. In the presence of the retinal chromophores 9-*cis*-retinal or 11-*cis*-retinal it absorbs photons. It requires high intensities of light of wavelengths between 420 and 480 nm, which leads to a photoisomerization of the chromophore into its all-*trans* conformation. Those photoreceptors are commonly expressed intrinsically in photosensitive retinal ganglion cells (ipRGCs). Because of its stable association with all-*trans* retinal, Melanopsin is unique among mammalian photopigments (Hankins et al., 2008). The induced conformational changes confer Gαq-type G-protein-mediated Ca^{2+} transport by phospholipase C (PLC). This Ca^{2+} transport enables downstream signaling pathways of protein kinase C (PKC) (Melyan et al., 2005; Beyer et al., 2015c; Spoida et al., 2016) (**Fig. 5**).

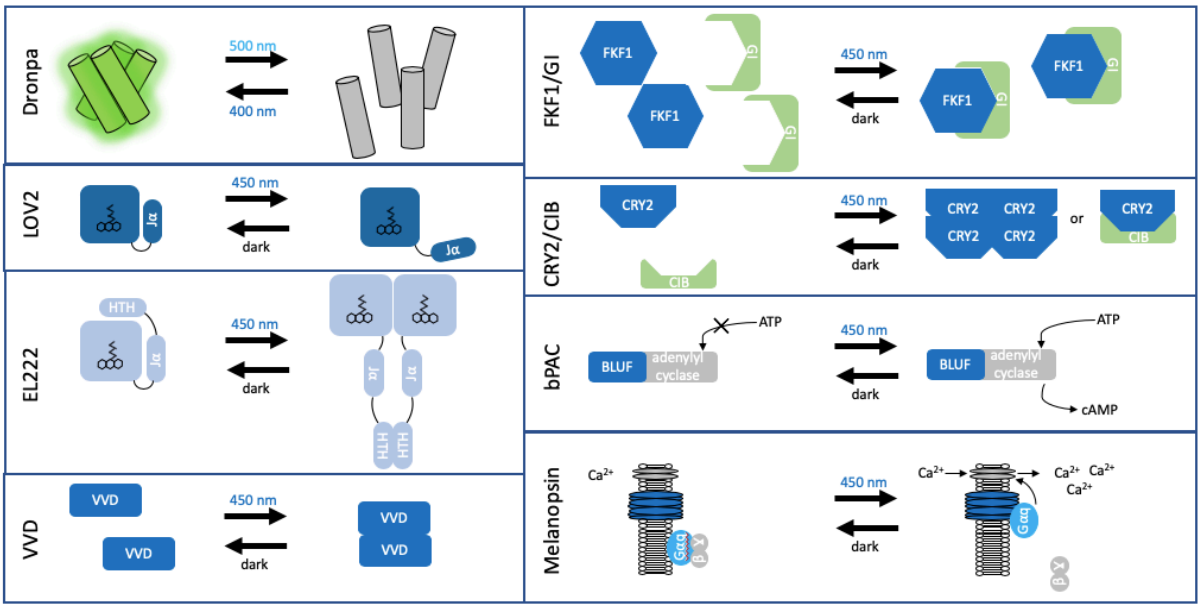

Fig. 5: Examples for blue light responsive photoreceptors used as switches in mammalian cells. Dronpa tetramer dissociate after illumination with blue-light and loses fluorescence. LOV2 unwinds its core-bound Jα-helix upon blue light illumination. EL222, VVD and CRY2 are able to form homodimers while FKF1/GI and CRY2/CIB form heterodimers upon illumination. Photon absorption of bPAC leads to an active adenylyl cyclase and cAMP production. Melanopsin activates the G-coupled receptor pathway which opens an ion channel upon blue light illumination. See text for detailed explanations and references of the receptor properties.

Green light

The bacterial B_{12}-dependent photoreceptor CarH, found in *Myxococcus xanthus*, was established as the first green light dependent light switch in model organisms, such as plants and mammalian cells (Cervantes and Murillo, 2002; Chatelle et al., 2018).

The monomeric apoprotein CarH binds in coenzyme B_{12} and forms tetramers in the dark. Those tetramers bind to their cognate operator DNA sequence (CarO) and repress transcription of downstream genes. Illumination with green light (between 478 nm – 509 nm) triggers dissociation of the tetramer followed by decreased binding affinity to the DNA and therefore transcription induced. (Ortiz-Guerrero et al., 2011; Tabor et al., 2011; Kutta et al., 2015). This green light-induced dissociation was used to engineer a green-off system. Therefore, a repressor domain was fused to CarH, which leads to transcriptional inhibition in the dark and dissociation in green light followed by transcriptional activity (**Fig. 6**).

Fig. 6: Example of a green light responsive photoreceptor. In dark CarH binds the chromophore AdoB12 and forms tetramers which are able to bind to their cognate DNA sequence. Upon illumination with green light AdoB12 gets photolysed and the tetramer dissociates (adapted from Chatelle et al., 2018).

Red light

Phytochromes are photoreceptors which can capture red and/or far-red light. For instance, *A. thaliana* has five different phytochromes able to sense red and far-red light (phytochrome A - E) (Clack et al., 1994). While phytochrome A and B are, as far as known, the physiologically most relevant proteins in red light-signaling pathways, phytochrome B is the best studied, characterized and used member of phytochromes in synthetic biology. In nature, plant phytochromes as for instance PhyA and PhyB tend to dimerize. They consist of two conserved modules, the photosensory core module (PCM) including an N-terminal extension (NTE), a PAS domain (Per-Arnt-Sim), a GAF domain (cGMP-stimulated phosphodiesterase, adenylyl

cyclase, FhlA) which is necessary for covalently chromophore binding and a Phy domain (phytochrome specific). The C-terminal output module (OPM) includes two PAS domains and a HKRD (histidine kinase-related domain) (Vierstra, 1993; Li et al., 2011; Burgie and Vierstra, 2014) (**Fig. 7 A**). As covalently bound chromophores plant phytochromes utilize the linear tetrapyrrole (bilin), phytochromobilin (PΘB) or phycocyanobilin (PCB). Phytochromes are synthesized in their inactive Pr form (Li et al., 2011). In the presence of the chromophore and upon red light-illumination (660 nm) the chromophore isomerizes from the Z to the E state which leads to a conformational change of the phytochrome and results in the active Pfr form (Remberg et al., 1999; Gyula et al., 2003). The active, Pfr form of phytochromes interacts with other proteins like transcription factors to regulate light-signaling pathways (Ni et al., 1999; Kircher et al., 2002; Lau and Deng, 2012). Conversely, irradiation with far-red light (740 nm) reverts the phytochrome back to its inactive Pr form (Andres et al., 2019). Since the absorption spectra of both forms overlap partially, an interconvertible, dynamic photo equilibrium is created depending on the wavelength (Rockwell et al., 2006). Additionally, the active Pfr form can revert light-independent via thermal relaxation (dark reversion) to its Pr form (Klose et al., 2015). Phys are involved in germination processes, seedling development and shade avoidance response (Casal, 2013). The red light-dependent translocation to the nucleus of the Pfr form of PhyB is therefore essential for biological responses. *In vitro* studies showed that the transport of PhyB depends on the interaction with transport-helper protein phytochrome interaction factor 3 (PIF3) (Pfeiffer et al., 2012). These results were verified using mammalian cells as an orthogonal platform (Beyer et al., 2015b). Based on the light-dependent interaction between PhyB and PIF3 or PIF6, several synthetic canonical light-switches were developed (Müller et al., 2013a; Toettcher et al., 2013; Müller et al., 2014; Wend et al., 2014; Beyer et al., 2015b) (**Fig. 7 B**). In contrast, PhyA (the exclusive photoreceptor for sensing and transducing far-red light-signals) is involved in the de-etiolation of seedlings and in high irradiance responses (Yanovsky et al., 1997; Shinomura et al., 2000; Quail, 2002). The PhyA protein is light-labile, whereas PhyB to PhyE are more light-stable (Hirschfeld et al., 1998; Hennig et al., 1999; Leivar et al., 2008b). Similar to PhyB, PhyA needs transport-helper proteins. Far-red elongated hypocotyl 1 (FHY1) and FHY1-like (FHL) interact red light-dependent with PhyA mediating the nuclear transport. Once transported to the nucleus, PhyA needs a second photon of far-red light to dissociate the interaction with FHY1 and FHL and be able to interact with transcription factors for biological light responses for this it needs to absorb red light again (Hiltbrunner et al., 2006; Genoud et al., 2008). While for PhyB several interactions partners were discovered, including components of the circadian clock like CCA1, TOC1 or ELF3, the role of PhyA is still unknown (Yeom et al., 2014).

Bathyphytochromes or bacteriophytochromes, utilize biliverdin (BV) as a chromophore which is abundant in mammalian cells as an intermediate in heme biosynthesis (Consiglieri et al.,

2019). One example for them is the far-red light-sensing photoreceptor BphP1 from *Rhodopseudomonas palustris.* BphP1 can, upon illumination with far-red light (740 – 780 nm), interact with the transcriptional repressor PpsR2 (Kojadinovic et al., 2008; Kaberniuk et al., 2016). In contrast to plant phytochromes, BphP1 cannot switch complete back to the inactive Pfr form with 636 nm illumination, probably because of its overlapping Pr and Pfr spectra at this wavelength. However, BphP1 has a dark relaxation half-life time of 900 s (Kaberniuk et al., 2016) (**Fig. 7 B**).

For applications in mammalian cells and higher organisms, phytochromes are particularly interesting because of the deep tissue penetration, the active switch ability between two conformations and the orthogonal usage.

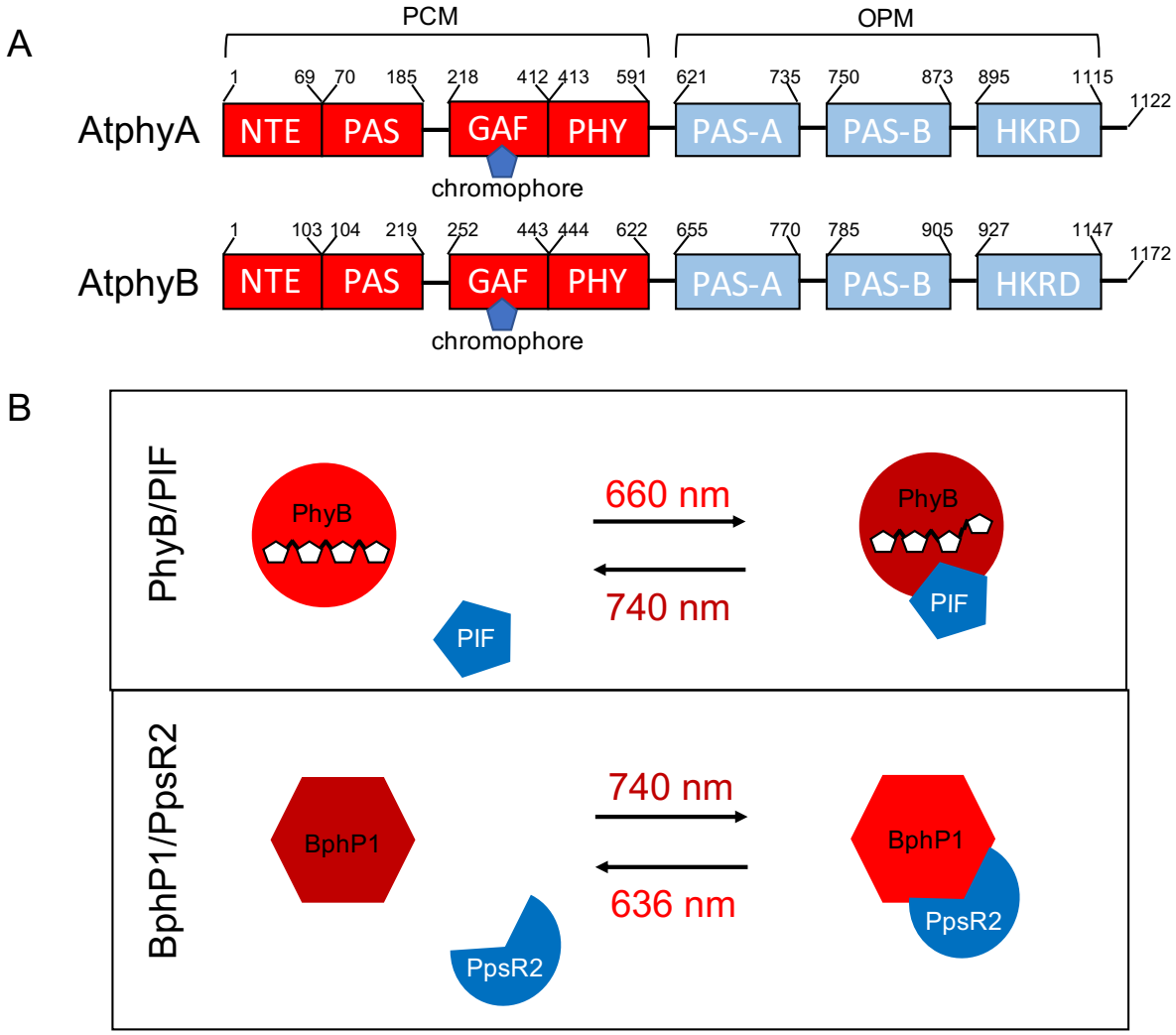

Fig. 7:Structure and examples for Red-light responsive photoreceptors used in optogenetic switches. A) Schematic domain structure of phytochrome A and B. Abbreviations: GAF (cGMP-stimulated phosphodiesterase); HKRD (histidine kinase-related domain); NTE (N-terminal extension); OPM (output module); PAS (Per (period circadian protein), Arnt (Ah receptor nuclear translocator protein), Sim (single-minded protein)); PCM (photosensory core module); PHY (phytochrome) (adapted from Li et al., 2011). **B)** Red-light responsive photoreceptor switches. Phytochrome B (PhyB) utilizes PΦB or PCB as chromophore and changes its conformation upon red-light illumination. This leads to a heteromeric interaction with PIF. This interaction can be actively dissociated via illumination with far-red light. BphP1 utilizes biliverdin (BV) as chromophore and changes its conformation after far-red light absorption. This provides the interaction with PpsR2. Via illumination with red-light the photoreceptor switches back to its inactive form, leading to the dissociation of PpsR2.

1.3 Plant transcription factors and regulators

Transcription is a strongly regulated process controlled mainly by transcription factors (TFs) or regulators that specify the spatial and temporal expression of eukaryotic genes. TFs are defined as sequence specific DNA-binding proteins regulating the initiation of transcription which are involved in different cell processes and pathways, from development to environmental adaptation (Brkljacic and Grotewold, 2017; Franco-Zorrilla and Solano, 2017). For instance, *A. thaliana* has ~2,000 TFs, separated in different TF super-families and most likely additional TF families remain to be identified from the ~8,000 proteins of unknown function (Davuluri et al., 2003; Gómez-Porras et al., 2007; Mitsuda and Ohme-Takagi, 2009; Brkljacic and Grotewold, 2017). These TF super-families include domains such as AP2 (ERF proteins), basic helix-loop-helix (bHLH; PIF proteins), bZIP and LFY (Fernández-Calvo et al., 2011; Chang et al., 2013; Weirauch et al., 2014; Mathelier et al., 2016; Franco-Zorrilla and Solano, 2017). Some families are explained further.

1.3.1 Phytochrome interacting factors (PIFs)

Phytochrome interacting factors (PIFs) belong to the bHLH superfamily of transcription factors (Toledo-Ortiz et al., 2003). The bHLH domain is essential for the specific DNA-binding to the G-PBE-box DNA motif (CACGTG, CACATG) to fulfill transcriptional regulation (Leivar and Quail, 2011). Additionally, they contain a weakly conserved N-terminal active phytochrome-B binding (APB) motif which is sufficient for PhyB Pfr binding and/or an active phytochrome-A binding (APA) motif which is necessary for binding of PhyA Pfr (Leivar and Quail, 2011; Lee and Choi, 2017). This binding is necessary for the phytochrome dependent light response such as seed germination, seedling photomorphogenesis, shade avoidance responses and leaf senescence (Lee and Choi, 2017). In *A. thaliana* eight family members of PIF (PIF1 - 8) exist and promote gene expression while they also appear in homo- and heterodimers with other proteins for transcriptional regulation (**Fig. 8 A**) (Martínez-García et al., 2000; Leivar and Quail, 2011; Pham et al., 2018).

PIF3 for instance, contains both phytochrome binding domains (APB & APA). Depending on the light conditions and in response to the interaction with either PhyA or PhyB, PIF3 regulates various physiological processes positively or negatively (Kim, 2003). Additionally, several studies showed, *in vitro* and *in vivo*, that PIF3 induces the nuclear transport of PhyB (Pfeiffer et al., 2012; Beyer et al., 2015b). Furthermore, PIF3 is removed from promoters of specific target genes by interacting with the phytochrome Pfr form, thereby transcription initiation is downregulated. Additionally, PhyA and -B Pfr forms intensify phosphorylation and polyubiquitination to diminish the repression of photomorphogenic signaling (Al-Sady et al., 2006; Park et al., 2012; Ni et al., 2014). This phytochrome dependent phosphorylation of PIF promotes 26S-proteasome mediated degradation. Half-life time dependent similarities were found for PIF1, 4 and 5 (Bauer et al., 2004; Lee et al., 2004; Al-Sady et al., 2006; Shen et al., 2008). Especially for this PIF-quartet (PIF1, 3, 4, 5), reports revealed a strong binding affinity to the G-PBE-box DNA motif (Martínez-García et al., 2000; Zhang et al., 2013). *A. thaliana* mutants lacking multiple PIFs from this quartet showed increased photomorphogenic development (Leivar et al., 2008a; Zhang et al., 2013) (**Fig. 8 A&B**).

PIF1 is a negative regulator of seedling de-etiolation by inhibiting chlorophyll biosynthesis, suppressing hypocotyl elongation and negative gravitropism of hypocotyls (Huq et al., 2004; Shen et al., 2005). Similar to PIF3, PIF1 interacts light-dependent via its APB or APA domains with PhyA and PhyB Pfr forms which promotes PIF1 phosphorylation and the following 26S-proteasome mediated degradation (Shen et al., 2005) (**Fig. 8 A&B**).

PIF2 (PIL1, recently renamed by Lee and Choi, 2017) is suggested to play a role as a positive regulator in photomorphogenesis. Reports revealed a physical interaction with PhyB and CONSTITUTIVELY PHOTOMORPHOGENIC1 (COP1) in an antagonistic manner (Luo et al., 2014). Additionally, PIF2 showed a suppression of the transcriptional activity of the PIF-quartet (PIF1, 3, 4, 5) together with LONG HYPOCOTYL IN FAR-RED1 (HFR1) (Luo et al., 2014). The 26S-proteasome mediated degradation of PIF2 depends on the interaction with COP1 instead of PhyB, suggesting an antagonistic mechanism of light to regulate transcriptional activity of bHLH transcription factors (Luo et al., 2014) (**Fig. 8 B**).

PIF4 and PIF5 are selectively involved in the PhyB light signaling pathway, regulating hypocotyl elongation, leaf senescence and shade avoidance (Lorrain et al., 2007; Leivar and Quail, 2011). These proteins are rapidly degraded by PhyB in response to high R/FR light ratio. Furthermore, both transcription factors are positive regulators of the shade avoidance response promoting shade-dependent auxin responses (Iglesias et al., 2018). Together with PIF1 and PIF3 these transcription factors can build a PIF-quartet to regulate cellular processes such as seedling skotomorphogenesis (Khanna et al., 2004; Leivar and Quail, 2011; Zhang et al., 2013).

The bHLH TF PIF6 has two alternative splicing variants, the α-form is the full-length version and the β-form, which has a different splicing of exon 3 leading to the loss of the bHLH domain. Surprisingly, only overexpression of PIF6-β leads to reduced seed dormancy suggesting the requirement of this splicing variant for the regulation of dormancy (Penfield et al., 2010). Similar to all other PIFs, PIF6 contains an APB domain for the interaction with the PhyB Pfr form. In contrast to other PIFs, interaction between PIF6 and PhyB inhibit the thermal relaxation of PhyB from its Pfr to its Pr form (Khanna et al., 2004; Penfield et al., 2010; Smith et al., 2017) (**Fig. 8 B**).

The light-stable protein PIF7 is implicated in various regulatory processes such as shade avoidance, seedling de-etiolation and circadian rhythm (Leivar et al., 2008a; Kidokoro et al., 2009; Huang et al., 2018). In contrast to other PIF proteins, PIF7 exhibits no evidence of phy-induced phosphorylation and the following degradation (Leivar et al., 2008a). On the contrary, activity of PIF7 is controlled by rapid de-phosphorylation in response to shade, which leads to shade avoidance responses (Li et al., 2012; Mizuno et al., 2015; de Wit et al., 2015; Huang et al., 2018). This shade response is delayed by other proteins that bind actively to PIF7 such as 14-3-3 proteins (Huang et al., 2018) (**Fig. 8 B**).

PIF8 is not well described yet, but the evidence of binding to PhyB and the presence of conserved domains (APB and bHLH) suggest the possibility that PIF8 participates at least in some of the red light responses (Leivar and Quail, 2011; Jeong and Choi, 2013).

Additionally, PIFs are involved in several developmental processes via crosstalk with plant hormone signaling pathways as those of gibberellins (GA), ethylene, abscisic acid (ABA) and jasmonates (JA).

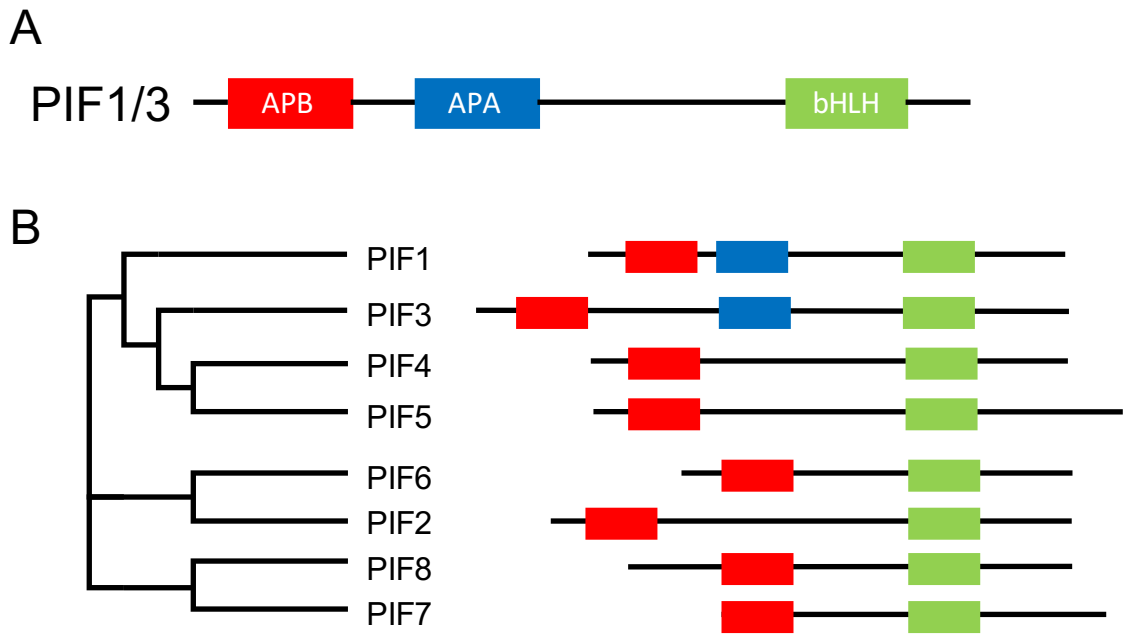

Fig. 8: The PIF-subfamily of basic helix-loop-helix (bHLH) transcription factors. A) Schematic PIF1/3 structure. The highly conserved binding sites for photoactivated phyB (APB) and phyA (APA) are necessary for the light dependent interaction. The bHLH domain, which defines this class of transcription factors, is necessary for dimerization and DNA-binding of the protein to its cognate DNA sequence (CACGTG). **B)** The PIF-subfamily of *A. thaliana* bHLH family demonstrating the phylogeny and domain structures. (adapted from Leivar and Quail, 2011).

The deeper analysis of PIF proteins regarding their interaction with phytochromes and further analysis of the APB domain would expand our knowledge of functional phytochrome binding and binding affinities depending on conserved regions within the APB domain. In this work, ligh-dependent phytochrome:PIF interaction studies in mammalian cells as an orthogonal platform were addressed. Furthermore, this platform was used to analyze the smallest conserved region inside of the APB domain, that is sufficient for the interaction with the phytochrome Pfr form, for differences in the binding affinity of PIF1, 3, 6.

1.3.2 Ethylene response factors (ERFs)

Ethylene is a gaseous plant hormone which induces in etiolated seedlings a response of short, thickened hypocotyl and a root with an exaggerated apical hook (Jeong et al., 2016). Synthesized from methionine, ethylene binds and inhibits ethylene receptors to stabilize the transcription factors ETHYLENE INSENSITIVE 3 (EIN3) and EIN3-LIKE 1 (EIL1). This stabilized transcription factors regulate then various downstream targets such as ETHYLENE RESPONSE FACTORs (ERFs) (Adams and Yang, 1979; Chao et al., 1997; Solano et al., 1998; Jeong et al., 2016). ERFs contain a conserved DNA-binding domain and belong to the AP2 transcription factor superfamily (Ohme-Takagi and Shinshi, 1995). With over 120 members the ERF family is the most prevalent representative family of the AP2 super family (Rao et al., 2015). However, as described above, PIFs are involved in several phytohormone signaling pathways and as reported PIF3 and PIF4 highly overlap in regulation with a set of target genes of EIN3 suggesting a transcriptional co-regulatory effect in ethylene response (Jeong et al., 2016). Furthermore, a direct physical interaction of PhyB with EIN3 and the resulting degradation of EIN3 via enhancement of the E3-ligase EBF1/EBF2 shows the light-triggered termination of ethylene signaling as an integral part of initiating the de-etiolation switch (Shi et al., 2016). Nevertheless, most of the integration of phytochrome mediated light-signaling in ethylene signaling is still unknown (Yang and Li, 2017). Especially, to discover the regulation and function of most of the ERFs is worth investigating further research. For instance, ERF family subgroup I-b contains ERF55-60 and the function of these genes is at this time still unknown (Nakano et al., 2006). However, characteristic for these proteins are four domains of unknown function (CMI-1 - 4) (Zhang and Li, 2018). ERF6 is involved in various stress responses, such as the pathogen defense or osmotic stress response and belongs to

the ERF subgroup IX (Nakano et al., 2006; Moffat et al., 2012; Van den Broeck et al., 2017). In this protein, domains of importance were identified such as an acidic region in the N-terminus and a putative MAP kinase phosphorylation site in the C-terminus designated as CMIX-5 motif (Nakano et al., 2006).

Due to the large number of processes mediated by ethylene response and the interfering proteins involved in such processes, studying and understanding the direct influence of light on ethylene signaling is particularly difficult to analyze *in planta.* In this work a minimal system, based on the red light split transcription factor system was used to study the light-dependent direct physical interaction between phytochrome A and ERFs in mammalian cells as orthogonal platform.

1.3.3 Jasmonate and JASMONATE-ZIM-DOMAINs (JAZs)

One important group of phytohormones includes jasmonic acid and its derivatives, termed jasmonates (JAs) with a multitude of roles in physiological processes such as growth, photosynthesis and reactions to the environment upon several abiotic and biotic stress conditions (Creelman and Mullet, 1997; Pauwels and Goossens, 2011). Most prominently, JAs activate defense mechanisms during biotic and abiotic stress, as they are essential for the production of secondary defense metabolites (Ballaré, 2011; Goossens et al., 2016). JAs are chemically closely mirror prostaglandins that mediate inflammatory response in animals (Hamberg and Gardner, 1992) and they are synthesized from polyunsaturated fatty acids from chloroplast membranes (Delker et al., 2006; Yan et al., 2007). Further processing leads to the final bioactive form of JA-Ile which is generated by the jasmonoyl-isoleucin synthase JASMONATE RESISTENT1 (JAR1) (Staswick and Tiryaki, 2004; Leon-Reyes et al., 2010; Sheard et al., 2010; Wasternack and Strnad, 2016). The response mechanism of JAs is quite similar to the one of other phytohormones. JA-Ile binds to the F-box protein CORONATINE INSENSITIVE1 (in *A. thaliana* COI1) and interacts with other proteins from the JAZ family (Feys et al., 1994; Chini et al., 2007; Okada et al., 2015). These JAZ proteins bind together with JA-Ile to the SCF^{COI1} receptor complex and become ubiquitinated and consequently degraded by the 26S-proteasome (Chini et al., 2007; Farmer, 2007; Thines et al., 2007). JAZ proteins are the predominantly negative regulators of JA signaling and possess a conserved TIFY motif inside of the ZINC-FINGER EXPRESSED IN FLUORESCENCE (ZIM) domain. This domain is necessary for the formation of hetero- and homodimers and the recruitment of negative regulators such as TOPLESS (TPL) via the adapter protein NINJA (NOVEL INTERACTOR OF JAZ) (VANHOLME et al., 2007; Chung and Howe, 2009; Wager and Browse, 2012). Additionally, every JAZ protein contains a C-terminal JA-associated (Jas) or Jas-like domain for binding the COI1 receptor or TFs and regulators in downstream signaling

(Sheard et al., 2010). In *A. thaliana* thirteen genes encoding JAZs (JAZ1-13), including JAZ13, an atypical JAZ protein lacking the TIFY motif, have been identified as regulators in the JA signaling (Thireault et al., 2015). While JAZ7, 8 and 13 lack the conserved amino acids necessary for binding COI1, all other JAZs are able to bind COI1 in a JA-Ile dependent manner (Pauwels and Goossens, 2011; Thireault et al., 2015). In addition, one study has shown that JAZ7, -8 and -13 have the ability to recruit TPL and repress the JA response via their ERF-associated amphiphilic repression (EAR) motif representing a possible negative feedback control or an essential fine-tuning mechanism (Campos et al., 2014; Thatcher et al., 2016). Alternative splicing events described for several JAZs increases the complexity of JA signaling indicating a fine-tuning mechanism (Campos et al., 2014; Chini et al., 2016). A crosstalk of phy-dependent light-signaling and JA signaling was shown in previous studies. For instance, Campos et al. could show, that decreased levels of the active PhyB form (Pfr), resulting from either a *phyB* mutation or shade conditions, compromise JA mediated resistance to a broad spectrum of biotic attackers (Casal, 2013; Campos et al., 2014). Additionally, one report showed that a JAZ-mediated interference with the DELLA-PIF interaction leads to modulation in plant growth suggesting an integration of light-signaling in the JA signaling pathway (Yang et al., 2012). Moreover, the transcriptional response of various genes involved in JA-dependent defense and resistance is impaired in *phyA cry1 cry2 A. thaliana* triple mutants. This indicates that the effects are not just results of different light conditions (Cagnola et al., 2018).

Even though the crosstalk of light-signaling and JA signaling is known, the precise influence and direct regulation of proteins is still undiscovered. While the analysis of pathway regulations and protein:protein interactions is particularly difficult in plants, the use of mammalian cells as orthogonal platform to study minimal systems provides advantages. In contrast to plants, studies in mammalian cells are possible with reduced complexity and without disturbing endogenous proteins. This allows the analysis of the interaction of plant proteins without any co-factors in a robust, quantitative platform. In this work, a system based on the red light-induced split transcription factor system was used to analyze physical light-dependent protein interactions between the main phytochromes, PhyA and PhyB, and all typical JAZ proteins (JAZ1-12) to show a direct light regulation of the main JA pathway transcription factors.

1.3.4 Further *A.thaliana* transcription factors and potential phytochrome interaction partners

Beside the mentioned big transcription factor families, a variety of transcription factors and regulators are equally interesting in case of crosstalk's with the light signaling pathway. As described above, FHY1 and FHL are essential for the nuclear transport of phytochrome A and therefore for the PhyA-dependent light signaling. Both proteins contain a nuclear localization signal (NLS), a nuclear export signal (NES) and septin-related domain (SRD), which promotes hetero- and homodimerization (Zhou et al., 2005). Although the shared identity is below 30 %, they show high similarity in their function and act as functional homologs. One example for the complementing functionality was shown by the workgroup of Zhou et al., 2005, where the overexpression of FHL successfully rescued the FHY1 deficient mutant (Zhou et al., 2005; Genoud et al., 2008). While FHY1 and FHL are commonly described as PhyA nuclear transporters, they also regulate downstream signaling by recruiting other transcription factors (Zhou et al., 2005; Yang et al., 2009).

The formation of nuclear bodies (NB) of PhyB is induced by interactions with proteins such as PIF3. The formation of NBs is promoted by PHOTOPERIODIC CONTROL OF HYPOCOTYL 1 (PCH1) and PCH1-LIKE (PCHL) proteins. They prevent the thermal relaxation of PhyB and they are indicated as parts of a memory prior illumination (Huang et al., 2016; Enderle et al., 2017). Additionally, it has been shown that PCH1 is upregulated through an interaction with the N-terminus of COP1, which is a key player in the UVR8 response and connects the red light signaling with the UVB-light signaling (Oravecz et al., 2006; Favory et al., 2009).

COP1 acts in the visible light spectrum as a negative regulator for photoreceptors, but in the UVB-light pathway, it is functional as positive regulator and interacts with UVR8 (Oravecz et al., 2006). Furthermore, COP1 can function as a E3 ubiquitin ligase, requiring the accessory of PHYTOCHROME A-105 (SPA1-4) proteins. Together with the kinase-like domain-CC-WD40 proteins, COP1 forms a tetrameric complex containing two COP and two SPA proteins to repress photomorphogenesis (Martínez et al., 2018). Photoreceptors such as PhyA, PhyB and Cry2 are also target substrates for COP1/SPA1 mediated ubiquitination and degradation. In contrast, light inhibits the activity of the COP1/SPA1 complex by dissociation through direct PhyA, PhyB and Cry1/2 interaction (Lu et al., 2015; Sheerin et al., 2015). Interestingly, the direct interaction of PhyA and the COP1/SPA1 complex depends on the phosphorylation state of PhyA. Only phosphorylated PhyA binds to the COP1/SPA1 complex, following by PhyA degradation while unphosphorylated PhyA has a higher binding affinity to FHY1 and FHL and promotes nuclear accumulation (Saijo et al., 2008; Martínez et al., 2018).

The influence of light signaling in the circadian clock of plants is known but not completely understood, especially the regulation of flowering via the light-dependent interaction of PhyA and PhyB with PIF3 by clock-dependent and clock-independent mechanisms (Martínez-García

et al., 2000; Leivar and Quail, 2011; Li et al., 2016a). One clock-dependent mechanism is the interaction of PhyB and the circadian clock transcription factor EARLY FLOWERING3 (ELF3) in *A. thaliana* (Reed et al., 2000). Furthermore, the circadian clock contains multiple transcriptional feedback loops where the integration of light signaling is still unknown (Sanchez and Yanovsky, 2013; Hsu and Harmer, 2014; McClung, 2014; Shim and Imaizumi, 2015; Li et al., 2016b). In those feedback loops, CIRCADIAN CLOCK ASSOCIATED1 (CCA1) and LATE ELONGATED HYPOCOTYL (LHY) repress the transcription of TIMING of CAB EXPRESSION1 (TOC1). TOC1 represses transcription of CCA1 and LHY (Huang et al., 2012). CCA1 and LHY also repress transcription of ELF3, ELF4, LUX ARRHYTHMO (LUX), TOC1 and GIGANTEA (GI) (Li et al., 2016b). Except from TOC1, all positively regulate the expression of CCA1 and LHY (Hazen et al., 2005; Kikis et al., 2005; Onai and Ishiura, 2005; Kamioka et al., 2016; Li et al., 2016b). However, information about the influence of the circadian clock on photoperiodic flowering, cold response and freezing tolerance are still limited (Chow et al., 2014). Identified in an Arabidopsis transcriptome profiling as cold-responsive genes, COLD-REGULATED GENE27 (COR27) and COR28 have been shown to be circadian clock regulated (Fowler and Thomashow, 2002; Mikkelsen and Thomashow, 2009). While the biological function is unknown, Li et al. could show downregulated transcription of COR27 an COR28 when Arabidopsis seedlings where illuminated with either red- or blue light suggesting that both proteins are regulated by temperature and light (Li et al., 2016b). A direct interaction could be observed with the circadian clock protein CCA1 proposing that they are key components connecting light and temperature signals and circadian clock (Li et al., 2016b).

The proteins NOT9a – c are involved in the CCR4-NOT complex in plants, which is a key player in eukaryotic gene expression (Collart, 2016; Arae et al., 2019). The CCR4-NOT complex, also containing NOT1 as a scaffold protein, determines the length of the poly-A tail of mRNAs (Tucker et al., 2002; Chen and Shyu, 2011). Orthologs of the CCR4-NOT complex have been identified in mammalian cells, including human and mouse cell derived cells (Arae et al., 2019). Additionally, Arae *et al*., identified various orthologs in *planta* but the complete composition and regulation of the CCR4-NOT complex is largely unknown (Arae et al., 2019). Furthermore, the workgroup of Andreas Hiltbrunner showed a direct interaction of NOT9b with PhyA in a yeast two hybrid screening (unpublished data) suggesting an integration of light signaling into the CCR4-NOT complex in *A. thaliana*.

In this yeast two hybrid screen, one protein termed in this work OPA (ONLY with PHYTOCHROME A) (AT1G48770) showed a light-dependent interaction with phytochrome A suggesting a biological function in the light signaling pathway. Nevertheless, until now this protein was described as hypothetical protein with a domain of unknown function (DUF1639).

Taken together the knowledge about the integration of light signaling into other signaling pathways is limited and not well understood. To get deeper insights into the light-dependent regulation of such pathways we analyzed the physical light-dependent interaction of phytochromes and the described proteins in an orthogonal mammalian cell-based system. In this work a light-regulated gene expression system was established and developed based on the discovered integration of light into another signaling pathway.

1.4 The application of light-switches

During the last years, various optogenetic switches, introduced above, were implemented in mammalian cells to study for instance signaling pathways, protein localization and cell-cell contact. Examples of these approaches are summarized in Table 1.

The control of cellular gene expression for several purposes was taken under the control of light. This control can be achieved with UV, blue, green and red / far-red light and the generally fused split-transcription factors which are reconstituted via illumination and the induced dimerization of the fused photoreceptors. The UV-system based on UVR8 and COP1 demonstrated high inductions of expression levels upon illumination. However, UVB light produces cytotoxic effects and therefore the intensity of UVB light has to be carefully adjusted (Crefcoeur et al., 2013; Müller et al., 2013b). Transgene expression systems were published for almost all blue light receptors mentioned before. For instance, the small LOV2 domain of *Avena sativa* was engineered as a tunable, light-controlled interacting protein tag (TULIP) for blue light-induced protein interactions (Strickland et al., 2012). Based on this interaction, a gene expression system was developed (Müller et al., 2014). The dimerization-based gene expression system of the bacterial EL222 domain was successfully developed for blue light-induced gene expression and induced inhibition of transcription (Motta-Mena et al., 2014; Baaske et al., 2018). Although the published gene expression system based on the interaction of FKF1 and GI (1.173 aa) is very large, it showed consistent induction of gene expression also in mammalian cells and was optimized throughout the years (Yazawa et al., 2009; Polstein and Gersbach, 2012; Quejada et al., 2017). The VVD system is one of the smallest systems and was one of the first light-regulated gene expression system in mammalian cells (Wang et al., 2012). Recently, a new optimized version of VVD, termed FUN-LOV, was published with increased induction up to 1300x fold in yeast (Salinas et al., 2018). Since the Cry2 homodimerization system was used for regulating kinase activity and the Cry2/CIB1 system was published as a tool for genome editing by blue light-induced CRISPR/Cas9, it is getting more prominent (Nihongaki et al., 2015). Gene expression systems based on the blue light-induced interaction between Cry2 and CIB1 were developed already in 2013 (Konermann et al., 2013) and used for various gene expression systems. Last year, an upgrade for the

chemical inducible tetracycline system based on Cry2/CIB1 was published, comparable to the LOV2-based upgrade published 2014 (Müller et al., 2014; Yamada et al., 2018). The bacterial cobalamin dependent carH based green light-switch, is the first green light-induced gene expression system in plants as well in mammalian cells (Chatelle et al., 2018). While the system is actually a green off system, it is able to regulate expression by forming tetramers, binding to the DNA, which are dissociated upon illumination with green light. Red and far-red light systems have some advantages compared to their wavelength counterparts as these wavelengths. Red and far-red light have a deeper tissue penetration and are less cytotoxic than any other wavelengths. Additionally, systems based on these wavelengths have the ability to be actively deactivated. For instance, the red light PhyB/PIF system was developed as gene expression toggle switches in yeast, plants and mammalian cells (Hughes et al., 2012; Müller et al., 2013a; Ochoa-Fernandez et al., 2016). Furthermore, this system was engineered and used for the activation of cell signaling approaches and light-dependent protein localization with a high spatiotemporal resolution (Levskaya et al., 2009; Toettcher et al., 2011; Beyer et al., 2015c). To study signaling pathways, a phytochrome B based opto-SOS system for activation and investigation of Ras signaling by recruitment of a Ras guanine nucleotide exchange factor domain (SOScat) via illumination with red light, was published (Toettcher et al., 2013). Since PΘB or PCB is not naturally available in eukaryotes like mammalian cells, the chromophore has to be supplemented exogenously for the PhyB-based system, to be functional. To overcome this limitation, systems based on bacterial phytochromes such as BphP1 were developed. These systems utilize as chromophore the endogenously available biliverdin and the emission wavelength is in the far-red region of the spectra (740 nm) (Kaberniuk et al., 2016). In addition to the gene expression system, BphP1 was published for far-red light-dependent functional protein localization processes (Redchuk et al., 2017). Further outstanding examples in the field of optogenetic switches include the reports on motor protein gearshifting via blue light (Nakamura et al., 2014). The authors used LOV2 domains and their Jα-heilx to regulate the speed and the direction of myosin and kinesin motor proteins. The spatiotemporal control of these proteins allows dynamic control of analyte transport in microfabricated devices in single cells (Nakamura et al., 2014). The light-dependent control of protein degradation was shown by constructing a LOV2 domain with fused degron, to allow proteasomal degradation of the LOV2 domain and the fused protein of interest upon blue light illumination (Bonger et al., 2014; Beyer et al., 2015b; Sun et al., 2017; Taxis, 2017; Baaske et al., 2018). Additionally, the combinability of the optogenetic systems was demonstrated in the last years. The combination of the PhyB/PIF system, the LOV2/ePDZ system and the UVR8/COP1 system allows multichromatic control of transgene expression of three different proteins at the same time (Müller et al., 2013b; Müller et al., 2014). Moreover, the combination of the LOV2-degron system and the EL222-KRAB system with a protein of interest (POI) leads

to a nearly complete downregulation of POI activity upon blue light illumination (Baaske et al., 2018). Therefore, the LOV2-degron protein was fused to the POI while the transcription of this fusion protein can be regulated by the EL222-KRAB repressor protein. This allows the downregulation of protein levels by regulation of transcription and protein stability at the same time via blue light (Baaske et al., 2018). Additionally, control over programmed cell death induced by pro-apoptotic proteins was achieved with this system (Fischbach et al., 2019a, Appendix 7.1).

Table 1: Examples of optogenetic approaches taking advantage of photoreceptors and switches described above.

Switch	Application	Reference
UVR8/COP1	gene expression	(Crefcoeur et al., 2013; Müller et al., 2013b)
UVR8/UVR8	protein secretion	(Chen et al., 2013)
	hydrogel formation	(Zhang et al., 2015)
	cytokinin release	(Sarris et al., 2016)
cPAC	cAMP production	(Blain-Hartung et al., 2018)
bPAC	cAMP production	(Stierl et al., 2011)
LOV2	nuclease protection	(Strickland et al., 2008)
	cell signaling	(Wu et al., 2009)
	gene expression	(Müller et al., 2014)
	apoptosis	(Smart et al., 2017)
	cell migration	(Guo et al., 2012)
	actin formation	(Rao et al., 2013)
	protein stability	(Bonger et al., 2014; Sun et al., 2017; Taxis, 2017; Baaske et al., 2018)
	receptor activation	(Schmidt et al., 2014)
	nuclear localization	(Niopek et al., 2014; Guntas et al., 2015; Yumerefendi et al., 2015; Niopek et al., 2016; Wehler et al., 2016)
	transport protein control	(Nakamura et al., 2014)
	ion channel	(Cosentino et al., 2015)
	peroxisomal transport	(Spiltoir et al., 2016)

	post-translational control	(Jones et al., 2016)
	kinase activity	(Gehrig et al., 2017)
EL222	gene expression	(Motta-Mena et al., 2014; Jayaraman et al., 2016; Baaske et al., 2018)
FKF1/GI	gene expression	(Yazawa et al., 2009; Polstein and Gersbach, 2012; Quejada et al., 2017)
	protein localization	(Yazawa et al., 2009)
	organelle tethering	(Shi et al., 2018)
VVD	gene expression	(Wang et al., 2012; Müller et al., 2013b; Salinas et al., 2018)
	receptor activation	(Grusch et al., 2014)
	cell-to-cell communication	(Isomura et al., 2017; Isomura and Kageyama, 2018)
	genome editing	(Nihongaki et al., 2015)
	protein localization	(Kawano et al., 2015)
Cry2/CIB1	gene expression	(Konermann et al., 2013; Pathak et al., 2017; Quejada et al., 2017; Yamada et al., 2018)
	receptor activation	(Bugaj et al., 2015)
	kinase activity	(Wend et al., 2014)
	cell signaling	(Ye et al., 2011; Bugaj et al., 2013; Lee et al., 2014; Chatelle et al., 2016)
	protein localization	(Kennedy et al., 2010)
	cell differentiation	(Polstein et al., 2017)
	genome editing	(Nihongaki et al., 2015)
	transport protein control	(Duan et al., 2015)
	apoptosis	(Hughes et al., 2015)
	DNA-methylation	(Choudhury et al., 2016)
	kinase activity	(Mühlhäuser et al., 2017)
Cry2/Cry2	kinase acitivity	(Wend et al., 2014)
	protein clustering	(Park et al., 2017)
Dronpa	cell signaling	(Zhou et al., 2012)
	protein localization	(Zhou et al., 2012)
	protein hydrogel	(Lyu et al., 2017)

CarH	gene expression	(Chatelle et al., 2018)
PhyA/FHY1 or FHL	gene expression	(Sorokina et al., 2009)
PhyB/PIF3 or PIF6	gene expression	(Shimizu-Sato et al., 2002; Müller et al., 2013a; Ochoa-Fernandez et al., 2016)
	protein localization	(Levskaya et al., 2009; Toettcher et al., 2011; Beyer et al., 2015b; Adrian et al., 2017)
	cell signaling	(Toettcher et al., 2011; Toettcher et al., 2013; Yu et al., 2016; Goglia et al., 2017; Yousefi et al., 2019)
	viral infectivity	(Gomez et al., 2016)
BphP1/PpsR2	gene expression	(Kaberniuk et al., 2016)
	protein localization	(Redchuk et al., 2017)

2 Aims

This work illustrates the use of synthetic biology approaches to engineer, develop and optimize optogenetic tools in mammalian cells for *in vivo* applicability and to control cellular processes, e.g. gene expression and viability. Additionally, this work addresses the screening and studying of potential phytochrome interactors and therefore their integration into plant light signaling pathways, with optogenetic tools in an orthogonal mammalian cells-based platform. This work focuses primarily on the following aims:

1. Optimization of the PhyB-based red light split transcription factor system for the applicability in *in vivo* situations. For this aim, the red light system was re-designed, truncated PIF variants were analyzed for their binding affinities to decrease the size of the system and a viral delivery system for the red light tool was established for use in neuronal-like cells.

2. Screening of potential phytochrome interactors and reconstruction of plant light signaling pathways. Towards this aim, the re-designed red light system was used to analyze and screen the light-dependent interaction of phytochrome A and B with various *A. thaliana* transcription factors to show integration of phytochrome signaling in such pathways in an orthogonal platform. Based on these results a novel PhyA-based red-light system was established showing the connection between basic research and applied optogenetics.

3. Blue light-induced protein knockout and endogenous mRNA targeting. Towards this aim tools to knockout protein levels in mammalian cells targeting transcription, mRNA or protein stability were developed. One optogenetic tool targeting transcription and protein stability and one targeting the mRNA level of protein based on CRISPR/Cas were engineered. In addition, the applicability was shown for programmed cell death and cell cycle control.

3 Results and Discussion

The following sections detail the most relevant data obtained during the studies and practical work of the Ph.D. thesis in context of the aims above. A more detailed description of most of the data can be found in the Appendix: Publications, Manuscripts.

3.1 Engineering of a red light toggle switch for *in vivo* application and screening of potential phytochrome interactors

3.1.1 New generation phytochrome B-based split transcription factor system

Light inducible transgene expression systems represent a cornerstone technology in synthetic biology and optogenetics. In contrast to its chemically inducible counterparts light has various advantages such as reversibility, reduced toxicity, high spatiotemporal resolution and minimized invasiveness. Especially the red light-inducible split transcription factor system based on the interaction of *A. thaliana* PhyB and PIF6 enables deeper tissue penetration because of its activation wavelength, compared with e.g. blue light systems (Kaberniuk et al., 2016). In addition, the system can be actively switched off by illumination with far-red light which is an advantage compared with blue or UV-B light systems (Müller et al., 2013a). While it was demonstrated that this system was applied to several mammalian cell lines, plants and yeast, a mammalian *in vivo* applicability is still missing (Müller et al., 2013a; Pathak et al., 2014; Ochoa-Fernandez et al., 2016). The applicability *in vivo,* implicates further modifications and optimizations of the system, for instance the need of tissue specific promoters and size limitations in transfection vectors. Additionally, this system has been used as a quantitative mammalian-based screening platform for interaction analysis of PIF variants and novel light-dependent phytochrome interactors, which needs the replacement of one or more modules by the protein of interest in the system. Since, the published PhyB-based system was constructed without specific restriction sites, an easy exchange of parts of the system were not possible. Therefore, we aimed to reconstruct and optimize the PhyB-based system for i) easy exchangeability, ii) applicability for *in vivo* use and iii) novel interaction studies with PhyA/B quantitatively. To engineer the PhyB system for an *in vivo* application and to use it for light-dependent interaction studies, the first step was to redesign the basic PhyB construct to make it customizable, which allows easy replace of needed and optimized modules. The basic published bicistronic construct contains, $PhyB^{1-650}$ fused to the trans activator virus protein 16 (VP16) under the control of a constitutive SV40 promoter, followed by an internal ribosomal entry site (IRES) which separates the tetracycline repressor (tetR) fused to $PIF6^{1-100}$ and a poly-A sequence (**Fig. 9 A**). The basic reporter construct used for the red light-induced toggle

switch comprises $tetO_{13}$ in front of a synthetic minimal promoter (P_{CMVmin}), followed by the human secreted alkaline phosphatase (SEAP) as a reporter (Müller et al., 2013a). In an experimental setup, upon red light illumination and available chromophore, $PhyB^{1-650}$ switches to its active Pfr form and interacts with $PIF6^{1-100}$ which is fused with the tetR protein bound to the DNA upstream of the synthetic minimal promoter. The interaction leads to a close proximity of the $PhyB^{1-650}$-VP16 fusion and induces transcription of the SEAP reporter (**Fig. 9 B**). Illumination with far-red light leads to dissociation of the interaction between PhyB and PIF6 and stops the transcription. To allow an easy exchange of every part, we reengineered the whole construct including specific unique restriction recognition sites between every module. For the specific exchange of the promoter a *NheI* and a *SpeI* restriction site were inserted. Since for *in vivo* applications, a tissue specific promoter such as hSynapsin or CamIIkα in neuronal cells is often necessary, the easy replaceability in such a system should be assured. For the replacement of $PhyB^{1-650}$ by shorter or mutated variants and other phytochromes, an *EcoRV* restriction site was implemented into the construct. While the tetR-based optoswitch is functional in mammalian cells in cell culture, there is a possibility that it is not functional in *in vivo* situations. To be prepared for such a situation we inserted a *NotI* and *BsrGI* restriction site to create an exchangeable tetR module for potential replacements of the DNA binding protein. Additionally, to have the ability to substitute $PIF6^{1-100}$ by smaller versions for limited size *in vivo* situations, potential interaction partners or other proteins, an *AscI* restriction site was introduced (**Fig. 9 A**). With the similar strategy for the red light-inducible system, we wanted to construct the reporter plasmid as modular as possible. Therefore, restrictions sites *AatII* and *NheI* were implemented to allow the replacement of the thirteen repeats of the tetracycline operon ($tetO_{13}$) by possible other operon sequences, fitting to the counterparts used in the red light-system. To provide a high flexibility in the choice of reporter genes we inserted *EcoRI* and *HindIII* recognition sites, in front and behind the reporter gene for the secreted embryonic alkaline phosphatase (SEAP), that allows quantitative determinations. As a normalization element we chose the secreted *Gaussia* luciferase (Gluc) constitutively expressed from an SV40 promoter in a second ORF cloned directly after the poly-A sequence of the first ORF. Restriction sites *EcoRV* and *NotI* were added for replaceability of the normalization element by other reporter genes such as fluorophores (**Fig. 9 A**).

Since normalization elements and constitutive controls are necessary to analyze transfection efficiency, expression differences and potential toxicity, we decided to add a constitutively expressed reporter (Wend et al., 2013; Baaske et al., 2018).

With these modifications, we constructed a fully customizable red light split transcription factor system with a ratiometric constitutively expressed normalization element for corrections of differences in transfection efficiency and expression levels. Additionally, the optimized system indicated higher induction folds in transfected CHO-K1 cells as the published basic system

(**Fig. 9 C**). After normalization, the new reporter construct showed higher relative expression levels, albeit the induction fold suffers from higher basal levels and therefore increased leakiness (**Fig. 9 D**). This results probably from the higher transfection efficiency of the reduced number of constructs, which leads to a higher overall expression level. Similar constructs with different constitutive reporter genes yielded similar results (data not shown). However, this new system allows the interaction analysis of two proteins of interest, which can be easily introduced. Furthermore, this system was engineered to optimize the red light system further for the applicability *in vivo* in view of size, tightness and delivery.

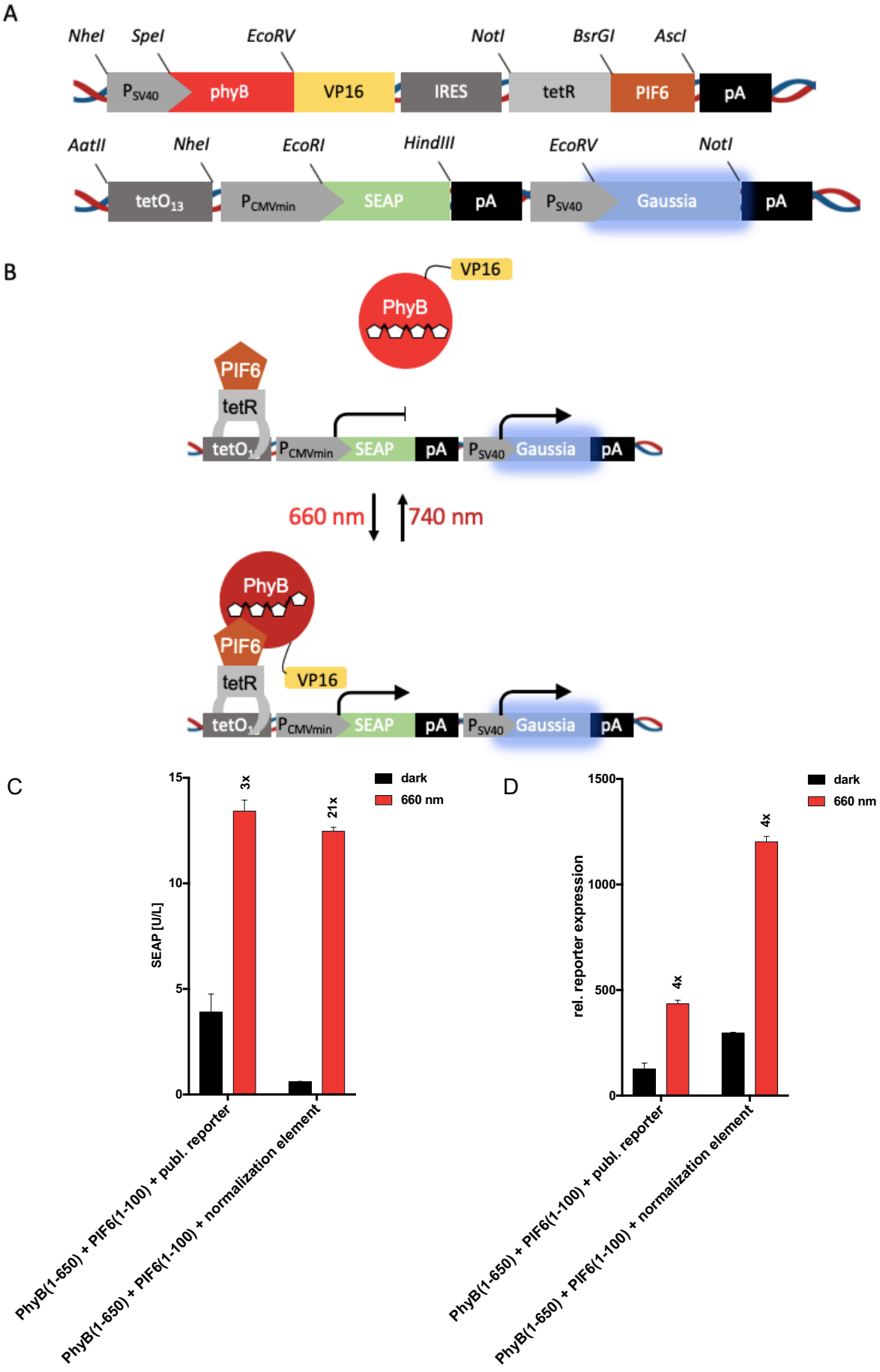
A
NheI
SpeI
EcoRV
NotI
BsrGI
AscI
P SV40
phyB
VP16
IRES
tetR
PIF6
pA
AatII
NheI
EcoRI
HindIII
EcoRV
NotI
tetO 13
P CMVmin
SEAP
pA
P SV40
Gaussia
pA
B
VP16
PhyB
PIF6
tetR
tetO 13
P CMVmin
SEAP
pA
P SV40
Gaussia
pA
660 nm
740 nm
PhyB
PIF6
tetR
VP16
tetO 13
P CMVmin
SEAP
pA
P SV40
Gaussia
pA
C
dark
660 nm
SEAP [U/L]
15
10
5
0
3x
21x
PhyB(1-650) + PIF6(1-100) + publ. reporter
PhyB(1-650) + PIF6(1-100) + normalization element
D
dark
660 nm
rel. reporter expression
1500
1000
500
0
4x
4x
PhyB(1-650) + PIF6(1-100) + publ. reporter
PhyB(1-650) + PIF6(1-100) + normalization element

Fig. 9: Design, optimization and validation of the newly generated red light-inducible split transcription factor system. A) Configuration of the modular red light-inducible split transcription factor system. The PhyB-PIF6 system is encoded on a bicistronic expression vector under the control of the constitutive SV40 promoter. $PhyB^{1-650}$ is C-terminally fused to a VP16 trans activator domain with an NLS sequence. $PIF6^{1-100}$ is N-terminally fused to the tetracycline repressor tetR and separated by an internal ribosome entry site (IRES) for induced translation from one mRNA. Specific restriction recognition sites were inserted as indicated for a fully exchangeable and customizable design. The inducible reporter construct contains thirteen repeats of a tetR specific operator sequence ($tetO_{13}$) in front of a minimal CMV promoter. As readout, the secreted alkaline phosphatase (SEAP) lies downstream of the minimal promoter. In a second ORF, the secreted Gaussia luciferase was under the control of a constitutive SV40 promoter. Similar to the PhyB/PIF6 construct, all parts were inserted with restriction sites for a modular design. **B)** Mode of function. In presence of the chromophore PCB and upon illumination with red light (660 nm), $PhyB^{1-650}$ fused the VP16 changes its conformation and interacts with $PIF6^{1-100}$ which is bound to the DNA via the fused tetR. The resulting close proximity of the VP16 trans activator and the minimal promoter induces recruitment of the transcriptional machinery and therefore expression of the SEAP reporter. Illumination with far-red light (740 nm) triggers dissociation from $PIF6^{1-100}$, thereby resulting in de-activation of the transcription of SEAP. As normalization element the secreted Gaussia luciferase is expressed constitutively in a second ORF (adapted from Müller et al., 2013). **C&D)** Validation of the reporter construct. CHO-K1 cells were transfected with the new generation PhyB system (pPF001) and either the published reporter (pKM006; Müller et al., 2013) together with a plasmid expressing Renilla luciferase consitutively or the new reporter with Gaussia as a normalization element on one construct (pPF034). Transfected cells were illuminated with 20 µmol m^{-2} s^{-1} red light or kept in dark for 24 h. SEAP expression was determined and normalized to the constitutive expression of the luciferase. Black and red bars indicate the mean of the absolute and normalized SEAP expression ± standard error of the mean for n = 4 under dark and red conditions. The numbers above the red bars indicate the induction fold between dark and red light conditions.

3.1.2 Repurposing of light-regulated PhyB/PIF interaction

This chapter is based on the collaborative work with David Golonka (AG Möglich, University of Bayreuth) presented in Golonka et al., 2019 (*accepted*) in Appendix Original studies and protocols 7.1.

Optogenetic approaches to date mostly employ the first 650 amino acids of PhyB containing the PCM and the N-terminal 100 amino acids of PIF3 (PIF3.100) or 6 (PIF6.100) constituting the APB domain (see 1.3.1) (Müller et al., 2013a; Beyer et al., 2015c). Quantitative data on the interaction strength or the underlying sequence determinants are missing. In view of getting deeper knowledge and quantitative data about the interaction of PhyB and PIF for future *in vivo* applications we constructed numerous derivates of the N-term region of PIF1,3 and 6. The aim was to find shorter PIF variants, to save space in the system with a higher dynamic range, decreased leakiness or higher activation of expression in view of *in vivo* applicability. Therefore, interaction studies with different approaches were necessary and hence the

optimization of the PhyB-based system we could easily replace PIF6$^{1-100}$ by truncated PIF variants and analyze their light-dependent interaction with PhyB$^{1-650}$ quantitatively.

A multiple sequence alignment of the APB region of PIF1-8 showed two highly conserved regions, termed A and B. The APB.A region showed stronger conservation and consists of 20 amino acid residues around the core sequence ELXXXXGQ. The APB.B region is shorter and less conserved compared to APB.A (**Fig. 10 A**). Based on the reference PIF3.100, PIF6.100 and additional PIF1.100 various derivates were constructed, starting with a deletion of non-conserved N-terminal residues (Px; x = 1,3 or 6). The interaction of all variants was first analyzed by David Golonka (AG Möglich, Uni Bayreuth) using an interaction assay in bacterial lysate which depends on the stabilization of PhyB due to PIF binding and retardation of the thermal reversion to the Pr form (Smith et al., 2017). Since all of this truncated PIF variants retained interaction we interrogated the linkage between the APB.A and APB.B parts which has a heterogenous length and sequence across PIF1-8. For this reason, constructed variants including i) linkers shortened by 10 residues at their N and C termini (Px.L1 and Px.L2); ii) linker substituted by the corresponding segment of PIF1, the shortest linker among all PIFs (Px.LP1); and iii) a synthetic linker consisting of a repetitive glycine-serine stretch of 10 residues (Px.LS). All these variants still interacted with PhyB$^{1-650}$ in a light-dependent manner implying that the linker is not necessary for this interaction (Golonka et al., 2019; Appendix 7.1). Therefore, Px.fus variants with linked APB.A and APB.B parts were constructed exhibiting still interaction with PhyB in the *in vitro* assay. To check if the interaction depends on a specific topology of the APB parts, Px.BA and Px.BAfus with inverted order and removed linker region were used. Additionally, to probe which APB motif is necessary for the interaction with PhyB we generated only APB.A and only APB.B motif containing constructs with and without the respective half of the linker (Px.A, Px.As, Px.B, Px.Bs) (**Fig. 10 B**). However, the APB.A containing variants showed interaction with PhyB while both APB.B containing variants exhibited no interaction. Duplication of the APB.A motif, Px.AA and Px.AAfus, preserved interactions with PhyB, and *vice versa,* duplication of APB.B, Px.BB and Px.BBfus failed to restore the interaction in the *in vitro* assay (Golonka et al., 2019; Appendix 7.1). For further analysis of the APB.A part, truncations of residues flanking the ELXXXXGQ core sequence were characterized (Px.A19, Px.A14, Px.A8) (**Fig. 10 B**).

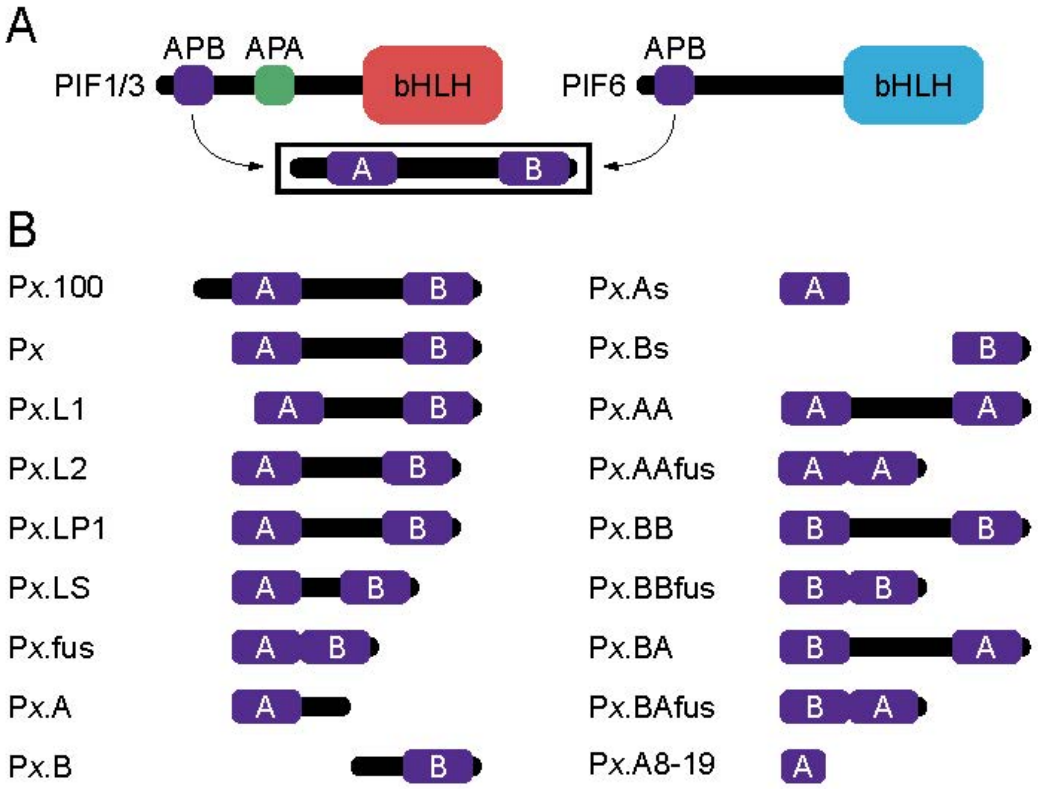

Fig. 10: Structure and composition of PIFs and truncated thereof. A) Modular composition of PIFs. The N-terminal segment with around 100 residues contains the APB domain which is necessary for the interaction with phytochrome B. Additionally PIF1 and 3 contain an APA domain for interaction with phytochrome A. The APB motif can be further subdivided into APB.A and APB.B parts. On the C-terminus all PIFs contain a bHLH DNA binding domain. **B)** Generated PIF variants. Based on the N-terminal APB domain, PIF variants and truncations of PIF1,3 and 6 were generated and tested for light-dependent interaction with the PCM of phytochrome B. Adapted from Golonka *et al*., 2019.

For quantitative analysis, verification of *in vitro* results and optogenetic applicability the described customizable modular red light-inducible system was used (see 3.1.1). In view for *in vivo* applications, the tetR split-transcription factor was replaced by an erythromycin-based system (E-protein and eight repeats of the DNA sequence etr_8) (**Fig. 11 A**). $PIF6^{1-100}$ was easily substituted by the different PIF variants and analyzed for light-depending interaction in CHO-K1 cells regarding the modular system. The reference constructs, P1.100, P3.100 and P6.100 induced normalized SEAP expression by 3-fold, 10-fold and 4-fold upon red light illumination (**Fig. 11 B**). The comparatively lower induction of P1.100 and P6.100 results from the substantial basal SEAP expression level. This suggests a light-independent binding in darkness as regulatory function. After the proof of functionality of the reference constructs, all variants described above and tested in the *in vitro* binding assays, were then characterized in our system. Consistent with the binding assays, PIF variants containing a functional APB.A motif were capable to induce SEAP expression upon red light illumination, even though to

different degrees. Whereas PIF variants with a truncated APB.A motif or only containing the APB.B variant showed no detectable light-dependent induction of SEAP expression, consistent with the *in vitro* measurements (**Fig. 11 B**). For instance, P6.A showed the highest induction among all variants, *ca*. 44-fold, again suggesting a regulatory effect of the linker region. Duplication of the APB.A motif resulted in increased total expression levels in almost all variants, but also a higher basal activity in darkness (**Fig. 11, "P6.A").** For instance, P6.AA showed an almost doubled SEAP expression compared to the variant containing the single APB.A motif but in contrast only an induction of 7-fold compared to the activity in darkness (**Fig. 11, "P6.AA"**). This higher SEAP expression could reflect the binding of two PhyB-VP16 fusion proteins to one Px.AA protein. Although, further studies in size-exclusion chromatography (SEC) analysis done by David Golonka (AG Möglich, Uni Bayreuth) did not show an evidence for simultaneous binding. Interestingly, all variants containing the remaining N-terminal part of the linker region showed decreased or no induction of expression. Maybe, this truncation results in structural changes, such as inadequate folding events of the PIF variants inhibiting the interaction with PhyB. Since some of the PIF variants showed a higher binding affinity or tighter induction of expression, we were curious if the interaction with this variant is still reversible. Therefore, based on Müller et al., 2013, ON-OFF experiments to show reversibility of all variants were performed (Müller et al., 2013a). All generated PIF variants showed reversibility of induced SEAP expression after illumination 24 h with far-red light after the induction with red-light (**Fig. 12**).

A

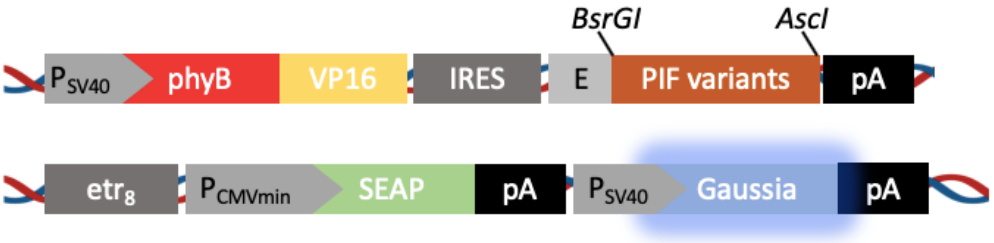
BsrGI
AscI
P SV40
phyB
VP16
IRES
E
PIF variants
pA
etr 8
P CMVmin
SEAP
pA
P SV40
Gaussia
pA

B

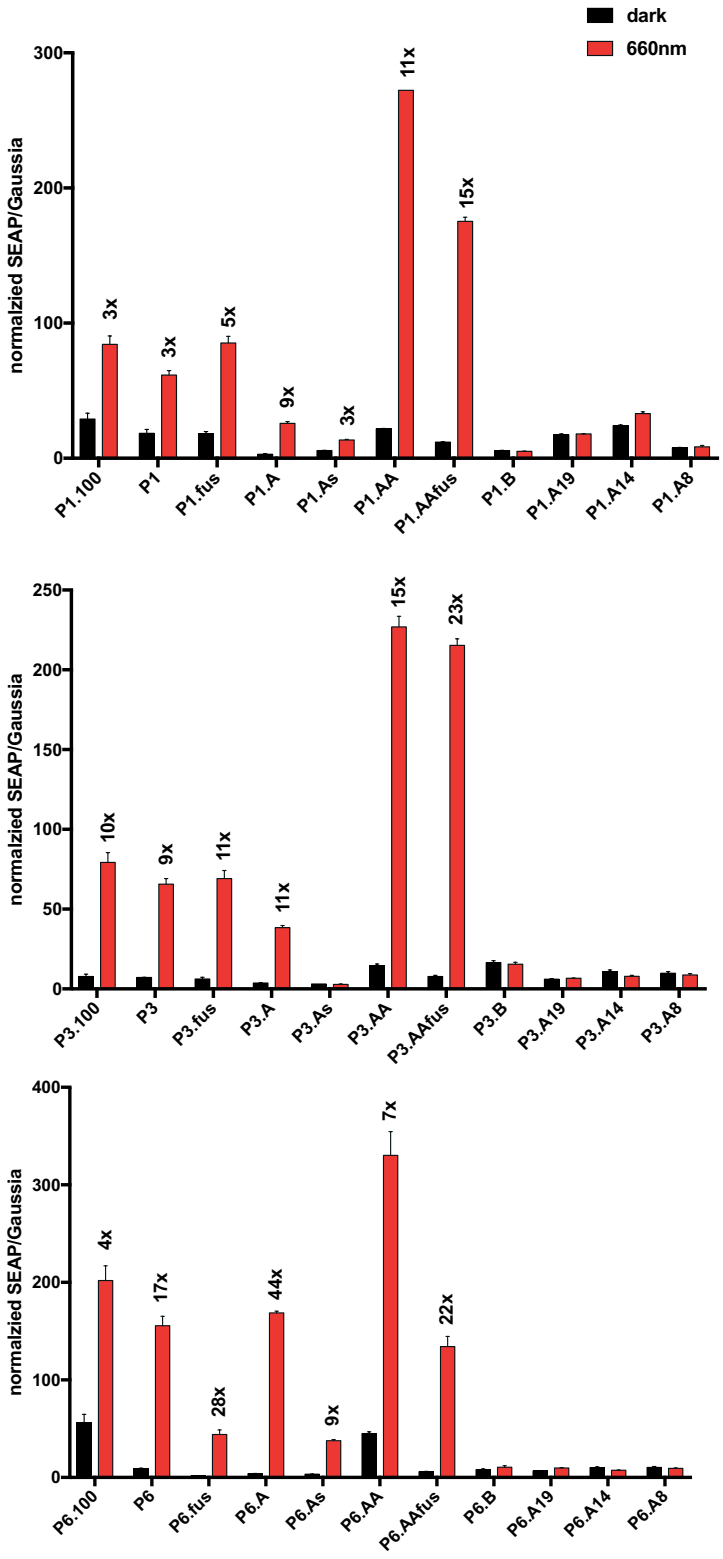
dark
660nm
normalzied SEAP/Gaussia
P1.100
P1
P1.fus
P1.A
P1.As
P1.AA
P1.AAfus
P1.B
P1.A19
P1.A14
P1.A8
P3.100
P3
P3.fus
P3.A
P3.As
P3.AA
P3.AAfus
P3.B
P3.A19
P3.A14
P3.A8
P6.100
P6
P6.fus
P6.A
P6.As
P6.AA
P6.AAfus
P6.B
P6.A19
P6.A14
P6.A8

Fig. 11: Utilizing PIF variants for the light dependent regulation of gene expression in mammalian cells. A) Schematic overview of the used constructs. Due to the customizable new generation red-light inducible split transcription factor construct, tetR and $tetO_{13}$ were easily replaced by the erythromycin derived E-protein and eight repeats of its cognate DNA operator sequence (etr8). Additionally, $PIF6^{1-100}$ was replaced by generated PIF variants to analyze their light dependent interaction with phyB. **B)** Results of the light dependent protein:protein interaction between generated PIF variants and phytochrome B. CHO-K1 cells were transfected with the new generation PhyB system containing the indicated PIF variant (PIF1, 3 or 6) and the new reporter construct with Gaussia as a normalization element (pPF034). Transfected cells were illuminated with 20 µmol m^{-2} s^{-1} red-light or kept in the dark for 24 h. SEAP expression was determined and normalized to the constitutive expression of the Gaussia luciferase. Black and red bars indicate the mean of the normalized SEAP expression ± standard error of the mean for n = 4 under dark and red-light conditions. The numbers above the red bars indicate the induction fold between dark and red-light conditions. Adapted from Golonka *et al.,* 2019.

In conclusion, we were able to acquire insights into the light-regulated protein:protein interaction between PhyB and PIFs, which underpin diverse adaptive responses in *planta* and various applications in optogenetics, including *in vivo* use. We implemented several approaches, such as interaction assay in bacterial lysate (David Golonka), SEC (David Golonka) and the described above reporter assays in mammalian cells (Golonka et al., 2019, Appendix 7.1), which result in qualitative and quantitative validation of this protein:protein interaction. Our results indicate a regulatory effect of the linker region inside of the APB domain and therefore a probably important regulatory basal binding of PIF6 to PhyB in darkness. However, temperature changes have an influence on the protein:protein interaction and may hence lead to unexpected PhyB Pfr-form binding (Legris et al., 2016; Smith et al., 2017).
In summary and in view of the optogenetic applicability, we have constructed and characterized a toolkit of novel PIF variants interacting with PhyB in a light-dependent manner with varying strength. The knowledge about the interaction strength can be important by choosing the right system for an application. We consider having a set of PIFs with known interaction strengths and varying properties is an advantage for the optogenetic toolbox and the red light-inducible split transcription factor system. Especially the variant P6.A with only 25 amino acids in length and a reduced basal activity, shows the advantages we wanted for further *in vivo* application and a further optimization of the red light system. Furthermore, we demonstrated the red light split transcription factor system as a platform for quantitative interaction studies in an orthogonal mammalian cell-based platform.

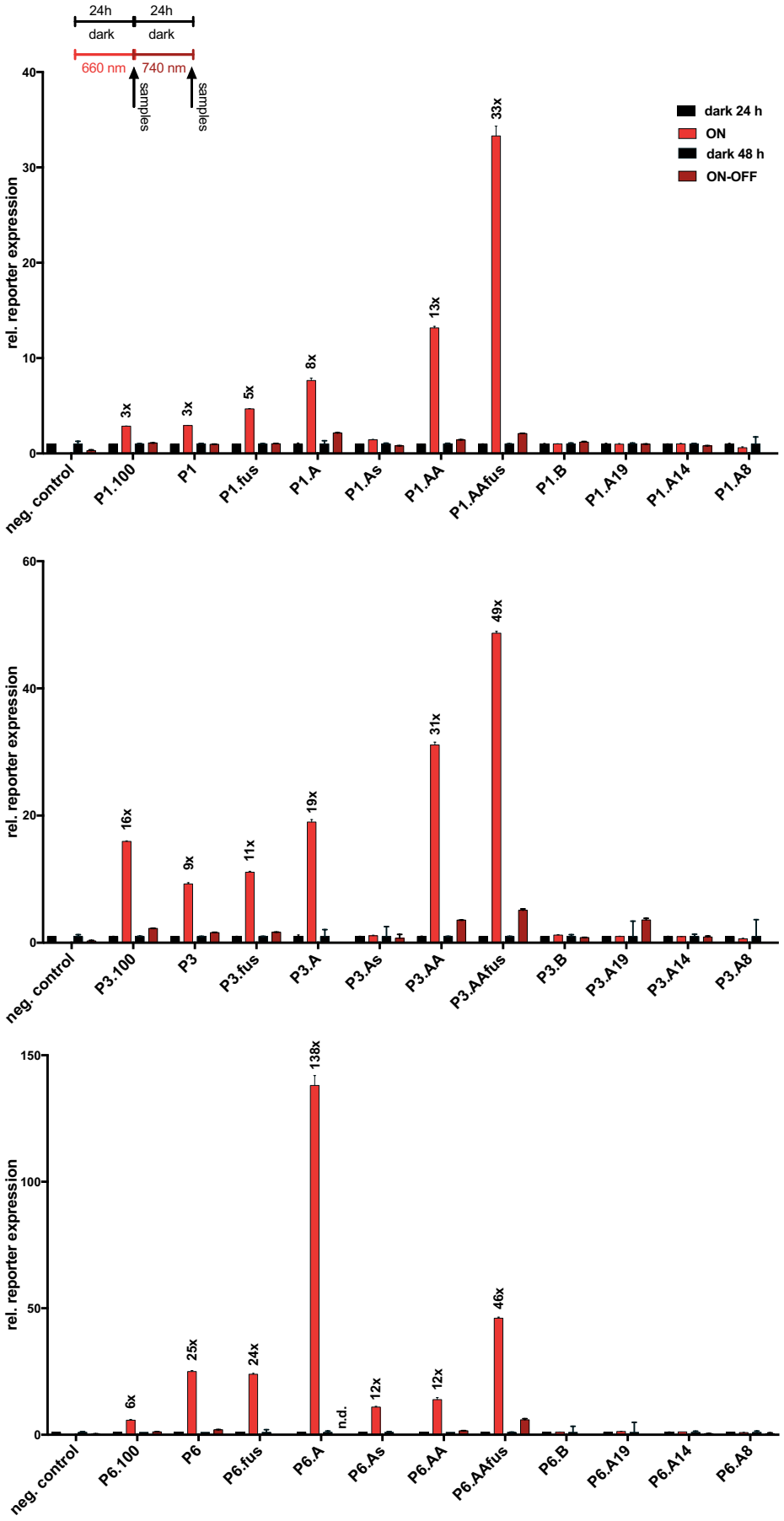
24h
dark
24h
dark
660 nm
740 nm
samples
samples
dark 24 h
ON
dark 48 h
ON-OFF
rel. reporter expression
neg. control
P1.100
P1
P1.fus
P1.A
P1.As
P1.AA
P1.AAfus
P1.B
P1.A19
P1.A14
P1.A8
3x
3x
5x
8x
13x
33x
P3.100
P3
P3.fus
P3.A
P3.As
P3.AA
P3.AAfus
P3.B
P3.A19
P3.A14
P3.A8
16x
9x
11x
19x
31x
49x
P6.100
P6
P6.fus
P6.A
P6.As
P6.AA
P6.AAfus
P6.B
P6.A19
P6.A14
P6.A8
6x
25x
24x
138x
n.d.
12x
12x
46x

Fig. 12: Reversibility of the protein:protein interaction of the PIF variants. Results of the ON-OFF protein:protein interaction between generated PIF variants and phytochrome B. CHO-K1 cells were transfected with the new generation PhyB system containing the indicated PIF variant (PIF1, 3 or 6) and the new reporter construct with Gaussia as a normalization element (pPF034). Transfected cells were illuminated with 20 µmol m^{-2} s^{-1} red-light or kept in the dark for 24 h. After sample preparation transfected cells were either kept in the dark or illuminated with 20 µmol m^{-2} s^{-1} far-red light for further 24 h. SEAP expression was determined and normalized to the constitutive expression of the Gaussia luciferase and is shown relatively to the basal expression level of the associated dark sample. Black, red and dark-red bars indicate the mean of the normalized SEAP expression ± standard error of the mean for n = 4 under dark, red- and far-red-light conditions. The numbers above the red bars indicate the induction fold change between dark and red-light conditions. Adapted from Golonka *et al*., 2019.

3.1.3 A novel PhyA-based red light-inducible split transcription factor system

This chapter is based on the collaborative work with the workgroup of Andreas Hiltbrunner (University of Freiburg) and David Golonka and Andreas Möglich (University of Bayreuth) presented in Fischbach et al., 2019b (*in preparation*) in Appendix Original studies and protocols 7.1.

3.1.3.1 Integration of red light signaling of phytochrome A and B into other pathways via direct physical interaction

As described in chapter 1.3, phytochromes are integrated in a variety of signaling pathways, such as phytohormone regulatory networks or the circadian clock (Casal, 2013; Sanchez and Yanovsky, 2013; Lee and Choi, 2017; Yang and Li, 2017). Even though a set of interactions with phytochromes were already demonstrated, showing integration in such pathways, an analysis in plants is particularly difficult because of genetic redundancy, influence of endogenous proteins and crosstalk events. Therefore, we decided to analyze the interaction of potential interactors, involved in several regulatory networks, with phytochrome A and B using the red light-inducible split transcription factor system in mammalian cells as an orthogonal platform. Compared to other interactions assays the mammalian-based platform benefits from i) relatively low costs, ii) highly quantitative results and iii) an *in vivo* comparable situation. By using the red light inducible split transcription factor system in mammalian cells, we get quantitative relevant information about the interaction of plant proteins in a minimal system without co-factors or other disturbing proteins. With these results we are able to reconstruct signaling pathways quantitatively in small pieces. Furthermore, we targeted the discovery of new light-dependent interactions for optogenetical applications to extend the optogenetic toolbox, since the PhyB-based system is the only red light-dependent toggle switch used in various organisms so far.

Towards these aims we generated a set of constructs containing a potential phytochrome interactor by replacing $PIF6^{1-100}$. Additionally, to check potential integration of PhyA into other

plant pathways, we replaced in the construct PhyB$^{1-650}$ with the PhyA or PhyB full-length gene. To demonstrate the functionality of the system as a screening platform we analyzed first the light-dependent interaction of full-length PIF1, 3-6 and 8 with PhyB. For PhyA we investigated the interaction with PIF1 and PIF3, since this PIFs are the only ones containing an APA domain for interaction with PhyA (Lee and Choi, 2017). As controls we transfected CHO-K1 cells either with the canonical optimized system with PhyB$^{1-650}$ and PIF6$^{1-100}$ or the reporter construct alone. The results of one representative experiment are shown in **Fig. 13 A**. As expected, PIF1 and PIF3 caused a light-dependent induction of SEAP expression via interaction with PhyA, albeit the induction of PIF1 suffered from the high basal expression level in darkness (**Fig. 13 B**). Similar results could be obtained with PhyB, while it, in addition, displayed an induction of SEAP expression of different strengths with PIF4,6 and 8 (**Fig. 13 C**). The high basal activity of PhyB and PIF1 resulting from a regulatory effect of the linker region was already observed and discussed in chapter 3.1.2. Interestingly, the interaction with PhyA demonstrated the same basal activity, suggesting a similar regulatory structure in the containing APA domain. In summary, we demonstrated that the system works as a screening platform for potential interactors of phytochromes. However, the lacking physical interaction between PhyB and PIF5 could be a result of a structural inhibition provided by the N-terminally fused tetracycline repressor, because the light-dependent interaction was already shown (Shen et al., 2007) (**Fig. 13 C**). Another possibility is the existence of an indirect interaction with PhyB over another PIF protein, because PIF5 is part of the PIF-quartet multiprotein complex consisting PIF1,3,4 and 5 (Leivar and Quail, 2011; Iglesias et al., 2018). For future perspectives, the change of the fusion order and the co-expression of potential interactors of PhyB and PIF5, functional as adapter proteins, could lead to the expected induction of expression with PIF5 and result in better knowledge about the interaction composition of the PIF-quartet.

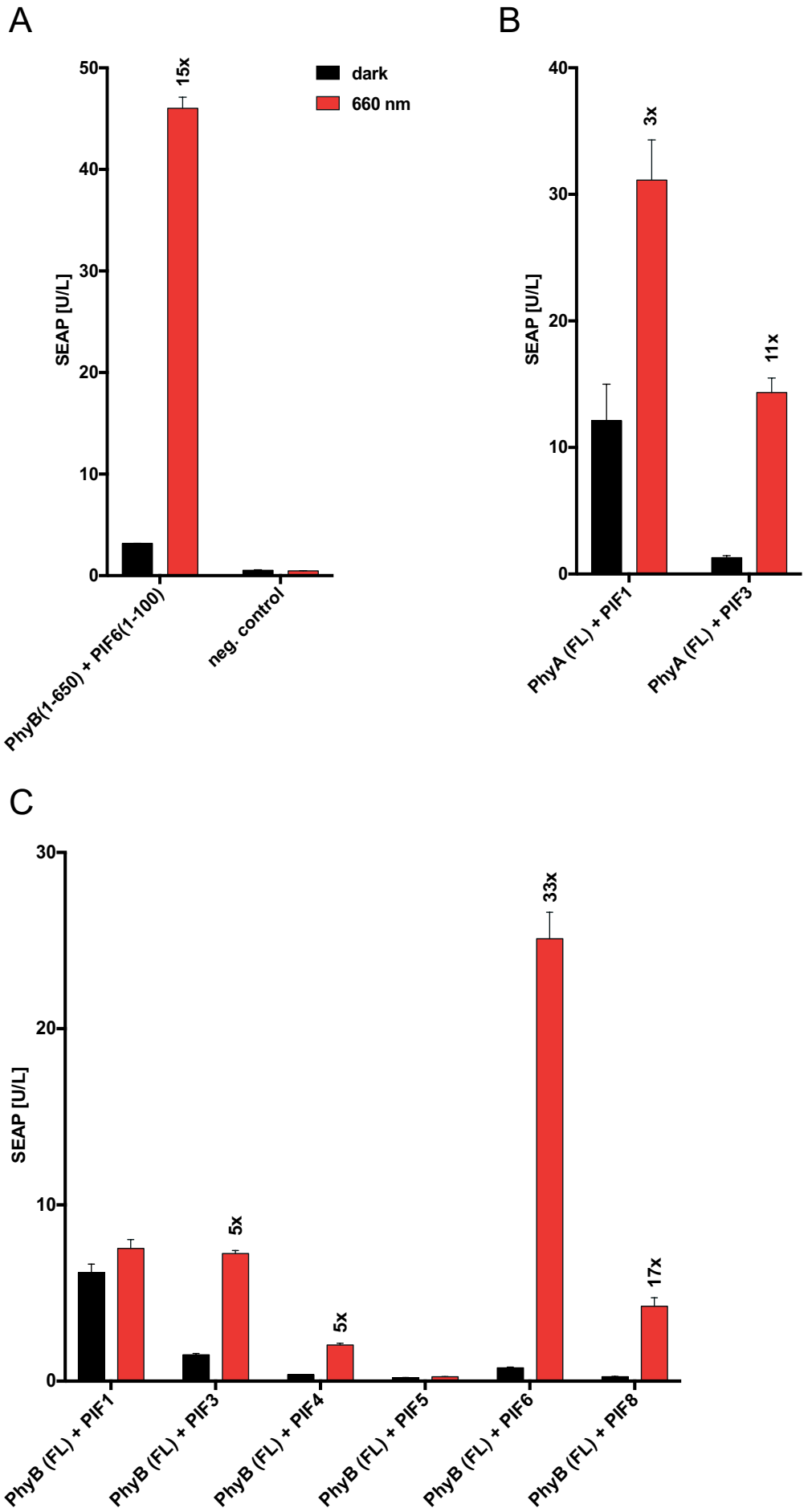
A
B
C
dark
660 nm
SEAP [U/L]
15x
3x
11x
5x
5x
33x
17x
PhyB(1-650) + PIF6(1-100)
neg. control
PhyA (FL) + PIF1
PhyA (FL) + PIF3
PhyB (FL) + PIF1
PhyB (FL) + PIF3
PhyB (FL) + PIF4
PhyB (FL) + PIF5
PhyB (FL) + PIF6
PhyB (FL) + PIF8

Fig. 13: Functionality of the system as a screening platform and interaction of phytochromes with PIFs. A) Representative result of the red light-inducible split transcription factor system controls for all following red-light system-based experiments. **B)** + **C)** Light-dependent interaction analysis of PIFs and phytochrome A and B. For **A – C:** CHO-K1 cells were transfected, kept 24 h in dark and afterwards supplemented with 15 µM PCB and either illuminated 24h with 20 µmol m^{-2} s^{-1} red-light or kept In the dark. SEAP expression was determined. Black and red bars indicate the mean of SEAP expression ± standard error of the mean for n = 4 under dark and red conditions. The numbers above the red bars indicate the induction fold between dark and red-light conditions.

Next, we tested proteins of the ethylene response family for their interaction with PhyA. While an integration of PhyB into the ethylene response pathway via PIFs was already shown (Jeong et al., 2016), knowledge about an integration of PhyA and an interaction with family members such as ERFs is missing. Similar to the experimental setup before, we exchanged $PIF6^{1-100}$ in the construct by ERF6 and 55-60, and analyzed the light-dependent interaction in CHO-K1 cells. Representative control data for the following screening results are demonstrated in **Fig. 13 A**. A light-dependent induction of SEAP expression of 5-fold was detectable for ERF058 (**Fig. 14**). Additionally, ERF056 showed a slight induction of expression, albeit the total expression level was low. All other tested ERFs showed no or a slight induction of SEAP expression suggesting no physical interaction or a light-independent interaction with PhyA, indicating that further analysis of these interactions is needed, starting with changing the protein fusion order (**Fig. 14**). With these results, we demonstrated for the first time an integration of light-labile PhyA into the ethylene response pathway. It has been shown that ERF058 is involved in transcriptional regulation of chloroplast peroxidases needed for the enzymatic inactivation of hydrogen peroxide generated during photosynthesis (Rudnik et al., 2017). This indicates a parallel light-dependent regulation of peroxidases during photosynthesis via PhyA.

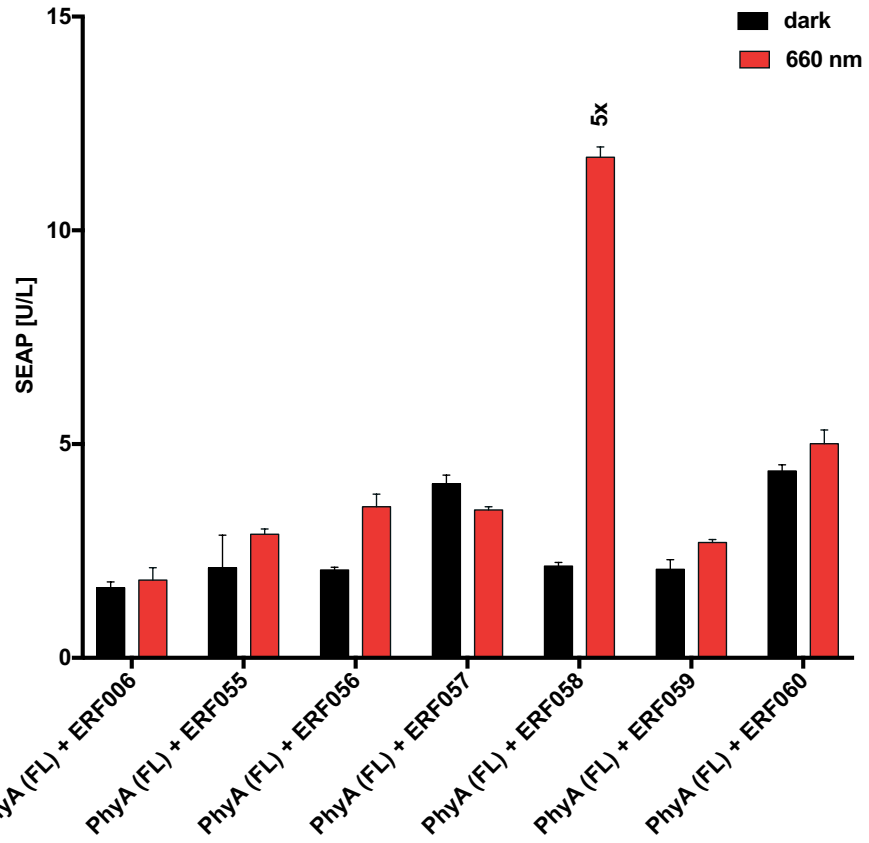

Fig. 14: Integration of phytochrome A into the ethylene response pathway. Light-dependent interaction analysis of ERF family members and PhyA. CHO-K1 cells were transfected, kept 24 h in dark and afterwards supplemented with 15 µM PCB and either illuminated 24h with 20 µmol m^{-2} s^{-1} red-light or kept in dark. SEAP expression was determined. Black and red bars indicate the mean of SEAP expression ± standard error of the mean for n = 4 under dark and red conditions. The numbers above the red bars indicate the induction fold between dark and red-light conditions.

The influence and integration of PhyA and PhyB into the jasmonic acid signaling pathway was already indicated by several observations, for instance changes in transcriptional JA expression patterns in triple *phya cry1 cry2* mutants or the interference of JAZs with the DELLA-PIF complex regulated by PhyB (Yang et al., 2012; Rossi et al., 2017; Cagnola et al., 2018). However, a direct influence and physical interaction of PhyA or PhyB and JAZ proteins is still unknown. Studies of this integration of light into hormone signaling pathways in plants are particularly difficult, because of co-factors or interfering proteins also involved in such pathways. To overcome this limitation and to get better knowledge about the integration of light signaling we aimed to analyze those direct interactions in our developed red light-inducible split transcription factor system in CHO-K1 cells. Surprisingly, only PhyA showed a light-dependent interaction with JAZ5 and 6 in our experiments, notwithstanding with different strength (**Fig. 15 A**). This indicates a light regulation of downstream targets via JAZ5 and 6 and underlines the observed changes in expression patterns in the *A. thaliana* triple mutant after illumination (Rossi et al., 2017; Cagnola et al., 2018). In addition, our results suggest an

indirect regulatory role of PhyB which demonstrates no direct interaction with JAZ proteins in our studies, over the DELLA-PIF complex (Yang et al., 2012; Campos et al., 2016) (**Fig. 15 B**). Furthermore, the undetectable induction of SEAP expression could be a result of stereochemical interference resulting from the N-terminal fusion of the tetR protein or the possibility that PhyA and PhyB are able to interact with specific splicing variants of JAZ proteins (Chini et al., 2016). In future experiments the fusion order can be changed and different JAZ splicing variants can be tested easy in this quantitative interaction system. In summary, we have the first results supporting the hypothesis of direct integration of PhyA signaling into the jasmonic acid signaling pathway. Furthermore, we could show that PhyB is not directly interacting with JAZ proteins under the same conditions.

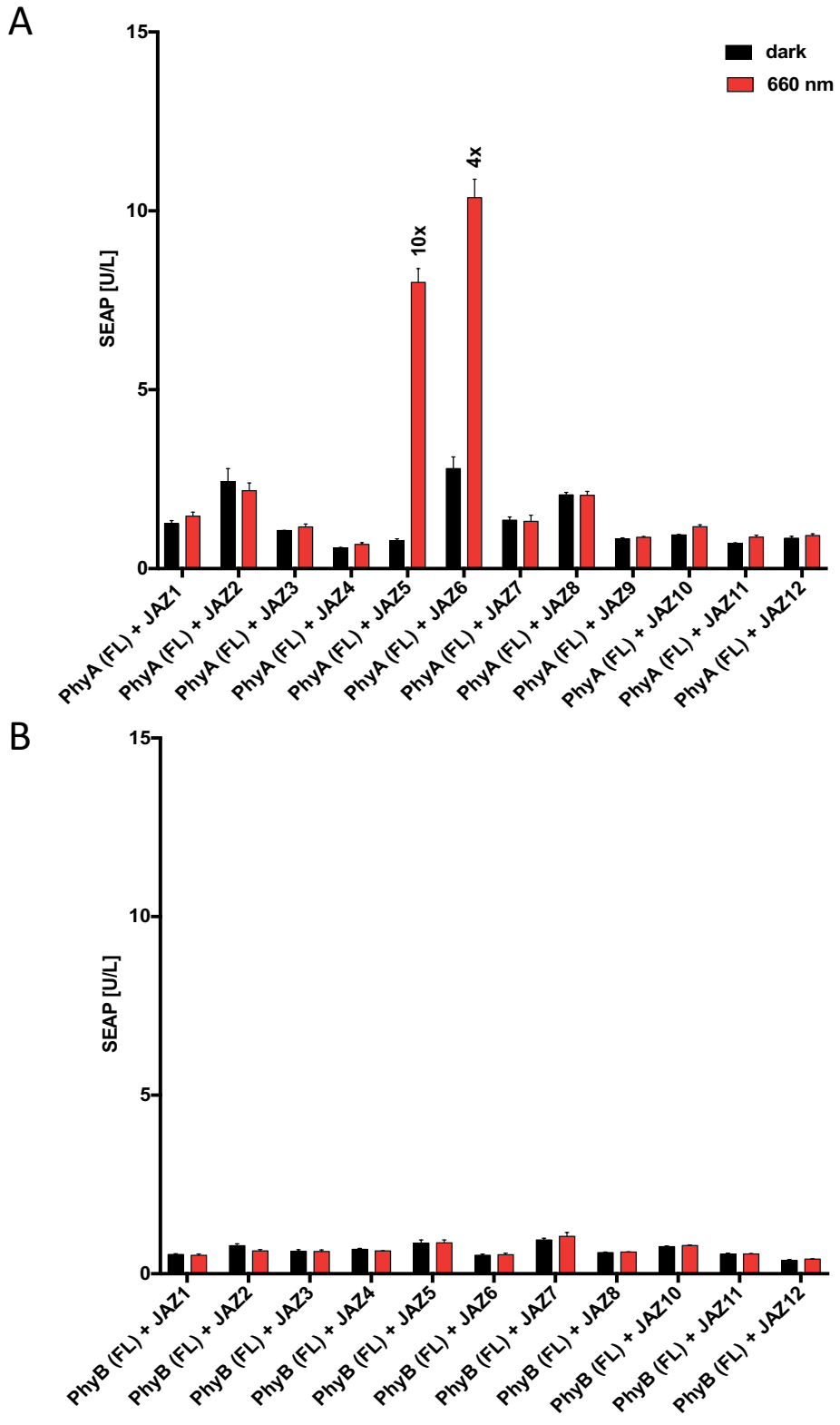

Fig. 15: Integration of phytochrome A & B into the jasmonate pathway. A) Light-dependent interaction analysis of JAZ family members and PhyA. **B)** Light-dependent interaction analysis of JAZ family members and PhyB. For **A + B**: CHO-K1 cells were transfected, kept 24 h in dark and afterwards supplemented with 15 µM PCB and either illuminated 24h with 20 µmol m^{-2} s^{-1} red-light or kept in dark. SEAP expression was determined. Black and red bars indicate the mean of SEAP expression ± standard error of the mean for n = 4 under dark and red conditions. The numbers above the red bars indicate the induction fold between dark and red-light conditions.

Besides the main hormone signaling pathways, we were also interested in the integration of PhyA and PhyB into *A. thaliana* cold response or the circadian clock. Additionally, potential interactors with partially unknown function, found in a yeast-two-hybrid screen (data not shown; workgroup A. Hiltbrunner), were analyzed for their light-dependent interaction with PhyA and PhyB in our red light system in CHO-K1 cells. First, we examined the interaction of PhyA with several proteins of the mentioned pathways. As expected, PhyA together with FHL and FHY1 demonstrated a high induction of 11-fold or 3-fold of SEAP expression in our system (**Fig. 16 A**). Since both proteins are necessary for the light-dependent nuclear transport of PhyA and the physical interaction was already shown, these quantitative results demonstrate the functionality of the system (Zhou et al., 2005; Genoud et al., 2008). Proteins involved in nuclear body formation such as PCH1 and PCHL showed also a light-dependent induction of reporter expression with PhyA by 12-or 6-fold, but a light-independent induction with PhyB (**Fig. 16 A & B**). While the interaction and stabilization of PhyB with PCH1 and PCHL is already known (Huang et al., 2016; Enderle et al., 2017), a light-dependent interaction of both proteins with PhyA suggested by our results is new. An explanation could be the integration of red light signaling into UV-B light signaling via COP1. Because phosphorylated PhyA can interact with the COP1/SPA complex which is an important complex in the UV-B signaling (Lu et al., 2015; Sheerin et al., 2015; Martínez et al., 2018). Furthermore, COP1 is able to interact with PCH1, showing the integration of PhyB into the UV-B light signaling (Favory et al., 2009). Taken together it is possible that the interaction of PhyA and PCH1 is an additional integration and regulation of the UV-B light signaling via red light. Additionally, it could be possible that this interaction between PhyA and PCH1 is an integration into the blue light signaling via cryptochromes, because Cry1 interacts with COP1 and SPA in a light dependent manner (X et al., 2017). This could be an indirect competitive light regulation of COP1 between red and blue light. Based on this, the observed missing induction of expression of PhyA and COP1 or SPA1 indicated in **Fig. 16 A**, suggests a missing third component in regulation of this proteins, such as PCH1. Additionally, in future experiments the stereochemical inhibition of COP1 and SPA1 proteins by the N-terminal fusion of tetR has to been proven, since the interaction was already reported in other systems (Seo et al., 2004; Sheerin et al., 2015).

Quite high inductions were obtained in the cells transfected with constructs containing PhyA and COR27 or COR28 upon illumination with red light (**Fig. 16 A**). Similar results could be observed for the interaction of COR28 and PhyB, while COR27 indicated a light-independent activation of the reporter system (**Fig. 16 B**). These results imply a novel integration of light into temperature signaling over COR27 and COR28, whose biological function is still unknown but transcriptional changes by light and temperature were reported (Li et al., 2016b). Since COR27 and 28 are involved also in the circadian clock, we investigated the interaction of PhyB with various proteins involved in the circadian clock mechanism (Chow et al., 2014). It has

been reported that PhyB is influencing the circadian clock direct over ELF3 and indirect over PIF3 (Martínez-García et al., 2000; Leivar and Quail, 2011; Li et al., 2016b). Therefore, we analyzed the light-dependent interaction of PhyB and circadian clock proteins, for instance TOC1, CCA1 and LHY1 which showed no induction in our system (**Fig. 16 B**). Since PhyB, as mentioned before, is regulating some circadian clock processes indirectly via PIF3, we co-expressed PIF3 in the same experimental setup. This co-expression led to a light-dependent induction of expression with all tested circadian clock proteins (**Fig. 16 C**). Our results show a novel quantitative analysis of indirect interaction via an adapter protein, such as PIF3 and additionally suggest an indirect regulation of TOC1, CCA1 and LHY1 via PhyB.

NOT9 is part of the CCR4/NOT1 complex and important for post-transcriptional modifications such as the poly-A tail of mRNA (Tucker et al., 2002). An integration of light into the CCR4/NOT1 complex has been completely unknown until now. However, our results demonstrated a light-dependent induction of expression with NOT9b, which is predicted to interact directly with NOT1 (Arae et al., 2019). Interestingly, although NOT9a-c have similar structures and conserved amino acid regions, only NOT9b showed this light-dependent interaction with PhyA compared to the other tested NOT9 proteins (**Fig. 16 A**).

Finally, we used our system to analyze the protein:protein interaction between PhyA and B and a hypothetical protein (AT1G48770), termed in this work OPA (ONLY with PHYTOCHROME A). **Fig. 16 A** displays the red light induction of SEAP expression for PhyA and OPA with a high dynamic range of 17-fold. Among all tested proteins OPA and COR28 showed the highest measured dynamic range but COR28 suffered from substantial basal expression in darkness (**Fig. 16 A**). In contrast, PhyB showed no induction of expression with OPA at all, suggesting a phytochrome A-only binding motif (**Fig. 16 A & B**). Further experiments and characterization of this interaction are following in the next chapter of this work.

In summary, we were able to show that PhyA and PhyB directly interact in different strengths, light-dependent or light-independently, with proteins involved in hormone signaling such as ethylene and jasmonate signaling, the circadian clock or cold response. This provides not only new knowledge about the integration of light signaling into other signaling pathways in plants, it also shows the applicability of the red light split transcription factor system as a quantitative, orthogonal screening platform for plant protein:protein interactions. In future experiments, further analysis of these interactions is needed to i) verify the interaction with other methods, ii) analyze the interaction in the changed fusion order (C-terminal) and iii) check for indirect regulation by third component adapter proteins such as PIF3.

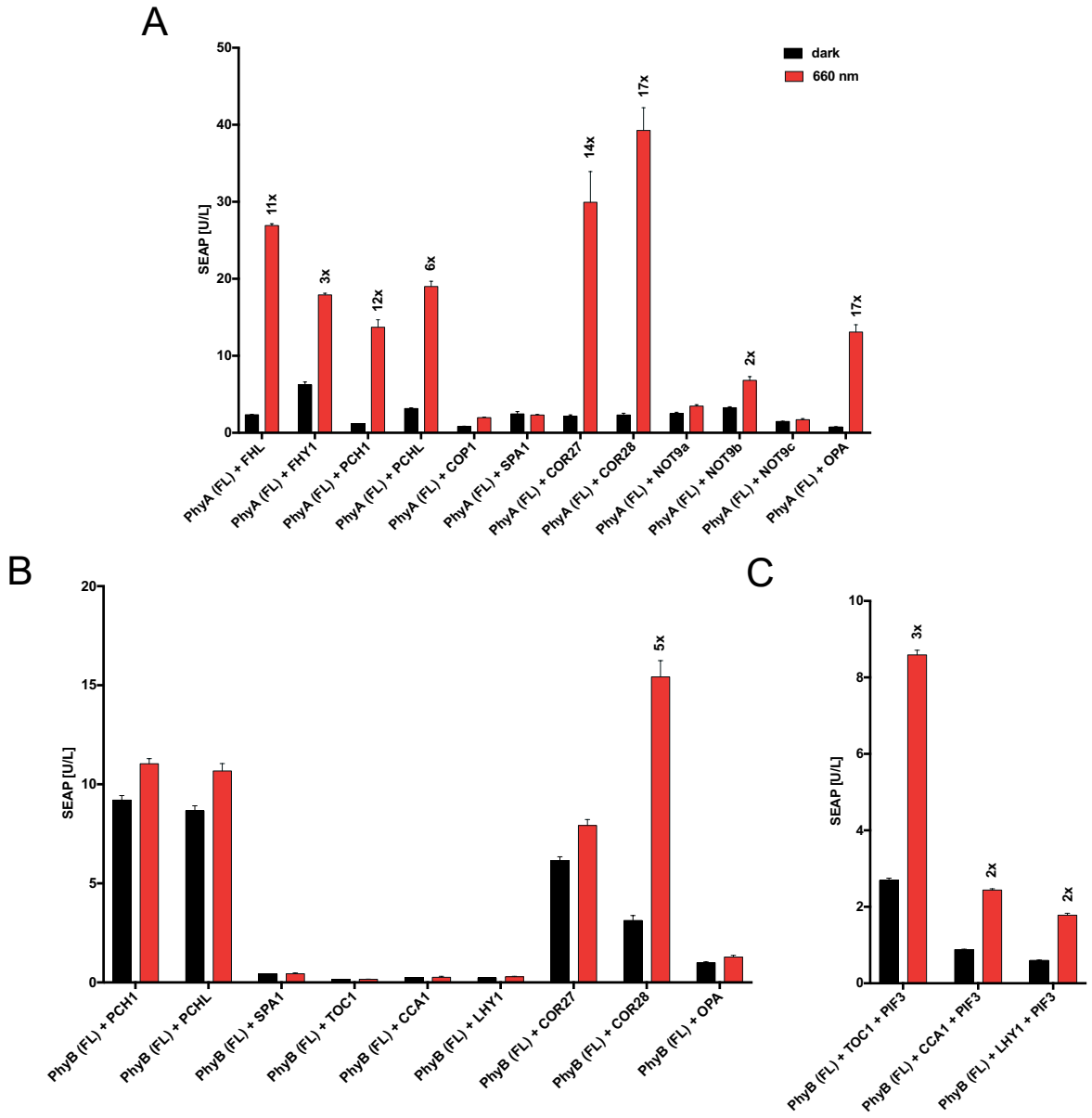

Fig. 16: Integration of phytochrome A & B into cold response and circadian clock of *A. thaliana*. A) Light-dependent interaction analysis of cold response proteins, known PhyA transporter and proteins of unknown function with PhyA. **B)** Light-dependent interaction analysis of circadian clock and cold response proteins with phyB. **C)** Analysis of light and PIF3-dependent interaction of circadian clock proteins with PhyB. For **A - C**: CHO-K1 cells were transfected, kept 24 h in dark and afterwards supplemented with 15 µM PCB and either illuminated 24h with 20 µmol m^{-2} s^{-1} red-light or kept in dark. SEAP expression was determined. Black and red bars indicate the mean of SEAP expression ± standard error of the mean for n = 4 under dark and red conditions. The numbers above the red bars indicate the induction fold between dark and red-light conditions.

3.1.3.2 Characterization of the light-dependent PhyA:OPA interaction and establishment of a novel red light split transcription factor system

As described above we found a novel red light-dependent PhyA:protein interaction, namely PhyA:OPA, during our screening of potential interactors in mammalian cells. This interaction showed a particularly interesting orthogonality to PhyB (**Fig. 17 A**). Therefore, we aimed to analyze this interaction further and to develop a novel red light-inducible system orthogonal to the PhyB based system for possible simultaneous applications. Towards this aim, we constructed similar to the PhyB system, truncations of PhyA and OPA to optimize the size of the system for possible applications in *in vivo* situations and to get better knowledge about their protein interaction domain. For this purpose, PhyA was shortened to 617 amino acids, including the PAS-GAF-PHY domain, and the interaction was analyzed in CHO-K1 cells, which resulted in a loss of SEAP expression (**Fig. 17 B**). OPA was separated into two parts of 90 amino acids (N-term and C-term) with the C-terminal part containing a domain of unknown function (DUF1639). Surprisingly, the N-terminal part without the predicted DUF domain still interacts with PhyA (**Fig. 17 B**). Based on these results, the truncated version of OPA^{1-90} was used for further characterization. Following, we characterized the interaction further by kinetics and dose response experiments (**Fig. 17 C** and Fischbach et al., 2019b Appendix 7.1). The results were comparable with the ones published for the PhyB system (Müller et al., 2013a).

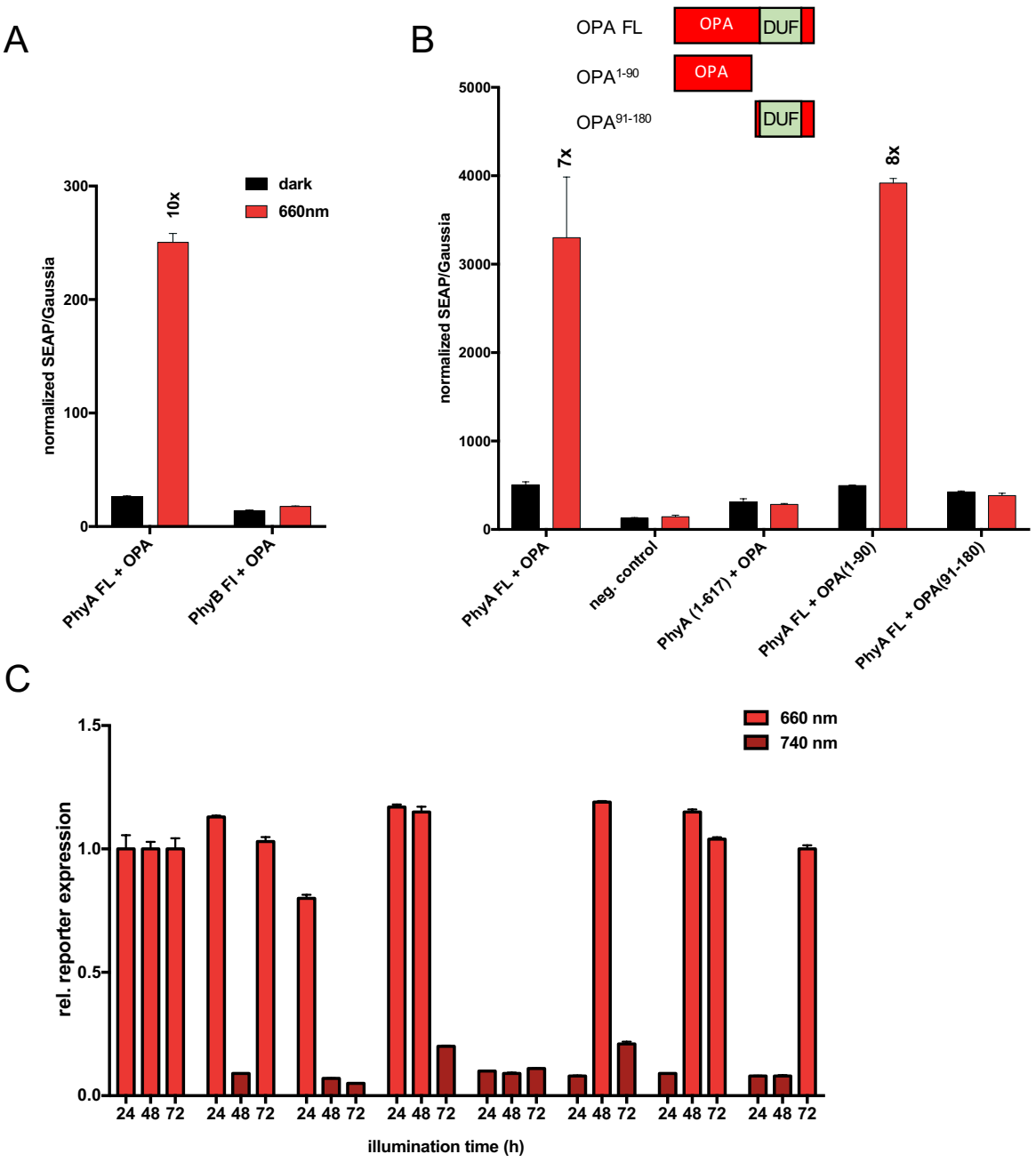
A
dark
660nm
10x
normalized SEAP/Gaussia
300
200
100
0
PhyA FL + OPA
PhyB Fl + OPA
B
OPA FL
OPA
DUF
OPA1-90
OPA
OPA91-180
DUF
5000
4000
3000
2000
1000
0
normalized SEAP/Gaussia
7x
8x
PhyA FL + OPA
neg. control
PhyA (1-617) + OPA
PhyA FL + OPA(1-90)
PhyA FL + OPA(91-180)
C
660 nm
740 nm
1.5
1.0
0.5
0.0
rel. reporter expression
24 48 72
illumination time (h)

Fig. 17: Characterization and engineering of the light-dependent phytochrome A:OPA interaction. A) Analysis of the orthogonality of the system. **B)** Scheme and analysis of OPA truncations and PhyA truncation. PhyA was truncated similar to the PhyB in the published red-light system directly after the PHY domain ($PhyA^{1-617}$) (Müller et al., 2013). OPA has a C-terminal predicted domain of unknown function (amino acids 125 – 176) (DUF1679). To analyze the necessity of this domain for a light dependent interaction with PhyA, OPA was cut into two parts (OPA^{1-90} and OPA^{91-180}). For **A & B:** CHO-K1 cells were transfected with plasmids coding for indicated genes, kept 24 h in darkness and afterwards supplemented with 15 µM PCB and either illuminated 24h with 20 µmol m^{-2} s^{-1} red-light or kept in dark. SEAP expression was determined and normalized with constitutive expressed Gaussia luciferase. Black and red bars indicate the mean of normalized SEAP expression ± standard error of the mean for n = 4 under dark and red conditions. The numbers above the red bars indicate the induction fold between dark and red-light conditions. **C)** Reversibility of the system. Cells were transfected with an inducible SEAP reporter plasmid with an additional Gaussia normalization element (pPF034) and a PhyA and OPA^{1-90} containing plasmid (pPF086). Transfected CHO-K1 cells were supplemented every 24 h with fresh medium containing 15 µM PCB and illuminated with indicated wavelengths with an intensity of 20 µmol m^{-2} s^{-1}. Expression of SEAP was determined every 24 h. SEAP values were normalized by values from constantly red-light illuminated cells, to correct changes in gene expression depending on growth over time. Red and dark-red bars indicate the mean of normalized SEAP expression ± standard error of the mean for n = 4 under red and far-red conditions

To define the binding affinity of OPA to PhyA we combined different approaches to characterize the interaction further. Therefore, we analyzed the interaction in a fluorescence anisotropy assay (described in Golonka *et al*., 2019, Appendix 7.1), where OPA showed a lower binding affinity to PhyA than PIF6 to PhyB (K_D= PhyA:OPA > PhyB:PIF6) (**Fig. 18 A**). Since the lower binding affinity could result in a faster dissociation of the interaction of PhyA and OPA, we performed light pulsing experiments in CHO-K1 cells. Therefore, transfected cells were illuminated for 30 s, 2 min, 30 min or 24 h with 2 µmol m^{-2} s^{-1} of red light and then incubated 24 h in darkness to analyze the following expression patterns. Since we saw differences in basal levels of expression when using lower reporter concentrations (data not shown), we did the experiments additionally with lower concentrations of the reporter construct (1:10). As expected, shorter illumination time results in lower SEAP expression (**Fig. 18 B**). Surprisingly, the system demonstrated when co-transfecting with lower reporter concentrations no response to short pulses of red light and therefore no expression of SEAP. Only continuous illumination resulted in 436-fold induction of SEAP expression (**Fig. 18 B**). This result indicated that both red light-inducible systems can be combined and independently regulated via different reporter concentrations and illumination periods and intensities. For future perspectives the independent regulation of expression and translocation (translocation as described in Golonka *et al*., 2019, Appendix 7.1) via one wavelength to activate a cellular pathway would be an interesting analysis in mammalian cells. With this approach one could reduce auto-activity of light regulated expression of proteins and therefore leakiness by adding an additional checkpoint. Furthermore, one could use this system to regulate the expression

of auto-active proteins before translocating them to their destination point independently with both orthogonal red light systems to avoid leakiness.

A

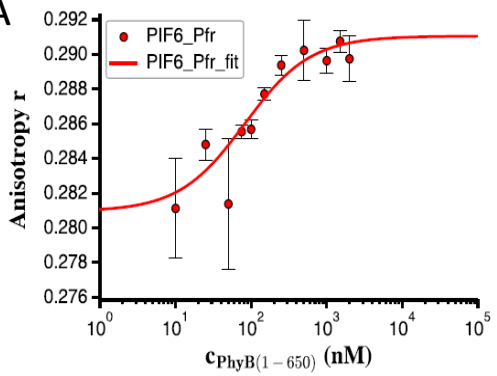

PhyB$^{1\text{-}650}$ + PIF6$^{1\text{-}100}$

$K_{D,650nm}$ = 82 nM

Error = 32 nM

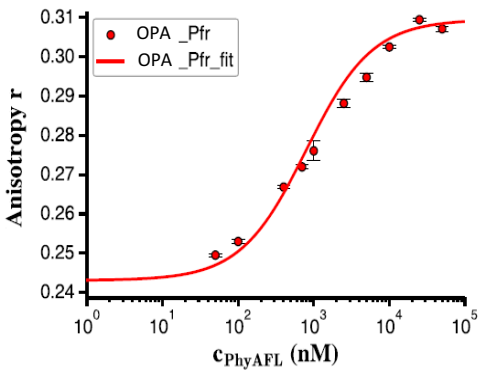

PhyA FL + OPA

$K_{D,650nm}$ = 797 nM

Error = 123 nM

B

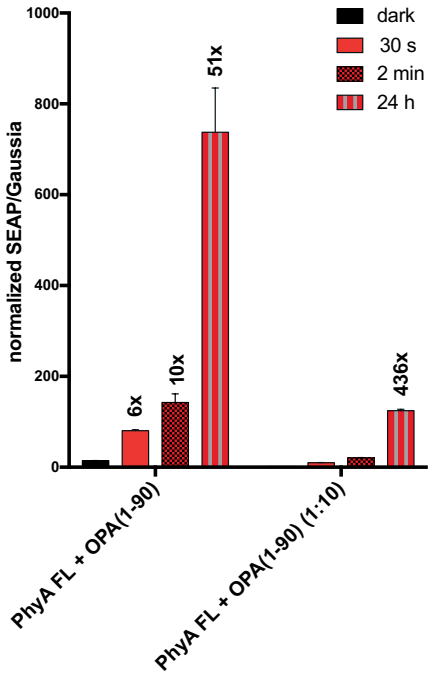

Fig. 18: Comparison and combination of the red-light inducible split transcription factor systems. A) Fluorescence anisotropy analysis of PhyA:OPA and PhyB$^{1-650}$:PIF6$^{1-100}$. Titration of 20 nM PIF6$^{1-100}$-EYFP / OPA-EYFP with increasing concentrations of dark-adapted (gray) or red-light-exposed PhyB$^{1-650}$ / PhyA FL (red), as monitored by anisotropy of the EYFP fluorescence. Data points show averages of three biological replicates. The red line denotes a fit to a single-site binding isotherm. Higher K_D indicates lower binding affinity (Experiments executed by David Golonka). **B)** Analysis of the sensitivity of the system. CHO-K1 cells were transfected with indicated plasmids, kept 24 h in darkness and afterwards supplemented with 15 µM PCB and either illuminated for 30 s, 2 min or 24 h with 2 µmol m^{-2} s^{-1} red-light or kept in dark. SEAP expression was determined and normalized with constitutive expressed Gaussia luciferase. Black and red bars indicate the mean of normalized SEAP expression ± standard error of the mean for n = 4 under dark and red conditions. The numbers above the red bars indicate the induction fold between dark and red-light conditions.

In summary, we engineered a novel red light-inducible split transcription factor system based on a novel discovered light-dependent interaction between phytochrome A and a protein of unknown function, hereafter termed OPA. We analyzed the interaction further and demonstrated not only an orthogonal interaction to PhyB and PIF6, we furthermore showed and utilized the differences in binding affinities and sensitivities. Additionally, our results indicated a multi-system control based on the variation of the light intensities and illumination time to control probably both red light systems. This demonstrates the tight linkage between basic research of light signaling pathways with the engineering of photoreceptor based optogenetic tools. Additionally, the new PhyA system shows a beneficial addition to the optogenetic toolbox and an important addition for the multi pathway control via one wavelength.

3.1.4 Introducing the red light-inducible split transcription factor system via viral gene delivery systems in neuronal-like cells

All results in this part were achieved in collaboration with Leonie-Alexa Koch, Institute of Synthetic Biology, Heinrich-Heine-University Düsseldorf.

A common method to transfer our red light system into mammalian cells is the chemical DNA transfection, but this method is inefficient in neuronal-like cells and *in vivo*. In these applications a common method is to transfer the DNA via viral particles containing the DNA of interest. Therefore, we decided to transfect mammalian cells and murine neuronal-like cells with the viral vectors containing the red light system as a quick test and for characterization. For final experiments and *in vivo* tests, we planned transduction experiments with produced viral particles. To increase the gene delivery efficiency in murine Neuro2a cells and in view of establishing the red light-inducible system *in vivo*, we constructed two customizable modularly exchangeable lentiviral vectors containing the whole optimized red light-inducible system (**Fig.**

19 A). The advantage of lentiviral vectors compared to the commonly used adeno-associated viruses (AAVs) (Betley and Sternson, 2011; Ojala et al., 2015; Deverman et al., 2016) is the packaging capacity. Since the full red light-inducible split transcription factor system together with the reporter gene consists of three ORFs and a size of almost 10 kb, one single AAV coding for the complete system with a packaging capacity of 4 kb is not sufficient (Grieger and Samulski, 2005; Vannucci et al., 2013). Due to the low co-transduction efficiency when using three AAVs (Duan et al., 2001; Carvalho et al., 2017) we decided to design two lentiviral vectors using their increased capacity of up to 10 kb. For this aim, we optimized the system by decreasing the number of needed plasmids, which should lead to higher transduction efficiency in neuronal cells. Due to the complexity of the lentiviral construct (LTRs, RRE, size) and the amount of sequence repeats an easy exchange of parts of the construct was not possible. To overcome these limitations the system was standardized and modularized as described in 3.1.1. The modularity of the construct led to fully-customizable modules, such as the gene of interest (channelrhodopsin-YFP) or the promoter (CMV). Additionally, the split transcription part (E/etr8) and the red light-dependent protein-interaction partner ($PhyB^{(1-650)}$/$PIF6^{(1-100)}$) are exchangeable by optimized variants or alternatives. Furthermore, the synthetic minimal promoter (CMVmin) and the viral trans-activator (VP16) are also exchangeable to give full control of the expression of the gene of interest (**Fig. 19 A**). To assay the functionality of the red light inducible system in the lentiviral vector, this vector and the mammalian expression vector containing the inducible synthetic minimal promoter followed by SEAP, were transfected into HEK293-T cells in 1:1 (w/w) ratio. After 24 hours of incubation in the dark, the cells were supplemented with the chromophore PCB and illuminated with 20 µmol m^{-2} s^{-1} and 660 nm light. The transfected cells showed a high induction of 55-fold of SEAP expression, indicating the functionality of the system in a lentiviral vector (**Fig. 19 B**). Based on this result, we constructed, similar to the mammalian reporter plasmid, a lentiviral vector coding for/comprising the inducible promoter and Channelrhodopsin fused to YFP instead of SEAP. To test this system also for applicability in neurons *in vivo*, both vectors were co-transfected in murine neuronal like cells (N2a) as described before. The transfected N2a cells kept in dark showed low or no detectable expression of YFP. In contrast, the illuminated cells showed high expression of Channelrhodopsin-YFP, which is localized mainly at the membrane (**Fig. 19 C**). These results show the functionality of the system transfected and expressed on a lentiviral vector and is the first step for the application *in vivo* by transducing the system into neuronal cells. Since the red light system is functional in lentiviral vectors, the constructed shorter PIF variants could be implemented to these constructs depending on their required activity. Additionally, analysis of the functionality of the novel red light-inducible PhyA based system in lentiviral vectors, would give the possibility of simultaneously controlling of two reporters with one wavelength *in vivo*.

In conclusion, we presented an optimized fully customizable red light-inducible split transcription factor system in a viral delivery system, functional in neuronal-like cells. Additionally, we gave insights on the interaction between PhyB and PIF while we generated a set of PIF variants with different binding affinities and therefore different activities, deployable in *in vivo* applications. Furthermore, we demonstrated physical interaction of different proteins with PhyA and B. These interactions suggest an integration of light into several cellular pathways and processes and based on these results we engineered an alternative red light-inducible system, completely orthogonal to the PhyB-based system.

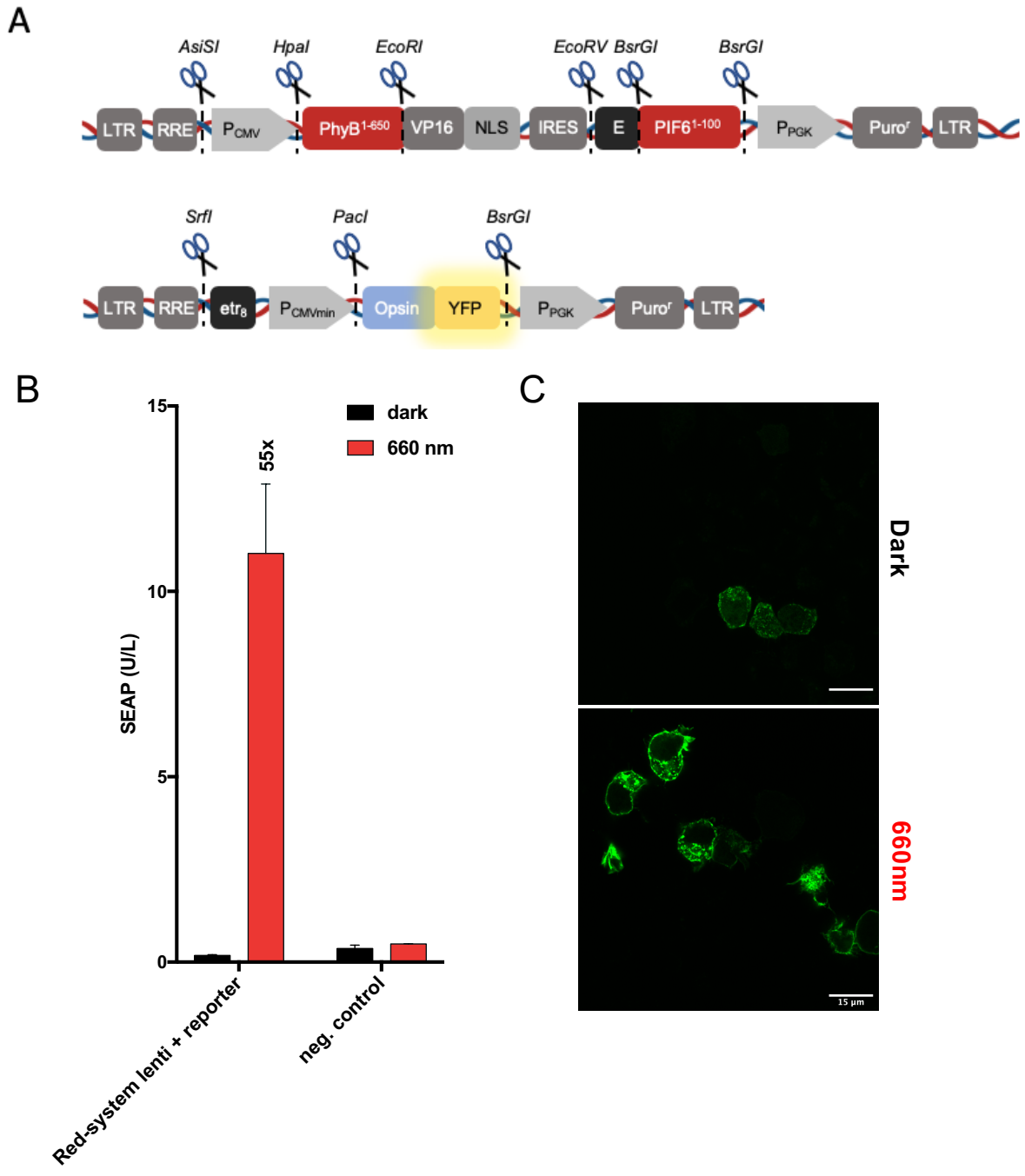

Fig. 19: Construction and validation of a red-light inducible system in a functional virus-derived gene delivery system. A) Configuration of the modular red-light split transcription factor in a lentiviral backbone. The whole new generation red-light split-transcription factor system (see 3.1.1) was inserted after the REV RESPONSE ELEMENT (RRE) into a lentiviral vector with containing puromycin resistance. Additionally, the inducible reporter was inserted in the same manner in a second lentiviral vector. $PhyB^{1-650}$ is C-terminally fused to a VP16 trans activator domain with an NLS sequence. $PIF6^{1-100}$ is N-terminally fused to the erythromycin protein (E) and separated by an internal ribosome entry site (IRES) for translation from one mRNA. Specific restriction recognition sites were inserted as indicated for a fully exchangeable and customizable design. The inducible reporter construct comprises eight repeats of an E protein specific operator sequence (etr_8) in front of a minimal CMV promoter. As readout, channelrhodopsin (opsin) fused to eYFP lies downstream of the minimal promoter. Similar to the PhyB/PIF6 construct, all parts were inserted with restrictions sites for a modular design. The inserted specific restriction sites were adapted to be unique in the backbone construct. **B)** Functionality of the lentiviral vector containing the red-light system. Neuro2A cells were transfected with the lentiviral vector containing the red-light inducible split transcription factor system and a mammalian reporter vector with SEAP as readout or with reporter alone (neg.control). Transfected cells were kept in dark for 24 h, supplemented with 15 µM PCB and illuminated 24 h with 20 µmol m^{-2} s^{-1} red-light (660 nm) or kept in darkness. SEAP expression was determined. Black and red bars indicate the mean of SEAP expression ± standard error of the mean for n = 4 under dark and red conditions. The numbers above the red bars indicate the induction fold between dark and red-light conditions. **C)** Functionality of the whole gene delivery system for application in neuronal cells. Neuro2A cells were transfected with lentiviral vectors shown in A) containing the red-light system and the reporter with opsin-YFP fusion as readout. After 24 h in darkness the cells were supplemented with 15 µM PCB and illuminated 24 h with 20 µmol m^{-2} s^{-1} red-light (660 nm) or kept in darkness. Afterwards, transfected cells were fixated and YFP fluorescence was determined under a confocal microscope.

3.2 Engineering of blue light-inducible optogenetic tools for rapid downregulation of protein and mRNA levels in mammalian cells

3.2.1 Blue light-induced control of protein stability and transcriptional activity to regulate programmed cell death

This chapter is based on the work presented in Baaske et al., 2018 and Fischbach et al., 2019a (*accepted*) in Appendix Original studies and protocols 7.1.

As described above, a common approach to study the function of a protein of interest is to regulate the expression level or the stability of the protein. While chemical-based activation, repression or degradation have limitations such as toxicity, irregular spatially controlled distribution and limited reversibility, light-regulated systems were developed to overcome these limitations (Weber and Fussenegger, 2011). The optogenetic toolbox contains various light-inducible systems for several applications but only a few were developed for downregulation or destabilization of a protein (Bonger et al., 2014; Pathak et al., 2017). Additionally, the combination of diverse optogenetic tools in one cell for independent control of processes is particularly difficult and needs further analysis (Müller et al., 2013b).
Therefore, our group developed a dual blue light-controlled system for transcriptional repression and simultaneous degradation of the protein of interest (Baaske et al., 2018, Appendix 7.1). The system consists of two switches: i) the photosensitive transcription factor EL222 from *Erythrobacter litoralis* fused to a KRAB transrepressor domain to repress transcriptional activity and ii) the POI fused to the blue light-induced degradation module (B-LID) for light-dependent proteasomal degradation (**Fig. 20 A**). The B-LID module consists of a LOV2 domain of *Avena sativa* Phototropin I (*As*LOV2) and is fused C-terminally to a RRRG degron. Upon blue light illumination, the Jα-helix unwinds and exposes the fused degron to induce proteasomal degradation of the POI-B-LID fusion protein. Additionally, this POI-B-LID module is under the control of a synthetic promoter comprising five repeats of the specific DNA target sequence of EL222-KRAB ($C120_5$) (**Fig. 20 A**). Blue light illumination leads to homodimerization of EL222-KRAB and therefore binding via its helix-turn-helix (HTH) domain to the cognate DNA sequence $C120_5$ to inhibit transcriptional activity.

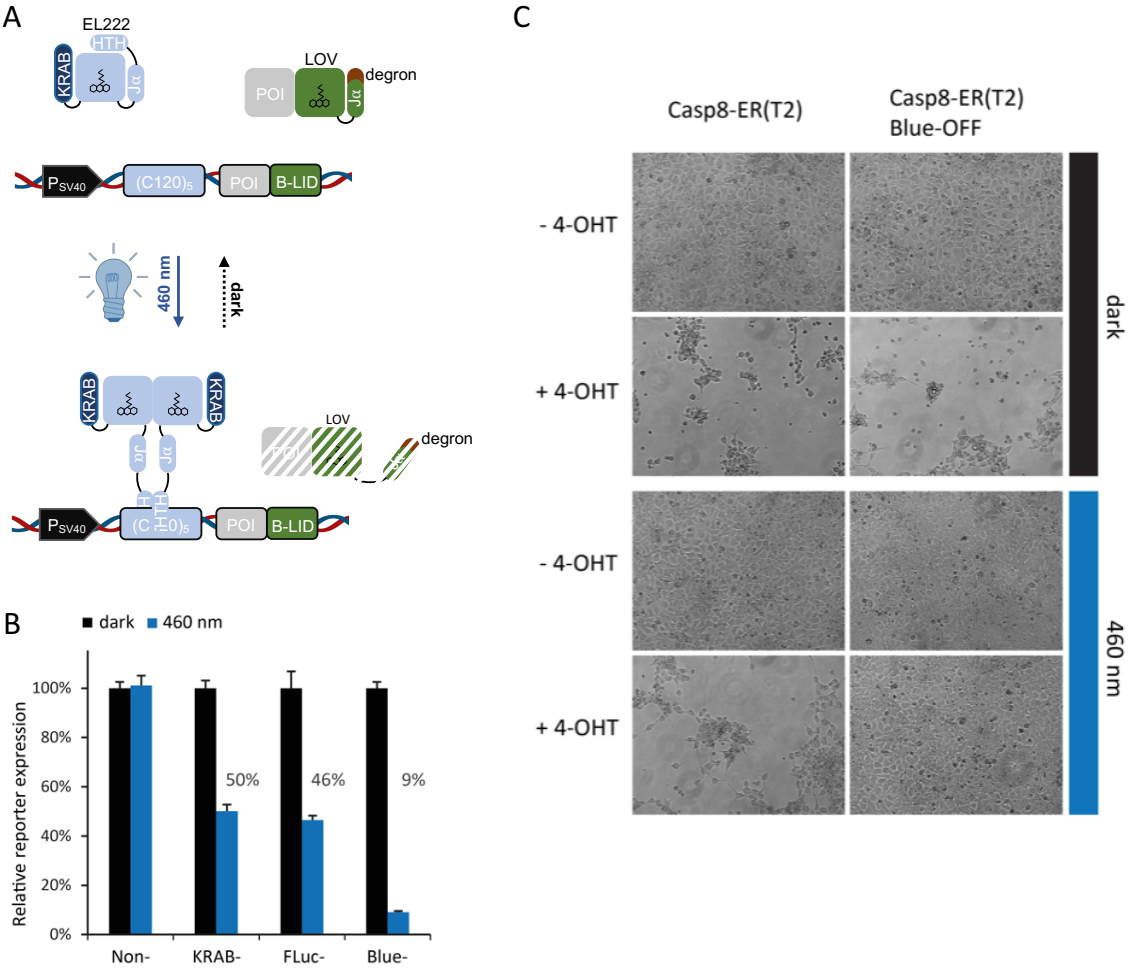

Fig. 20: Design, validation and application of the Blue-OFF system. A) Mode of function of the Blue-OFF system. The SV40 promoter sequence is followed by five copies of the EL222-binding sequence ($C120_5$). The photosensory transcription factor EL222 is fused to the inhibitory KRAB domain. In the dark, the KRAB-EL222 fusion is not bound to the target sequence on the DNA and the B-LID system is inactive leading to accumulation of the POI. Upon blue light illumination, the Jα helix unwinds, exposing the docked degradation peptide (RRRG) which leads to proteasome mediated protein degradation. Simultaneously, the EL222 transcription factor dimerizes and binds to the $C120_5$ sequence inhibiting transcription via the fused KRAB repressor domain. **B)** Validation of the combined regulation of transcription and post-translation. HEK-293T cells were transfected with plasmids containing indicated genes. Transfected cells were kept in darkness for 24 h or for 16 h in dark conditions followed by 8 h illumination with 20 µmol m^{-2} s^{-1} 460 nm light. Firefly luciferase levels were determined and normalized to their dark control. Data are means ± standard error of the mean of four biological replicates. **C)** Control of Caspase-induced programmed cell death. HEK-293T cells were transfected either with Casp8-ER(T2) or Casp8-ER(T2)-Blue-OFF and form a uniform monolayer under all conditions in absence of 4-OHT. Addition of 4-OHT induces caspase8 and therefore cell death in darkness for Casp8-ER(T2) and Casp8-ER(T2)-Blue-OFF and under blue light for Casp8-ER(T2) transfected cells. Only cells transfected with Casp8-ER(T2)-Blue-OFF show a higher survival rate by forming a uniform monolayer comparable to the control cells in dark without 4-OHT. Adapted from Fischbach et al., 2019a and Baaske et al., 2018.

First, we evaluated the functionality of the system by the downregulation of firefly (FLuc) as a reporter in HEK293-T cells. Transfected cells were kept in darkness for 16 h and afterwards illuminated 8 h with 460 nm and 20 µmol m^{-2} s^{-1} light. Cells transfected with only with EL222-KRAB exhibited a decrease in expression of 50 % compared to the cells kept in dark (**Fig. 20 B).** Quite similar results were achieved with cells transfected only with the POI-B-LID module, they demonstrated 46 % of the expression of protein levels in non-illuminated cells. As expected, the combination of both modules showed a stronger repression down to 9 % of the control cells expression level (**Fig. 20 B**). This shows the non-linear synergistic effect of the two optogenetic modules. Since the system represses transcriptional activity and target protein degradation, there is no effect on mRNA level, meaning the remaining expression might be from previously synthesized RNA. However, after full characterization and development of a quantitative model of the Blue-OFF system (Baaske et al., 2018; Appendix 7.1), we implemented the system to achieve light control over apoptosis in mammalian cells. Therefore, we integrated the tamoxifen inducible caspase protein caspase 8 (Casp8-ER(T2)) into the Blue-OFF system, for blue light control of caspase stability (Cachat et al., 2017). The predominantly present monomer of caspase 8 is inactive, but addition of 4-hydroxytamoxifen (4-OHT) leads to dimerization and therefore to activation and triggering of apoptosis (Chu et al., 2008). HEK-293T cells transfected with caspase 8 expressing constructs demonstrated significant decrease in cell growth upon addition of 4-OHT in darkness and under blue light (**Fig. 20 C**). In contrast, cells transfected with a Casp8-ER(T2)-Blue-OFF module showed monolayer formation and normal growth under blue light, despite 4-OHT addition (**Fig. 20 C**). These results demonstrate that the Blue-OFF system can efficiently be used for optogenetic control of programmed cell death in mammalian cells.

Finally, to study the control of programmed cell death further, we implemented the pro-apoptotic proteins PUMA and BID into the Blue-OFF system. These pro-apoptotic proteins are targets of the transcription factor p53 keeping the balance between cell cycle arrest and cell death upon DNA damage or cell death insults (Nakano and Vousden, 2001; Sax et al., 2002; Deng, 2017). Overexpression of PUMA and BID in mammalian cells leads to cell death. Therefore, we aimed to regulate with the Blue-OFF system induced apoptosis by reducing the levels of constitutively, ectopically expressed pro-apoptotic proteins. Towards this aim, we transfected HEK-293T cells with the Blue-OFF system containing either PUMA or BID. Additionally, constitutively PUMA and BID expressing constructs with a deleted degron were transfected as controls. As a negative control, the basic Blue-OFF system containing FLuc was used (**Fig. 21 A**). Transfected cells were illuminated with for 48 h with 460 nm blue light and an intensity of 10 µmol m^{-2} s^{-1} directly after transfection or kept in darkness for 48 h. The illumination starts directly after transfection to avoid accumulation of pro-apoptotic proteins and the followed cell death. We observed that cells incubated in darkness showed a high death

rate indicating more apoptosis, in contrast to the control cells which formed a uniform monolayer (**Fig. 21 B**). As expected, cells transfected with the Blue-OFF system showed a higher survival rate when illuminated with blue light. This showed the high functionality and the rapid downregulation of protein levels of the Blue-OFF system.

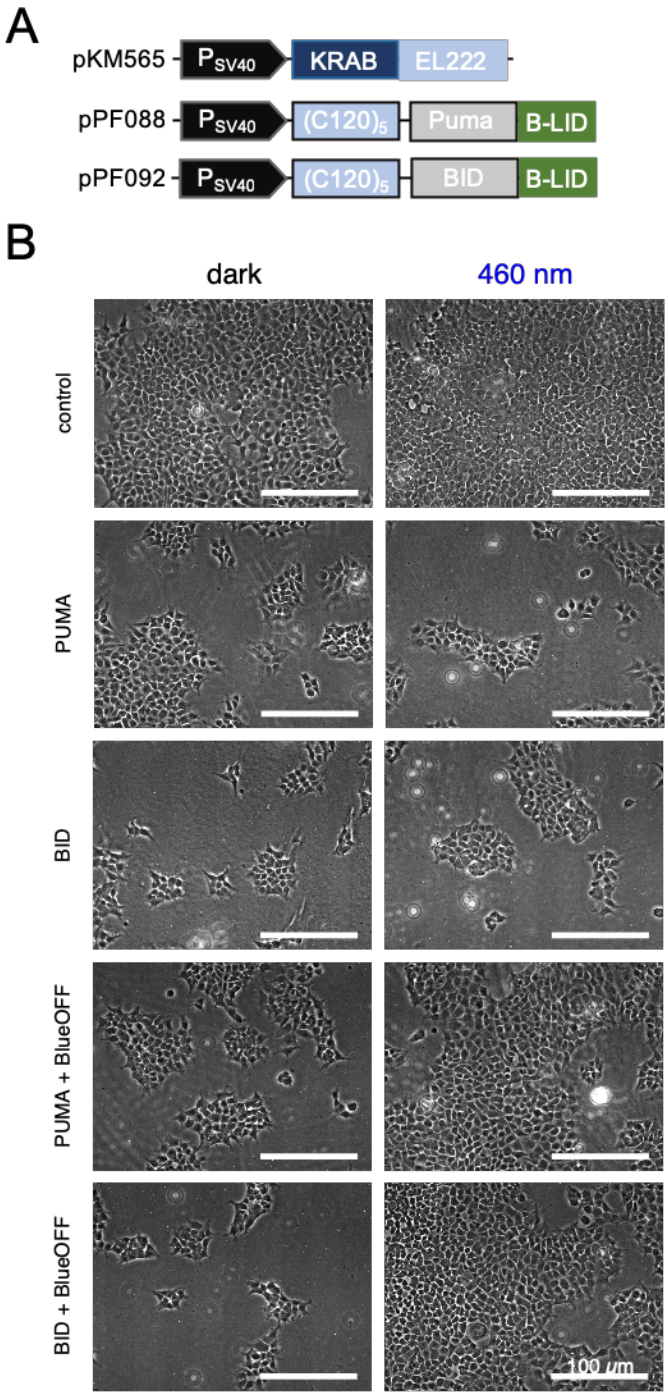

Fig. 21: Control of programmed cell death. A) Schematic design of the constructed plasmids of pro-apoptotic proteins. Puma and BID were inserted in the Blue-OFF system, directly fused to the B-LID domain. **B)** Control of pro-apoptotic protein induced cell death. HEK-293Tcells were transfected with indicated plasmids. Transfected cells were illuminated for 48 h with 10 µmol m^{-2} s^{-1} 460 nm blue light. Cells transfected with the control plasmid forming a uniform monolayer under both conditions. Constitutive expression of PUMA and BID in darkness and blue light and PUMA-Blue-OFF and BID-Blue-OFF in darkness leads to increased cell death. In contrast, PUMA and BID in the Blue-OFF system showed a higher survival rate compared to the control cells, upon blue light illumination. Adapted from Fischbach et al., 2019a.

In conclusion, we engineered and demonstrated the use of a novel Blue-OFF optogenetic approach for controlling protein levels. The simultaneous transcriptional and post-translational control of protein levels, leads to a fast and strong reduction of the protein of interest. In addition, these results open novel perspectives for the regulation of programmed cell death and further applications in basic research, such as study of carcinogenic cellular mechanisms or apoptotic events (Lee et al., 2004; Giotopoulou et al., 2015). Furthermore, the high spatiotemporal resolution might be an advantage for the establishment of cellular patterns in tissue engineering. Moreover, this system is applicable for *in vivo* applications, especially because it uses the endogenously available FMN (flavin mononucleotide) as a chromophore. However, since the Blue-OFF system is not targeting mRNA, a complete blue light-induced and reversible protein knock-out is still missing. This issue and an optogenetic solution for it is described in the next chapter.

3.2.2 Development and engineering of a blue light-activated CRISPR/Cas13b mediated mRNA knockout (BLACKout) system

The presented results in this part of the thesis are achieved in collaborative work with Tim Blomeier, Institute of Synthetic Biology, Heinrich-Heine-University Düsseldorf and based on Fischbach et al., 2019c (*in preparation*) in Appendix Original studies and protocols 7.1.

As described before, common approaches to control RNA levels are usually based on the translational and CRISPR/Cas9 interference or knock down of miRNAs or mRNAs (Chang et al., 2016; Unniyampurath et al., 2016). While, light-dependent DNA cleavage CRISPR/Cas9 tools are already developed, tools for light-dependent regulation of RNA levels are still missing (Vogel et al., 2017; Brooks and Gaj, 2018). Further, optogenetic tools which are able to target endogenous proteins are rare and needed in many *in vivo* applications. Additionally, as we demonstrated above, the regulation of mRNA levels is necessary for a rapid and reversible light-induced downregulation of proteins. Therefore, we aimed to develop the first light-inducible tool for mRNA level regulation in a reversible manner with the high spatiotemporal resolution common for optogenetic tools with the possibility to target endogenous proteins.
Towards this aim, we employed a CRISPR/Cas13b effector protein derived from *Prevotella sp*., which is targeting RNA instead of DNA with high precision and PAM motif independent (Cox et al., 2017). Based on this Cas13b protein we constructed the blue light-activated Cas13b induced mRNA knockout (BLACKout) system. The BLACKout system, which regulates the gene expression of Cas13b, consists out of four parts: i) a LOV2 domain, from Phototropin I of *Avena sativa*, hiding a specific tag on the Jα helix and N-terminally fused to a GAL4 DNA binding domain (Strickland et al., 2012); ii) an ePDZ domain fused to a virus derived

trans activator VP16 (Huang et al., 2008; Strickland et al., 2012); iii) a reporter construct with a synthetic minimal promoter containing GAL4 target sequence repeats upstream of the PspCas13b gene and iv) a construct containing the specific gRNA for the target of interest (**Fig. 22 A**). Via illumination with blue light the system turns active, the LOV2 domain exposes the hidden tag and interacts with the ePDZ domain. This interaction leads to a close proximity of the fused trans activator and the synthetic minimal promoter, inducing the transcription of Cas13b. Guided by the specific customizable gRNA, Cas13b is cleaving the mRNA of interest (**Fig. 22 A**). With this blue light system, we are able to indirectly control mRNA levels via the regulation of Cas13b expression. To test the functionality of the system, and in view of further combination of the systems, we targeted the mRNA of the firefly luciferase used as a reporter of the Blue-OFF system.

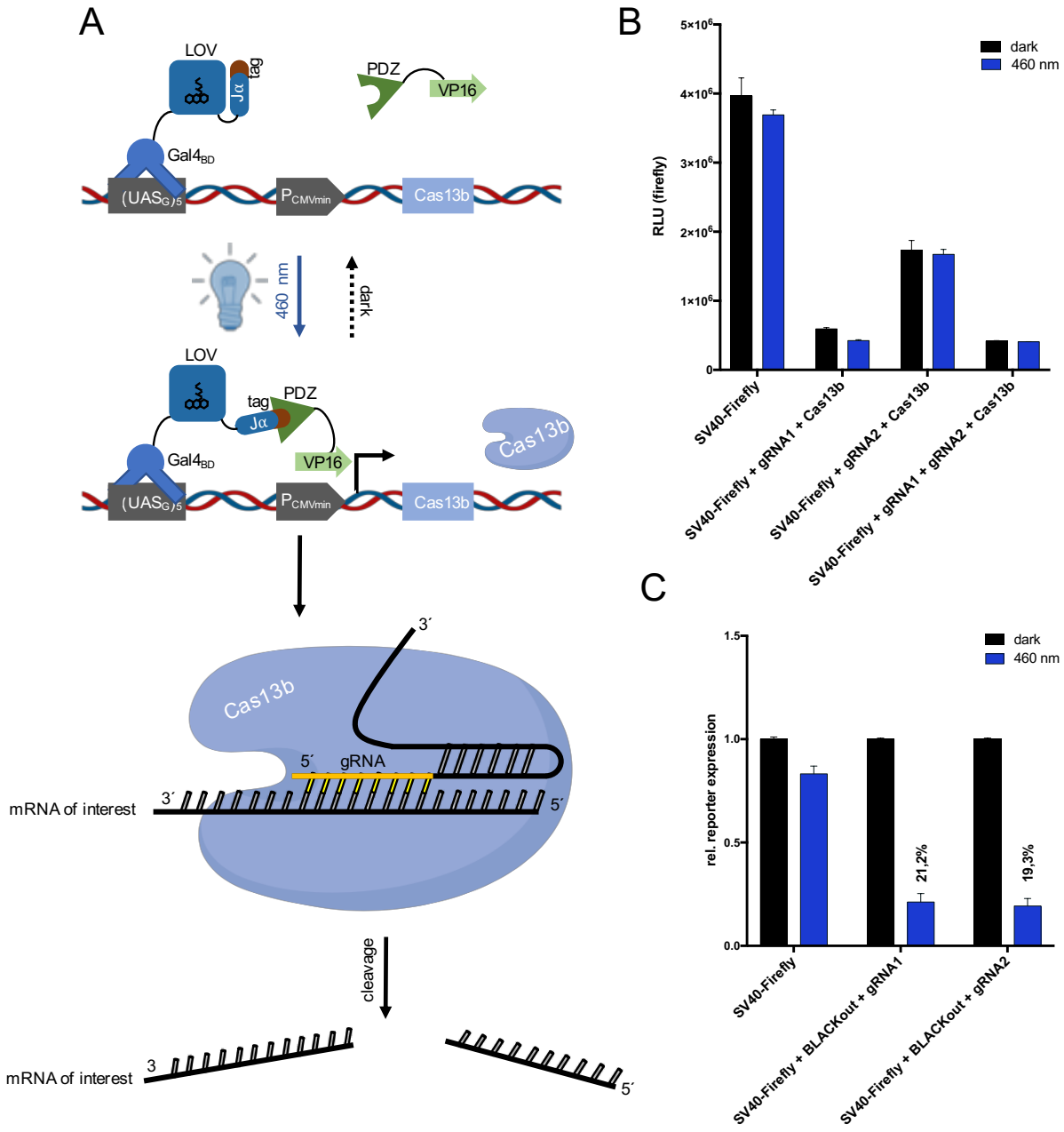
A
LOV
tag
Jα
PDZ
VP16
Gal4BD
(UASG)5
PCMVmin
Cas13b
460 nm
dark
LOV
tag
PDZ
Jα
Gal4BD
VP16
Cas13b
(UASG)5
PCMVmin
Cas13b
3´
Cas13b
5´
gRNA
mRNA of interest
3´
5´
cleavage
mRNA of interest
3
5´
B
RLU (firefly)
5×10^6
4×10^6
3×10^6
2×10^6
1×10^6
0
dark
460 nm
SV40-Firefly
SV40-Firefly + gRNA1 + Cas13b
SV40-Firefly + gRNA2 + Cas13b
SV40-Firefly + gRNA1 + gRNA2 + Cas13b
C
rel. reporter expression
1.5
1.0
0.5
0.0
dark
460 nm
21,2%
19,3%
SV40-Firefly
SV40-Firefly + BLACKout + gRNA1
SV40-Firefly + BLACKout + gRNA2

Fig. 22: Design and validation of the BLACKout system. A) Mode of function. The photosensitive LOV2 peptide with an ePDZ specific tag is fused to the GAL4 DNA binding domain and separated by an internal ribosome entry site (IRES) from the ePDZ-VP16 fusion protein. On the reporter construct, five repeats of the GAL4 DNA sequence followed by a TATA box are upstream of the PspCas13b gene. Blue light illumination provides the unwinding of the Jα-helix and therefore exposing of the tag, which leads to interaction with the ePDZ-VP16 fusion. This interaction brings the viral trans activator in close proximity to the TATA box and recruits the transcriptional machinery. The expressed Cas13b protein is guided via the U6-promoter driven specific gRNA to the mRNA of interest to cleave it. **B)** Functionality of the gRNAs. Specific gRNAs targeting two separate sites of Firefly luciferase were designed and tested for their functionality with constitutively expressed Cas13b. HEK293-T were transfected with a construct containing constitutive expressed Cas13b, a construct expressing FLuc constitutively and either gRNA1, gRNA2 or both together. Transfected cells were kept in darkness for 24 h post-transfection and afterwards illuminated with blue light (10 µmol m^{-2} s^{-1} 460 nm) or kept in darkness for 24 h. FLuc expression was determined. Black and blue bars indicate the mean of FLuc expression ± standard error of the mean for n = 4 under dark and blue conditions. **C)** Functionality of the BLACKout system. HEK293-T were transfected with constructs containing the BLACKout system, a construct expressing FLuc constitutively and either gRNA1 or gRNA2. Transfected cells were kept in darkness for 24 h post-transfection and afterwards illuminated with blue light (10 µmol m^{-2} s^{-1} 460 nm) or kept in darkness for 24 h. FLuc expression was determined and normalized to the corresponding dark expression level. Black and blue bars indicate the relative mean of FLuc expression ± standard error of the mean for n = 4 under dark and blue conditions. Numbers above the blue bars indicate the blue-light expression level compared to the dark level in percentage.

Therefore, we designed two different gRNAs and after verification of the functionality (**Fig. 22 B**), the transfection of the complete BLACKout system demonstrated a blue light-induced decrease of ~ 80 % of the FLuc protein level (**Fig. 22 C**). Furthermore, we could show that the BLACKout system is able to knockdown fluorescence proteins such as GFP in a blue light-dependent manner (**Fig. 23**). To characterize the system further we measured kinetics of the mRNA cleavage and performed dose response experiments to get better insight into the performance of the BLACKout system. Additionally, we analyzed the reversibility, since this is a key advantage of a light-inducible system (Fischbach et al., 2019c, Appendix Original studies and protocols 7.1).

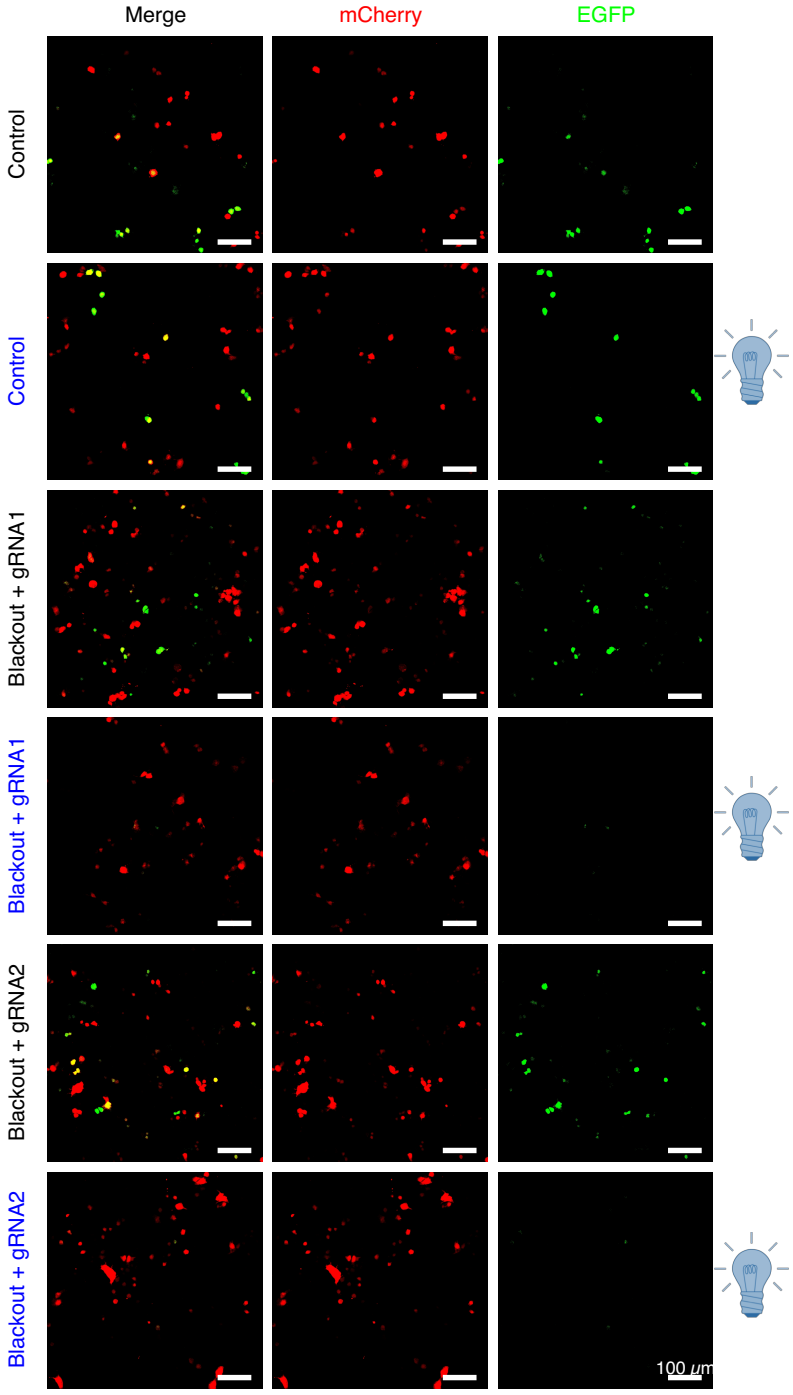

Fig. 23*:* Blue light-induced GFP knock out. In darkness GFP accumulates similar to the mCherry signal in transfected cells. Upon blue light illumination the GFP level decreases in cells transfected with BLACKout system and either gRNA1 or gRNA2. HEK-293T cells were transfected with PGK-GFP (pTBPF018), SV40-mCherry (pTBPF014), the BLACKout system (pTBPF001, pKM516) and either gRNA1 or gRNA2 (pTBPF005, pTBPF006). After transfection cells were kept in dark for 24 h and illuminated for 48 h with 10 µmol m^{-2} s^{-1} and 460 nm light. Afterwards cells were fixated and imaged by confocal microscopy.

To investigate a complete knockout of a protein of interest we combined the described Blue-OFF with the BLACKout system, to target transcriptional activity, mRNA level and protein stability simultaneously with one wavelength. As indicated in **Fig. 24 A** we were able to decrease the protein level down to ~ 1 % after an illumination time of 24 h. These results showed the rapid and high efficiency of protein downregulation when combining both systems and indicated the high combinability of the BLACKout system. Finally, to demonstrate the applicability of the system for knock out of endogenous proteins we targeted hCDK1 in HEK-293T cells. hCDK1 is an important key player for the G2 cell cycle check point and regulates the induction of mitosis (Liao et al., 2017). To investigate the BLACKout system for blue light-regulated G2 cell cycle arrest we designed gRNAs targeting the kinase domain of hCDK1. Our results in transfected HEK-293T showed a decreased growth of the cells compared to the un-transfected cells (**Fig. 24 B**).

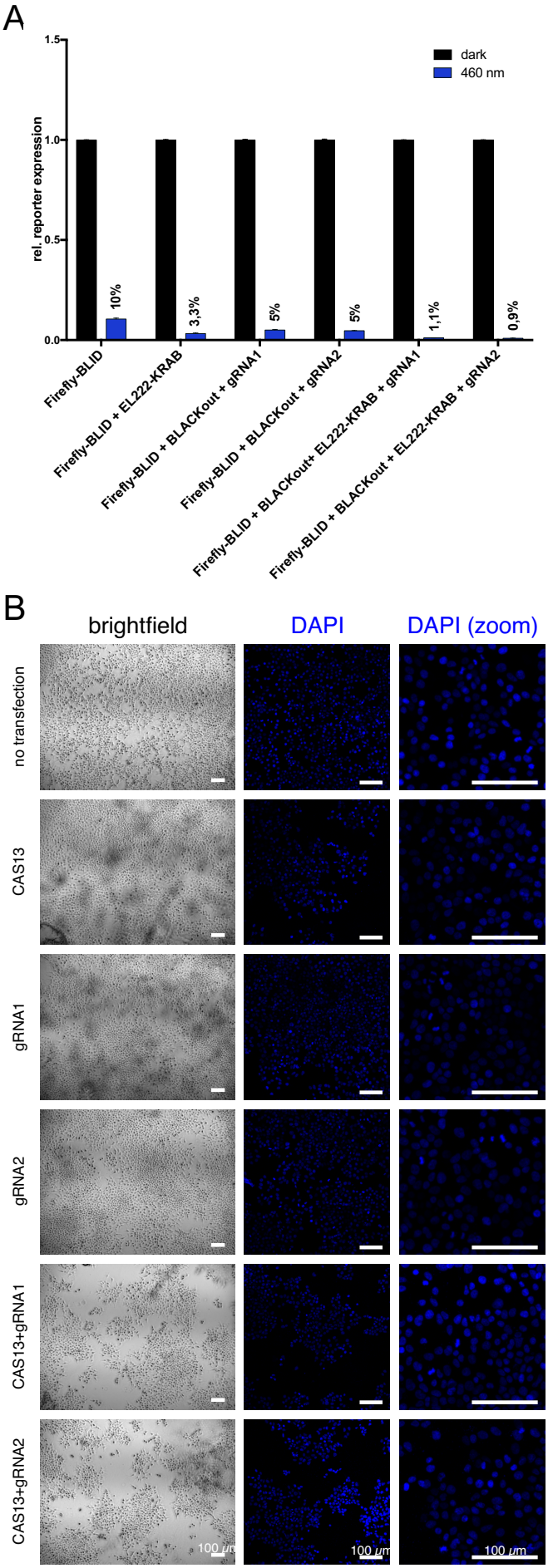
A
dark
460 nm
rel. reporter expression
1.5
1.0
0.5
0.0
10%
3,3%
5%
5%
1,1%
0,9%
Firefly-BLID
Firefly-BLID + EL222-KRAB
Firefly-BLID + BLACKout + gRNA1
Firefly-BLID + BLACKout + gRNA2
Firefly-BLID + BLACKout+ EL222-KRAB + gRNA1
Firefly-BLID + BLACKout + EL222-KRAB + gRNA2
B
brightfield
DAPI
DAPI (zoom)
no transfection
CAS13
gRNA1
gRNA2
CAS13+gRNA1
CAS13+gRNA2
100 µm
100 µm
100 µm

Fig. 24: Application and combinability of the BLACKout system. A) Full knockout by combination of the Blue-OFF system with the BLACKout system. HEK293-T were transfected with indicated constructs. Transfected cells were kept in darkness for 24 h post-transfection and afterwards illuminated with blue light (10 µmol m^{-2} s^{-1} 460 nm) or kept in darkness for 24 h. FLuc expression was determined and normalized to the corresponding dark expression level. Black and blue bars indicate the relative mean of FLuc expression ± standard error of the mean for n = 4 under dark and blue conditions. Numbers above the blue bars indicate the blue-light expression level compared to the dark level in percentage. **B)** Functionality of gRNAs for cell cycle control. HEK-293Tcells were transfected with plasmids expressing indicated genes. Transfected cells were kept in dark for 48 h post-transfection. Un-transfected cells and cells transfected with either gRNA1 or 2 (targeting hCDK1) or constitutive Cas13b forming a uniform monolayer. Constitutive expression of Cas13b and either gRNA1 or 2 in darkness led to reduced cell growth suggesting a BLACKout induced cell cycle arrest. Cells were stained with DAPI.

In conclusion, we engineered the first blue light-inducible mRNA cleavage tool based on a CRISPR/Cas effector protein. We showed that a reversible knock out of proteins is possible with a high spatiotemporal resolution. Furthermore, this tool could be applied for fundamental research of splicing variants, cancer or essential proteins in living cells or organisms in *in vivo* applications. In addition, due to the high customizability of the gRNA, this system allows to target nearly every protein of interest in a reversible manner and it is combinable with other optogenetic tools. Finally, we could show the functionality for endogenous target mRNAs to control the cell cycle in mammalian cells which allows further applications. However, this result needs to be verified by using the whole BLACKout system to control the cell cycle in a reversible manner, but anyway the designed gRNAs are functional and the transfected cells showed reduced growth. In future studies, one could analyze the efficiency and possible off-targets of the Cas system by qPCR analysis of the mRNA of interest, since there are no data available so far. Furthermore, to increase the transfection efficiency it is possible to reduce the number of needed constructs by combining for example the blue light system construct with the gRNA plasmid. Another possibility to increase the efficiency of the system would be to engineer the Cas13b protein to a have an own light-dependent activity, therefore the transcription-based accumulation time of Cas13b would be decreased and the induction time of Cas13b would be increased (Nihongaki et al., 2015).

4 Conclusion

In summary, this work addresses the establishment and engineering of optogenetic tools to control cellular processes, gene expression, programmed cell death and cell cycle in mammalian cell culture and *in vivo* systems. Furthermore, this work shows the usage of optogenetic tools for deciphering fundamental biological processes such as the reconstruction of light signaling pathways and the development of new optogenetic tools resulting out of this knowledge.

First, we re-designed the PhyB-based split transcription factor system to be customizable for a simplified applicability in *in vivo* systems. In addition, we targeted the size of the transcription factor PIF to not only get a better understanding of the interaction between PhyB and PIF but also discover truncated and optimized PIF variants with decreased basal activity in view of the *in viv*o applicability. In fact, we implemented the optimized, modular red light system in a lenti viral delivery system and demonstrated the functionality in neuronal like cells.

Second, we aimed to screen new potential interactors of phytochrome A and B and therefore to reconstruct plant light signaling pathways in an orthogonal system. Successfully, thanks to the optimized PhyB-based system we showed light-dependent interaction of these pathways with several of the tested transcription factors and PhyA or B. With these results we demonstrated the integration of phytochrome signaling into hormone signaling for example jasmonate signaling, the circadian clock and cold regulation. Moreover, contributing to optogenetics, we developed a novel PhyA-based red light-dependent toggle switch completely orthogonal to the PhyB system and therefore combinable to control two processes with one pulse of red light. Furthermore, we demonstrated the functionality of the split transcription factor system as a orthogonal screening platform for plant protein:protein interactions and therefore reconstruction of light signaling pathways.

Finally, as novel upgrades for the optogenetic toolbox, we targeted the control of transcription, mRNA levels and protein stability via one wavelength. Specifically, we engineered a blue light-dependent tool which inhibits transcriptional activity and simultaneously induces protein degradation to knockdown protein levels. Additionally, we successfully developed the first blue light-induced mRNA cleavage tool based on a CRISPR/Cas effector protein to regulate mRNA levels. These tools were successfully used to control programmed cell death and cell cycle arrest in mammalian cells.

Taken together, this work resulted in the establishment of various optogenetic tools which are an advantage to answer various scientific questions for example in splicing variant analysis, cancer research, programmed cell death or fundamental research in the future. All this with the benefits of optogenetic tools like the high spatiotemporal resolution, reversibility and in a non-invasive manner.

5 Material and Methods

5.1 Plasmid generation and construction

Generated plasmids, oligos and gRNAs are described in detail in tables **Tab. 2**, **Tab. 3** and **Tab. 4**.

5.2 Cell culture and transfection

Chinese hamster ovary cells (CHO-K1, DSMZ, Braunschweig, Germany) were cultivated and transfected as described Golonka et al., 2019 and Fischbach et al., 2019b.
Human embryonic kidney cells (HEK-293T, DSMZ, Braunschweig, Germany) were cultivated and transfected as described in Baaske et al., 2018 and Fischbach et al., 2019a+c.

5.3 Light experiments

If not indicated otherwise, medium was exchanged 24 h post-transfection either supplemented with chromophore (15 µM) or without. All work-steps were done under 530 nm green safe-light to avoid activation of the optogenetic systems. Cells were illuminated with various LED light-boxes with the indicated wavelength and intensities. LED light-boxes were constructed as described in Fischbach et al., 2019a.

5.4 SEAP reporter assay

The supernatant of transfected cells was transferred to 96-well round-bottom MTPs and incubated at 68°C for 1 h to inactivate endogenous phosphatases. Afterwards, 80 µL of the supernatant were transferred to a 96-well flat-bottom MTPs, and per well 100 µL SEAP buffer (20 mM homoarginine, 1 mM $MgCl_2$, 21% (v/v) diethanolamine) was added (Müller et al., 2013a). After addition of 20 µL 120 mM para-nitrophenyl phosphate, the absorption at 405 nm was measured for 1 h using a BMG Labtech CLARIOstar or a TriStar2 S LB 942 multimode plate reader (Berthold Technologies, Bad Wildbad, Germany). The slope of obtained curves (OD/min) was calculated and SEAP activity (U/L) was determined using Lambert-Beers´s-law:

$$E = \varepsilon \, x \, c \, x \, d$$

ε = 18600 M^{-1} cm^{-1}

c = increase of OD/min (slope)

d = length of light path, 0,6 cm

5.5 *Gaussia* Luciferase assay

20 – 80 µL of the supernatant of the transfected cells were transferred to a 96-well white MTP and diluted in 0 - 60 µL phosphate-buffered saline (PBS; 2.68 mM KCl, 1.47 mM KH_2PO_4, 8.03 mM Na_2PO_4, 137 mM NaCl). After addition of 20 µL coelenterazine (472mM stock solution in methanol, diluted 1:1,500 in PBS; Carl Roth, Karlsruhe, Germany, no. 4094.4), the luminescence was measured for 20 min using TriStar2 LB 941 or LB 942 multimode plate readers (Golonka *et al*., 2019).

5.6 Firefly Luciferase assay

Luciferase expression was quantified by lysing cells on ice with 250 µl luciferase lysis buffer (25 mM Tris/HCl, pH 7.8, 1 % Triton X-100, 15 mM $MgSO_4$, 4 mM ethylene glycol tetraacetic acid (EGTA), 1 mM DTT) per well on ice for 15 min. 80 µl lysate was transferred to Costar® 96-well flat-bottom white plates (Corning Incorporated, Germany). Firefly luciferase luminescence was directly monitored using Berthold Centro XS^3 LB960 reader (Berthold Technologies, Bad Wildbad, Germany) after addition of 20 µl of firefly luciferase substrate (20 mM Tricine, 2.67 mM $MgSO_4$, 0.1 mM EDTA, 33.3 mM DTT, 0.52 mM ATP, 0.27 mM Acetyl-CoA, 5 mM NaOH, 50 mM $MgCO_3$, 0.47 mM luciferin) (Baaske et al., 2018).

5.7 Statistical analysis

Statistical analysis was performed by using two-way ANOVA with GraphPad Prism 7.0.
Outlier were determined and excluded in all experiments as described in (Jacobs and Dinman, 2004).

5.8 Software

Geneious R10 Version 10.2.3 for plasmid design and construction.
GraphPad Prism 7.0 for data analysis and statistical analysis.
Microsoft Office 2019 for data analysis & graphic design.
Biorender.com for graphic design.

Tab. 2: Generation and description of plasmids used in this work. All plasmids were constructed using Gibson or AQUA assembly (Gibson et al., 2009; Beyer et al., 2015a).

Plasmid	Description	Reference or Source
pKM006	**$tetO_{13}$-CMV_{min}-SEAP-TA**	(Müller et al., 2013a)
pKM022	**SV40-PhyB$^{1-650}$-VP16-tetR-PIF6$^{1-100}$-TA**	(Müller et al., 2013a)
pKM082	**etr_8-CMV_{min}-SEAP-TA**	(Müller et al., 2014)
pKM083	**SV40-GLuc-TA**	Unpublished (Konrad Müller)
pKM516	**SV40-GAL4BD-$LOV2_{tag}$-IRES-ePDZ-VP16-NLS-TA**	(Müller et al., 2014)
pKM565	**SV40-KRAB-EL222-TA**	(Baaske et al., 2018)
StrigoQuant	**P35S-Renilla-2A-SMXL6-Firefly-myc-pA;** Vector for the expression of a ratiometric luminescent biosensor with SMXL6 as a sensor module.	(Samodelov et al., 2016)
pMZ333	**SV40-PhyB$^{1-650}$-mCherry-TA**	(Müller et al., 2013a)
pMZ1160	**SV40-PhyA FL-VP16-IRES-tetR-SPA1-TA**	Unpublished (Matias Zurbriggen)
pMZ1161	**SV40-PhyA FL-VP16-IRES-tetR-PIF3-TA**	Unpublished (Matias Zurbriggen)
pMZ1163	**SV40-PhyA FL-VP16-IRES-tetR-COR27-TA**	Unpublished (Matias Zurbriggen)

pMZ1164	**SV40-PhyA FL-VP16-IRES-tetR-COR28-TA**	Unpublished (Matias Zurbriggen)
pMZ1165	**SV40-PhyA FL-VP16-IRES-tetR-JAZ1-TA**	Unpublished (Matias Zurbriggen)
pMZ1166	**SV40-PhyA FL-VP16-IRES-tetR-JAZ5-TA**	Unpublished (Matias Zurbriggen)
pMZ1167	**SV40-PhyA FL-VP16-IRES-tetR-ERF006-TA**	Unpublished (Matias Zurbriggen)
pMZ1168	**SV40-PhyA FL-VP16-IRES-tetR-ERF058-TA**	Unpublished (Matias Zurbriggen)
pMZ1169	**SV40-PhyB FL-VP16-IRES-tetR-SPA1-TA**	Unpublished (Matias Zurbriggen)
pMZ1170	**SV40-PhyB FL-VP16-IRES-tetR-PIF3-TA**	Unpublished (Matias Zurbriggen)
pMZ1171	**SV40-PhyB FL-VP16-IRES-tetR-COR27-TA**	Unpublished (Matias Zurbriggen)
pMZ1172	**SV40-PhyB FL-VP16-IRES-tetR-COR28-TA**	Unpublished (Matias Zurbriggen)
pMZ1200	**SV40-VP16-IRES-tetR-TA**	(Müller et al., 2013a)
pMZ1203	**SV40-C_{120}-Firefly-B-LID-TA**	(Baaske et al., 2018)

pMZ1427	**SV40-PUMA-LOV-TA**	Unpublished (Matias Zurbriggen)
pTB034	**SV40-PhyB FL-VP16-IRES-tetR-PIF4-TA**	Unpublished (Tim Blomeier)
pTB035	**SV40-PhyB FL-VP16-IRES-tetR-PIF5-TA**	Unpublished (Tim Blomeier)
pTB036	**SV40-PhyB FL-VP16-IRES-tetR-PIF6-TA**	Unpublished (Tim Blomeier)
pTB038	**SV40-PhyB FL-VP16-IRES-tetR-PIF8-TA**	Unpublished (Tim Blomeier)
pTB039	**SV40-PhyB FL-VP16-IRES-tetR-TOC1-TA;** pPF009 linearized by *AscI* and *AsiSI*; TOC1 amplified with oTB169+170 from TOC1 containing plasmid (DKLAT5G61380.1; ABRC) and assembled by AQUA.	**This work**
pTB040	**SV40-PhyB FL-VP16-IRES-tetR-CCA1-TA;** pPF009 linearized by *AscI* and *AsiSI*; CCA1 amplified with oTB171+172 from CCA1 containing plasmid (DKLAT2G46830; ABRC) and assembled by AQUA.	**This work**
pTB043	**SV40-PhyB FL-VP16-IRES-tetR-LHY1-TA;** pPF009 linearized by *AscI* and *AsiSI*; LHY1 amplified with oTB177+178 from LHY1 containing plasmid (DKLAT1G01060; ABRC) and assembled by AQUA.	**This work**
pTB505	**SV40-BID-LOV-TA**	Unpublished (Tim Blomeier)

pLK001	**SV40-PhyB$^{1-650}$-VP16-E-PIF6$^{1-100}$-TA**	Unpublished (Leonie-Alexa Koch)
pLK002	**etr$_8$-CMV$_{min}$-SEAP-TA$_{BGH}$-SV40-Renilla-TA$_{SV40}$;** pKM082 linearized by *HindIII* and *SpeI*, BGH-TA was amplified by oPF007+oPF008 from pKM528, SV40 Promotor was amplified by oPF009+oPF010 from pKM022, Renilla was amplified by oPF011+oPF012 from StrigoQuant. All fragments were assembled by AQUA Cloning.	**This work**
pLK017	**´5LTR-etr3-CMV$_{min}$-SEAP-YFP-SV40-PhyB$^{1-650}$-VP16-IRES-E-PIF6$^{1-100}$-´3LTR**	Unpublished (Leonie-Alexa Koch)
pJA086	**SV40-GFP-TA;**	Unpublished (Jennifer Andres)
PIF1dNSL	**SV40-PhyB$^{1-650}$-VP16-E-PIF1.LS-TA**	Received from David Golonka
PIF1dN	**SV40-PhyB$^{1-650}$-VP16-E-PIF1-TA**	Received from David Golonka
PIF1dNsplitA	**SV40-PhyB$^{1-650}$-VP16-E-PIF1.A-TA**	Received from David Golonka
PIF1dNsplitB	**SV40-PhyB$^{1-650}$-VP16-E-PIF1.B-TA**	Received from David Golonka
PIF1	**SV40-PhyB$^{1-650}$-VP16-E-PIF1.100-TA**	Received from David Golonka
PIF1dNAPBfus	**SV40-PhyB$^{1-650}$-VP16-E-PIF1.fus-TA**	Received from David Golonka
pDG386	**SV40-PhyB$^{1-650}$-VP16-E-PIF1.Bs-TA**	Received from David Golonka
pDG394	**SV40-PhyB$^{1-650}$-VP16-E-PIF1.A8-TA**	Received from David Golonka

pDG406	**SV40-PhyB$^{1-650}$-VP16-E-PIF1.AA-TA**	Received from David Golonka
pDG407	**SV40-PhyB$^{1-650}$-VP16-E-PIF1.BB-TA**	Received from David Golonka
pDG409	**SV40-PhyB$^{1-650}$-VP16-E-PIF1.BA-TA**	Received from David Golonka
PIF1AA14	**SV40-PhyB$^{1-650}$-VP16-E-PIF1.A14-TA**	Received from David Golonka
PIF1AS19	**SV40-PhyB$^{1-650}$-VP16-E-PIF1.A19-TA**	Received from David Golonka
PIF1dNBAfus	**SV40-PhyB$^{1-650}$-VP16-E-PIF1.BAfus-TA**	Received from David Golonka
PIF1dNBBfus	**SV40-PhyB$^{1-650}$-VP16-E-PIF1.BBfus-TA**	Received from David Golonka
PIF1dNsAs	**SV40-PhyB$^{1-650}$-VP16-E-PIF1.As-TA**	Received from David Golonka
PIF1dNAAfus	**SV40-PhyB$^{1-650}$-VP16-E-PIF1.AAfus-TA**	Received from David Golonka
PIF3dNhk	**SV40-PhyB$^{1-650}$-VP16-E-PIF3.L1-TA**	Received from David Golonka
PIF3dNSL	**SV40-PhyB$^{1-650}$-VP16-E-PIF3.LS-TA**	Received from David Golonka
PIF3dNvk	**SV40-PhyB$^{1-650}$-VP16-E-PIF3.L2-TA**	Received from David Golonka
PIF3dN	**SV40-PhyB$^{1-650}$-VP16-E-PIF3-TA**	Received from David Golonka
PIF3	**SV40-PhyB$^{1-650}$-VP16-E-PIF3.100-TA**	Received from David Golonka
PIF3dNP1L	**SV40-PhyB$^{1-650}$-VP16-E-PIF3.LP1-TA**	Received from David Golonka
PIF3dNsplitA	**SV40-PhyB$^{1-650}$-VP16-E-PIF3.A-TA**	Received from David Golonka

PIF3dNsplitB	**SV40-PhyB$^{1-650}$-VP16-E-PIF3.B-TA**	Received from David Golonka
PIF3dNAA	**SV40-PhyB$^{1-650}$-VP16-E-PIF3.AA-TA**	Received from David Golonka
PIF3dNBB	**SV40-PhyB$^{1-650}$-VP16-E-PIF3.BB-TA**	Received from David Golonka
pDG366	**SV40-PhyB$^{1-650}$-VP16-E-PIF3.AAfus-TA**	Received from David Golonka
pDG367	**SV40-PhyB$^{1-650}$-VP16-E-PIF3.BBfus-TA**	Received from David Golonka
pDG379	**SV40-PhyB$^{1-650}$-VP16-E-PIF3.As-TA**	Received from David Golonka
pDG389	**SV40-PhyB$^{1-650}$-VP16-E-PIF3.A8-TA**	Received from David Golonka
pDG396	**SV40-PhyB$^{1-650}$-VP16-E-PIF3.Bs-TA**	Received from David Golonka
pDG398	**SV40-PhyB$^{1-650}$-VP16-E-PIF3.BA-TA**	Received from David Golonka
pDG400	**SV40-PhyB$^{1-650}$-VP16-E-PIF3.BAfus-TA**	Received from David Golonka
pDG410	**SV40-PhyB$^{1-650}$-VP16-E-PIF3.A-TA**	Received from David Golonka
PIF3AS14	**SV40-PhyB$^{1-650}$-VP16-E-PIF3.A14-TA**	Received from David Golonka
PIF3AS19	**SV40-PhyB$^{1-650}$-VP16-E-PIF3.A19-TA**	Received from David Golonka
PIF6	**SV40-PhyB$^{1-650}$-VP16-E-PIF6.100-TA**	Received from David Golonka
PIF6dN	**SV40-PhyB$^{1-650}$-VP16-E-PIF6-TA**	Received from David Golonka
PIF6dNAPBfus	**SV40-PhyB$^{1-650}$-VP16-E-PIF6.fus-TA**	Received from David Golonka

PIF6dNP1L	**SV40-PhyB$^{1-650}$-VP16-E-PIF6.LP1-TA**	Received from David Golonka
PIF6dsplitA	**SV40-PhyB$^{1-650}$-VP16-E-PIF6.A-TA**	Received from David Golonka
PIF6dNSL	**SV40-PhyB$^{1-650}$-VP16-E-PIF6.LS-TA**	Received from David Golonka
PIF6dNvk	**SV40-PhyB$^{1-650}$-VP16-E-PIF6.L2-TA**	Received from David Golonka
pDG373	**SV40-PhyB$^{1-650}$-VP16-E-PIF6.B-TA**	Received from David Golonka
pDG381	**SV40-PhyB$^{1-650}$-VP16-E-PIF6.Bs-TA**	Received from David Golonka
pDG390	**SV40-PhyB$^{1-650}$-VP16-E-PIF6.A8-TA**	Received from David Golonka
pDG397	**SV40-PhyB$^{1-650}$-VP16-E-PIF6.BB-TA**	Received from David Golonka
pDG399	**SV40-PhyB$^{1-650}$-VP16-E-PIF6.BA-TA**	Received from David Golonka
pDG401	**SV40-PhyB$^{1-650}$-VP16-E-PIF6.BBfus-TA**	Received from David Golonka
pDG402	**SV40-PhyB$^{1-650}$-VP16-E-PIF6.BAfus-TA**	Received from David Golonka
pDG403	**SV40-PhyB$^{1-650}$-VP16-E-PIF6.LS-TA**	Received from David Golonka
pDG404	**SV40-PhyB$^{1-650}$-VP16-E-PIF6.L2-TA**	Received from David Golonka
pDG405	**SV40-PhyB$^{1-650}$-VP16-E-PIF6.AA-TA**	Received from David Golonka
pDG408	**SV40-PhyB$^{1-650}$-VP16-E-PIF6.As-TA**	Received from David Golonka
PIF6AS14	**SV40-PhyB$^{1-650}$-VP16-E-PIF6.A14-TA**	Received from David Golonka

PIF6AS19	**SV40-PhyB$^{1-650}$-VP16-E-PIF6.A19-TA**	Received from David Golonka
PIF6dNAAfus	**SV40-PhyB$^{1-650}$-VP16-E-PIF6.AAfus-TA**	Received from David Golonka
pAAV-hSyn-ChR2	**ITR-hSyn-ChR2-YFP-WPRE-ITR**	Received from Ilka Diester
pC0043	**U6-PspCas13bDR-TA**	pC0043-PspCas13b crRNA backbone was a gift from Feng Zhang (Addgene plasmid # 103854 ; http://n2t.net/addgene:103854 ; RRID:Addgene_103854)
pC0046	**EF1α-PspCas13b-NES-TA**	pC0046-EF1a-PspCas13b-NES-HIV was a gift from Feng Zhang (Addgene plasmid # 103862)
pLJM1-GFP	**´5LTR-CMV-GFP-PGK-Puro^{r}-´3LTR**	pLJM1-EGFP was a gift from David Sabatini (Addgene plasmid # 19319 ; http://n2t.net/addgene:19319 ; RRID:Addgene_19319)
pTREX-B-LID-mCherry-2A-myrcasp8-ER(T2)	**SV40-B-LID-mCherry-2A-myrcasp8-ER(T2);**	(Baaske et al., 2018)

pTREX-myrcasp8-ER(T2)-IRES-mCherry	**SV40-myrcasp8-ER(T2)-IRES-mCherry;**	(Baaske et al., 2018)
pLKPF010	**´5LTR-etr3-CMV$_{min}$-SEAP-YFP-CMV-PhyB$^{1-650}$-VP16-IRES-E-PIF6$^{1-100}$-´3LTR;** pLK017 was linearized by *HpaI* + *AsiSI*, CMV was amplified from pLJM1-GFP with oLKPF026 + 27 and assembled by Gibson.	**This work**
pLKPF011	**´5LTR-etr$_8$-CMV$_{min}$-SEAP-YFP-CMV-PhyB$^{1-650}$-VP16-IRES-E-PIF6$^{1-100}$-´3LTR;** pLKPF010 was linearized by *PacI* + *SnaBI*, etr$_8$-CMV$_{min}$ was amplified from pLK002 with oPF071 + 50 and assembled by Gibson.	**This work**
pLKPF015	**´5LTR-etr$_8$-CMV$_{min}$-ChR2-YFP-CMV-PhyB$^{1-650}$-VP16-IRES-E-PIF6$^{1-100}$-´3LTR;** pLKPF011 was linearized by *PacI* + *AsiSI*, ChR2 was amplified from pAAV-hSyn-ChR2 plasmid with oLKPF036 + 37 and assembled by Gibson.	**This work**
pLKPF033	**´5LTR-etr$_8$-CMV$_{min}$-ChR2-YFP-´3LTR;** pLKPF015 was linearized by *AscI* + *AsiSI*, PGK was amplified from pLKPF015 plasmid with oLKPF069 + 70 and assembled by Gibson.	**This work**
pLKPF034	**´5LTR-CMV-PhyB$^{1-650}$-VP16-IRES-E-PIF6$^{1-100}$-´3LTR;** pLKPF015 was linearized by *SrfI* + *AsiSI*, BB was amplified from pPF001 plasmid with oLKPF071 + 72 and assembled by Gibson.	**This work**

pTBPF001	**Gal4UAS-PspCas13b-NES-HA-TA -** pKM083 was amplified with oTBPF003 + 004, PspCas13b was amplified from pC0046 with oTBPF001 + 002 an assembled by AQUA.	**This work**
pTBPF003	**U6-Firefly gRNA1-PspCas13bDR-TA -** pC0043 was linearized by *BbsI-HF* and assembled with oTBPF009 by AQUA.	**This work**
pTBPF004	**U6-Firefly gRNA2-PspCas13bDR-TA -** pC0043 was linearized by *BbsI-HF* and assembled with oTBPF010 by AQUA.	**This work**
pTBPF005	**U6-GFP gRNA1-PspCas13bDR-TA -** pC0043 was linearized by *BbsI-HF* and assembled with oTBPF011 by AQUA.	**This work**
pTBPF006	**U6-GFP gRNA2-PspCas13bDR-TA -** pC0043 was linearized by *BbsI-HF* and assembled with oTBPF012 by AQUA.	**This work**
pTBPF014	**SV40-mCherry-TA;** pJA086 was linearized by *NotI* + *XbaI*, mCherry was amplified from pMZ333 with oTBPF034 + 35 and were assembled by AQUA Cloning.	**This work**
pTBPF015	**SV40-Firefly-TA;** pLKPTBPF001 was linearized with *XhoI* + *BamHI*, SV40 was amplified from pMZ1203 with oTBPF036 + 37 and assembled with AQUA.	**This work**
pTBPF018	**PGK-GFP-TA;** pJA086 was linearized with *NheI* + *XhoI*, PGK was amplified from pLJM1-GFP with oTBPF041+42 and assembled with AQUA.	**This work**

pTBPF021	**U6-hCDK1 gRNA1-PspCas13bDR-TA -** pC0043 was linearized by *BbsI-HF* and assembled with oTBPF047 by AQUA.	**This work**
pTBPF022	**U6-hCDK1 gRNA2-PspCas13bDR-TA -** pC0043 was linearized by *BbsI-HF* and assembled with oTBPF048 by AQUA.	**This work**
pLKTBPF001	**CMV-Firefly-TA;**	Unpublished (Leonie-Alex Koch)
pPF001	**Modular pKM022 (SV40-PhyB$^{1-650}$-VP16-tetR-PIF6$^{1-100}$-TA);** pKM022 was amplified with oPF001/oPF002 and added *SpeI* and *AscI* site, PhyB$^{1-650}$ was amplified from pKM022 with oPF003/oPF004 and added *EcoRV* site, PIF6$^{1-100}$ was amplified from pKM022 with oPF005/oPF006 and added *BsrGI* site, VP16-IRES-tetR was excised by *EcoRV* from pMZ1200. All fragments were assembled by AQUA.	**This work**
pPF002	**tetO$_{13}$-CMV$_{min}$-SEAP-TA$_{BGH}$-SV40-Renilla-TA$_{SV40}$;** pKM006 linearized by *HindIII* and *SpeI*, BGH-TA was amplified by oPF007+oPF008 from pKM528, SV40 Promotor was amplified by oPF009+oPF010 from pKM022, Renilla was amplified by oPF011+oPF012 from StrigoQuant. All fragments were assembled by AQUA Cloning.	**This work**
pPF007	**SV40-PhyA FL-VP16-IRES-tetR-PIF6$^{1-100}$-TA;** pPF001 was linearized by *SpeI* and *EcoRV*, PhyA was amplified from pMZ1160 with oPF025 + oPF026 and assembled by AQUA	**This work**

pPF009	**SV40-PhyB FL-VP16-IRES-tetR-(BsrGI)PIF6(1-100)-TA);** pPF039 was linearised by *SpeI* and *EcoRV*, PhyB FL was amplified from pMZ333 with oPF027 + oPF028 and assembled by AQUA	**This work**
pPF012	**SV40-PhyA FL-VP16-IRES-tetR-NOT9a-TA;** pPF007 linearized by *AscI* and *BsrGI,* NOT9a was amplified with oPF106+oPF107 from NOT9a containing plasmid. All fragments were assembled by AQUA.	**This work**
pPF013	**SV40-PhyA FL-VP16-IRES-tetR-OPA-TA;** pPF007 linearized by *AscI* and *BsrGI,* OPA was amplified with oPF100+oPF101 from OPA containing plasmid. All fragments were assembled by AQUA.	**This work**
pPF014	**SV40-PhyA FL-VP16-IRES-tetR-ERF057-TA;** pPF007 linearized by *AscI* and *BsrGI,* ERF057 was amplified with oPF104+oPF105 from ERF057 containing plasmid. All fragments were assembled by AQUA.	**This work**
pPF015	**SV40-PhyA FL-VP16-IRES-tetR-JAZ9-TA;** pPF007 linearized by *AscI* and *BsrGI,* JAZ9 was amplified with oPF102+oPF103 from JAZ9 containing plasmid. All fragments were assembled by AQUA.	**This work**
pPF016	**SV40-PhyA FL-VP16-IRES-tetR-ERF055-TA;** pPF007 linearized by *AscI* and *BsrGI,* ERF055 was amplified with oPF108+oPF109 from ERF055 containing plasmid. All fragments were assembled by AQUA.	**This work**

pPF017	**SV40-PhyA(FL)-VP16-IRES-tetR-ERF056-TA;** pPF007 linearized by *AscI* and *BsrGI,* ERF056 was amplified with oPF110+oPF111 from ERF056 containing plasmid. All fragments were assembled by AQUA.	**This work**
pPF018	**SV40-PhyA FL-VP16-IRES-tetR-ERF059-TA;** pPF007 linearized by *AscI* and *BsrGI,* ERF059 was amplified with oPF112+oPF113 from ERF059 containing plasmid. All fragments were assembled by AQUA.	**This work**
pPF019	**SV40-PhyA FL-VP16-IRES-tetR-ERF060-TA;** pPF007 linearized by *AscI* and *BsrGI,* ERF060 was amplified with oPF114+oPF115 from ERF060 containing plasmid. All fragments were assembled by AQUA.	**This work**
pPF020	**SV40-PhyA FL-VP16-IRES-tetR-JAZ2-TA;** pPF007 linearized by *AscI* and *BsrGI,* JAZ2 was amplified with oPF116+oPF117 from JAZ2 containing plasmid. All fragments were assembled by AQUA.	**This work**
pPF021	**SV40-PhyA FL-VP16-IRES-tetR-JAZ6-TA;** pPF007 linearized by *AscI* and *BsrGI,* JAZ6 was amplified with oPF118+oPF119 from JAZ6 containing plasmid. All fragments were assembled by AQUA.	**This work**
pPF022	**SV40-PhyA FL-VP16-IRES-tetR-PIF1-TA;** pPF007 linearized by *AscI* and *BsrGI,* PIF1 was	**This work**

	amplified with oPF120+oPF121 from PIF1 containing plasmid. All fragments were assembled by AQUA.	
pPF023	**SV40-PhyA FL-VP16-IRES-tetR-NOT9b-TA;** pPF007 linearized by *AscI* and *BsrGI,* NOT9b was amplified with oPF122+oPF123 from NOT9b containing plasmid. All fragments were assembled by AQUA.	**This work**
pPF024	**SV40-PhyA FL-VP16-IRES-tetR-NOT9c-TA;** pPF007 linearized by *AscI* and *BsrGI,* NOT9c was amplified with oPF124+oPF125 from NOT9c containing plasmid. All fragments were assembled by AQUA.	**This work**
pPF025	**SV40-PhyA FL-VP16-IRES-tetR-COP1-TA;** pPF007 linearized by *AscI* and *BsrGI,* COP1 was amplified with oPF126+oPF127 from COP1 containing plasmid. All fragments were assembled by AQUA.	**This work**
pPF026	**SV40-PhyA FL-VP16-IRES-tetR-PCH1-TA;** pPF007 linearized by *AscI* and *BsrGI,* PCH1 was amplified with oPF128+oPF129 from PCH1 containing plasmid. All fragments were assembled by AQUA.	**This work**
pPF027	**SV40-PhyA FL-VP16-IRES-tetR-PCHL-TA;** pPF007 linearized by *AscI* and *BsrGI,* PCHL was amplified with oPF130+oPF131 from PCHL containing plasmid. All fragments were assembled by AQUA.	**This work**

pPF028	**SV40-PhyA FL-VP16-IRES-tetR-FHL-TA;** pPF007 linearized by *AscI* and *BsrGI,* FHL was amplified with oPF132+oPF133 from FHL containing plasmid. All fragments were assembled by AQUA.	**This work**
pPF029	**SV40-PhyA FL-VP16-IRES-tetR-FHY1-TA;** pPF007 linearized by *AscI* and *BsrGI,* FHY1 was amplified with oPF134+oPF135 from FHY1 containing plasmid. All fragments were assembled by AQUA.	**This work**
pPF034	**$tetO_{13}$-CMV_{min}-SEAP-TA_{BGH}-SV40-GLuc-TA_{SV40};** pPF002 linearized by *EcoRV* and *NotI*, Gluc was amplified by oPF047+oPF048 from pKM083 and were assembled by AQUA Cloning.	**This work**
pPF035	**etr_8-CMV_{min}-SEAP-TA_{BGH}-SV40-GLuc-TA_{SV40};** pLK002 linearized by *EcoRV* and *NotI*, Gluc was amplified by oPF047+oPF049 from pKM083 and were assembled by AQUA Cloning.	**This work**
pPF039	**SV40-$PhyB^{1-650}$-VP16-IRES-tetR-$PIF6^{1-}$100-TA**; pPF001 was amplified by oPF002 and oPF067, second part was amplified from pPF001 with oPF003+oPF068; All fragments were assembled by AQUA.	**This work**
pPF044	**SV40-PIF3-TA**; pMZ333 was linearised by *NotI* and *XbaI*, PIF3 was amplified from PIF3 containing plasmid with oPF076+oPF077; All fragments were assembled by AQUA.	**This work**

pPF058	**SV40-PhyA$^{1-651}$-VP16-IRES-tetR-PIF6$^{1-100}$-TA;** pPF001 was linearized by *SpeI* and *EcoRV*, PhyA$^{1-651}$ was amplified from pMZ1160 with oPF025 + oPF098 and assembled by AQUA	**This work**
pPF078	**SV40-PhyB FL-VP16-IRES-tetR-OPA;** pPF009 was linearized by *AsiSI* + *AscI* and OPA was amplified by oPF339+oPF340 from pPF013. All fragments were assembled by AQUA.	**This work**
pPF085	**SV40-PhyA$^{1-651}$-VP16-IRES-tetR-OPA-TA;** pPF058 was linearized by *BsrGI* + *AscI*, OPA was amplified from pPF013 with oPF100 + 101 and assembled by AQUA.	**This work**
pPF086	**SV40-PhyA FL-VP16-IRES-tetR-OPA$^{1-90}$-TA;** pPF007 was linearized by *BsrGI* + *AscI*, OPA$^{1-90}$ was amplified from pPF013 with oPF353 + 101 and assembled by AQUA.	**This work**
pPF087	**SV40-PhyA FL-VP16-IRES-tetR-OPA$^{91-180}$-TA;** pPF007 was linearized by *BsrGI* + *AscI*, OPA$^{91-180}$was amplified from pPF013 with oPF354 + 100 and assembled by AQUA.	**This work**
pPF088	**SV40-C$_{120}$-PUMA-LOV-Degron-TA;** pMZ1203 was amplified by oPF355+356, PUMA was amplified from PUMA containing plasmid with oPF357+358 and assembled with AQUA.	**This work**
pPF089	**SV40-PhyB FL-VP16-IRES-tetR-OPA$^{1-90}$-TA -** pPF009 was linearized by *AsiSI* + *AscI*, OPA$^{1-90}$	**This work**

	was amplified from pPF013 with oPF353 + 359 and assembled by AQUA.	
pPF090	**SV40-PhyA$^{1-617}$-VP16-IRES-tetR-OPA-TA -** pPF085 was amplified by oPF360 + 361 and assembled by AQUA.	**This work**
pPF092	**SV40-C$_{120}$-BID-LOV-Degron-TA;** pMZ1203 was amplified by oPF355+356, BID was amplified from BID containing plasmid with oPF364+365 and assembled with AQUA	**This work**
pPF131	**SV40-PhyB FL-VP16-IRES-tetR-PIF1;** pPF009 linearized by *AscI* and *AsiSI*; PIF1 amplified with oPF142+oPF121 from PIF containing plasmid and assembled by AQUA.	**This work**
pPF132	**SV40-PhyB FL-VP16-IRES-tetR-PCH1;** pPF009 linearized by *AscI* and *AsiSI*; PIF1 amplified with oPF143+oPF129 from PCH1 containing plasmid and assembled by AQUA.	**This work**
pPF133	**SV40-PhyB FL-VP16-IRES-tetR-PCHL;** pPF009 linearized by *AscI* and *AsiSI*; PIF1 amplified with oPF144+oPF131 from PCHL containing plasmid and assembled by AQUA.	**This work**
pPF139	**SV40-PhyB FL-VP16-IRES-tetR-JAZ1;** pPF009 linearized by *AscI* and *AsiSI*; JAZ1 amplified with oPF147+oPF148 from JAZ1 containing plasmid and assembled by AQUA.	**This work**
pPF140	**SV40-PhyB FL-VP16-IRES-tetR-JAZ2;** pPF009 linearized by *AscI* and *AsiSI*; JAZ2 amplified with	**This work**

	oPF149+oPF150 from JAZ2 containing plasmid and assembled by AQUA.	
pPF141	**SV40-PhyB FL-VP16-IRES-tetR-JAZ3;** pPF009 linearized by *AscI* and *AsiSI*; JAZ3 amplified with oPF151+oPF152 from JAZ3 containing plasmid and assembled by AQUA.	**This work**
pPF142	**SV40-PhyB FL-VP16-IRES-tetR-JAZ4;** pPF009 linearized by *AscI* and *AsiSI*; JAZ4 amplified with oPF153+oPF154 from JAZ4 containing plasmid and assembled by AQUA.	**This work**
pPF143	**SV40-PhyB FL-VP16-IRES-tetR-JAZ5;** pPF009 linearized by *AscI* and *AsiSI*; JAZ5 amplified with oPF155+oPF156 from JAZ5 containing plasmid and assembled by AQUA.	**This work**
pPF144	**SV40-PhyB FL-VP16-IRES-tetR-JAZ6;** pPF009 linearized by *AscI* and *AsiSI*; JAZ6 amplified with oPF157+oPF158 from JAZ6 containing plasmid and assembled by AQUA.	**This work**
pPF145	**SV40-PhyB FL-VP16-IRES-tetR-JAZ7;** pPF009 linearized by *AscI* and *AsiSI*; JAZ7 amplified with oPF159+oPF160 from JAZ7 containing plasmid and assembled by AQUA.	**This work**
pPF146	**SV40-PhyB FL-VP16-IRES-tetR-JAZ8;** pPF009 linearized by *AscI* and *AsiSI*; JAZ8 amplified with oPF161+oPF162 from JAZ8 containing plasmid and assembled by AQUA.	**This work**

pPF147	**SV40-PhyB FL-VP16-IRES-tetR-JAZ9;** pPF009 linearized by *AscI* and *AsiSI*; JAZ9 amplified with oPF163+oPF164 from JAZ9 containing plasmid and assembled by AQUA.	**This work**
pPF148	**SV40-PhyB FL-VP16-IRES-tetR-JAZ10;** pPF009 linearized by *AscI* and *AsiSI*; JAZ10 amplified with oPF165+oPF166 from JAZ10 containing plasmid and assembled by AQUA.	**This work**
pPF149	**SV40-PhyB FL-VP16-IRES-tetR-JAZ11;** pPF009 linearized by *AscI* and *AsiSI*; JAZ11 amplified with oPF167+oPF168 from JAZ11 containing plasmid and assembled by AQUA.	**This work**
pPF150	**SV40-PhyB FL-VP16-IRES-tetR-JAZ12;** pPF009 linearized by *AscI* and *AsiSI*; JAZ12 amplified with oPF169+oPF170 from JAZ12 containing plasmid and assembled by AQUA.	**This work**
pPF151	**SV40-PhyA FL-VP16-IRES-tetR-JAZ3;** pPF007 was linearized by *AscI* and *BsrGI*; JAZ3 was amplified with oPF171+oPF152 from JAZ3 containing plasmid and assembled by AQUA.	**This work**
pPF152	**SV40-PhyA FL-VP16-IRES-tetR-JAZ4;** pPF007 was linearized by *AscI* and *BsrGI*; JAZ4 was amplified with oPF172+oPF154 from JAZ4 containing plasmid and assembled by AQUA.	**This work**
pPF153	**SV40-PhyA FL-VP16-IRES-tetR-JAZ7;** pPF007 was linearized by *AscI* and *BsrGI*; JAZ7 was	**This work**

	amplified with oPF173+oPF160 from JAZ7 containing plasmid and assembled by AQUA.	
pPF154	**SV40-PhyA FL-VP16-IRES-tetR-JAZ8;** pPF007 was linearized by *AscI* and *BsrGI*; JAZ8 was amplified with oPF174+oPF162 from JAZ8 containing plasmid and assembled by AQUA.	**This work**
pPF155	**SV40-PhyA FL-VP16-IRES-tetR-JAZ10;** pPF007 was linearized by *AscI* and *BsrGI*; JAZ10 was amplified with oPF175+oPF166 from JAZ10 containing plasmid and assembled by AQUA.	**This work**
pPF156	**SV40-PhyA FL-VP16-IRES-tetR-JAZ11;** pPF007 was linearized by *AscI* and *BsrGI*; JAZ11 was amplified with oPF176+oPF168 from JAZ11 containing plasmid and assembled by AQUA.	**This work**
pPF157	**SV40-PhyA FL-VP16-IRES-tetR-JAZ12;** pPF007 was linearized by *AscI* and *BsrGI*; JAZ12 was amplified with oPF177+oPF170 from JAZ12 containing plasmid and assembled by AQUA.	**This work**

Tab. 3: Oligonucleotides used in this work.

Oligo	Sequence (5´→ 3´)
oTB169	GGCGGTGGAAGTGGTGGCGGAGGTAGCGATGCGATCGCTATGGATTTGAACGGTGAGTG
oTB170	TATCTTATCATGTCTGGATCGAAGCTTTTAGGCGCGCCTCAAGTTCCCAAAGCATCAT
oTB171	GGCGGTGGAAGTGGTGGCGGAGGTAGCGATGCGATCGCTATGGAGACAAATTCGTCTGG

oTB172	TATCTTATCATGTCTGGATCGAAGCTTTTAGGCGCGCCTCATGTGGAAGCTTGAGTTTC
oTB177	GGCGGTGGAAGTGGTGGCGGAGGTAGCGATGCGATCGCTATGGATACTAATACATCTGGAGAA
oTB178	TATCTTATCATGTCTGGATCGAAGCTTTTAGGCGCGCCTCATGTAGAAGCTTCTCCTT
oPF001	TGTTCCAGATTACGCTGGCGCGCCTAAAAGCTTCGATCCAGACATGATAAGATACATTG
oPF002	CGGAAACCATGGTGGGACTAGTCAATTCCGATCCGGGACCTGAAATAAAAGA
oPF003	TCCCGGATCGGAATTGACTAGTCCCACCATGGTTTCCGGAGTCG
oPF004	GCACTACCAGCACTACCAGCACTATCGAATTCGATATCACCTAACTCATCAATCCCCTGTTCCC
oPF005	GAGGCGGTGGAAGTGGTGGCGGAGGTAGCGATTGTACAATGATGTTCTTACCAACCGATTATTGTTGCAGG
oPF006	TTATCATGTCTGGATCGAAGCTTTTAGGCGCGCCAGCGTAATCTGGAACATCGTATGGGTAGT
oPF007	ACCTACAGCCCAGTGGCCTCGAGCTGCAGAAAGCTTCTTAAGCGACTGTGCCTTCTAGTTGCCAGC
oPF008	GACACACATTCCACAGCCATAGAGCCCACCGCATCCC
oPF009	GCGGTGGGCTCTATGGCTGTGGAATGTGTGTCAGTTAGGGTG
oPF010	TTCGAAGTCATGGTGGGATATCGCAATTCCGATCCGGGACCTGAAATAAAA
oPF011	CCCGGATCGGAATTGCGATATCCCACCATGACTTCGAAAGTTTATGATCCAG
oPF012	AACGCGTATTTAAATTAATTAAGCGATCGCACTAGTGCGGCCGCTTATTGTTCATTTTTGAGAACTCGCTCAACGAAC
oPF025	TTTGTCTTTTATTTCAGGTCCCGGATCGGAATTGACTAGTCCACCATGGATTCAGGCTCTAGGC
oPF026	GCACTACCAGCACTACCAGCACTATCGAATTCGATCTTGTTTGCTGCAGCGAGTTCCGC

oPF027	TTTGTCTTTTATTTCAGGTCCCGGATCGGAATTGACTAGTCCACCATG GTTTCCGGAGTCGG
oPF028	GCACTACCAGCACTACCAGCACTATCGAATTCGATATATGGCATCATC AGCATCATGTCACCACT
oPF047	TTTTATTTCAGGTCCCGGATCGGAATTGCGATATCCCACCATGGGAGT CAAAGTTCTGTTTG
oPF048	TAAATTAATTAAGCGATCGCACTAGTGCGGCCGCTTAGTCACCACCG GCCCCCTTG
oPF049	GTTTAAACATCGATTGATCAGGCGCGGCGGCCGCTTAGTCACCACCG GCCCCCTTG
oPF050	AGCAGCAGCATGCAGGAAGCTGACTCTAGAGGATCCCCGGGCGAGT TAATTAACGGTACCGGGGCCGCGG
oPF067	CTGGAGGCGGTGGAAGTGGTGGCGGAGGTAGCGATGCGATCGCTAT GATGTTCTTACCAACCGATTATTGTTGCAGG
oPF068	AACCTGCAACAATAATCGGTTGGTAAGAACATCATAGCGATCGCATC GCTACCTCCGCCACCACTTC
oPF071	CCTTATGGGACTTTCCTACTTGGCAGTACATCTACGCCCGGGCCGTC GACGATCGACCTGCAGG
oPF076	TTTTGTCTTTTATTTCAGGTCCCGGATCGAATTGCGGCCGCCCACCAT GCCTCTGTTTGAGCTTTTCAGGCTCAC
oPF077	TCTGGATCGAAGCTTGGGCTGCAGGTCGACTCTAGTTACGACGATCC ACAAAACTGATCAGAAGAC
oPF098	GCACTACCAGCACTACCAGCACTATCGAATTCGATCTCAGCAATTTTC GTGTTCCAACCATTAACC
oPF100	ATCATGTCTGGATCGAAGCTTTTAGGCGCGCCTTAAGCTCCATTATAC GAATCAATCGTCACTTCTTC
oPF101	CTGGAGGCGGTGGAAGTGGTGGCGGAGGTAGCGATTGTACAATGGA GCCTCCTTTTGAAAGATCGAAAC
oPF102	ATCATGTCTGGATCGAAGCTTTTAGGCGCGCCTTATGTAGGAGAAGT AGAAGAGTAATTCATTCCACTG
oPF103	CTGGAGGCGGTGGAAGTGGTGGCGGAGGTAGCGATTGTACAATGGA AAGAGATTTTCTGGGTTTGAGCGA

oPF104	ATCATGTCTGGATCGAAGCTTTTAGGCGCGCCTTAGAAGAGTTTCTCT ATAGCGTCCCAATCAATCT
oPF105	CTGGAGGCGGTGGAAGTGGTGGCGGAGGTAGCGATTGTACAATGGC TTTAAACATGAATGCTTACGTAGACGA
oPF106	ATCATGTCTGGATCGAAGCTTTTAGGCGCGCCTACACTTTCCGCTTTT TCTTGGGAAGCATGTGCTCAAATCCTCCACCTTGAT
oPF107	CTGGAGGCGGTGGAAGTGGTGGCGGAGGTAGCGATTGTACAATGGC GAATCTACCTTCTTCTCTCTCCAT
oPF108	ATCATGTCTGGATCGAAGCTTTTAGGCGCGCCTTACGATAAAATTGAA GCCCAATCTATCTCATAAGAAG
oPF109	CTGGAGGCGGTGGAAGTGGTGGCGGAGGTAGCGATTGTACAATGGC GGATCTCTTCGGTGGTG
oPF110	ATCATGTCTGGATCGAAGCTTTTAGGCGCGCCTTAAGAATTGGCCAG TTTACTAATTGCATCCCAATC
oPF111	CTGGAGGCGGTGGAAGTGGTGGCGGAGGTAGCGATTGTACAATGGA AACTGCTTCTCTTTCTTTCCCTGTC
oPF112	ATCATGTCTGGATCGAAGCTTTTAGGCGCGCCTTAAGCTAGAATCGA ATCCCAATCGATCTCGTA
oPF113	CTGGAGGCGGTGGAAGTGGTGGCGGAGGTAGCGATTGTACAATGGC AGCTGCTATGAATTTGTACACTTGTA
oPF114	ATCATGTCTGGATCGAAGCTTTTAGGCGCGCCTTAAGATTCGGACAAT TTGCTAATCGCATCCCAAT
oPF115	CTGGAGGCGGTGGAAGTGGTGGCGGAGGTAGCGATTGTACAATGGC AGCCATAGATATGTTCAATAGCAACA
oPF116	ATCATGTCTGGATCGAAGCTTTTAGGCGCGCCTTACCGTGAACTGAG CCAAGCTGGGT
oPF117	CTGGAGGCGGTGGAAGTGGTGGCGGAGGTAGCGATTGTACAATGTC GAGTTTTTCTGCCGAGTGTTG
oPF118	ATCATGTCTGGATCGAAGCTTTTAGGCGCGCCTTAAAGCTTGAGTTCA AGGTTTTTGGAAGATTGTCC
oPF119	CTGGAGGCGGTGGAAGTGGTGGCGGAGGTAGCGATTGTACAATGTC AACGGGACAAGCGCC

oPF120	TGGAGGCGGTGGAAGTGGTGGCGGAGGTAGCGATTGTACAATGCAT CATTTTGTCCCTGACTTCGATACCG
oPF121	ATGTATCTTATCATGTCTGGATCGAAGCTTTTAGGCGCGCCTTAACCT GTTGTGTGGTTTCCGTGATCCTC
oPF122	GTTCTGGAGGCGGTGGAAGTGGTGGCGGAGGTAGCGATTGTACAAT GGCTAATCTTCCTCCTCCGCTCTCC
oPF123	CAATGTATCTTATCATGTCTGGATCGAAGCTTTTAGGCGCGCCCTACA CTTTCCGCTTTTTCTTGGGATTCACAAACATATGAGCCAACCCTTGAG GTG
oPF124	GTTCTGGAGGCGGTGGAAGTGGTGGCGGAGGTAGCGATTGTACAAT GTCGGAAAACATGGTGAATCTACCGGATTCT
oPF125	CAATGTATCTTATCATGTCTGGATCGAAGCTTTTAGGCGCGCCCTACA CTTTCCGCTTTTTCTTGGGGTTGTCCAGATTCTGAAGCAGCTGAATTC GA
oPF126	CTGGAGGCGGTGGAAGTGGTGGCGGAGGTAGCGATTGTACAATGGA AGAGATTTCGACGGACCCGGT
oPF127	CAATGTATCTTATCATGTCTGGATCGAAGCTTTTAGGCGCGCCCTACG CAGCGAGTACCAGAACTTTGATGG
oPF128	CTGGAGGCGGTGGAAGTGGTGGCGGAGGTAGCGATTGTACAATGTC TGAACATGTTATGGTTTTGGGTAAAGGTAACAAAG
oPF129	CAATGTATCTTATCATGTCTGGATCGAAGCTTTTAGGCGCGCCCTACC TCAAATCCCTTGCATTCCAAACCATGAGA
oPF130	CTGGAGGCGGTGGAAGTGGTGGCGGAGGTAGCGATTGTACAATGTC TGAACATTTTATGGGCTTAAGCAAGATTAAGACAGAA
oPF131	CAATGTATCTTATCATGTCTGGATCGAAGCTTTTAGGCGCGCCCTAAC TTAAATCCTCAGCATTCCAAACGAAGAGGGA
oPF132	CTGGAGGCGGTGGAAGTGGTGGCGGAGGTAGCGATTGTACAATGAT AGTTGCTGTGGAATCTCTAGACACAAGCA
oPF133	CAATGTATCTTATCATGTCTGGATCGAAGCTTTTAGGCGCGCCCTACA TCATGAGTGTAGAAAAGTACTGCTCAAACTCTTGATCA
oPF134	CAATGTATCTTATCATGTCTGGATCGAAGCTTTTAGGCGCGCCCTACA GCATTAGCGTTGAGAAGTATTGTTCAAATTCTTGATCA

oPF135	CTGGAGGCGGTGGAAGTGGTGGCGGAGGTAGCGATTGTACACCTGAAGTGGAAGTGGATAACAACAACGAGAA
oPF142	GGAGGCGGTGGAAGTGGTGGCGGAGGTAGCGATGCGATCGCTATGCATCATTTTGTCCCTGACTTCGATACCG
oPF143	GGAGGCGGTGGAAGTGGTGGCGGAGGTAGCGATGCGATCGCTATGTCTGAACATGTTATGGTTTTGGGTAAAGGTAACAAAG
oPF144	GGAGGCGGTGGAAGTGGTGGCGGAGGTAGCGATGCGATCGCTATGTCTGAACATTTTATGGGCTTAAGCAAGATTAAGACAGAA
oPF147	GGAGGCGGTGGAAGTGGTGGCGGAGGTAGCGATGCGATCGCTATGTCGAGTTCTATGGAATGTT
oPF148	CAATGTATCTTATCATGTCTGGATCGAAGCTTTTAGGCGCGCCTCATATTTCAGCTGCTAAACCGAG
oPF149	GGAGGCGGTGGAAGTGGTGGCGGAGGTAGCGATGCGATCGCTATGTCGAGTTTTTCTGCCG
oPF150	CAATGTATCTTATCATGTCTGGATCGAAGCTTTTAGGCGCGCCTTACCGTGAACTGAGCCAAG
oPF151	GGAGGCGGTGGAAGTGGTGGCGGAGGTAGCGATGCGATCGCTATGGAGAGAGATTTTCTCGGGTTGGG
oPF152	CAATGTATCTTATCATGTCTGGATCGAAGCTTTTAGGCGCGCCTTAGGTTGCAGAGCTGAGAGAAGAACT
oPF153	GGAGGCGGTGGAAGTGGTGGCGGAGGTAGCGATGCGATCGCTATGGAGAGAGATTTTCTCGGGCTGG
oPF154	CAATGTATCTTATCATGTCTGGATCGAAGCTTTTAGGCGCGCCTTAGTGCAGATGATGAGCTGGAGGAC
oPF155	GGAGGCGGTGGAAGTGGTGGCGGAGGTAGCGATGCGATCGCTATGTCGTCGAGCAATGAAAATGCTAAGG
oPF156	CAATGTATCTTATCATGTCTGGATCGAAGCTTTTAGGCGCGCCCTATAGCCTTAGATCGAGATCTTTCGAACTTTGG
oPF157	GGAGGCGGTGGAAGTGGTGGCGGAGGTAGCGATGCGATCGCTATGTCAACGGGACAAGCGCC
oPF158	CAATGTATCTTATCATGTCTGGATCGAAGCTTTTAGGCGCGCCCTAAAGCTTGAGTTCAAGGTTTTTGGAAGATTGT

oPF159	GGAGGCGGTGGAAGTGGTGGCGGAGGTAGCGATGCGATCGCTATGA TCATCATCATCAAAAACTGCGACAAGC
oPF160	CAATGTATCTTATCATGTCTGGATCGAAGCTTTTAGGCGCGCCCTATC GGTAACGGTGGTAAGGGGAAG
oPF161	GGAGGCGGTGGAAGTGGTGGCGGAGGTAGCGATGCGATCGCTATGA AGCTACAGCAAAATTGTGACTTGGAA
oPF162	CAATGTATCTTATCATGTCTGGATCGAAGCTTTTAGGCGCGCCTTATC GTCGTGAATGGTACGGTGAAGTAG
oPF163	GGAGGCGGTGGAAGTGGTGGCGGAGGTAGCGATGCGATCGCTATG GAAAGAGATTTTCTGGGTTTGAGCG
oPF164	CAATGTATCTTATCATGTCTGGATCGAAGCTTTTAGGCGCGCCTTATG TAGGAGAAGTAGAAGAGTAATTCATTCCAC
oPF165	GGAGGCGGTGGAAGTGGTGGCGGAGGTAGCGATGCGATCGCTATGT CGAAAGCTACCATAGAACTCGATTTCC
oPF166	CAATGTATCTTATCATGTCTGGATCGAAGCTTTTAGGCGCGCCTTAGG CCGATGTCGGATAGTAAGGAGA
oPF167	GGAGGCGGTGGAAGTGGTGGCGGAGGTAGCGATGCGATCGCTATG GCTGAGGTAAACGGAGATTTCCC
oPF168	CAATGTATCTTATCATGTCTGGATCGAAGCTTTTAGGCGCGCCTCATG TCACAATGGGGCTGGTTTC
oPF169	GGAGGCGGTGGAAGTGGTGGCGGAGGTAGCGATGCGATCGCTATGA CTAAGGTGAAAGATGAGCCACG
oPF170	CAATGTATCTTATCATGTCTGGATCGAAGCTTTTAGGCGCGCCCTAAG CAGTTGGAAATTCCTCCTTGATAGAGA
oPF171	CTGGAGGCGGTGGAAGTGGTGGCGGAGGTAGCGATTGTACAATGGA GAGAGATTTTCTCGGGTTGGG
oPF172	CTGGAGGCGGTGGAAGTGGTGGCGGAGGTAGCGATTGTACAATGGA GAGAGATTTTCTCGGGCTGG
oPF173	CTGGAGGCGGTGGAAGTGGTGGCGGAGGTAGCGATTGTACAATGAT CATCATCATCAAAAACTGCGACAAG
oPF174	CTGGAGGCGGTGGAAGTGGTGGCGGAGGTAGCGATTGTACAATGAA GCTACAGCAAAATTGTGACTTGGAA

oPF175	CTGGAGGCGGTGGAAGTGGTGGCGGAGGTAGCGATTGTACAATGTC GAAAGCTACCATAGAACTCGATTTC
oPF176	CTGGAGGCGGTGGAAGTGGTGGCGGAGGTAGCGATTGTACAATGGC TGAGGTAAACGGAGATTTCCC
oPF177	CTGGAGGCGGTGGAAGTGGTGGCGGAGGTAGCGATTGTACAATGAC TAAGGTGAAAGATGAGCCACGC
oPF339	GGCGGTGGAAGTGGTGGCGGAGGTAGCGATGCGATCGCATGGAGC CTCCTTTTGAAAGATCGAAACG
oPF340	ATCTTATCATGTCTGGATCGAAGCTTTTAGGCGCGCCTTAAGCTCCAT TATACGAATCAATCGTCACTTCTTC
oPF353	ATCTTATCATGTCTGGATCGAAGCTTTTAGGCGCGCCTTAAGGTTCAC TACACGCAGCTCTTCTCATC
oPF354	TGGAGGCGGTGGAAGTGGTGGCGGAGGTAGCGATTGTACAATGGGA GAAGAAATTGAAATTGGCGTTAATAAGAG
oPF355	TTTTTGGCTACTACACTTGAACGTATTGAGAAG
oPF356	GGTGGCTTTACCAACAGTACCGGATTG
oPF357	CAGCTTGGCAATCCGGTACTGTTGGTAAAGCCACCATGGCCCGCGCA CGCCAG
oPF358	TTCTTCTCAATACGTTCAAGTGTAGTAGCCAAAAAGGCGCCGGCGCC GCTAGCGTTGGGCTCCATTTCTGGGGCTC
oPF359	GGCGGTGGAAGTGGTGGCGGAGGTAGCGATGCGATCGCTATGGAG CCTCCTTTTGAAAGATCGAAACG
oPF360	ATCTCAAAATTGATGGTATACAAGAACTAGAAGCTATCGAATTCGATA GTGCTGGTAGTGCTG
oPF361	GCACTACCAGCACTACCAGCACTATCGAATTCGATAGCTTCTAGTTCT TGTATACCATCAATTTTGAGATC
oPF364	CAGCTTGGCAATCCGGTACTGTTGGTAAAGCCACCATGGACTGTGAG GTCAACAACGGTTC
oPF365	TTCTTCTCAATACGTTCAAGTGTAGTAGCCAAAAAGGCGCCGGCGCC GCTAGCGTCCATCCCATTTCTGGCTAAGCTC
oLKPF026	GGCACCACCGACGCCGCGCACCCGGGTTAAGCGATCGCGTGATGCG GTTTTGGCAGTACATCAATG

oLKPF027	TGAAATAAAAGACAAAAAGACTAAACTTACCAGTTAACGATCTGACGG TTCACTAAACCAGCTC
oLKPF036	ACCGATCCAGCCTCCGCGGCCCCGGTACCGTTAATTAACCACCATGG ACTATGGCGGCG
oLKPF037	CGCCCATTGATGTACTGCCAAAACCGCATCACGCGATCGCTTACTTG TACAGCTCGTCCATGCCGAG
oLKPF069	ACTCTCGGCATGGACGAGCTGTACAAGTAAGCGATCGCATTTTAAAA GAAAAGGGGGGATTGGGGGG
oLKPF070	CGCACCGCCCCTTCCCGGCCGCTGCTCTCGGCGCGCCCTGCTGAGC AGCCGCTATTG
oLKPF071	GGACTTTCCTACTTGGCAGTACATCTACGTAGCCCGGGCTTAATTAAC GAAAAGTGCCACCTGACGTCTAAG
oLKPF072	CGCCCATTGATGTACTGCCAAAACCGCATCACGCGATCGCCAGAAGC TAGCTTATCGATGATAAGCTGTC
oTBPF001	CGTTCGAGATCTGCGATCTAAGTAAGCTTGGCCACCATGAACATCCC CGCTCTGGTGGAAAAC
oTBPF002	CTCCCATTCATAAGTTCCATAGGATGGGCGGCCGCTTAGGCATAGTC GGGGACATCATATGG
oTBPF003	GCGGCCGCCCATCCTATGG
oTBPF004	GGTGGCCAAGCTTACTTAGATCGCAG
oTBPF009	ATAGCCCCTCAAAACTGGACCTTCCACAACGAGGTGGACATTACCTA CGCCGAGTACTTCGGTGTTTCGTCCTTTCCACAAGATATATAA
oTBPF010	ATAGCCCCTCAAAACTGGACCTTCCACAACCACGGTAAAACCATGAC CGAGAAGGAGATCGGTGTTTCGTCCTTTCCACAAGATATATAA
oTBPF011	ATAGCCCCTCAAAACTGGACCTTCCACAACCTGGACGGCGACGTAAA CGGCCACAAGTTCGGTGTTTCGTCCTTTCCACAAGATATATAA
oTBPF012	ATAGCCCCTCAAAACTGGACCTTCCACAACACCCAGTCCAAGCTGAG CAAAGACCCCAACCGGTGTTTCGTCCTTTCCACAAGATATATA
oTBPF034	TTTTGTCTTTTATTTCAGGTCCCGGATCGAATTGCGGCCGCATGGTGA GCAAGGGCGAGGAGG
oTBPF035	CTGGATCGAAGCTTGGGCTGCAGGTCGACTTCTAGACTACTTGTACA GCTCGTCCATGCCG

oTBPF036	CATGTTTGACAGCTTATCATCGATAAGCTAGCTTGGATCCCTGTGGAA TGTGTGTCAGTTAGGGTG
oTBPF037	TTACCAGTTAACTTTCTGGTTTTCCAGTTCCTCGAGAGCTTTTTGCAAA AGCCTAGGCCTCC
oTBPF041	TTCTCATGTTTGACAGCTTATCATCGATAAGCTAGCTTGGGGTTGCGC CTTTTCCAAGGC
oTBPF042	TTACCAGTTAACTTTCTGGTTTTCCAGTTCCTCGAGCTGGGGAGAGAG GTCGGTGATTC
oTBPF047	ATAGCCCCTCAAAACTGGACCTTCCACAACGCCAGAGCTTTTGGAAT ACCTATCAGAGTAGGTGTTTCGTCCTTTCCACAAGATATATAA
oTBPF048	ATAGCCCCTCAAAACTGGACCTTCCACAACGGGCACTCCCAATAATG AAGTGTGGCCAGAGGTGTTTCGTCCTTTCCACAAGATATATAA

Tab. 4: Designed gRNAs to target mRNA in this work.

gRNA plasmid	Target	Sequence (5´→ 3´)
pTBPF003	Firefly luciferase	GAGGTGGACATTACCTACGCCGAGTACTTC
pTBPF004	Firefly luciferase	CACGGTAAAACCATGACCGAGAAGGAGATC
pTBPF005	eGFP	CTGGACGGCGACGTAAACGGCCACAAGTTC
pTBPF006	eGFP	ACCCAGTCCAAGCTGAGCAAAGACCCCAAC
pTBPF020	hCDK1	CCAGAGCTTTTGGAATACCTATCAGAGT
pTBPF021	hCDK1	GGCACTCCCAATAATGAAGTGTGGCCAG

6 References

Adamantidis AR, Zhang F, Aravanis AM, Deisseroth K, de Lecea L (2007) Neural substrates of awakening probed with optogenetic control of hypocretin neurons. Nature **450**: 420–424

Adams DO, Yang SF (1979) Ethylene biosynthesis: Identification of 1-aminocyclopropane-1-carboxylic acid as an intermediate in the conversion of methionine to ethylene. Proc Natl Acad Sci **76**: 170–174

Adrian M, Nijenhuis W, Hoogstraaten RI, Willems J, Kapitein LC (2017) A Phytochrome-Derived Photoswitch for Intracellular Transport. ACS Synth Biol **6**: 1248–1256

Akinc A, Querbes W, De S, Qin J, Frank-Kamenetsky M, Jayaprakash KN, Jayaraman M, Rajeev KG, Cantley WL, Dorkin JR, et al (2010) Targeted Delivery of RNAi Therapeutics With Endogenous and Exogenous Ligand-Based Mechanisms. Mol Ther **18**: 1357–1364

Al-Sady B, Ni W, Kircher S, Schäfer E, Quail PH (2006) Photoactivated phytochrome induces rapid PIF3 phosphorylation prior to proteasome-mediated degradation. Mol Cell **23**: 439–46

Anderson JC, Clarke EJ, Arkin AP, Voigt CA (2006) Environmentally Controlled Invasion of Cancer Cells by Engineered Bacteria. J Mol Biol **355**: 619–627

Andres J, Blomeier T, Zurbriggen MD (2019) Synthetic Switches and Regulatory Circuits in Plants. Plant Physiol **179**: 862–884

Arae T, Morita K, Imahori R, Suzuki Y, Yasuda S, Sato T, Yamaguchi J, Chiba Y (2019) Identification of Arabidopsis CCR4-NOT Complexes with Pumilio RNA-Binding Proteins, APUM5 and APUM2. Plant Cell Physiol **60**: 2015–2025

Archer E, Süel GM (2013) Synthetic biological networks. Reports Prog Phys **76**: 096602

Arenkiel BR, Peca J, Davison IG, Feliciano C, Deisseroth K, Augustine GJ, Ehlers MD, Feng G (2007) In vivo light-induced activation of neural circuitry in transgenic mice expressing channelrhodopsin-2. Neuron **54**: 205–18

Ausländer D, Wieland M, Ausländer S, Tigges M, Fussenegger M (2011) Rational design of a small molecule-responsive intramer controlling transgene expression in mammalian cells. Nucleic Acids Res **39**: e155

Baaske J, Gonschorek P, Engesser R, Dominguez-Monedero A, Raute K, Fischbach P, Müller K, Cachat E, Schamel WWA, Minguet S, et al (2018) Dual-controlled optogenetic system for the rapid down-regulation of protein levels in mammalian cells. Sci Rep **8**: 15024

Ballaré CL (2011) Jasmonate-induced defenses: a tale of intelligence, collaborators and rascals. Trends Plant Sci **16**: 249–257

Barnea G, Strapps W, Herrada G, Berman Y, Ong J, Kloss B, Axel R, Lee KJ (2008) The genetic design of signaling cascades to record receptor activation. Proc Natl Acad Sci **105**: 64–69

Barrangou R, Doudna JA (2016) Applications of CRISPR technologies in research and beyond. Nat Biotechnol **34**: 933–941

Bauer D, Viczián A, Kircher S, Nobis T, Nitschke R, Kunkel T, Panigrahi KCS, Adám E, Fejes E, Schäfer E, et al (2004) Constitutive photomorphogenesis 1 and multiple photoreceptors control degradation of phytochrome interacting factor 3, a transcription factor required for light signaling in Arabidopsis. Plant Cell **16**: 1433–45

Beerli RR, Dreier B, Barbas CF (2000) Positive and negative regulation of endogenous genes by

designed transcription factors. Proc Natl Acad Sci **97**: 1495–1500

Betley JN, Sternson SM (2011) Adeno-associated viral vectors for mapping, monitoring, and manipulating neural circuits. Hum Gene Ther **22**: 669–77

Beyer HM, Gonschorek P, Samodelov SL, Meier M, Weber W, Zurbriggen MD (2015a) AQUA Cloning: A Versatile and Simple Enzyme-Free Cloning Approach. PLoS One **10**: e0137652

Beyer HM, Juillot S, Herbst K, Samodelov SL, Müller K, Schamel WW, Römer W, Schäfer E, Nagy F, Strähle U, et al (2015b) Red Light-Regulated Reversible Nuclear Localization of Proteins in Mammalian Cells and Zebrafish. ACS Synth Biol **4**: 951–958

Beyer HM, Naumann S, Weber W, Radziwill G (2015c) Optogenetic control of signaling in mammalian cells. Biotechnol J **10**: 273–283

Bikard D, Jiang W, Samai P, Hochschild A, Zhang F, Marraffini LA (2013) Programmable repression and activation of bacterial gene expression using an engineered CRISPR-Cas system. Nucleic Acids Res **41**: 7429–7437

Blain-Hartung M, Rockwell NC, Moreno M V., Martin SS, Gan F, Bryant DA, Lagarias JC (2018) Cyanobacteriochrome-based photoswitchable adenylyl cyclases (cPACs) for broad spectrum light regulation of cAMP levels in cells. J Biol Chem **293**: 8473–8483

Bonger KM, Rakhit R, Payumo AY, Chen JK, Wandless TJ (2014) General Method for Regulating Protein Stability with Light. ACS Chem Biol **9**: 111–115

Brkljacic J, Grotewold E (2017) Combinatorial control of plant gene expression. Biochim Biophys Acta - Gene Regul Mech **1860**: 31–40

Van den Broeck L, Dubois M, Vermeersch M, Storme V, Matsui M, Inzé D (2017) From network to phenotype: the dynamic wiring of an Arabidopsis transcriptional network induced by osmotic stress. Mol Syst Biol **13**: 961

Brooks AK, Gaj T (2018) Innovations in CRISPR technology. Curr Opin Biotechnol **52**: 95–101

Bugaj LJ, Choksi AT, Mesuda CK, Kane RS, Schaffer D V (2013) Optogenetic protein clustering and signaling activation in mammalian cells. Nat Methods **10**: 249–252

Bugaj LJ, Spelke DP, Mesuda CK, Varedi M, Kane RS, Schaffer D V. (2015) Regulation of endogenous transmembrane receptors through optogenetic Cry2 clustering. Nat Commun **6**: 6898

Burgie ES, Vierstra RD (2014) Phytochromes: An Atomic Perspective on Photoactivation and Signaling. Plant Cell **26**: 4568–4583

Cachat E, Liu W, Davies JA (2017) Synthetic self-patterning and morphogenesis in mammalian cells: a proof-of-concept step towards synthetic tissue development. Eng Biol **1**: 71–76

Cagnola JI, Cerdan PD, Pacin M, Andrade A, Rodriguez MV, Zurbriggen MD, Legris M, Buchovsky S, Carrillo N, Chory J, et al (2018) Long-day photoperiod enhances jasmonic acid-related plant defense. Plant Physiol **178**: pp.00443.2018

Calderón Villalobos LIA, Lee S, De Oliveira C, Ivetac A, Brandt W, Armitage L, Sheard LB, Tan X, Parry G, Mao H, et al (2012) A combinatorial TIR1/AFB–Aux/IAA co-receptor system for differential sensing of auxin. Nat Chem Biol **8**: 477–485

Callura JM, Dwyer DJ, Isaacs FJ, Cantor CR, Collins JJ (2010) Tracking, tuning, and terminating microbial physiology using synthetic riboregulators. Proc Natl Acad Sci U S A **107**: 15898–903

Cameron DE, Bashor CJ, Collins JJ (2014) A brief history of synthetic biology. Nat Rev Microbiol **12**: 381–390

Campos ML, Kang J-H, Howe GA (2014) Jasmonate-Triggered Plant Immunity. J Chem Ecol **40**: 657–675

Campos ML, Yoshida Y, Major IT, de Oliveira Ferreira D, Weraduwage SM, Froehlich JE, Johnson BF, Kramer DM, Jander G, Sharkey TD, et al (2016) Rewiring of jasmonate and phytochrome B signalling uncouples plant growth-defense tradeoffs. Nat Commun **7**: 12570

Carvalho LS, Turunen HT, Wassmer SJ, Luna-Velez M V, Xiao R, Bennett J, Vandenberghe LH (2017) Evaluating Efficiencies of Dual AAV Approaches for Retinal Targeting. Front Neurosci **11**: 503

Casal JJ (2013) Photoreceptor Signaling Networks in Plant Responses to Shade. Annu Rev Plant Biol **64**: 403–427

Cervantes M, Murillo FJ (2002) Role for Vitamin B12 in Light Induction of Gene Expression in the Bacterium Myxococcus xanthus. J Bacteriol **184**: 2215–2224

Chang H, Yi B, Ma R, Zhang X, Zhao H, Xi Y (2016) CRISPR/cas9, a novel genomic tool to knock down microRNA in vitro and in vivo. Sci Rep **6**: 22312

Chang KN, Zhong S, Weirauch MT, Hon G, Pelizzola M, Li H, Huang SC, Schmitz RJ, Urich MA, Kuo D, et al (2013) Temporal transcriptional response to ethylene gas drives growth hormone cross-regulation in Arabidopsis. Elife **2**: e00675

Chao Q, Rothenberg M, Solano R, Roman G, Terzaghi W, Ecker† JR (1997) Activation of the Ethylene Gas Response Pathway in Arabidopsis by the Nuclear Protein ETHYLENE-INSENSITIVE3 and Related Proteins. Cell **89**: 1133–1144

Chatelle C, Ochoa-Fernandez R, Engesser R, Schneider N, Beyer HM, Jones AR, Timmer J, Zurbriggen MD, Weber W (2018) A Green-Light-Responsive System for the Control of Transgene Expression in Mammalian and Plant Cells. ACS Synth Biol **7**: 1349–1358

Chatelle C V., Hövermann D, Müller A, Wagner HJ, Weber W, Radziwill G (2016) Optogenetically controlled RAF to characterize BRAF and CRAF protein kinase inhibitors. Sci Rep **6**: 23713

Chen C-YA, Shyu A-B (2011) Mechanisms of deadenylation-dependent decay. Wiley Interdiscip Rev RNA **2**: 167–83

Chen D, Gibson ES, Kennedy MJ (2013) A light-triggered protein secretion system. J Cell Biol **201**: 631–640

Chen M, Tao Y, Lim J, Shaw A, Chory J (2005) Regulation of Phytochrome B Nuclear Localization through Light-Dependent Unmasking of Nuclear-Localization Signals. Curr Biol **15**: 637–642

Chini A, Fonseca S, Fernández G, Adie B, Chico JM, Lorenzo O, García-Casado G, López-Vidriero I, Lozano FM, Ponce MR, et al (2007) The JAZ family of repressors is the missing link in jasmonate signalling. Nature **448**: 666–71

Chini A, Gimenez-Ibanez S, Goossens A, Solano R (2016) Redundancy and specificity in jasmonate signalling. Curr Opin Plant Biol **33**: 147–156

Cho SW, Kim S, Kim JM, Kim J-S (2013) Targeted genome engineering in human cells with the Cas9 RNA-guided endonuclease. Nat Biotechnol **31**: 230–232

Choudhury SR, Cui Y, Narayanan A, Gilley DP, Huda N, Lo C-L, Zhou FC, Yernool D, Irudayaraj

J (2016) Optogenetic regulation of site-specific subtelomeric DNA methylation. Oncotarget **7**: 50380–50391

Chow BY, Sanchez SE, Breton G, Pruneda-Paz JL, Krogan NT, Kay SA (2014) Transcriptional Regulation of LUX by CBF1 Mediates Cold Input to the Circadian Clock in Arabidopsis. Curr Biol **24**: 1518–1524

Christie JM, Arvai AS, Baxter KJ, Heilmann M, Pratt AJ, O'Hara A, Kelly SM, Hothorn M, Smith BO, Hitomi K, et al (2012) Plant UVR8 Photoreceptor Senses UV-B by Tryptophan-Mediated Disruption of Cross-Dimer Salt Bridges. Science (80-) **335**: 1492–1496

Chu Y, Senghaas N, Köster RW, Wurst W, Kühn R (2008) Novel caspase-suicide proteins for tamoxifen-inducible apoptosis. Genesis **46**: 530–6

Chung HS, Howe GA (2009) A Critical Role for the TIFY Motif in Repression of Jasmonate Signaling by a Stabilized Splice Variant of the JASMONATE ZIM-Domain Protein JAZ10 in *Arabidopsis*. Plant Cell **21**: 131–145

Cironi P, Swinburne IA, Silver PA (2008) Enhancement of Cell Type Specificity by Quantitative Modulation of a Chimeric Ligand. J Biol Chem **283**: 8469–8476

Clack T, Mathews S, Sharrock RA (1994) The phytochrome apoprotein family in Arabidopsis is encoded by five genes: the sequences and expression of PHYD and PHYE. Plant Mol Biol **25**: 413–27

Collart MA (2016) The Ccr4-Not complex is a key regulator of eukaryotic gene expression. Wiley Interdiscip Rev RNA **7**: 438–454

Consiglieri E, Gutt A, Gärtner W, Schubert L, Viappiani C, Abbruzzetti S, Losi A (2019) Dynamics and efficiency of photoswitching in biliverdin-binding phytochromes. Photochem Photobiol Sci **18**: 2484–2496

Cosentino C, Alberio L, Gazzarrini S, Aquila M, Romano E, Cermenati S, Zuccolini P, Petersen J, Beltrame M, Van Etten JL, et al (2015) Engineering of a light-gated potassium channel. Science (80-) **348**: 707–710

Cox DBT, Gootenberg JS, Abudayyeh OO, Franklin B, Kellner MJ, Joung J, Zhang F (2017) RNA editing with CRISPR-Cas13. Science (80-) **358**: 1019–1027

Creelman RA, Mullet JE (1997) BIOSYNTHESIS AND ACTION OF JASMONATES IN PLANTS. Annu Rev Plant Physiol Plant Mol Biol **48**: 355–381

Crefcoeur RP, Yin R, Ulm R, Halazonetis TD (2013) Ultraviolet-B-mediated induction of protein-protein interactions in mammalian cells. Nat Commun **4**: 1779

Davuluri R V, Sun H, Palaniswamy SK, Matthews N, Molina C, Kurtz M, Grotewold E (2003) AGRIS: Arabidopsis gene regulatory information server, an information resource of Arabidopsis cis-regulatory elements and transcription factors. BMC Bioinformatics **4**: 25

Deans TL, Cantor CR, Collins JJ (2007) A tunable genetic switch based on RNAi and repressor proteins for regulating gene expression in mammalian cells. Cell **130**: 363–72

Delker C, Stenzel I, Hause B, Miersch O, Feussner I, Wasternack C (2006) Jasmonate Biosynthesis in Arabidopsis thaliana - Enzymes, Products, Regulation. Plant Biol **8**: 297–306

Deltcheva E, Chylinski K, Sharma CM, Gonzales K, Chao Y, Pirzada ZA, Eckert MR, Vogel J, Charpentier E (2011) CRISPR RNA maturation by trans-encoded small RNA and host factor

RNase III. Nature **471**: 602–7

Deng J (2017) How to unleash mitochondrial apoptotic blockades to kill cancers? Acta Pharm Sin B **7**: 18–26

Deverman BE, Pravdo PL, Simpson BP, Kumar SR, Chan KY, Banerjee A, Wu W-L, Yang B, Huber N, Pasca SP, et al (2016) Cre-dependent selection yields AAV variants for widespread gene transfer to the adult brain. Nat Biotechnol **34**: 204–9

DiCarlo JE, Norville JE, Mali P, Rios X, Aach J, Church GM (2013) Genome engineering in Saccharomyces cerevisiae using CRISPR-Cas systems. Nucleic Acids Res **41**: 4336–4343

Doudna JA, Charpentier E (2014) The new frontier of genome engineering with CRISPR-Cas9. Science (80-) **346**: 1258096–1258096

Duan D, Yue Y, Engelhardt JF (2001) Expanding AAV Packaging Capacity with Trans-splicing or Overlapping Vectors: A Quantitative Comparison. Mol Ther **4**: 383–391

Duan L, Che D, Zhang K, Ong Q, Guo S, Cui B (2015) Optogenetic Control of Molecular Motors and Organelle Distributions in Cells. Chem Biol **22**: 671–682

Elowitz MB, Leibler S (2000) A synthetic oscillatory network of transcriptional regulators. Nature **403**: 335–338

Enderle B, Sheerin DJ, Paik I, Kathare PK, Schwenk P, Klose C, Ulbrich MH, Huq E, Hiltbrunner A (2017) PCH1 and PCHL promote photomorphogenesis in plants by controlling phytochrome B dark reversion. Nat Commun **8**: 2221

Engler C, Marillonnet S (2014) Golden Gate Cloning. Methods Mol. Biol. pp 119–131

Etzel M, Mörl M (2017) Synthetic Riboswitches: From Plug and Pray toward Plug and Play. Biochemistry **56**: 1181–1198

Farmer EE (2007) Jasmonate perception machines. Nature **448**: 659–660

Favory J-J, Stec A, Gruber H, Rizzini L, Oravecz A, Funk M, Albert A, Cloix C, Jenkins GI, Oakeley EJ, et al (2009) Interaction of COP1 and UVR8 regulates UV-B-induced photomorphogenesis and stress acclimation in Arabidopsis. EMBO J **28**: 591–601

Fernández-Calvo P, Chini A, Fernández-Barbero G, Chico J-M, Gimenez-Ibanez S, Geerinck J, Eeckhout D, Schweizer F, Godoy M, Franco-Zorrilla JM, et al (2011) The *Arabidopsis* bHLH Transcription Factors MYC3 and MYC4 Are Targets of JAZ Repressors and Act Additively with MYC2 in the Activation of Jasmonate Responses. Plant Cell **23**: 701–715

Feys B, Benedetti CE, Penfold CN, Turner JG (1994) Arabidopsis Mutants Selected for Resistance to the Phytotoxin Coronatine Are Male Sterile, Insensitive to Methyl Jasmonate, and Resistant to a Bacterial Pathogen. Plant Cell **6**: 751–759

Fire A, Xu S, Montgomery MK, Kostas SA, Driver SE, Mello CC (1998) Potent and specific genetic interference by double-stranded RNA in Caenorhabditis elegans. Nature **391**: 806–811

Folcher M, Morris RP, Dale G, Salah-Bey-Hocini K, Viollier PH, Thompson CJ (2001) A Transcriptional Regulator of a Pristinamycin Resistance Gene in *Streptomyces coelicolor*. J Biol Chem **276**: 1479–1485

Fowler S, Thomashow MF (2002) Arabidopsis transcriptome profiling indicates that multiple regulatory pathways are activated during cold acclimation in addition to the CBF cold response pathway. Plant Cell **14**: 1675–90

Franco-Zorrilla JM, Solano R (2017) Identification of plant transcription factor target sequences. Biochim Biophys Acta - Gene Regul Mech **1860**: 21–30

Gardner TS, Cantor CR, Collins JJ (2000) Construction of a genetic toggle switch in Escherichia coli. Nature **403**: 339–342

Garg A, Lohmueller JJ, Silver PA, Armel TZ (2012) Engineering synthetic TAL effectors with orthogonal target sites. Nucleic Acids Res **40**: 7584–95

Geering B, Fussenegger M (2015) Synthetic immunology: modulating the human immune system. Trends Biotechnol **33**: 65–79

Gehrig S, Macpherson JA, Driscoll PC, Symon A, Martin SR, MacRae JI, Kleinjung J, Fraternali F, Anastasiou D (2017) An engineered photoswitchable mammalian pyruvate kinase. FEBS J **284**: 2955–2980

Genoud T, Schweizer F, Tscheuschler A, Debrieux D, Casal JJ, Schäfer E, Hiltbrunner A, Fankhauser C (2008) FHY1 Mediates Nuclear Import of the Light-Activated Phytochrome A Photoreceptor. PLoS Genet **4**: e1000143

Gibson DG, Benders GA, Andrews-Pfannkoch C, Denisova EA, Baden-Tillson H, Zaveri J, Stockwell TB, Brownley A, Thomas DW, Algire MA, et al (2008) Complete chemical synthesis, assembly, and cloning of a Mycoplasma genitalium genome. Science **319**: 1215–20

Gibson DG, Glass JI, Lartigue C, Noskov VN, Chuang R-Y, Algire MA, Benders GA, Montague MG, Ma L, Moodie MM, et al (2010) Creation of a Bacterial Cell Controlled by a Chemically Synthesized Genome. Science (80-) **329**: 52–56

Gibson DG, Young L, Chuang R-Y, Venter JC, Hutchison CA, Smith HO (2009) Enzymatic assembly of DNA molecules up to several hundred kilobases. Nat Methods **6**: 343–345

Gilbert LA, Larson MH, Morsut L, Liu Z, Brar GA, Torres SE, Stern-Ginossar N, Brandman O, Whitehead EH, Doudna JA, et al (2013) CRISPR-Mediated Modular RNA-Guided Regulation of Transcription in Eukaryotes. Cell **154**: 442–451

Giotopoulou N, Valiakou V, Papanikolaou V, Dubos S, Athanassiou E, Tsezou A, Zacharia LC, Gkretsi V (2015) Ras suppressor-1 promotes apoptosis in breast cancer cells by inhibiting PINCH-1 and activating p53-upregulated-modulator of apoptosis (PUMA); verification from metastatic breast cancer human samples. Clin Exp Metastasis **32**: 255–265

Goglia AG, Wilson MZ, DiGiorno DB, Toettcher JE (2017) Optogenetic Control of Ras/Erk Signaling Using the Phy–PIF System. pp 3–20

Gómez-Porras JL, Riaño-Pachón D, Dreyer I, Mayer JE, Mueller-Roeber B (2007) Genome-wide analysis of ABA-responsive elements ABRE and CE3 reveals divergent patterns in Arabidopsis and rice. BMC Genomics **8**: 260

Gomez EJ, Gerhardt K, Judd J, Tabor JJ, Suh J (2016) Light-Activated Nuclear Translocation of Adeno-Associated Virus Nanoparticles Using Phytochrome B for Enhanced, Tunable, and Spatially Programmable Gene Delivery. ACS Nano **10**: 225–237

Goossens J, Fernández-Calvo P, Schweizer F, Goossens A (2016) Jasmonates: signal transduction components and their roles in environmental stress responses. Plant Mol Biol **91**: 673–689

Gossen M, Bujard H (1992) Tight control of gene expression in mammalian cells by tetracycline-

responsive promoters. Proc Natl Acad Sci **89**: 5547–5551

Grieger JC, Samulski RJ (2005) Packaging capacity of adeno-associated virus serotypes: impact of larger genomes on infectivity and postentry steps. J Virol **79**: 9933–44

Grusch M, Schelch K, Riedler R, Reichhart E, Differ C, Berger W, Inglés-Prieto Á, Janovjak H (2014) Spatio-temporally precise activation of engineered receptor tyrosine kinases by light. EMBO J **33**: 1713–1726

Guet C ;I. C, Elowitz MB, Hsing W, Leibler S (2002) Combinatorial Synthesis of Genetic Networks. Science (80-) **296**: 1466–1470

Guntas G, Hallett RA, Zimmerman SP, Williams T, Yumerefendi H, Bear JE, Kuhlman B (2015) Engineering an improved light-induced dimer (iLID) for controlling the localization and activity of signaling proteins. Proc Natl Acad Sci **112**: 112–117

Guo Q, Wang X, Tibbitt MW, Anseth KS, Montell DJ, Elisseeff JH (2012) Light activated cell migration in synthetic extracellular matrices. Biomaterials **33**: 8040–8046

Gyula P, Schäfer E, Nagy F (2003) Light perception and signalling in higher plants. Curr Opin Plant Biol **6**: 446–52

Habuchi S, Dedecker P, Hotta J, Flors C, Ando R, Mizuno H, Miyawaki A, Hofkens J (2006) Photo-induced protonation/deprotonation in the GFP-like fluorescent protein Dronpa: mechanism responsible for the reversible photoswitching. Photochem Photobiol Sci **5**: 567

Hamberg M, Gardner HW (1992) Oxylipin pathway to jasmonates: biochemistry and biological significance. Biochim Biophys Acta **1165**: 1–18

Hankins MW, Peirson SN, Foster RG (2008) Melanopsin: an exciting photopigment. Trends Neurosci **31**: 27–36

Harper SM, Christie JM, Gardner KH (2004) Disruption of the LOV-Jalpha helix interaction activates phototropin kinase activity. Biochemistry **43**: 16184–92

Hasadsri L, Kreuter J, Hattori H, Iwasaki T, George JM (2009) Functional Protein Delivery into Neurons Using Polymeric Nanoparticles. J Biol Chem **284**: 6972–6981

Hattar S, Lyons LC, Dryer L, Eskin A (2002) Circadian regulation of a transcription factor, ApC/EBP, in the eye of Aplysia californica. J Neurochem **83**: 1401–1411

Hazen SP, Schultz TF, Pruneda-Paz JL, Borevitz JO, Ecker JR, Kay SA (2005) LUX ARRHYTHMO encodes a Myb domain protein essential for circadian rhythms. Proc Natl Acad Sci U S A **102**: 10387–92

Hegemann P, Möglich A (2011) Channelrhodopsin engineering and exploration of new optogenetic tools. Nat Methods **8**: 39–42

Hennig L, Büche C, Eichenberg K, Schäfer E (1999) Dynamic Properties of Endogenous Phytochrome A in Arabidopsis Seedlings. Plant Physiol **121**: 571–578

Hershko A, Ciechanover A (1998) THE UBIQUITIN SYSTEM. Annu Rev Biochem **67**: 425–479

Hille F, Charpentier E (2016) CRISPR-Cas: biology, mechanisms and relevance. Philos Trans R Soc Lond B Biol Sci **371**: 20150496

Hiltbrunner A, Tscheuschler A, Viczián A, Kunkel T, Kircher S, Schäfer E (2006) FHY1 and FHL Act Together to Mediate Nuclear Accumulation of the Phytochrome A Photoreceptor. Plant Cell Physiol **47**: 1023–1034

Hirschfeld M, Tepperman JM, Clack T, Quail PH, Sharrock RA (1998) Coordination of phytochrome levels in phyB mutants of Arabidopsis as revealed by apoprotein-specific monoclonal antibodies. Genetics **149**: 523–35

Hörner M, Chatelle C, Mühlhäuser WWD, Stocker DR, Coats M, Weber W, Radziwill G (2018) Optogenetic control of focal adhesion kinase signaling. Cell Signal **42**: 176–183

Hsu PY, Harmer SL (2014) Wheels within wheels: the plant circadian system. Trends Plant Sci **19**: 240–249

Huang H, Yoo CY, Bindbeutel R, Goldsworthy J, Tielking A, Alvarez S, Naldrett MJ, Evans BS, Chen M, Nusinow DA (2016) PCH1 integrates circadian and light-signaling pathways to control photoperiod-responsive growth in Arabidopsis. Elife **5**: e13292

Huang J, Koide A, Makabe K, Koide S (2008) Design of protein function leaps by directed domain interface evolution. Proc Natl Acad Sci U S A **105**: 6578–83

Huang W, Pérez-García P, Pokhilko A, Millar AJ, Antoshechkin I, Riechmann JL, Mas P (2012) Mapping the Core of the *Arabidopsis* Circadian Clock Defines the Network Structure of the Oscillator. Science (80-) **336**: 75–79

Huang X, Zhang Q, Jiang Y, Yang C, Wang Q, Li L (2018) Shade-induced nuclear localization of PIF7 is regulated by phosphorylation and 14-3-3 proteins in Arabidopsis. Elife. doi: 10.7554/eLife.31636

Hughes RM, Bolger S, Tapadia H, Tucker CL (2012) Light-mediated control of DNA transcription in yeast. Methods **58**: 385–91

Hughes RM, Freeman DJ, Lamb KN, Pollet RM, Smith WJ, Lawrence DS (2015) Optogenetic Apoptosis: Light-Triggered Cell Death. Angew Chemie Int Ed **54**: 12064–12068

Huq E, Al-Sady B, Hudson M, Kim C, Apel K, Quail PH (2004) Phytochrome-interacting factor 1 is a critical bHLH regulator of chlorophyll biosynthesis. Science **305**: 1937–41

Iglesias MJ, Sellaro R, Zurbriggen MD, Casal JJ (2018) Multiple links between shade avoidance and auxin networks. J Exp Bot **69**: 213–228

Isomura A, Kageyama R (2018) An Optogenetic Method to Control and Analyze Gene Expression Patterns in Cell-to-cell Interactions. J Vis Exp. doi: 10.3791/57149

Isomura A, Ogushi F, Kori H, Kageyama R (2017) Optogenetic perturbation and bioluminescence imaging to analyze cell-to-cell transfer of oscillatory information. Genes Dev **31**: 524–535

Jackson RN, Wiedenheft B (2015) A Conserved Structural Chassis for Mounting Versatile CRISPR RNA-Guided Immune Responses. Mol Cell **58**: 722–728

Jacobs JL, Dinman JD (2004) Systematic analysis of bicistronic reporter assay data. Nucleic Acids Res **32**: e160

James JR, Vale RD (2012) Biophysical mechanism of T-cell receptor triggering in a reconstituted system. Nature **487**: 64–69

Jayaraman P, Devarajan K, Chua TK, Zhang H, Gunawan E, Poh CL (2016) Blue light-mediated transcriptional activation and repression of gene expression in bacteria. Nucleic Acids Res **44**: 6994–7005

Jeong J, Choi G (2013) Phytochrome-interacting factors have both shared and distinct biological roles. Mol Cells **35**: 371–380

Jeong J, Kim K, Kim ME, Kim HG, Heo GS, Park OK, Park Y-I, Choi G, Oh E (2016) Phytochrome and Ethylene Signaling Integration in Arabidopsis Occurs via the Transcriptional Regulation of Genes Co-targeted by PIFs and EIN3. Front Plant Sci **7**: 1055

Jewett MC (2017) Editorial overview: Synthetic biology: Frontiers in synthetic biology. Curr Opin Chem Biol **40**: A1–A3

Jiang F, Doudna JA (2017) CRISPR–Cas9 Structures and Mechanisms. Annu Rev Biophys **46**: 505–529

Jinek M, Chylinski K, Fonfara I, Hauer M, Doudna JA, Charpentier E (2012) A Programmable Dual-RNA-Guided DNA Endonuclease in Adaptive Bacterial Immunity. Science (80-) **337**: 816–821

Jones DC, Mistry IN, Tavassoli A (2016) Post-translational control of protein function with light using a LOV-intein fusion protein. Mol Biosyst **12**: 1388–93

Kaberniuk AA, Shemetov AA, Verkhusha V V (2016) A bacterial phytochrome-based optogenetic system controllable with near-infrared light. Nat Methods **13**: 591–597

Kamioka M, Takao S, Suzuki T, Taki K, Higashiyama T, Kinoshita T, Nakamichi N (2016) Direct Repression of Evening Genes by CIRCADIAN CLOCK-ASSOCIATED1 in the Arabidopsis Circadian Clock. Plant Cell **28**: 696–711

Kawano F, Suzuki H, Furuya A, Sato M (2015) Engineered pairs of distinct photoswitches for optogenetic control of cellular proteins. Nat Commun **6**: 6256

Kennedy MJ, Hughes RM, Peteya LA, Schwartz JW, Ehlers MD, Tucker CL (2010) Rapid blue-light–mediated induction of protein interactions in living cells. Nat Methods **7**: 973–975

Khanna R, Huq E, Kikis EA, Al-Sady B, Lanzatella C, Quail PH (2004) A novel molecular recognition motif necessary for targeting photoactivated phytochrome signaling to specific basic helix-loop-helix transcription factors. Plant Cell **16**: 3033–44

Kidokoro S, Maruyama K, Nakashima K, Imura Y, Narusaka Y, Shinwari ZK, Osakabe Y, Fujita Y, Mizoi J, Shinozaki K, et al (2009) The phytochrome-interacting factor PIF7 negatively regulates DREB1 expression under circadian control in Arabidopsis. Plant Physiol **151**: 2046–57

Kikis EA, Khanna R, Quail PH (2005) ELF4 is a phytochrome-regulated component of a negative-feedback loop involving the central oscillator components CCA1 and LHY. Plant J **44**: 300–13

Kim J (2003) Functional Characterization of Phytochrome Interacting Factor 3 in Phytochrome-Mediated Light Signal Transduction. PLANT CELL ONLINE **15**: 2399–2407

Kircher S, Gil P, Kozma-Bognár L, Fejes E, Speth V, Husselstein-Muller T, Bauer D, Ádám É, Schäfer E, Nagy F (2002) Nucleocytoplasmic Partitioning of the Plant Photoreceptors Phytochrome A, B, C, D, and E Is Regulated Differentially by Light and Exhibits a Diurnal Rhythm. Plant Cell **14**: 1541–1555

Klose C, Venezia F, Hussong A, Kircher S, Schäfer E, Fleck C (2015) Systematic analysis of how phytochrome B dimerization determines its specificity. Nat Plants **1**: 15090

Kojadinovic M, Laugraud A, Vuillet L, Fardoux J, Hannibal L, Adriano J-M, Bouyer P, Giraud E, Verméglio A (2008) Dual role for a bacteriophytochrome in the bioenergetic control of Rhodopsdeudomonas palustris: Enhancement of photosystem synthesis and limitation of respiration. Biochim Biophys Acta - Bioenerg **1777**: 163–172

Konermann S, Brigham MD, Trevino A, Hsu PD, Heidenreich M, Cong L, Platt RJ, Scott DA, Church GM, Zhang F (2013) Optical control of mammalian endogenous transcription and epigenetic states. Nature **500**: 472–476

Konermann S, Brigham MD, Trevino AE, Joung J, Abudayyeh OO, Barcena C, Hsu PD, Habib N, Gootenberg JS, Nishimasu H, et al (2015) Genome-scale transcriptional activation by an engineered CRISPR-Cas9 complex. Nature **517**: 583–588

Kong S-G, Okajima K (2016) Diverse photoreceptors and light responses in plants. J Plant Res **129**: 111–4

Kutta RJ, Hardman SJO, Johannissen LO, Bellina B, Messiha HL, Ortiz-Guerrero JM, Elías-Arnanz M, Padmanabhan S, Barran P, Scrutton NS, et al (2015) The photochemical mechanism of a B12-dependent photoreceptor protein. Nat Commun **6**: 7907

Lagos-Quintana M, Rauhut R, Lendeckel W, Tuschl T (2001) Identification of Novel Genes Coding for Small Expressed RNAs. Science (80-) **294**: 853–858

Laity JH, Lee BM, Wright PE (2001) Zinc finger proteins: new insights into structural and functional diversity. Curr Opin Struct Biol **11**: 39–46

Lau OS, Deng XW (2012) The photomorphogenic repressors COP1 and DET1: 20 years later. Trends Plant Sci **17**: 584–593

Lee JH, Soung YH, Lee JW, Park WS, Kim SY, Cho YG, Kim CJ, Seo SH, Kim HS, Nam SW, et al (2004) Inactivating mutation of the pro-apoptotic geneBID in gastric cancer. J Pathol **202**: 439–445

Lee N, Choi G (2017) Phytochrome-interacting factor from Arabidopsis to liverwort. Curr Opin Plant Biol **35**: 54–60

Lee S, Park H, Kyung T, Kim NY, Kim S, Kim J, Heo W Do (2014) Reversible protein inactivation by optogenetic trapping in cells. Nat Methods **11**: 633–636

Legris M, Klose C, Burgie ES, Rojas CCR, Neme M, Hiltbrunner A, Wigge PA, Schäfer E, Vierstra RD, Casal JJ (2016) Phytochrome B integrates light and temperature signals in *Arabidopsis*. Science (80-) **354**: 897–900

Leivar P, Monte E, Al-Sady B, Carle C, Storer A, Alonso JM, Ecker JR, Quail PH (2008a) The *Arabidopsis* Phytochrome-Interacting Factor PIF7, Together with PIF3 and PIF4, Regulates Responses to Prolonged Red Light by Modulating phyB Levels. Plant Cell **20**: 337–352

Leivar P, Monte E, Oka Y, Liu T, Carle C, Castillon A, Huq E, Quail PH (2008b) Multiple Phytochrome-Interacting bHLH Transcription Factors Repress Premature Seedling Photomorphogenesis in Darkness. Curr Biol **18**: 1815–1823

Leivar P, Quail PH (2011) PIFs: pivotal components in a cellular signaling hub. Trends Plant Sci **16**: 19–28

Leon-Reyes A, Van der Does D, De Lange ES, Delker C, Wasternack C, Van Wees SCM, Ritsema T, Pieterse CMJ (2010) Salicylate-mediated suppression of jasmonate-responsive gene expression in Arabidopsis is targeted downstream of the jasmonate biosynthesis pathway. Planta **232**: 1423–1432

Levskaya A, Chevalier AA, Tabor JJ, Simpson ZB, Lavery LA, Levy M, Davidson EA, Scouras A, Ellington AD, Marcotte EM, et al (2005) Synthetic biology: engineering Escherichia coli to see

light. Nature **438**: 441–2

Levskaya A, Weiner OD, Lim WA, Voigt CA (2009) Spatiotemporal control of cell signalling using a light-switchable protein interaction. Nature **461**: 997–1001

Li J, Li G, Wang H, Wang Deng X (2011) Phytochrome Signaling Mechanisms. Arab B **9**: e0148

Li K, Yu R, Fan L-M, Wei N, Chen H, Deng XW (2016a) DELLA-mediated PIF degradation contributes to coordination of light and gibberellin signalling in Arabidopsis. Nat Commun **7**: 11868

Li L, Ljung K, Breton G, Schmitz RJ, Pruneda-Paz J, Cowing-Zitron C, Cole BJ, Ivans LJ, Pedmale U V, Jung H-S, et al (2012) Linking photoreceptor excitation to changes in plant architecture. Genes Dev **26**: 785–90

Li X, Ma D, Lu SX, Hu X, Huang R, Liang T, Xu T, Tobin EM, Liu H (2016b) Blue Light- and Low Temperature-Regulated COR27 and COR28 Play Roles in the Arabidopsis Circadian Clock. Plant Cell **28**: 2755–2769

Liang J, Luo Y, Zhao H (2011) Synthetic biology: putting synthesis into biology. Wiley Interdiscip Rev Syst Biol Med **3**: 7–20

Liao H, Ji F, Ying S (2017) CDK1: beyond cell cycle regulation. Aging (Albany NY) **9**: 2465–2466

Lienert F, Lohmueller JJ, Garg A, Silver PA (2014) Synthetic biology in mammalian cells: next generation research tools and therapeutics. Nat Rev Mol Cell Biol **15**: 95–107

Liu H, Yu X, Li K, Klejnot J, Yang H, Lisiero D, Lin C (2008) Photoexcited CRY2 Interacts with CIB1 to Regulate Transcription and Floral Initiation in Arabidopsis. Science (80-) **322**: 1535–1539

Liu L, Huang W, Huang J-D (2017) Synthetic circuits that process multiple light and chemical signal inputs. BMC Syst Biol **11**: 5

Liu T, Pan S, Li Y, Peng N, She Q (2018) Type III CRISPR-Cas System: Introduction And Its Application for Genetic Manipulations. Curr Issues Mol Biol **26**: 1–14

Lorrain S, Allen T, Duek PD, Whitelam GC, Fankhauser C (2007) Phytochrome-mediated inhibition of shade avoidance involves degradation of growth-promoting bHLH transcription factors. Plant J **53**: 312–323

Lu X-D, Zhou C-M, Xu P-B, Luo Q, Lian H-L, Yang H-Q (2015) Red-light-dependent interaction of phyB with SPA1 promotes COP1-SPA1 dissociation and photomorphogenic development in Arabidopsis. Mol Plant **8**: 467–78

Luo Q, Lian H-L, He S-B, Li L, Jia K-P, Yang H-Q (2014) COP1 and phyB Physically Interact with PIL1 to Regulate Its Stability and Photomorphogenic Development in *Arabidopsis*. Plant Cell **26**: 2441–2456

Lutz R, Bujard H (1997) Independent and tight regulation of transcriptional units in Escherichia coli via the LacR/O, the TetR/O and AraC/I1-I2 regulatory elements. Nucleic Acids Res **25**: 1203–10

Lyu S, Fang J, Duan T, Fu L, Liu J, Li H (2017) Optically controlled reversible protein hydrogels based on photoswitchable fluorescent protein Dronpa. Chem Commun **53**: 13375–13378

Marchisio MA, Huang Z (2017) CRISPR-Cas type II-based Synthetic Biology applications in eukaryotic cells. RNA Biol **14**: 1286–1293

Marraffini LA (2015) CRISPR-Cas immunity in prokaryotes. Nature **526**: 55–61

Martínez-García JF, Huq E, Quail PH (2000) Direct targeting of light signals to a promoter element-

bound transcription factor. Science **288**: 859–63

Martínez C, Nieto C, Prat S (2018) Convergent regulation of PIFs and the E3 ligase COP1/SPA1 mediates thermosensory hypocotyl elongation by plant phytochromes. Curr Opin Plant Biol **45**: 188–203

Mathelier A, Xin B, Chiu T-P, Yang L, Rohs R, Wasserman WW (2016) DNA Shape Features Improve Transcription Factor Binding Site Predictions In Vivo. Cell Syst **3**: 278-286.e4

McClung CR (2014) Wheels within wheels: new transcriptional feedback loops in the Arabidopsis circadian clock. F1000Prime Rep **6**: 2

Mekler V, Kuznedelov K, Minakhin L, Murugan K, Sashital DG, Severinov K (2019) CRISPR-Cas molecular beacons as tool for studies of assembly of CRISPR-Cas effector complexes and their interactions with DNA. Methods Enzymol **616**: 337–363

Melyan Z, Tarttelin EE, Bellingham J, Lucas RJ, Hankins MW (2005) Addition of human melanopsin renders mammalian cells photoresponsive. Nature **433**: 741–5

Mikkelsen MD, Thomashow MF (2009) A role for circadian evening elements in cold-regulated gene expression in Arabidopsis. Plant J **60**: 328–39

Mitsuda N, Ohme-Takagi M (2009) Functional Analysis of Transcription Factors in Arabidopsis. Plant Cell Physiol **50**: 1232–1248

Mizuno T, Oka H, Yoshimura F, Ishida K, Yamashino T (2015) Insight into the mechanism of end-of-day far-red light (EODFR)-induced shade avoidance responses in Arabidopsis thaliana. Biosci Biotechnol Biochem **79**: 1987–94

Moffat CS, Ingle RA, Wathugala DL, Saunders NJ, Knight H, Knight MR (2012) ERF5 and ERF6 play redundant roles as positive regulators of JA/Et-mediated defense against Botrytis cinerea in Arabidopsis. PLoS One **7**: e35995

Mojica FJM, Díez-Villaseñor C, García-Martínez J, Almendros C (2009) Short motif sequences determine the targets of the prokaryotic CRISPR defence system. Microbiology **155**: 733–40

MONOD J, JACOB F (1961) Teleonomic mechanisms in cellular metabolism, growth, and differentiation. Cold Spring Harb Symp Quant Biol **26**: 389–401

Moore R, Chandrahas A, Bleris L (2014) Transcription Activator-like Effectors: A Toolkit for Synthetic Biology. ACS Synth Biol **3**: 708–716

Motta-Mena LB, Reade A, Mallory MJ, Glantz S, Weiner OD, Lynch KW, Gardner KH (2014) An optogenetic gene expression system with rapid activation and deactivation kinetics. Nat Chem Biol **10**: 196–202

Mühlhäuser WWD, Hörner M, Weber W, Radziwill G (2017) Light-Regulated Protein Kinases Based on the CRY2-CIB1 System. Methods Mol. Biol. pp 257–270

Müller K, Engesser R, Metzger S, Schulz S, Kämpf MM, Busacker M, Steinberg T, Tomakidi P, Ehrbar M, Nagy F, et al (2013a) A red/far-red light-responsive bi-stable toggle switch to control gene expression in mammalian cells. Nucleic Acids Res **41**: e77–e77

Müller K, Engesser R, Schulz S, Steinberg T, Tomakidi P, Weber CC, Ulm R, Timmer J, Zurbriggen MD, Weber W (2013b) Multi-chromatic control of mammalian gene expression and signaling. Nucleic Acids Res **41**: e124–e124

Müller K, Engesser R, Timmer J, Zurbriggen MD, Weber W (2014) Orthogonal Optogenetic Triple-

Gene Control in Mammalian Cells. ACS Synth Biol **3**: 796–801

Murugan K, Babu K, Sundaresan R, Rajan R, Sashital DG (2017) The Revolution Continues: Newly Discovered Systems Expand the CRISPR-Cas Toolkit. Mol Cell **68**: 15–25

Nagel G, Szellas T, Huhn W, Kateriya S, Adeishvili N, Berthold P, Ollig D, Hegemann P, Bamberg E (2003) Channelrhodopsin-2, a directly light-gated cation-selective membrane channel. Proc Natl Acad Sci **100**: 13940–13945

Nakamura M, Chen L, Howes SC, Schindler TD, Nogales E, Bryant Z (2014) Remote control of myosin and kinesin motors using light-activated gearshifting. Nat Nanotechnol **9**: 693–697

Nakano K, Vousden KH (2001) PUMA, a novel proapoptotic gene, is induced by p53. Mol Cell **7**: 683–94

Nakano T, Suzuki K, Fujimura T, Shinshi H (2006) Genome-Wide Analysis of the ERF Gene Family in Arabidopsis and Rice. Plant Physiol **140**: 411–432

Nakasone Y, Zikihara K, Tokutomi S, Terazima M (2010) Kinetics of conformational changes of the FKF1-LOV domain upon photoexcitation. Biophys J **99**: 3831–9

Nash AI, McNulty R, Shillito ME, Swartz TE, Bogomolni RA, Luecke H, Gardner KH (2011) Structural basis of photosensitivity in a bacterial light-oxygen-voltage/helix-turn-helix (LOV-HTH) DNA-binding protein. Proc Natl Acad Sci **108**: 9449–9454

Ni M, Tepperman JM, Quail PH (1999) Binding of phytochrome B to its nuclear signalling partner PIF3 is reversibly induced by light. Nature **400**: 781–784

Ni W, Xu S-L, Tepperman JM, Stanley DJ, Maltby DA, Gross JD, Burlingame AL, Wang Z-Y, Quail PH (2014) A mutually assured destruction mechanism attenuates light signaling in Arabidopsis. Science **344**: 1160–1164

Nihongaki Y, Kawano F, Nakajima T, Sato M (2015) Photoactivatable CRISPR-Cas9 for optogenetic genome editing. Nat Biotechnol **33**: 755–760

Nihongaki Y, Suzuki H, Kawano F, Sato M (2014) Genetically engineered photoinducible homodimerization system with improved dimer-forming efficiency. ACS Chem Biol **9**: 617–21

Niopek D, Benzinger D, Roensch J, Draebing T, Wehler P, Eils R, Di Ventura B (2014) Engineering light-inducible nuclear localization signals for precise spatiotemporal control of protein dynamics in living cells. Nat Commun **5**: 4404

Niopek D, Wehler P, Roensch J, Eils R, Di Ventura B (2016) Optogenetic control of nuclear protein export. Nat Commun **7**: 10624

Nishimura K, Fukagawa T, Takisawa H, Kakimoto T, Kanemaki M (2009) An auxin-based degron system for the rapid depletion of proteins in nonplant cells. Nat Methods **6**: 917–922

Ochoa-Fernandez R, Samodelov SL, Brandl SM, Wehinger E, Müller K, Weber W, Zurbriggen MD (2016) Optogenetics in Plants: Red/Far-Red Light Control of Gene Expression. Methods Mol. Biol. pp 125–139

OESTERHELT D, STOECKENIUS W (1971) Rhodopsin-like Protein from the Purple Membrane of Halobacterium halobium. Nat New Biol **233**: 149–152

Ohme-Takagi M, Shinshi H (1995) Ethylene-inducible DNA binding proteins that interact with an ethylene-responsive element. Plant Cell **7**: 173–182

Ojala DS, Amara DP, Schaffer D V. (2015) Adeno-Associated Virus Vectors and Neurological Gene

Therapy. Neurosci **21**: 84–98

Okada K, Abe H, Arimura G (2015) Jasmonates induce both defense responses and communication in monocotyledonous and dicotyledonous plants. Plant Cell Physiol **56**: 16–27

Onai K, Ishiura M (2005) PHYTOCLOCK 1 encoding a novel GARP protein essential for the Arabidopsis circadian clock. Genes to Cells **10**: 963–972

Oravecz A, Baumann A, Máté Z, Brzezinska A, Molinier J, Oakeley EJ, Ádám É, Schäfer E, Nagy F, Ulm R (2006) CONSTITUTIVELY PHOTOMORPHOGENIC1 Is Required for the UV-B Response in *Arabidopsis*. Plant Cell **18**: 1975–1990

Ortiz-Guerrero JM, Polanco MC, Murillo FJ, Padmanabhan S, Elias-Arnanz M (2011) Light-dependent gene regulation by a coenzyme B12-based photoreceptor. Proc Natl Acad Sci **108**: 7565–7570

Ortiz-Sánchez E, Helguera G, Daniels TR, Penichet ML (2008) Antibody–cytokine fusion proteins: applications in cancer therapy. Expert Opin Biol Ther **8**: 609–632

Park E, Park J, Kim J, Nagatani A, Lagarias JC, Choi G (2012) Phytochrome B inhibits binding of phytochrome-interacting factors to their target promoters. Plant J **72**: 537–46

Park H, Kim NY, Lee S, Kim N, Kim J, Heo W Do (2017) Optogenetic protein clustering through fluorescent protein tagging and extension of CRY2. Nat Commun **8**: 30

Park IS, Han Y gi, Chung HJ, Jung YW, Kim Y, Kim H (2016) SUMOylation regulates nuclear localization and stability of TRAIP/RNF206. Biochem Biophys Res Commun **470**: 881–7

Pathak GP, Spiltoir JI, Höglund C, Polstein LR, Heine-Koskinen S, Gersbach CA, Rossi J, Tucker CL (2017) Bidirectional approaches for optogenetic regulation of gene expression in mammalian cells using Arabidopsis cryptochrome 2. Nucleic Acids Res **45**: e167–e167

Pathak GP, Strickland D, Vrana JD, Tucker CL (2014) Benchmarking of optical dimerizer systems. ACS Synth Biol **3**: 832–8

Pauwels L, Goossens A (2011) The JAZ Proteins: A Crucial Interface in the Jasmonate Signaling Cascade. Plant Cell **23**: 3089–3100

Pellagatti A, Dolatshad H, Valletta S, Boultwood J (2015) Application of CRISPR/Cas9 genome editing to the study and treatment of disease. Arch Toxicol **89**: 1023–1034

Penfield S, Josse E-M, Halliday KJ (2010) A role for an alternative splice variant of PIF6 in the control of Arabidopsis primary seed dormancy. Plant Mol Biol **73**: 89–95

Pfeiffer A, Nagel M-K, Popp C, Wüst F, Bindics J, Viczián A, Hiltbrunner A, Nagy F, Kunkel T, Schäfer E (2012) Interaction with plant transcription factors can mediate nuclear import of phytochrome B. Proc Natl Acad Sci U S A **109**: 5892–7

Pham VN, Kathare PK, Huq E (2018) Phytochromes and Phytochrome Interacting Factors. Plant Physiol **176**: 1025–1038

Polstein LR, Gersbach CA (2012) Light-Inducible Spatiotemporal Control of Gene Activation by Customizable Zinc Finger Transcription Factors. J Am Chem Soc **134**: 16480–16483

Polstein LR, Juhas M, Hanna G, Bursac N, Gersbach CA (2017) An Engineered Optogenetic Switch for Spatiotemporal Control of Gene Expression, Cell Differentiation, and Tissue Morphogenesis. ACS Synth Biol **6**: 2003–2013

Quail PH (2002) Phytochrome photosensory signalling networks. Nat Rev Mol Cell Biol **3**: 85–93

Quejada JR, Park S-HE, Awari DW, Shi F, Yamamoto HE, Kawano F, Jung JC, Yazawa M (2017) Optimized light-inducible transcription in mammalian cells using Flavin Kelch-repeat F-box1/GIGANTEA and CRY2/CIB1. Nucleic Acids Res **45**: e172

Rao G, Sui J, Zeng Y, He C, Zhang J (2015) Genome-wide analysis of the AP2/ERF gene family in Salix arbutifolia. FEBS Open Bio **5**: 132–7

Rao MV, Chu P-H, Hahn KM, Zaidel-Bar R (2013) An optogenetic tool for the activation of endogenous diaphanous-related formins induces thickening of stress fibers without an increase in contractility. Cytoskeleton **70**: 394–407

Redchuk TA, Omelina ES, Chernov KG, Verkhusha V V (2017) Near-infrared optogenetic pair for protein regulation and spectral multiplexing. Nat Chem Biol **13**: 633–639

Reed JW, Nagpal P, Bastow RM, Solomon KS, Dowson-Day MJ, Elumalai RP, Millar AJ (2000) Independent Action of ELF3 and phyB to Control Hypocotyl Elongation and Flowering Time. Plant Physiol **122**: 1149–1160

Remberg A, Schmidt P, Braslavsky SE, Gartner W, Schaffner K (1999) Differential effects of mutations in the chromophore pocket of recombinant phytochrome on chromoprotein assembly and Pr-to-Pfr photoconversion. Eur J Biochem **266**: 201–208

Rinaudo K, Bleris L, Maddamsetti R, Subramanian S, Weiss R, Benenson Y (2007) A universal RNAi-based logic evaluator that operates in mammalian cells. Nat Biotechnol **25**: 795–801

Rivera-Cancel G, Motta-Mena LB, Gardner KH (2012) Identification of Natural and Artificial DNA Substrates for Light-Activated LOV–HTH Transcription Factor EL222. Biochemistry **51**: 10024–10034

Rizk SS, Luchniak A, Uysal S, Brawley CM, Rock RS, Kossiakoff AA (2009) An engineered substance P variant for receptor-mediated delivery of synthetic antibodies into tumor cells. Proc Natl Acad Sci **106**: 11011–11015

Rizzini L, Favory J-J, Cloix C, Faggionato D, O'Hara A, Kaiserli E, Baumeister R, Schafer E, Nagy F, Jenkins GI, et al (2011) Perception of UV-B by the Arabidopsis UVR8 Protein. Science (80-) **332**: 103–106

Rockwell NC, Su Y-S, Lagarias JC (2006) PHYTOCHROME STRUCTURE AND SIGNALING MECHANISMS. Annu Rev Plant Biol **57**: 837–858

Rossi FR, Krapp AR, Bisaro F, Maiale SJ, Pieckenstain FL, Carrillo N (2017) Reactive oxygen species generated in chloroplasts contribute to tobacco leaf infection by the necrotrophic fungus Botrytis cinerea. Plant J **92**: 761–773

Rudnik R, Bulcha JT, Reifschneider E, Ellersiek U, Baier M (2017) Specificity versus redundancy in the RAP2.4 transcription factor family of Arabidopsis thaliana: transcriptional regulation of genes for chloroplast peroxidases. BMC Plant Biol **17**: 144

Saijo Y, Zhu D, Li J, Rubio V, Zhou Z, Shen Y, Hoecker U, Wang H, Deng XW (2008) Arabidopsis COP1/SPA1 complex and FHY1/FHY3 associate with distinct phosphorylated forms of phytochrome A in balancing light signaling. Mol Cell **31**: 607–13

Salinas F, Rojas V, Delgado V, López J, Agosin E, Larrondo LF (2018) Fungal Light-Oxygen-Voltage Domains for Optogenetic Control of Gene Expression and Flocculation in Yeast. MBio. doi: 10.1128/mBio.00626-18

Samodelov SL, Beyer HM, Guo X, Augustin M, Jia K-P, Baz L, Ebenhöh O, Beyer P, Weber W, Al-Babili S, et al (2016) StrigoQuant: A genetically encoded biosensor for quantifying strigolactone activity and specificity. Sci Adv **2**: e1601266

Sanchez SE, Yanovsky MJ (2013) Time for a change. Elife **2**: e00791

Sander JD, Joung JK (2014) CRISPR-Cas systems for editing, regulating and targeting genomes. Nat Biotechnol **32**: 347–355

Sarris M, Olekhnovitch R, Bousso P (2016) Manipulating leukocyte interactions in vivo through optogenetic chemokine release. Blood **127**: e35-41

Sax JK, Fei P, Murphy ME, Bernhard E, Korsmeyer SJ, El-Deiry WS (2002) BID regulation by p53 contributes to chemosensitivity. Nat Cell Biol **4**: 842–849

Schafmeier T, Diernfellner ACR (2011) Light input and processing in the circadian clock of *Neurospora*. FEBS Lett **585**: 1467–1473

Schmidt D, Tillberg PW, Chen F, Boyden ES (2014) A fully genetically encoded protein architecture for optical control of peptide ligand concentration. Nat Commun **5**: 3019

Schröder-Lang S, Schwärzel M, Seifert R, Strünker T, Kateriya S, Looser J, Watanabe M, Kaupp UB, Hegemann P, Nagel G (2007) Fast manipulation of cellular cAMP level by light in vivo. Nat Methods **4**: 39–42

Schwank G, Koo B-K, Sasselli V, Dekkers JF, Heo I, Demircan T, Sasaki N, Boymans S, Cuppen E, van der Ent CK, et al (2013) Functional Repair of CFTR by CRISPR/Cas9 in Intestinal Stem Cell Organoids of Cystic Fibrosis Patients. Cell Stem Cell **13**: 653–658

Seo HS, Watanabe E, Tokutomi S, Nagatani A, Chua N-H (2004) Photoreceptor ubiquitination by COP1 E3 ligase desensitizes phytochrome A signaling. Genes Dev **18**: 617–22

Sheard LB, Tan X, Mao H, Withers J, Ben-Nissan G, Hinds TR, Kobayashi Y, Hsu F-F, Sharon M, Browse J, et al (2010) Jasmonate perception by inositol-phosphate-potentiated COI1-JAZ co-receptor. Nature **468**: 400–5

Sheerin DJ, Menon C, zur Oven-Krockhaus S, Enderle B, Zhu L, Johnen P, Schleifenbaum F, Stierhof Y-D, Huq E, Hiltbrunner A (2015) Light-Activated Phytochrome A and B Interact with Members of the SPA Family to Promote Photomorphogenesis in Arabidopsis by Reorganizing the COP1/SPA Complex. Plant Cell **27**: 189–201

Shen H, Moon J, Huq E (2005) PIF1 is regulated by light-mediated degradation through the ubiquitin-26S proteasome pathway to optimize photomorphogenesis of seedlings in Arabidopsis. Plant J **44**: 1023–1035

Shen H, Zhu L, Castillon A, Majee M, Downie B, Huq E (2008) Light-induced phosphorylation and degradation of the negative regulator PHYTOCHROME-INTERACTING FACTOR1 from Arabidopsis depend upon its direct physical interactions with photoactivated phytochromes. Plant Cell **20**: 1586–602

Shen Y, Khanna R, Carle CM, Quail PH (2007) Phytochrome induces rapid PIF5 phosphorylation and degradation in response to red-light activation. Plant Physiol **145**: 1043–51

Shi F, Kawano F, Park SE, Komazaki S, Hirabayashi Y, Polleux F, Yazawa M (2018) Optogenetic Control of Endoplasmic Reticulum–Mitochondria Tethering. ACS Synth Biol **7**: 2–9

Shi H, Shen X, Liu R, Xue C, Wei N, Deng XW, Zhong S (2016) The Red Light Receptor

Phytochrome B Directly Enhances Substrate-E3 Ligase Interactions to Attenuate Ethylene Responses. Dev Cell **39**: 597–610

Shim JS, Imaizumi T (2015) Circadian Clock and Photoperiodic Response in *Arabidopsis* : From Seasonal Flowering to Redox Homeostasis. Biochemistry **54**: 157–170

Shimizu-Sato S, Huq E, Tepperman JM, Quail PH (2002) A light-switchable gene promoter system. Nat Biotechnol **20**: 1041–4

Shinomura T, Uchida K, Furuya M (2000) Elementary Processes of Photoperception by Phytochrome A for High-Irradiance Response of Hypocotyl Elongation in Arabidopsis. Plant Physiol **122**: 147–156

Smart AD, Pache RA, Thomsen ND, Kortemme T, Davis GW, Wells JA (2017) Engineering a light-activated caspase-3 for precise ablation of neurons in vivo. Proc Natl Acad Sci **114**: E8174–E8183

Smith RW, Helwig B, Westphal AH, Pel E, Borst JW, Fleck C (2017) Interactions Between phyB and PIF Proteins Alter Thermal Reversion Reactions in vitro. Photochem Photobiol **93**: 1525–1531

Solano R, Stepanova A, Chao Q, Ecker JR (1998) Nuclear events in ethylene signaling: a transcriptional cascade mediated by ETHYLENE-INSENSITIVE3 and ETHYLENE-RESPONSE-FACTOR1. Genes Dev **12**: 3703–3714

Song YH, Estrada DA, Johnson RS, Kim SK, Lee SY, MacCoss MJ, Imaizumi T (2014) Distinct roles of FKF1, Gigantea, and Zeitlupe proteins in the regulation of Constans stability in Arabidopsis photoperiodic flowering. Proc Natl Acad Sci U S A **111**: 17672–7

Sorokina O, Kapus A, Terecskei K, Dixon LE, Kozma-Bognar L, Nagy F, Millar AJ (2009) A switchable light-input, light-output system modelled and constructed in yeast. J Biol Eng **3**: 15

Spiltoir JI, Strickland D, Glotzer M, Tucker CL (2016) Optical Control of Peroxisomal Trafficking. ACS Synth Biol **5**: 554–560

Spoida K, Eickelbeck D, Karapinar R, Eckhardt T, Mark MD, Jancke D, Ehinger BV, König P, Dalkara D, Herlitze S, et al (2016) Melanopsin Variants as Intrinsic Optogenetic On and Off Switches for Transient versus Sustained Activation of G Protein Pathways. Curr Biol **26**: 1206–1212

Staswick PE, Tiryaki I (2004) The oxylipin signal jasmonic acid is activated by an enzyme that conjugates it to isoleucine in Arabidopsis. Plant Cell **16**: 2117–27

Sternberg SH, Redding S, Jinek M, Greene EC, Doudna JA (2014) DNA interrogation by the CRISPR RNA-guided endonuclease Cas9. Nature **507**: 62–67

Stierl M, Stumpf P, Udwari D, Gueta R, Hagedorn R, Losi A, Gärtner W, Petereit L, Efetova M, Schwarzel M, et al (2011) Light modulation of cellular cAMP by a small bacterial photoactivated adenylyl cyclase, bPAC, of the soil bacterium Beggiatoa. J Biol Chem **286**: 1181–8

Strickland D, Lin Y, Wagner E, Hope CM, Zayner J, Antoniou C, Sosnick TR, Weiss EL, Glotzer M (2012) TULIPs: tunable, light-controlled interacting protein tags for cell biology. Nat Methods **9**: 379–84

Strickland D, Moffat K, Sosnick TR (2008) Light-activated DNA binding in a designed allosteric protein. Proc Natl Acad Sci U S A **105**: 10709–14

Strickland D, Yao X, Gawlak G, Rosen MK, Gardner KH, Sosnick TR (2010) Rationally improving LOV domain-based photoswitches. Nat Methods **7**: 623–6

Sun W, Zhang W, Zhang C, Mao M, Zhao Y, Chen X, Yang Y (2017) Light-induced protein degradation in human-derived cells. Biochem Biophys Res Commun **487**: 241–246

Tabor JJ, Levskaya A, Voigt CA (2011) Multichromatic Control of Gene Expression in Escherichia coli. J Mol Biol **405**: 315–324

Tabor JJ, Salis HM, Simpson ZB, Chevalier AA, Levskaya A, Marcotte EM, Voigt CA, Ellington AD (2009) A Synthetic Genetic Edge Detection Program. Cell **137**: 1272–1281

Taslimi A, Vrana JD, Chen D, Borinskaya S, Mayer BJ, Kennedy MJ, Tucker CL (2014) An optimized optogenetic clustering tool for probing protein interaction and function. Nat Commun **5**: 4925

Taxis C (2017) Development of a Synthetic Switch to Control Protein Stability in Eukaryotic Cells with Light. Methods Mol Biol **1596**: 241–255

Thatcher LF, Cevik V, Grant M, Zhai B, Jones JDG, Manners JM, Kazan K (2016) Characterization of a *JAZ7* activation-tagged Arabidopsis mutant with increased susceptibility to the fungal pathogen *Fusarium oxysporum*. J Exp Bot **67**: 2367–2386

Thines B, Katsir L, Melotto M, Niu Y, Mandaokar A, Liu G, Nomura K, He SY, Howe GA, Browse J (2007) JAZ repressor proteins are targets of the SCF(COI1) complex during jasmonate signalling. Nature **448**: 661–5

Thireault C, Shyu C, Yoshida Y, St Aubin B, Campos ML, Howe GA (2015) Repression of jasmonate signaling by a non-TIFY JAZ protein in Arabidopsis. Plant J **82**: 669–79

Toettcher JE, Gong D, Lim WA, Weiner OD (2011) Light-based feedback for controlling intracellular signaling dynamics. Nat Methods **8**: 837–9

Toettcher JE, Weiner OD, Lim WA (2013) Using optogenetics to interrogate the dynamic control of signal transmission by the Ras/Erk module. Cell **155**: 1422–34

Toledo-Ortiz G, Huq E, Quail PH (2003) The Arabidopsis Basic/Helix-Loop-Helix Transcription Factor Family. Plant Cell **15**: 1749–1770

Tucker M, Staples RR, Valencia-Sanchez MA, Muhlrad D, Parker R (2002) Ccr4p is the catalytic subunit of a Ccr4p/Pop2p/Notp mRNA deadenylase complex in *Saccharomyces cerevisiae*. EMBO J **21**: 1427–1436

Unniyampurath U, Pilankatta R, Krishnan MN (2016) RNA Interference in the Age of CRISPR: Will CRISPR Interfere with RNAi? Int J Mol Sci **17**: 291

VANHOLME B, GRUNEWALD W, BATEMAN A, KOHCHI T, GHEYSEN G (2007) The tify family previously known as ZIM. Trends Plant Sci **12**: 239–244

Vannucci L, Lai M, Chiuppesi F, Ceccherini-Nelli L, Pistello M (2013) Viral vectors: a look back and ahead on gene transfer technology. New Microbiol **36**: 1–22

Vierstra RD (1993) Illuminating Phytochrome Functions (There Is Light at the End of the Tunnel). Plant Physiol **103**: 679–684

Vogel P, Hanswillemenke A, Stafforst T (2017) Switching Protein Localization by Site-Directed RNA Editing under Control of Light. ACS Synth Biol **6**: 1642–1649

Wager A, Browse J (2012) Social Network: JAZ Protein Interactions Expand Our Knowledge of

Jasmonate Signaling. Front Plant Sci **3**: 41

Wang H, Yang H, Shivalila CS, Dawlaty MM, Cheng AW, Zhang F, Jaenisch R (2013) One-Step Generation of Mice Carrying Mutations in Multiple Genes by CRISPR/Cas-Mediated Genome Engineering. Cell **153**: 910–918

Wang X, Chen X, Yang Y (2012) Spatiotemporal control of gene expression by a light-switchable transgene system. Nat Methods **9**: 266–269

Wasternack C, Strnad M (2016) Jasmonate signaling in plant stress responses and development – active and inactive compounds. N Biotechnol **33**: 604–613

Weber W, Fussenegger M (2006) Pharmacologic transgene control systems for gene therapy. J Gene Med **8**: 535–556

Weber W, Fussenegger M (2011) Emerging biomedical applications of synthetic biology. Nat Rev Genet **13**: 21–35

Weber W, Fux C, Daoud-el Baba M, Keller B, Weber CC, Kramer BP, Heinzen C, Aubel D, Bailey JE, Fussenegger M (2002) Macrolide-based transgene control in mammalian cells and mice. Nat Biotechnol **20**: 901–7

Weber W, Link N, Fussenegger M (2006) A genetic redox sensor for mammalian cells. Metab Eng **8**: 273–280

Wehler P, Niopek D, Eils R, Di Ventura B (2016) Optogenetic Control of Nuclear Protein Import in Living Cells Using Light-Inducible Nuclear Localization Signals (LINuS). Curr. Protoc. Chem. Biol. John Wiley & Sons, Inc., Hoboken, NJ, USA, pp 131–145

Weirauch MT, Yang A, Albu M, Cote AG, Montenegro-Montero A, Drewe P, Najafabadi HS, Lambert SA, Mann I, Cook K, et al (2014) Determination and Inference of Eukaryotic Transcription Factor Sequence Specificity. Cell **158**: 1431–1443

Wend S, Bosco CD, Kämpf MM, Ren F, Palme K, Weber W, Dovzhenko A, Zurbriggen MD (2013) A quantitative ratiometric sensor for time-resolved analysis of auxin dynamics. Sci Rep **3**: 2052

Wend S, Wagner HJ, Müller K, Zurbriggen MD, Weber W, Radziwill G (2014) Optogenetic Control of Protein Kinase Activity in Mammalian Cells. ACS Synth Biol **3**: 280–285

Whitfield TW, Wang J, Collins PJ, Partridge EC, Aldred S, Trinklein ND, Myers RM, Weng Z (2012) Functional analysis of transcription factor binding sites in human promoters. Genome Biol **13**: R50

Win MN, Smolke CD (2008) Higher-order cellular information processing with synthetic RNA devices. Science **322**: 456–60

de Wit M, Ljung K, Fankhauser C (2015) Contrasting growth responses in lamina and petiole during neighbor detection depend on differential auxin responsiveness rather than different auxin levels. New Phytol **208**: 198–209

Di Wu, Hu Q, Yan Z, Chen W, Yan C, Huang X, Zhang J, Yang P, Deng H, Wang J, et al (2012) Structural basis of ultraviolet-B perception by UVR8. Nature **484**: 214–219

Wu YI, Frey D, Lungu OI, Jaehrig A, Schlichting I, Kuhlman B, Hahn KM (2009) A genetically encoded photoactivatable Rac controls the motility of living cells. Nature **461**: 104–108

X H, J P, M A, U H (2017) The Blue Light-Induced Interaction of Cryptochrome 1 With COP1 Requires SPA Proteins During Arabidopsis Light Signaling. PLoS Genet. doi:

10.1371/JOURNAL.PGEN.1007044

Xiao H, Edwards TE, Ferré-D'Amaré AR (2008) Structural Basis for Specific, High-Affinity Tetracycline Binding by an In Vitro Evolved Aptamer and Artificial Riboswitch. Chem Biol **15**: 1125–1137

Yamada M, Suzuki Y, Nagasaki SC, Okuno H, Imayoshi I (2018) Light Control of the Tet Gene Expression System in Mammalian Cells. Cell Rep **25**: 487-500.e6

Yan Y, Stolz S, Chételat A, Reymond P, Pagni M, Dubugnon L, Farmer EE (2007) A Downstream Mediator in the Growth Repression Limb of the Jasmonate Pathway. Plant Cell **19**: 2470–2483

Yang C, Li L (2017) Hormonal Regulation in Shade Avoidance. Front Plant Sci **8**: 1527

Yang D-L, Yao J, Mei C-S, Tong X-H, Zeng L-J, Li Q, Xiao L-T, Sun T -p., Li J, Deng X-W, et al (2012) Plant hormone jasmonate prioritizes defense over growth by interfering with gibberellin signaling cascade. Proc Natl Acad Sci **109**: E1192–E1200

Yang J, Reth M (2010) Oligomeric organization of the B-cell antigen receptor on resting cells. Nature **467**: 465–9

Yang SW, Jang I-C, Henriques R, Chua N-H (2009) FAR-RED ELONGATED HYPOCOTYL1 and FHY1-LIKE Associate with the *Arabidopsis* Transcription Factors LAF1 and HFR1 to Transmit Phytochrome A Signals for Inhibition of Hypocotyl Elongation. Plant Cell **21**: 1341–1359

Yanovsky MJ, Casal JJ, Luppi JP (1997) The *VLF* loci, polymorphic between ecotypes Landsberg *erecta* and Columbia, dissect two branches of phytochrome A signal transduction that correspond to very-low-fluence and high-irradiance responses. Plant J **12**: 659–667

Yazawa M, Sadaghiani AM, Hsueh B, Dolmetsch RE (2009) Induction of protein-protein interactions in live cells using light. Nat Biotechnol **27**: 941–945

Ye H, Baba MD-E, Peng R-W, Fussenegger M (2011) A Synthetic Optogenetic Transcription Device Enhances Blood-Glucose Homeostasis in Mice. Science (80-) **332**: 1565–1568

Yen H-CS, Xu Q, Chou DM, Zhao Z, Elledge SJ (2008) Global Protein Stability Profiling in Mammalian Cells. Science (80-) **322**: 918–923

Yeom M, Kim H, Lim J, Shin A-Y, Hong S, Kim J-I, Nam HG (2014) How do phytochromes transmit the light quality information to the circadian clock in Arabidopsis? Mol Plant **7**: 1701–1704

Yin R, Arongaus AB, Binkert M, Ulm R (2015) Two Distinct Domains of the UVR8 Photoreceptor Interact with COP1 to Initiate UV-B Signaling in Arabidopsis. Plant Cell **27**: 202–213

Yousefi OS, Günther M, Hörner M, Chalupsky J, Wess M, Brandl SM, Smith RW, Fleck C, Kunkel T, Zurbriggen MD, et al (2019) Optogenetic control shows that kinetic proofreading regulates the activity of the T cell receptor. Elife. doi: 10.7554/eLife.42475

Yu G, Onodera H, Aono Y, Kawano F, Ueda Y, Furuya A, Suzuki H, Sato M (2016) Optical manipulation of the alpha subunits of heterotrimeric G proteins using photoswitchable dimerization systems. Sci Rep **6**: 35777

Yu X, Sayegh R, Maymon M, Warpeha K, Klejnot J, Yang H, Huang J, Lee J, Kaufman L, Lin C (2009) Formation of Nuclear Bodies of *Arabidopsis* CRY2 in Response to Blue Light Is Associated with Its Blue Light–Dependent Degradation. Plant Cell **21**: 118–130

Yumerefendi H, Dickinson DJ, Wang H, Zimmerman SP, Bear JE, Goldstein B, Hahn K, Kuhlman B (2015) Control of Protein Activity and Cell Fate Specification via Light-Mediated

Nuclear Translocation. PLoS One **10**: e0128443

Zetsche B, Volz SE, Zhang F (2015) A split-Cas9 architecture for inducible genome editing and transcription modulation. Nat Biotechnol **33**: 139–142

Zhang F, Tzanakakis ES (2017) Optogenetic regulation of insulin secretion in pancreatic β-cells. Sci Rep **7**: 9357

Zhang X, Dong C, Huang W, Wang H, Wang L, Ding D, Zhou H, Long J, Wang T, Yang Z (2015) Rational design of a photo-responsive UVR8-derived protein and a self-assembling peptide-protein conjugate for responsive hydrogel formation. Nanoscale **7**: 16666–70

Zhang Y, Mayba O, Pfeiffer A, Shi H, Tepperman JM, Speed TP, Quail PH (2013) A Quartet of PIF bHLH Factors Provides a Transcriptionally Centered Signaling Hub That Regulates Seedling Morphogenesis through Differential Expression-Patterning of Shared Target Genes in Arabidopsis. PLoS Genet **9**: e1003244

Zhang Z, Li X (2018) Genome-wide identification of AP2/ERF superfamily genes and their expression during fruit ripening of Chinese jujube. Sci Rep **8**: 15612

Zhou Q, Hare PD, Yang SW, Zeidler M, Huang L-F, Chua N-H (2005) FHL is required for full phytochrome A signaling and shares overlapping functions with FHY1. Plant J **43**: 356–70

Zhou XX, Chung HK, Lam AJ, Lin MZ (2012) Optical control of protein activity by fluorescent protein domains. Science **338**: 810–4

Zoltowski BD, Gardner KH (2011) Tripping the Light Fantastic: Blue-Light Photoreceptors as Examples of Environmentally Modulated Protein−Protein Interactions. Biochemistry **50**: 4–16

7 Appendix: Publications, Manuscripts

7.1 Original studies and protocols

David Golonka, **Patrick Fischbach**, Siddhartha G. Jena, Julius W. Kleeberg, Lars-Oliver Essen, Jared E. Toettcher, Matias D. Zurbriggen, Andreas Möglich. Deconstructing and repurposing the light-regulated interplay between *Arabidopsis* phytochromes and interacting factors. *Commun Biol* **2,** 448 (2019) doi:10.1038/s42003-019-0687-9

Contribution: Design, performance and analysis of light regulated gene expression experiments. Writing of the manuscript.

Patrick Fischbach, David Golonka, Sergey Fedotov, Andreas Hiltbrunner, Andreas Möglich, Matias D. Zurbriggen. Alternative red-light inducible split transcription factor system. *In preparation,* December 2019.

Contribution: Design, performance and analysis of experiments together with Sergey Fedotov (in the course of his M.Sc. thesis under my supervision). Preparation of all figures and writing of the manuscript.

Julia Baaske, Patrick Gonschorek, Raphael Engesser, Alazne Dominguez-Monedero, Katrin Raute, **Patrick Fischbach**, Konrad Müller, Elise Chachat, Wolfgang W.A. Schamel, Susana Minguet, Jamie A. Davies, Jens Timmer, Wilfried Weber, Matias D. Zurbriggen. Dual-controlled optogenetic system for rapid down-regulation of protein levels in mammalian cells. *Scientific Reports,* 2018 Oct 9,8(1):15024. Doi: 10.1038/s41598-018-32929-7.

Contribution: Performance and analysis of first Caspase experiments.

Patrick Fischbach, Patrick Gonschorek, Julia Baaske, Jamie A. Davies, Wilfried Weber, Matias D. Zurbriggen. Optogenetic downregulation of protein levels to control programmed cell death in mammalian cells with dual blue-light-switch. *Accepted, Methods in Molecular Biology*, December 2019.

Contribution: Design, performance and analysis of experiments. Preparation of all figures and writing of the manuscript.

Patrick Fischbach, Tim Blomeier, Matias D. Zurbriggen. Fast and reversible blue light activated CRISPR/Cas13b mediated mRNA knockout (BLACKout). *In preparation,* December 2019.

Contribution: Design, performance and analysis of experiments. Preparation of all figures and writing of the manuscript.

7.2 Additional publications

Sofia Romero-Montepaone, Sofia Poodts, **Patrick Fischbach**, Romina Sellaro, Matias D. Zurbriggen, Jorge J. Casal. Shade-avoidance responses become more aggressive in warm evironments. *bioRxiv,* 22 July 2019. Doi: https://doi.org/10.11.01/710004.

Contribution: Performance and analysis of experiments.

Markus Pauly, Niklas Gawenda, Christine Wagner, **Patrick Fischbach**, Vicente Ramirez, Ilka Axmann, Catalin Voiniciuc. Suitability of Orthogonal Hosts to Study Plant Cell Wall Biosynthesis. Plants (Basel). 2019;8(11):E516. Published 2019 Nov 17. doi:10.3390/plants8110516

Contribution: Writing the manuscript.

COMMUNICATIONS BIOLOGY

ARTICLE

https://doi.org/10.1038/s42003-019-0687-9 OPEN

Deconstructing and repurposing the light-regulated interplay between *Arabidopsis* phytochromes and interacting factors

David Golonka [1], Patrick Fischbach [2], Siddhartha G. Jena [3], Julius R.W. Kleeberg [1], Lars-Oliver Essen [4], Jared E. Toettcher [3], Matias D. Zurbriggen [2*] & Andreas Möglich [1,5,6,7*]

Phytochrome photoreceptors mediate adaptive responses of plants to red and far-red light. These responses generally entail light-regulated association between phytochromes and other proteins, among them the phytochrome-interacting factors (PIF). The interaction with *Arabidopsis thaliana* phytochrome B (*At*PhyB) localizes to the bipartite APB motif of the *A. thaliana* PIFs (*At*PIF). To address a dearth of quantitative interaction data, we construct and analyze numerous *At*PIF3/6 variants. Red-light-activated binding is predominantly mediated by the APB N-terminus, whereas the C-terminus modulates binding and underlies the differential affinity of *At*PIF3 and *At*PIF6. We identify *At*PIF variants of reduced size, monomeric or homodimeric state, and with *At*PhyB affinities between 10 and 700 nM. Optogenetically deployed in mammalian cells, the *At*PIF variants drive light-regulated gene expression and membrane recruitment, in certain cases reducing basal activity and enhancing regulatory response. Moreover, our results provide hitherto unavailable quantitative insight into the *At*PhyB:*At*PIF interaction underpinning vital light-dependent responses in plants.

[1] Lehrstuhl für Biochemie, Universität Bayreuth, 95447 Bayreuth, Germany. [2] Institute of Synthetic Biology and CEPLAS, Heinrich Heine University Düsseldorf, 40225 Düsseldorf, Germany. [3] Department of Molecular Biology, Princeton University, Princeton, NJ 08544, USA. [4] Department of Chemistry, Center for Synthetic Microbiology, Philipps University Marburg, 35032 Marburg, Germany. [5] Research Center for Bio-Macromolecules, Universität Bayreuth, 95447 Bayreuth, Germany. [6] Bayreuth Center for Biochemistry & Molecular Biology, Universität Bayreuth, 95447 Bayreuth, Germany. [7] North-Bavarian NMR Center, Universität Bayreuth, 95447 Bayreuth, Germany. *email: matias.zurbriggen@uni-duesseldorf.de; andreas.moeglich@uni-bayreuth.de

First discovered among the plant photoreceptors[1], phytochromes (Phy) sense red and far-red light to control a range of physiological responses, including seedling germination, shade avoidance, entrainment of the circadian clock, and the transition from vegetative to reproductive growth[2]. Beyond plants, Phys also occur in bacteria and fungi where they mediate chromatic adaptation and pigmentation among other processes[3,4]. Receptors of the Phy family generally exhibit a bipartite architecture with an N-terminal photosensory core module (PCM) and a C-terminal output module (OPM) (Fig. 1a). The PCM of canonical Phys comprises consecutive PAS (Per/ARNT/Sim), GAF (cGMP-specific phosphodiesterase, adenylyl cyclase, and FhlA), and PHY (Phy-specific) domains and binds within its GAF domain a linear tetrapyrrole (bilin) chromophore[3,5] (Fig. 1b). Phys of higher plants naturally employ phytochromobilin (PΦB), covalently attached to a cysteine residue within the GAF domain, but can be functionally reconstituted with phycocyanobilin (PCB) of cyanobacterial origin. In darkness, conventional Phys adopt their red-absorbing Pr state with the bilin chromophore in the 15*Z* configuration; absorption of red light triggers rapid bilin isomerization to the 15*E* state and population of the metastable, far-red-absorbing Pfr state (Fig. 1b). The Pfr → Pr reversion occurs thermally or can be actively driven by far-red light. Insight from bacterial Phys illustrates that the *Z*/*E* isomerization is coupled to refolding of the so-called PHY tongue, a protrusion of the PHY domain, from a β-hairpin to an α-helix conformation, in turn prompting quaternary structural rearrangements[6–10]. Bacterial Phys mostly form part of two-component signaling cascades[11] with OPMs acting as histidine kinases (HKs). By contrast, the Phy OPMs of land plants comprise two PAS domains, PAS-A and PAS-B, and a homologous HK-related domain that, however, lacks key residues essential for function and is thus devoid of HK activity. Rather, plant Phys have been reported to exhibit serine/threonine kinase activity[12,13]. Plant Phys exert their biological effects via light-regulated cytonucleoplasmic shuttling and protein:protein interactions (PPIs), which manifest in transcriptional responses and proteolytic degradation of cellular target proteins[14–16]. As one prominent protein family, the so-called phytochrome-interacting factors (PIFs) undergo light-regulated PPIs with plant Phys and act as basic helix–loop–helix transcription factors[14,17–20] (Fig. 1c and Supplementary Fig. 1).

Arabidopsis thaliana possesses five Phys, denoted *At*PhyA–E, that engage with a set of at least eight PIFs, denoted *At*PIF1–8[14,17]. For the arguably best-studied Phy, *At*PhyB, preferential interactions of the Pfr state vs. the Pr state were identified with all eight *At*PIFs[14,17,21–23]. Notably, the PCM of *At*PhyB is necessary and sufficient for red-light-activated and far-red-light-reversible *At*PIF binding[19,24–26]. Although a pioneering study on the optogenetic use of *At*PhyB reported that reversible interactions with *At*PIF6 required the presence of PAS-A and PAS-B[27], numerous later studies demonstrated that the PCM suffices for photoreversible interactions with *At*PIFs[28–30]. That notwithstanding, the C-terminal OPM likely contributes to light-regulated PPIs and is integral to eliciting physiological responses[14,15]. Likewise, the light-activated interaction with *At*PhyB maps to the weakly conserved APB (active phytochrome B binding) consensus motif within the N-terminal region of *At*PIF orthologs that precedes the basic helix–loop–helix domain[24] (Fig. 1d). The APB motif consists of two segments, termed APB.A and APB.B, the first of which exhibits higher sequence conservation (Supplementary Fig. 1) and dominates light-activated *At*PhyB binding as indicated by site-directed mutagenesis[24]. In the case of *At*PhyA, the isolated PCM also suffices for light-regulated interactions with *At*PIF1 and *At*PIF3, which localize to the APA motifs (active phytochrome A binding) of these PIFs, somewhat C-terminal of the APB motifs[31,32].

Early on, the light-regulated *At*Phy:*At*PIF PPI has been harnessed for the control of cellular processes in heterologous hosts by red and far-red light[25,27], an approach now known as optogenetics[33]. As manifold natural processes are intrinsically governed by PPIs, the *At*Phy:*At*PIF system provides a widely applicable means for the bimodal control of cellular phenomena

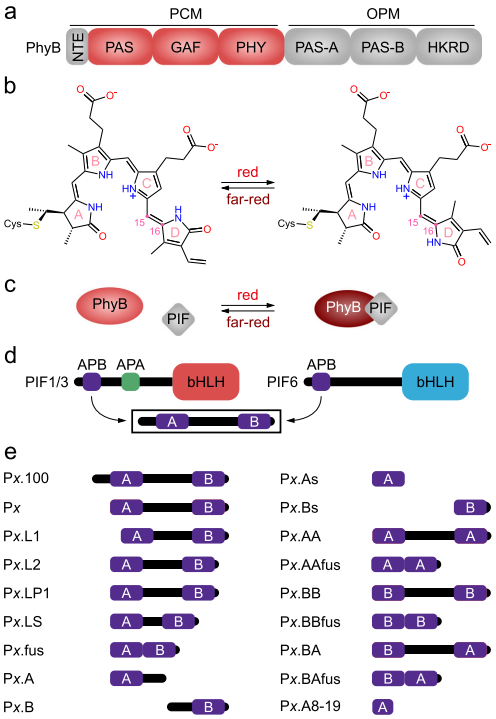

Fig. 1 Architecture and function of plant phytochromes (Phy) and their cognate phytochrome-interacting factors (PIFs). **a** Modular composition of plant phytochromes. An N-terminal extension (NTE) is succeeded by the photosensory core module (PCM) consisting of consecutive PAS, GAF, and PHY domains, with a phytochromobilin (PΦB) chromophore covalently bound as a thioether within the GAF domain. The C-terminal output module (OPM) comprises two additional PAS domains (PAS-A and PAS-B), succeeded by a histidine-kinase-related domain (HKRD). **b** In the dark-adapted Pr (red-absorbing) state of the Phy, the PΦB chromophore adopts its 15*Z* form. Red light drives isomerization to the 15*E* form to give rise to the Pfr state (far-red-absorbing). Vice versa, far-red light drives the Pfr → Pr transition. **c** In their Pr state (red), plant Phys show no or at most weak interactions with PIFs. Following red-light absorption, the Pfr state (brown) is populated and affinity for the PIFs enhanced. **d** Modular composition of PIFs. An N-terminal region of around 100 residues contains the so-called APB motif that mediates interactions with phytochrome B. The APB motif further subdivides into the ABP.A and APB.B segments[24]. Certain PIFs also possess a more C-terminal APA motif engaged in interactions with phytochrome A. The C-terminal part comprises a basic helix–loop–helix (bHLH) DNA-binding domain. **e** Based on the N-terminal fragments of *Arabidopsis thaliana* PIFs 3 and 6, a panel of PIF variants were generated and probed for light-dependent protein:protein interactions with the PCM of *A. thaliana* PhyB (cf. Supplementary Table 1 for a detailed description of these derivatives).

with supreme resolution in space and time[34]. As a case in point, the expression of transgenes in yeast and mammalian cells has been subjected to red-/far-red-light control via a two-hybrid strategy[25,35,36]. To this end, a split transcription factor was engineered with one component of the *At*Phy:*At*PIF pair connected to a sequence-specific DNA-binding domain and the other to a transcriptional *trans*-activating domain. Exposure to red light prompts colocalization of the two entities and onset of expression from synthetic target promoters. In another approach[27,37,38], the *At*Phy:*At*PIF pair conferred light sensitivity on plasma membrane recruitment and cellular signaling cascades in mammalian cells. Although details differ, optogenetic applications to date mostly employ the isolated PCM of *At*PhyB and the N-terminal 100 amino acids of *At*PIF3/6, denoted P3.100 and P6.100, that comprise the APB motif.

Despite the eminent role of the *At*Phy:*At*PIF interaction in nature and optogenetics, quantitative data on the interaction strength and the underlying sequence determinants are scarce. To fill this gap, we dissected and analyzed the light-dependent interaction between *At*PhyB and *At*PIF3/6 by several qualitative and quantitative approaches. Whereas the *At*PhyB PCM bound P6.100 with about 10 nM affinity in its Pfr state and showed no detectable affinity in the Pr state, P3.100 exhibited weaker Pfr-state affinity and elevated basal affinity in Pr. By deconstructing *At*PIF3/6 and engineering a wide set of shortened variants, we pinpointed APB.A as decisive for light-regulated PPIs, with a modulatory role for APB.B. Quantitative analyses informed the construction of minimal *At*PIF3/6 fragments of 25 and 23 residues, respectively, that retained stringently light-regulated PPIs with *At*PhyB. When deployed for the optogenetic control of gene expression and membrane recruitment, the novel *At*PIF variants with a range of interaction strengths achieved stratified and enhanced light responses.

Results

Deconstructing the *At*PhyB:*At*PIF interaction. Starting from the *At*PIF constructs P3.100 and P6.100, we generated numerous derivatives with residues deleted from the N terminus, the linker between the APB.A and APB.B segments varied, or either segment omitted or duplicated (Fig. 1e, Supplementary Table 1). All *At*PIF variants were C-terminally tagged with enhanced yellow fluorescent protein (EYFP) to promote protein solubility and facilitate concentration determination. We implemented a screening assay to efficiently probe interactions of these variants with the Pfr state of the *At*PhyB PCM. The screen exploits the fact that *At*PIF binding stabilizes the Pfr state of *At*PhyB and decelerates the thermal reversion to the Pr state in the dark[39] (Fig. 2a). For this assay, the *At*PIF-EYFP variants were expressed in *Escherichia coli*, purified *At*PhyB PCM was added to the crude cell lysate in substoichiometric amounts, and the Pfr → Pr reversion kinetics were monitored by absorption spectroscopy (Fig. 2b, c). The initial kinetics were normalized to an EYFP-negative control and provide a convenient readout for interactions (Fig. 2d). Although qualitative in nature, this first screening platform offers important advantages: (i) owing to the specificity of the *At*PhyB:*At*PIF interaction, the assay can be conducted in crude bacterial lysate, without the need for protein purification; and (ii) it can be easily multiplexed to test many variants in a single experiment.

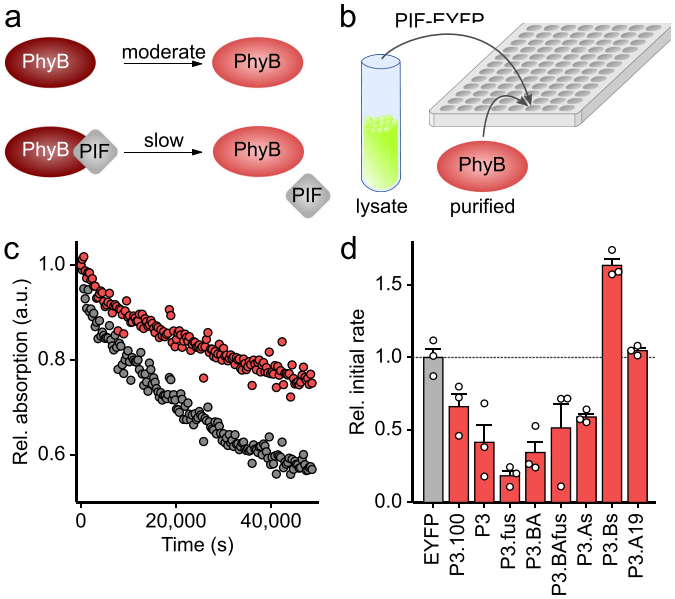

Fig. 2 Screening *At*PIF variants for protein:protein interactions with the *At*PhyB PCM. **a** The light-adapted Pfr state (brown) of *At*PhyB thermally recovers to the dark-adapted Pr state (red) in a moderately paced reaction. When binding to an *At*PIF variant, the recovery reaction is delayed. **b** *At*PIF variants were C-terminally tagged with EYFP, expressed in *Escherichia coli*, cells were lysed, and *At*PhyB PCM was added to the crude lysate. Samples were exposed to red light, and the recovery reaction was monitored over time by absorption measurements. **c** Normalized absorption of the *At*PhyB PCM measured at 720 nm after red-light absorption in the presence of P3.100 (red) or the EYFP-negative control (gray). **d** The initial rates of the recovery reaction were determined and normalized to the reading obtained for the EYFP-negative control. Data indicate mean ± SEM of $n = 3$ independent biological replicates.

A multiple sequence alignment of the N-terminal regions of *At*PIF1–8 delineates two regions of conservation that define the A and B segments of the APB motif (Supplementary Fig. 1[24]). The APB.A segment shows stronger conservation and comprises around 20 residues centered around the consensus core sequence ELXXXXGQ[24]; by comparison, the APB.B region is considerably shorter and less conserved. As the very N-terminal region preceding APB.A varies substantially among the *At*PIFs in length and sequence, we deemed it non-essential for *At*PhyB interactions and removed it from P3.100 and P6.100. The resultant P*x* variants (here and in the following, $x = 3, 6$) retained interaction with the *At*PhyB PCM, and all subsequent *At*PIF variants were thus based on these N-terminally truncated forms (Fig. 2d and Supplementary Fig. 2). Next, we interrogated the linkage between the constituent APB.A and APB.B segments, which is of heterogenous length and sequence across *At*PIF1–8. We generated a set of variants, including (i) P*x*.L1 and P*x*.L2 in which the linkers of P3/P6 are shortened by 10 residues at their N and C termini, respectively; (ii) P*x*.LP1 in which said linker is substituted for the corresponding segment of *At*PIF1, the shortest among all *At*PIFs; and (iii) P*x*.LS in which the linker is replaced by a repetitive glycine–serine stretch of 10 residues. As gauged by their effect on dark-reversion kinetics (cf. Supplementary Fig. 2), all these variants still interacted with the Pfr state of the *At*PhyB PCM. These results imply that the linker connecting the APB.A and APB.B segments is dispensable, which is confirmed in the P*x*.fus variants that directly link these two segments without any linker and still exhibit interaction with the *At*PhyB PCM (cf. Fig. 2d and Supplementary Fig. 2). To assess whether productive *At*PhyB binding mandates a specific topology of the APB segments, we generated the variants P*x*.BA and P*x*.BAfus with inverted sequential order of APB.A and APB.B, and the original linker sequence kept or removed, respectively. Again, these variants retained interactions with the Pfr state of the *At*PhyB PCM (cf. Fig. 2d and Supplementary Fig. 2). Site-directed mutagenesis had previously ascribed a dominant role to APB.A in mediating the light-dependent interaction with *At*PhyB[24], and we hence probed the two segments of the composite APB motif separately. Both the APB.A-containing variants P*x*.A and the P*x*.As, with or without the N-terminal half of the respective linker, still showed interactions with the *At*PhyB PCM as judged by the effect on dark-reversion kinetics (cf. Fig. 2d and Supplementary Fig. 2). By contrast, neither the APB.B-based P*x*.B nor the P*x*.Bs variants, with or without the C-terminal half of the linker, respectively, exhibited interactions in this assay. Duplication of the A part in the variants P*x*.AA and P*x*.AAfus preserved interactions with the *At*PhyB PCM, and vice versa, duplication of the B segment in P*x*.BB and P*x*.BBfus failed to restore them (cf. Supplementary Fig. 2). Taken together, our findings emphasize the dominant role of APB.A for mediating interactions with *At*PhyB. To further characterize the APB.A segment, we successively trimmed residues flanking its ELXXXXGQ core sequence. However, even the removal of five weakly conserved C-terminal residues in the variants P*x*.A19 abolished interactions with *At*PhyB, as judged by their inability to slow down the *At*PhyB-PCM Pfr → Pr reversion kinetics (cf. Fig. 2d and Supplementary Fig. 2). Likewise, no interaction with the *At*PhyB PCM was detected for more extensive truncations of the APB.A segment (cf. Supplementary Fig. 2).

Biochemical analyses of the *At*PhyB:*At*PIF interaction. The above screening platform affords a qualitative first-pass assessment of the *At*PIF variants but does not quantify the strength of interactions with *At*PhyB. Moreover, the assay is limited to interactions within the Pfr state but not the Pr state. We hence selected several of the above *At*PIF candidates for in-depth analysis. Following expression and purification, we assessed the oligomeric state of these variants and of the *At*PhyB PCM by size-exclusion chromatography (SEC). In its Pr state, the isolated *At*PhyB PCM elutes as a monomer with a minor homodimeric fraction, consistent with a recent SEC analysis[40] (Fig. 3a). In the Pfr state, the predominantly monomeric state is maintained but the retention from the SEC column is slightly delayed, which arguably reflects light-induced conformational changes, i.e., a compaction, of the PCM that may resemble those observed in bacterial Phys[6–8,10] (Fig. 3b). At a concentration of 10 µM, P3.100 and P6.100 largely eluted as homodimers with a minor monomeric population (Fig. 3c, Supplementary Fig. 3 and Table 1). Dimerization is not caused by the EYFP tag as the fluorescent protein itself eluted as a monomer (Fig. 3d, Table 1). Notably, the homodimeric state of *At*PIFs is also observed in nature and critical for their physiological function as basic helix–loop–helix transcription factors[41]. Size reduction of the *At*PIFs impaired homodimerization in several variants to different extent

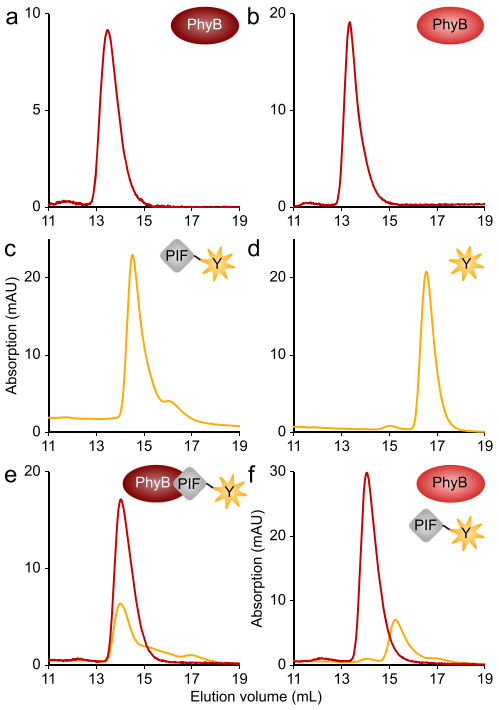

Fig. 3 Oligomeric state of the *At*PIF variants and light-dependent interactions with the *At*PhyB PCM. **a** 50 µM *At*PhyB PCM were exposed to red light and analyzed by size-exclusion chromatography (SEC), where the yellow and red lines represent absorption at 513 and 650 nm, respectively. **b** As in **a** but the *At*PhyB PCM was exposed to far-red light prior to chromatography. **c** 10 µM P3.100-EYFP were analyzed by SEC. Elution profiles were independent of illumination. **d** 10 µM of the negative control EYFP were analyzed by SEC. Elution profiles were independent of light. **e** A mixture of 10 µM P3.100-EYFP and 50 µM *At*PhyB PCM was exposed to red light and analyzed by SEC. **f** As in **e** but samples were illuminated with far-red light, rather than red light. Experiments were repeated twice with similar results.

Table 1 Biochemical analyses of the *At*PIF3/6 variants.

Name	Oligomeric state[a]	*At*PhyB-PCM interaction[a,b]	Pfr state K_D (nM)[c]	Pr state K_D (nM)[c]
P3.100	Homodimer	+	200 ± 70	>2000
P6.100	Homodimer	+	10 ± 8	n.d.
P3	Homodimer	+	220 ± 40	>10,000
P6	Homodimer/monomer	+	10 ± 7	n.d.
P3.fus	Monomer	+	270 ± 60	>10,000
P6.fus	Homodimer	+	200 ± 90	>10,000
P3.A	Homodimer	+	220 ± 40	>10,000
P6.A	Monomer	+	280 ± 100	>2000
P3.As	Monomer	+	680 ± 60	>10,000
P6.As	Monomer	+	710 ± 80	>10,000
P3.AA	Homodimer	+	370 ± 40	>3000
P6.AA	Homodimer	+	360 ± 40	>2000
P3.AAfus	Homodimer/monomer	+	230 ± 50	>10,000
P6.AAfus	Homodimer/monomer	+	230 ± 30	>10,000
P3.A19	Monomer	–	>1000	n.d.
P6.A19	Monomer	–	>2000	n.d.
P3.A14	Monomer	–	n.d.	n.d.
P6.A14	Monomer	–	n.d.	n.d.
P3.A8	Monomer	–	n.d.	n.d.
P6.A8	Monomer	–	n.d.	n.d.
P3.B	Monomer	–	n.d.	n.d.
P6.B	Monomer	–	n.d.	n.d.
EYFP	Monomer	–	n.d.	n.d.

n.d. not detectable
[a]As determined by size-exclusion chromatography
[b]A "+" sign indicates that an interaction could be detected by size-exclusion chromatography, a "–" sign denotes that no interaction was observed
[c]As determined by fluorescence anisotropy

(Supplementary Fig. 3, Table 1). If the APB.A segment was truncated, as in P3.A and P6.A, or excluded altogether, as in P3.Bs and P6.Bs, homodimerization was lost completely. Taken together, these findings point toward a contribution of the APB.A segment to homodimerization of the current *At*PIF variants and, by extension, of the intact *At*PIF3 and *At*PIF6 proteins[41].

We next investigated the interactions between the *At*PIF3/6 variants and the *At*PhyB PCM by SEC (Fig. 3e, Supplementary Fig. 4 and Table 1). To this end, we first converted the *At*PhyB PCM to its Pfr state by illumination with red light (640 nm), incubated it at a 5:1 molar ratio with the different *At*PIF variants, and analyzed the mixture by SEC. In full agreement with the first-pass screening (cf. Fig. 2 and Supplementary Fig. 2), all variants that we had identified as binding-competent exhibited interactions with *At*PhyB PCM at an apparent 1:1 stoichiometry. Vice versa, the *At*PIF variants that had failed to decelerate *At*PhyB reversion kinetics (cf. Fig. 2 and Supplementary Fig. 2) lacked any interactions (Supplementary Fig. 4). We also assessed interactions between the *At*PIF variants and the *At*PhyB PCM in the Pr state following exposure to far-red light (720 nm) (Fig. 3f and Supplementary Fig. 5). None of the variants showed interactions under these conditions. Insofar red-light-activated binding to the *At*PhyB PCM had been retained in the truncated *At*PIF variants, far-red light hence abolished it.

Having engineered a suite of *At*PIF variants undergoing light-regulated PPIs with the *At*PhyB PCM, we next sought to quantify the strength of these interaction in both the Pr and Pfr states. Notably, detailed quantitative data of that type are largely unavailable but would tremendously improve our understanding of the *At*PhyB:*At*PIF PPI and inform its optimization. To this end, we resorted to fluorescence anisotropy measurements of the EYFP moiety C-terminally appended to all the *At*PIF variants. Binding of a given *At*PIF-EYFP variant to the *At*PhyB PCM would increase its effective hydrodynamic radius, slow down rotational diffusion, and thus increase fluorescence anisotropy (Fig. 4a). We hence incubated a constant 20 nM of the *At*PIF-EYFP variants with increasing amounts of *At*PhyB PCM under red or far-red light and recorded binding isotherms. The reference construct P6.100 exhibited strong binding to the *At*PhyB PCM under red light but no detectable binding under far-red light even at *At*PhyB-PCM concentrations of 2 µM (Fig. 4b). When calculating dissociation constants (K_D), one must consider that red light not only drives the Pr → Pfr transition of Phys but also the reverse Pfr → Pr process. Consequently, continuous illumination with red light (640 nm) leads to population of a photostationary state with a mixed Pfr/Pr population at a ratio of ~0.56/0.44[42] (Fig. 4c). Correcting for the actual fraction in the Pfr state, we determined a K_D for the P6.100:*At*PhyB-PCM pair of 10 ± 8 nM (Table 1). This value is in good agreement with an earlier estimate for this pair of 20-100 nM within mammalian cells based on fluorescence microscopy[27]. In comparison to P6.100, P3.100 exhibited a weaker K_D of 200 ± 70 nM in Pfr and an elevated basal affinity in Pr, with an estimated K_D on the order of low micromolar (Fig. 4d and Table 1). This residual interaction could in principle be due to partial population of the Pfr state of the *At*PhyB PCM under the chosen illumination conditions; however, the absence of basal affinity in case of P6.100 strongly argues against this notion. The slightly weaker affinity and much less pronounced light effect in P3.100 compared to P6.100 may account for the previously reported inability to detect light-regulated interactions of *At*PIF3 with the *At*PhyB PCM in mammalian cells[27]. We then recorded binding isotherms under red and far-red light for all the *At*PIF variants we had purified and analyzed by SEC (Supplementary Figs. 4 and 5, Table 1). Consistent with our first-pass assessment (cf. Fig. 2d and Supplementary Fig. 2), the removal of the non-conserved N-terminal residues preceding the APB.A segment had no influence on the Pfr interaction. Unexpectedly, omission of these residues in the *At*PIF3 context substantially attenuated the basal Pr-state affinity. For the *At*PIF3 variants, removal of the linker and the APB.B part had no or at most modest effects on affinity to the Pfr state (Supplementary Fig. 6, Table 1). By contrast, in *At*PIF6, the removal of the linker and the APB.B part more severely attenuated the affinity to the Pfr state to values between 200 and 700 nM. In

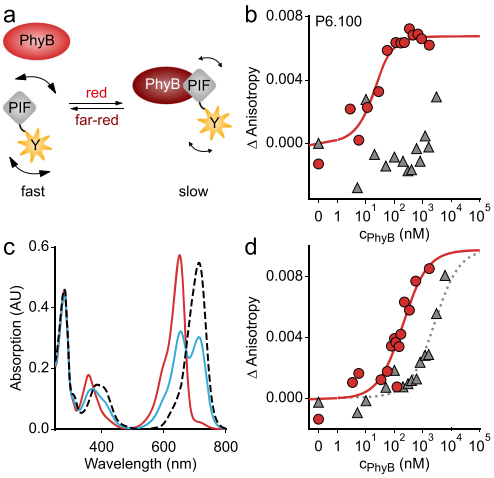

Fig. 4 Quantitative analyses of the light-dependent protein:protein interaction between *At*PIF variants and the *At*PhyB PCM. **a** In its Pr state, the *At*PhyB PCM exhibits weak or no affinity to *At*PIF, but upon red-light exposure, the affinity is enhanced. Binding to the AtPhyB PCM increases the effective hydrodynamic radius of the *At*PIF variants and slows down rotational diffusion. In turn, the fluorescence anisotropy of an EYFP tag C-terminally appended to the *At*PIF increases. **b** Titration of 20 nM P6.100-EYFP with increasing concentrations of dark-adapted (gray) or red-light-exposed *At*PhyB PCM (red), as monitored by anisotropy of the EYFP fluorescence. Data points show mean of $n = 3$ biological replicates. The red line denotes a fit to a single-site-binding isotherm. **c** Absorption spectra of the *At*PhyB PCM in its dark-adapted Pr state (red line) and as a Pfr/Pr mixture following red-light exposure (blue). The dashed line denotes the absorption spectrum of the pure Pfr state, calculated according to ref. [42]. **d** As in **b** but for P3.100-EYFP rather than P6.100-EYFP. Experiments were repeated twice with similar results.

addition, the affinity to the Pr state, non-detectable for the variants P6.100 and P6, increased as well. As a corollary, *At*PIF3 and *At*PIF6 variants lacking the APB.B segment exhibited closely similar K_D values for a given construct topology. As a case in point, the P3.As and the P6.As variants, comprising 25 and 23 residues, respectively, both interacted with the *At*PhyB PCM with an affinity of ~700 nM in the Pfr and weaker than 10 µM in the Pr state. These data for P6As are consistent with a recent report that demonstrated light-dependent PPI for an *At*PIF6 construct of closely similar length and sequence[43]. Duplication of the APB.A segments in the *At*PIF3/6 backgrounds resulted in variants with affinities in the range of 200–400 nM for Pfr and weaker than 2 µM for Pr. We also analyzed several *At*PIF3/6 variants entirely lacking the APB.A segment or possessing shortened versions of it, neither of which showed any interaction with *At*PhyB PCM when probed by SEC nor by their effect on Pr reversion kinetics. In almost all these variants, fluorescence anisotropy failed to detect interactions either (Supplementary Fig. 6 and Table 1); merely, the P3.A19 and P6.A19 variants with C-terminally trimmed APB.A segments exhibited weak affinity for the Pfr state in the low micromolar range (Supplementary Fig. 6 and Table 1). In summary, these results confirm the APB.A segment as the main interaction epitope in both *At*PIF3 and *At*PIF6. Intriguingly, *At*PIF6 differs from *At*PIF3 by higher affinity for Pfr and much reduced affinity for Pr. As the removal of the APB.B segment largely cancels these differences, we conclude that APB.B in *At*PIF6, but not in *At*PIF3, enhances the affinity for Pfr and diminishes that for Pr. In *At*PIF3, the N-terminal amino acids contribute to elevated basal affinity for Pr.

Repurposing the *At*PhyB:*At*PIF interaction for optogenetics. Through sequence variations and quantitative analyses, we generated modules for light-regulated PPIs spanning an affinity for the Pfr state from around 10 to 700 nM. We next investigated whether this set of novel *At*PIF variants can be leveraged for optogenetics in mammalian cells. In a first line of experiments, we embedded the variants into a previously reported system for red-/far-red-light-regulated gene expression that provides an in-cell readout of relative PPI affinities[36,44]. To this end, the *At*PhyB PCM was covalently attached to a VP16 *trans*-activating domain, and the different *At*PIF variants were linked to the E-protein DNA-binding domain, which binds to a cognate operator sequence upstream of a minimal promoter driving expression of secreted alkaline phosphatase (SEAP) (Fig. 5a). Through light-induced *At*PhyB:*At*PIF interactions, the *trans*-activating domain localizes to the DNA-binding domain and the promoter and thereby induces SEAP expression. SEAP activity levels are quantified and normalized to the levels of constitutively expressed *Gaussia* luciferase to correct for variations of cell density, transfection efficiency, and overall expression. We found that the P3.100 and P6.100 reference constructs upregulated normalized SEAP expression by tenfold and fourfold, respectively, under red light compared to darkness when expressed in Chinese hamster ovary cells (CHO-K1). The comparatively small regulatory effect for P6.100 results from substantial basal SEAP expression. We then subjected all the *At*PIF3/6 variants we had previously characterized to the same analysis (Fig. 5b, c and Supplementary Fig. 7). Consistent with the above measurements, *At*PIF variants that lacked detectable interactions with the *At*PhyB PCM, e.g., P*x*.B and P*x*.A19, failed to stimulate reporter expression regardless of illumination. By contrast, variants that exhibited interactions with the *At*PhyB PCM were generally capable of inducing SEAP expression under red light, albeit to different degree. Overall, the expression levels observed for the individual *At*PIF variants scaled with binding affinity, in that low measured K_D values correlated with strong SEAP activity. For instance, all *At*PIF3/6 variants containing the intact APB.A segment exhibited strong expression under red light. Whereas P6.100 suffered from relatively high basal expression, the shortened *At*PIF6 derivatives generally showed reduced SEAP expression in darkness, translating into much more pronounced regulatory effects. For instance, in the variant P6.A the SEAP expression increased by 43-fold under red light relative to darkness. Duplication of APB.A in the variants P6.AA and P3.AA elevated SEAP expression under red light and, to lesser extent, in darkness, thereby enhancing the regulatory effect. The overall higher SEAP expression under red light for these variants could reflect the binding of two *At*PhyB-VP16 modules to one P*x*.AA protein. However, we note that, under the conditions employed for the SEC analysis, we did not find evidence for simultaneous binding of two *At*PhyB PCM entities to the P*x*.AA variants. We also assessed the photoreversibility of the gene-expression systems based on the *At*PIF derivatives (Supplementary Fig. 8). When the cells were first exposed to red light for 24 h, followed by far-red illumination for another 24 h, they exhibited basal SEAP expression levels comparable to cells incubated in darkness throughout. Given that gene expression for the different sequence variations followed similar trends in both the *At*PIF3 and the *At*PIF6 backgrounds, we wondered whether the emerging underlying principles extend to other *At*PIF orthologs. We hence generated the corresponding sequence variations in the *At*PIF1 background and assessed their impact on

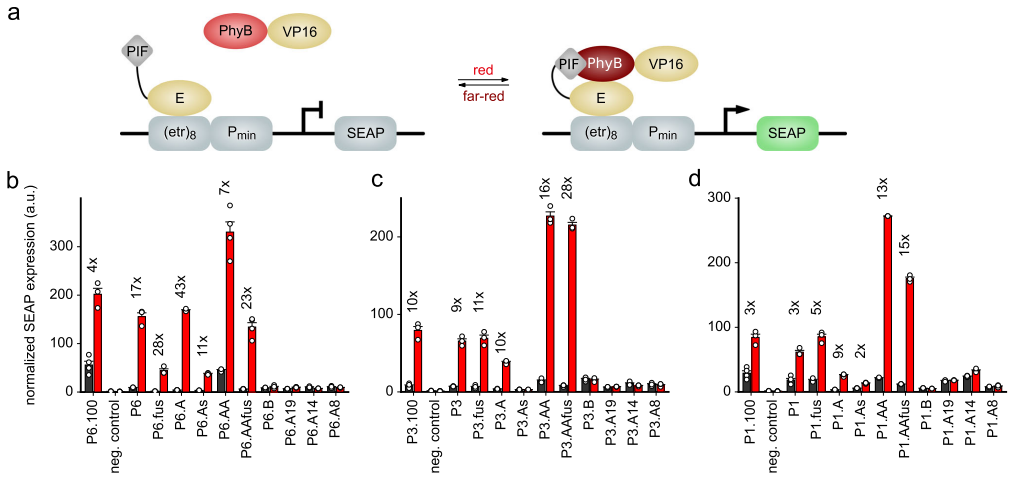

Fig. 5 Harnessing the *At*PIF variants for the light-dependent regulation of gene expression in mammalian cells. **a** The *At*PhyB PCM and *At*PIF variants are connected to a VP16 *trans*-activating domain and an E-protein DNA-binding domain that binds to a synthetic promoter sequence. Red light promotes association of the *At*PhyB:*At*PIF pair and thereby activates the expression of a secreted alkaline phosphatase (SEAP) reporter gene. **b** SEAP expression was determined in Chinese hamster ovary cells (CHO-K1) for the diverse *At*PIF6 variants and normalized to the constitutive expression of *Gaussia* luciferase. Black and red bars denote mean ± SEM normalized SEAP expression for $n = 4$ independent biological replicates under dark or red-light conditions, respectively. Cells were kept in darkness for 24 h, supplemented with PCB, and then either kept in darkness for 24 h or illuminated for 24 h with 20 µmol m^{-2} s^{-1} 660-nm light. As a negative control, the reporter construct alone was transfected. The numbers above the bars indicate the factor difference between dark and red-light conditions for a given *At*PIF6 variant. **c** As **b** but for the *At*PIF3 variants. **d** As **b** but for the *At*PIF1 variants.

light-regulated gene expression (Fig. 5d and Supplementary Fig. 7). Several of the resultant *At*PIF1 variants supported light-activated SEAP expression, although generally with slightly attenuated maximal levels and regulatory effects. Nonetheless, the *At*PIF1 variants conformed to the general activity pattern observed for the *At*PIF3/6 variants; specifically, only the *At*PIF1 variants preserving an intact APB.A segment were capable of upregulating SEAP expression under red light. Taken together, these experiments demonstrate the utility of the cellular set-up for the efficient appraisal of light-regulated PPIs in mammalian cells. By capitalizing on this set-up, we obtained derivative systems with enhanced dynamic range and reduced leakiness that outperformed the original reference systems.

In a second set of experiments, we deployed several of the newly generated *At*PIF6 variants for light-regulated recruitment of target proteins to the plasma membrane of NIH-3T3 cells. To this end, we equipped the *At*PhyB PCM with a C-terminal CAAX prenylation motif for membrane targeting and the *At*PIF6 variants with an N-terminal EYFP tag[27,37,38] (Fig. 6a). Cell lines stably expressing both the *At*PhyB PCM and one of the *At*PIF6 variants, linked by an internal ribosome entry site (IRES), were created through lentiviral transduction. Cells were exposed to red (650 nm) and far-red light (750 nm), respectively, and the subcellular distribution of the EYFP-*At*PIF6 variants was monitored by fluorescence microscopy (Fig. 6b–e). Under far-red light, the reference variant P6.100 mostly localized to the cytoplasm, but under red light it partially translocated to the plasma membrane (Fig. 6c–f). Whereas the variants P6.A, P6.As, and P6.AA exhibited overall similar subcellular distribution under red and far-red light as P6.100, the variant P6.fus failed to show any light response of subcellular localization. Although subtle performance differences between the individual *At*PIF6 variants cannot be ruled out, these are exceeded by the cell-to-cell variability of light-dependent translocation (Fig. 6f). Nonetheless, the experiments show that the new *At*PIF6 variants with a much smaller footprint support light-regulated plasma membrane recruitment at similar efficiencies as the reference P6.100. This notion is further supported by the overall comparable expression level of the *At*PIF6 variants and its effect on the magnitude of light-regulated membrane recruitment (Fig. 6g).

Discussion

In this study, we have dissected the light-regulated PPIs between the *At*PhyB PCM and the *At*PIFs 3 and 6, which underpin diverse adaptive responses in planta and multiple applications in optogenetics. To this end, we implemented a set of complementary experimental approaches ranging from SEC and fluorescence anisotropy to reporter assays in mammalian cells that deliver both qualitative and quantitative information on the PPIs. At a qualitative level, these assays consistently showed the APB.A segment to be necessary and sufficient for *At*PhyB-PCM interactions, in line with previous reports[24]. By contrast, the APB.B segment alone did not promote detectable interactions. Our quantitative analyses put concrete numbers on the affinity of the *At*PhyB:*At*PIF3/6 pairs, information that hitherto was largely lacking. Strikingly, P6.100 exhibited a K_D of only ~10 nM for *At*PhyB PCM in its Pfr state but entirely lacked interaction with the Pr state, from which we estimate an at least 1000-fold affinity difference. By contrast, the light dependence of the P3.100:*At*PhyB-PCM interaction was less pronounced, with dissociation constants of ~200 nM in the Pfr state and low micromolar in the Pr state. We tied the more stringent red-light response in *At*PIF6 to its APB.B segment, which enhances affinity for the Pfr state of the *At*PhyB PCM while simultaneously attenuating basal affinity for the Pr state. We speculate that these inherent differences between AtPIF3 and *At*PIF6 might reflect their natural roles in planta. Whereas *At*PIF3 predominantly serves as a negative regulator of photomorphogenesis by modulating the abundance of

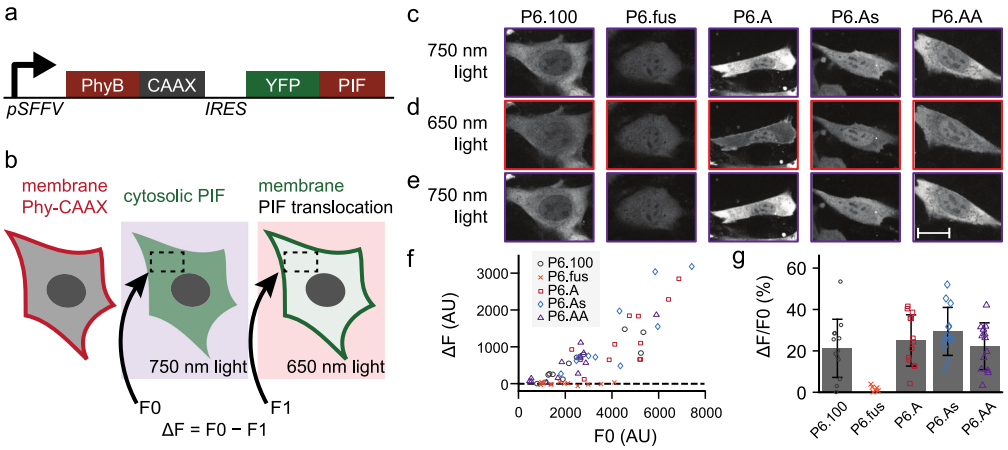

Fig. 6 Photoreversible recruitment to the plasma membrane. **a** *At*PhyB and one of the several new *At*PIF6 variants, equipped with a C-terminal CAAX prenylation motif or an N-terminal EYFP tag, respectively, were encoded on a bicistronic vector with an intervening IRES sequence and expressed in NIH-3T3 cells. **b** Owing to the CAAX tag, *At*PhyB localizes to the plasma membrane, while the EYFP-*At*PIF6 variants shuttle between cytosol and plasma membrane as a function of light. Under far-red light (750 nm), the EYFP-*At*PIF6 variants exhibit cytosolic localization; under red light (650 nm), they can bind to *At*PhyB and translocate to the membrane. **c**–**e** Fluorescence micrographs of NIH-3T3 cells expressing *At*PhyB-CAAX and different EYFP-*At*PIF6 variants under far-red light (**c**), after red-light exposure (**d**), and after additional exposure to far-red light (**e**). The scale bar denotes 20 µm. **f** The relative depletion of cytosolic EYFP fluorescence under red light compared to far-red light for the EYFP-*At*PIF6 variants. Data represent mean ± SD of $n \geq 12$ individual cells. **g** Dependence of the relative fluorescence change on the overall EYFP-*At*PIF6 expression level.

*At*PhyB[45–47], *At*PIF6 acts as a positive regulator by inhibiting hypocotyl elongation under red light, at least when over-expressed[48]. To prevent untimely inhibition of hypocotyl growth, a more stringent light response with very low basal affinity in Pr may be required for this particular PIF. Recently, it has been reported that PIFs, and in particular *At*PIF3, are constantly turned over both in darkness and under red light as a mechanism of achieving optimal levels for tight regulation of the skotomorphogenic and photomorphogenic responses[14]. A more permissive binding of *At*PIF3 to the Pr state of *At*PhyB as observed here might facilitate the regulation of PIF abundance in darkness. This concurs with reports that *At*PhyB mediates phosphorylation by PPK-family kinases and subsequent degradation of *At*PIF3 in both the Pr and Pfr states[49]. The differential affinities of the individual PIFs might therefore contribute to the fine-tuning of physiological responses[14,49]. In fact, our study now provides a means of gradually adjusting the interaction strength of a given PIF, which could benefit the analysis of signal transduction mechanisms in planta. In a similar vein, the quantitative data on the *At*PhyB:*At*PIF PPI may help rationalize the phenotypes of pertinent *pif* mutant alleles. Finally, the comparatively smaller regulatory effect in *At*PhyB:*At*PIF3, compared to *At*PhyB:*At*PIF6, may explain why this PPI pair proved inferior for generic optogenetic applications[27].

By deconstructing and quantitatively analyzing *At*PIF3/6, we devised a suite of interaction modules with several beneficial traits (Table 1): First, the *At*PIF variants span an affinity range from 10 to 700 nM, thus enabling the precise tuning of light-regulated PPIs as demanded by a specific application. Second, the *At*PIFs can be reduced to around 23–25 residues while largely retaining light-regulated PPIs with the *At*PhyB PCM. As we demonstrate, the smaller size facilitates the construction of tandem repeats of the APB.A motif, which, depending upon context, may enhance light-dependent responses. Third, the reduction in size also affected the oligomeric state of the *At*PIFs, which are homodimeric at full length[41] but predominantly monomeric in several of the truncated variants studied presently. As we showcase for the scenarios of light-regulated gene expression and membrane recruitment, the set of novel *At*PIF variants can indeed improve absolute activity and degree of light regulation in optogenetics. As a case in point, despite stringently light-regulated PPIs with the *At*PhyB PCM, the original P6.100 variant promoted substantial basal gene expression in darkness, thus degrading the regulatory effect of light. We tentatively ascribe the relatively poor performance of P6.100 to its high Pfr-state affinity; even limited population of the *At*PhyB Pfr state, e.g., due to light pollution or temperature changes[50], may hence activate the PPI to considerable extent and over prolonged periods[39]. In support of this notion, the attenuation of the Pfr-state affinity in the shortened *At*PIF6 variants led to reduced basal activity and enhanced regulatory efficiency. Duplication of the APB.A segment improved the performance for light-regulated expression, although the Pfr-state affinity of the P*x*.AA variants is almost unchanged relative to the corresponding P*x*.A variants. We hence ascribe this improvement to avidity and cooperativity effects. Our analyses readily extended to the *At*PIF1 context, where shortened variants exhibited similar patterns of activity and light regulation as the *At*PIF3/6 variants (cf. Fig. 5b–d). We speculate that the underlying principles can be generalized to APB-containing PIF proteins from *A. thaliana* and other plants[51,52]. The performance of individual *At*PIF variants in a given experiment can considerably vary and may be difficult to gauge upfront, not least because it likely depends on application context. We thus consider it an advantage to have now a set of *At*PIF variants with known interaction strengths and varying properties. With this suite of *At*PIF variants in hand, additional processes may be unlocked for optogenetic control by red and far-red light. As recently summarized[53], numerous cellular parameters and pathways depend on PPIs and can thus be controlled by certain photoreceptors that associate or dissociate

under blue light. The underlying regulatory strategy should readily extend to the present *At*PhyB:*At*PIF pairs and thereby to red and far-red light. Other potential use cases for the new *At*PIF variants include immunoreceptor signaling[30] and light-regulated biomaterials[54]. As one shortcoming, optogenetic applications of plant Phys currently require the exogenous addition of PCB or PΦB chromophores, which do not widely occur outside cyanobacteria and plants. This contrasts with bacterial Phys, which utilize biliverdin (BV) that is available in mammals as a heme degradation product[55–58]. In particular, a recently described bacterial Phy undergoes PPIs depending on red and far-red light and has been harnessed for light-regulated gene expression[59–61]. The reliance on BV in this system obviates exogenous chromophore addition, which may prove advantageous for applications in vivo.

In summary, we have constructed and characterized a toolkit of novel *At*PIF variants with varying interaction strength, size, and oligomeric state. Beyond application in optogenetics, the availability of these variants also stands to benefit the biophysical analyses of the Phy:PIF interaction. Although previous studies had localized this interaction to the N-terminal extension of Phys, atomically resolved information on the Phy:PIF complex is lacking[40,62–64]. Minimized *At*PIFs may well facilitate X-ray crystallographic analysis and thus pave the way toward elucidation of the complex structure. Moreover, the qualitative and quantitative interaction assays presently established can be deployed to chart Phys and interacting factors from *A. thaliana* and other plants.

Methods

Molecular biology and protein purification. Genes encoding *A. thaliana* PhyB PCM (residues 1–651), PIF3 (1–100), and PIF6 (1–100) were synthesized with codon usage adapted for expression in *E. coli* (GeneArt, Invitrogen, Regensburg, Germany). Via Gibson assembly[65], the *At*PhyB PCM was furnished with a C-terminal hexahistidine tag and subcloned onto the pCDFDuet1 vector (Novagen, Merck, Darmstadt, Germany) under control of a T7-lacO promoter; the plasmid, designated pDG282, additionally harbors a bicistronic cassette of *Synechocystis* sp. heme oxygenase 1 and pcyA[66], also under the control of T7-lacO. For the expression of *At*PIF3/6, the corresponding genes were subcloned onto a pET-19b vector (Novagen) under the control of a T7-lacO promoter by Gibson assembly or AQUA cloning[67] and thereby equipped with an N-terminal His_6-SUMO tag[68] and a C-terminal EYFP tag, attached via a short linker (DSAGSAGSAG). For interaction studies in bacterial lysate, the *At*PIF3/6 genes were subcloned onto a pET-28c vector (Novagen) under the control of a T7-lacO promoter, again with C-terminal linkers and EYFP. Variants of the *At*PIF proteins were generated in both plasmid contexts, and the identity of all constructs was confirmed by Sanger DNA sequencing (GATC, Konstanz, Germany or Microsynth Seqlab, Göttingen, Germany).

For *At*PhyB expression, the plasmid pDG282 was transformed into the *E. coli* BL21(DE3) strain. Transformant cells were grown in 2× 1000 mL terrific-broth (TB) medium, supplemented with 100 μg mL^{-1} streptomycin, at 37 °C in darkness until an optical density at 600 nm (OD_{600}) of 0.6–0.8 was reached. δ-Aminolevulinic acid was added at 0.5 mM to assist chromophore production[69], and the expression was induced by adding 1 mM β-D-1-thiogalactopyranoside (IPTG). Cultivation continued overnight at 18 °C, before cells were harvested by centrifugation, resuspended in lysis buffer [50 mM Tris/HCl pH 8.0, 20 mM NaCl, 20 mM imidazole; supplemented with protease inhibitor mix (cOmplete Ultra, Roche Diagnostics, Mannheim, Germany)], and lysed by sonification. The cleared lysate was purified by immobilized ion affinity chromatography (IMAC) on Protino Ni-NTA 1 mL columns (Macherey-Nagel, Düren, Germany) and eluted with a linear imidazole gradient from 20 to 500 mM. Elution fractions were analyzed by denaturing polyacrylamide gel electrophoresis (PAGE), where 1 mM Zn^{2+} was added to enable detection of covalently incorporated bilin chromophores via zinc-induced fluorescence[70]. Suitable fractions were pooled and dialyzed overnight into AEX buffer (20 mM Tris/HCl pH 8.0, 50 mM NaCl, 5 mM 2-mercaptoethanol), applied to a HiTrap Q HP 1 mL anion-exchange column (GE Healthcare Europe GmbH, Freiburg, Germany), and eluted using two successive linear gradients from 50 to 300 mM NaCl and from 300 to 500 mM. Eluted fractions were analyzed by PAGE, appropriately pooled, dialyzed against storage buffer [10 mM Tris/HCl pH8, 10 mM NaCl, 10 % (w/v) glycerol], and stored at −80 °C.

Purification of the *At*PIF3/6-EYFP variants employed a similar protocol with the following differences. No δ-aminolevulinic acid was added, and incubation after induction continued at 16 °C for 40 h. Following IMAC, the N-terminal His_6-SUMO was cleaved overnight at 4 °C during dialysis into 50 mM Tris/HCl pH 8.0 and 20 mM NaCl using SENP2-protease. The His_6-SUMO tag was removed by IMAC, and the flow-through containing the *At*PIF3/6 construct was collected and analyzed by PAGE. Depending upon purity, the proteins were optionally further purified by anion-exchange chromatography as described above. Pure *At*PIF3/6-EYFP variants were dialyzed into storage buffer and stored at −80 °C. An analysis by denaturing PAGE of the purified *At*PIF3/6-EYFP constructs and the *At*PhyB PCM is shown as Supplementary Fig. 9.

Spectroscopic analysis. The concentration of purified *At*PhyB PCM and the *At*PIF3/6-EYFP variants were determined at 22 °C by absorption measurements on an Agilent 8453 UV-visible spectrophotometer (Agilent Technologies, Waldbronn, Germany). In case of the *At*PIF3/6-EYFP variants, a molar extinction coefficient at 513 nm of 84,300 M^{-1} cm^{-1} was used[71]. Photoreversible Pr ↔ Pfr conversion of *At*PhyB PCM was ascertained by illumination with light-emitting diodes (LED) with emission wavelengths of 650 ± 15 nm (5.6 μW cm^{-2}) and 720 ± 15 nm (0.7 μW cm^{-2}), respectively. Spectra recorded after illumination revealed isosbestic points at 374 and 672 nm. Absorption spectra were also recorded after denaturation in 6.5 M guanidinium hydrochloride. By referencing to the previously reported extinction coefficient for PCB under these conditions[72], we calculated an extinction coefficient at the isosbestic point 672 nm for *At*PhyB PCM in its native state of 47,600 M^{-1} cm^{-1}. The fraction of *At*PhyB PCM in the Pfr state upon saturating red-light illumination (640 nm) was determined as described in ref. [42].

Interaction assay in bacterial lysate. pET-28c plasmids harboring *At*PIF3-EYFP or *At*PIF6-EYFP variants were transformed into chemically competent BL21(DE3) cells. Three replicate clones were used to inoculate 3× 5 mL TB medium supplemented with 50 μg mL^{-1} kanamycin. Cultures were incubated at 37 °C up to an OD_{600} of 0.6–0.8, at which point temperature was lowered to 16 °C and expression was induced by addition of 1 mM IPTG. Incubation continued overnight, and cells were harvested by centrifugation at 3000 × *g* for 10 min. Pelleted cells were resuspended in 300 μL lysis buffer [1× FastBreak Cell Lysis Reagent (Promega GmbH, Mannheim, Germany), 10 μg mL^{-1} DNaseI (PanReac AppliChem, Darmstadt, Germany), 200 μg mL^{-1} lysozyme (Sigma-Aldrich, Darmstadt, Germany)] and rotated at 22 °C for 10 min. Cell debris was removed by centrifugation at 186,000 × *g* for 45 min using an Optima MAX-XP Ultracentrifuge (Beckman-Coulter, Krefeld, Germany). The concentration of a given *At*PIF3/6-EYFP variant in the lysate was determined by absorption measurements at 513 nm using a CLARIOstar microtiter plate reader (MTP) (BMG Labtech, Ortenberg, Germany). *At*PhyB PCM at 2.5 μM concentration was mixed with a threefold molar excess of the *At*PIF3/6-EYFP variants in 384-well clear MTPs (Thermo Fisher Scientific, Waltham, USA). After illumination with red light (650 ± 15 nm, 5.6 μW cm^{-2}) for 4 min, the MTPs were covered with a clear lid, and absorption at 720 and 850 nm was measured every 5 min at 28 °C in an Infinite M200 PRO plate reader (Tecan, Männedorf, Switzerland) for 12 h. After background correction, data at 720 nm were normalized to the signal of the L-EYFP (Supplementary Table 1) negative control, and the relative initial velocity was determined over the data acquired during the first 4 h.

Interaction assays with purified components. *Size-exclusion chromatography*: The light-dependent interaction between *At*PhyB PCM and the *At*PIF3/6-EYFP variants was assessed by gel filtration chromatography using a Superdex 200 Increase 10/300 GL (GE Healthcare) column on an ÄKTApure system, equipped with multi-wavelength detection (GE Healthcare). To this end, a mixture of 50 μM *At*PhyB-PCM and 10 μM PIF-EYFP in 67 mM sodium phosphate buffer pH 8.0 and 200 mM NaCl was prepared and illuminated with 650- or 720-nm light for 2 min before sample application. Twenty-five microliters of this mixture was applied to the column and separated at a constant 0.75 mL min^{-1} flow rate. Absorption of EYFP and the *At*PhyB PCM was measured at 513 and 650 nm, respectively. All proteins were also tested individually, where the *At*PIF3/6-EYFP and EYFP samples were not illuminated prior to application.

Fluorescence anisotropy: *At*PhyB PCM was illuminated with 640- or 750-nm light for 2 min immediately prior to the experiment (640 ± 15 nm; 65 μW cm^{-2} and 750 ± 15 nm; 420 μW cm^{-2}). Samples containing 20 nM *At*PIF3/6-EYFP and increasing *At*PhyB-PCM concentrations between 0 and 10 μM were prepared in 20 mM HEPES/HCl pH 7.3, 10 mM NaCl, and 100 μg mL^{-1} bovine serum albumin, transferred into black 384-well MTPs (Brand, Wertheim, Germany), and illuminated with 640- or 750-nm light. Fluorescence anisotropy of EYFP fluorophore was measured on a CLARIOstar MTP reader (BMG Labtech) with an excitation wavelength of 482 ± 16 nm, a 504-nm long-pass dichroic filter, and a detection wavelength of 530 ± 40 nm. The fluorescence gains for the horizontal and vertical detection channels were adjusted to a fluorescence anisotropy value of 0.315, as determined for EYFP with an Olis DSM 172 spectrophotometer (On-Line Instrument Systems, Bogart, USA). Anisotropy data were evaluated with the Fit-o-mat software[73] using a single-site binding isotherm:

$$r = r_0 + r_1 \frac{[\mathrm{PhyB}]}{[\mathrm{PhyB}] + K_\mathrm{D}}$$

where r represents the anisotropy of the PIF-EYFP fluorescence, [PhyB] is the concentration of the *At*PhyB PCM in either the Pr or Pfr state, and K_D is the dissociation constant. For the case of strong binding exhibited by the variants P6.100 and P6, we used a modified single-site binding isotherm that takes into account that the relevant [PhyB] concentrations are on the same order of magnitude as the constant concentration c_{total} of the PIF-EYFP protein:

$$r = r_0 + r_1/2 \times \left\{1 + [\mathrm{PhyB}]/c_{\mathrm{total}} + K_{\mathrm{D}}/c_{\mathrm{total}} - \sqrt{(1 + [\mathrm{PhyB}]/c_{\mathrm{total}} + K_{\mathrm{D}}/c_{\mathrm{total}})^2 - 4[\mathrm{PhyB}]/c_{\mathrm{total}}}\right\}$$

Light-regulated gene expression in mammalian cells. The split transcription factor system for light-controlled gene expression in eukaryotic cells was based on a previously reported set-up[36,44]. To allow ratiometric analysis, this earlier set-up was expanded by cloning the *Gaussia* luciferase under the control of a constitutive promoter onto the same plasmid as the SEAP reporter gene. For testing of the *At*PIF variants, *At*PIF6 (1–100) was replaced by the corresponding *At*PIF1/3/6 derivatives. CHO-K1 (DSMZ, Braunschweig, Germany) were cultivated in HAM's F12 medium (PAN Biotech, Aidenbach, Germany; no. P04–14500) supplemented with 10% (v/v) tetracycline-free fetal bovine serum (PAN Biotech; no. P30–3602; batch no. P080317TC) and 1.4% (v/v) streptomycin (PAN Biotech; no. P06–07100). In all, 5×10^4 CHO-K1 cells were transfected using polyethyleneimine (PEI; Polysciences Inc. Europe, Hirschberg, Germany; no. 23966–1)[74]. DNA (0.75 µg) was diluted in 50 µL OptiMEM (Invitrogen, Thermo Fisher Scientific) and mixed with a PEI/OptiMEM mix (2.5 µL PEI solution in 50 µL OptiMEM). The DNA–PEI mix was added to the cells after 15 min of incubation at room temperature. At 4 h post-transfection, the medium was exchanged. CHO-K1 cells were transfected with the reporter plasmid etr8-CMVmin-SEAP-BGH-SV40-Gaussia (pPF035) and the different *At*PhyB:*At*PIF variants. All plasmids were transfected in equal amounts (w/w). At 24 h post-transfection, the cells were supplemented with 15 µM phycocyanobilin (24 mM stock solution in DMSO; Frontier Scientific, Logan, UT, USA; no. P14137) and incubated for 1 h. The cells were then illuminated with 660-nm light for 24 h at an intensity of 20 µmol m^{-2} s^{-1}, delivered by custom-built LED light boxes[36], or kept in darkness. As a negative control, the reporter construct alone was transfected. Photoreversibility was tested by incubating cells for 24 h under red light, followed by exchange of the media and incubation under far-red light for 24 h. In parallel, cells were incubated in darkness for 48 h with media exchange after 24 h. Exchange of media and other cell handling was done under 522-nm safe light, to prevent inadvertent actuation of the light-sensitive systems.

SEAP activity assay: The supernatant of transfected cells was transferred to 96-well round-bottom MTPs and incubated at 68 °C for 1 h to inactivate endogenous phosphatases. Afterwards, 80 µL of the supernatant were transferred to 96-well flat-bottom MTPs, and per well 100 µL SEAP buffer [20 mM homoarginine, 1 mM $MgCl_2$, 21% (v/v) diethanolamine] was added[36]. After addition of 20 µL 120 mM para-nitrophenyl phosphate, the absorption at 405 nm was measured for 1 h using a BMG Labtech CLARIOstar or a TriStar2 S LB 942 multimode plate reader (Berthold Technologies, Bad Wildbad, Germany)[36]. Outliers were statistically determined and excluded[75].

Gaussia luciferase assay: Twenty microliters of the supernatant of the transfected cells were transferred to a 96-well white MTP and diluted in 60 µL phosphate-buffered saline (PBS; 2.68 mM KCl, 1.47 mM KH_2PO_4, 8.03 mM Na_2PO_4, 137 mM NaCl). After addition of 20 µL coelenterazine (472 mM stock solution in methanol, diluted 1:1500 in PBS; Carl Roth, Karlsruhe, Germany, no. 4094.4), the luminescence was measured for 20 min using TriStar2 LB 941 or LB 942 multimode plate readers.

Light-mediated membrane recruitment in mammalian cells. For each *At*PIF6 variant tested, a lentiviral vector (pHR) was constructed containing a membrane-bound *At*PhyB PCM (PHY-CAAX, residues 1–650) and a YFP-conjugated *At*PIF6 variant. An IRES was introduced between the two coding sequences to ensure regulation of dual expression. Lentivirus was created by transfecting HEK-293T cells with pHR constructs and harvesting filtered media 48 h post-transfection. Mouse fibroblasts (NIH-3T3) were cultured in Dulbecco's Modified Eagle Medium (DMEM) containing 10% (v/v) fetal bovine serum. Fibroblasts were treated with lentivirus containing the constructs of interest. For all fibroblast experiments, cells were cultured in a 96-well glass-bottomed plate. Wells were pretreated with fibronectin for 30 min, following which fibronectin was aspirated and cells were plated and spun down for 5 min at 800 rpm. Cells were plated in 96-well glass-bottom plates and allowed to adhere for at least 12 h. Imaging was performed using a ×60 oil immersion objective (NA 1.4) on a Nikon TI Eclipse microscope with a CSU-X1 confocal spinning disk, an EM-CCD camera, and appropriate laser lines, dichroics, and filters. DMEM was supplemented with phycocyanobilin 30 min prior to the start of the experiment. Cells were exposed to infrared light followed by red light to cause membrane recruitment and the resulting change in cytoplasmic fluorescence was measured using ImageJ by selecting a cytoplasmic region and computing the average pixel intensity before and after photostimulation. The change in cytoplasmic YFP-PIF level was normalized to the total YFP-PIF fluorescence in the nucleus under infrared conditions, to normalize to total expression level differences caused by lentivirus. In these experiments, light was delivered through the microscope using a Mightex Polygon digital micromirror device (DMD), X-Cite XLED1 LED light sources at 635 ± 20 and 730 ± 20 nm, and a ×40 objective lens. The duration of LED illumination was 1 min. To estimate the light dose delivered to the cell, we measured the light intensity using a ThorLabs power meter (PM100D) when the DMD was set to 100% transmission and obtained 100 µW for 635-nm light and 20 µW for 730-nm light, over a field of view of about 100 µm squared. For all experiments, we set the DMDs to 5% dithering (so each region was only illuminated for 5% of the time), translating into a final calculated intensity of 5 µW 635-nm light and 1 µW of 730-nm light. The light was delivered over an approximately 100 µm × 100 µm field of view, leading to an overall LED power density of 50 mW cm^{-2} at 635 nm and 10 mW cm^{-2} at 730 nm. Notably, these values are slightly higher but of comparable magnitude to those used by Pathak et al. for the *At*PhyB:*At*PIF3/6 system in the context of light-regulated gene expression[76].

Statistics and reproducibility. Data are reported as mean ± SD or as mean ± SEM of $n \geq 3$ biologically independent replicates. Details are specified in the legends to the figures and tables. All experiments could be reproduced with similar results.

Reporting summary. Further information on research design is available in the Nature Research Reporting Summary linked to this article.

Data availability

The data underlying Figs. 2–6 are available in Supplementary Data 1. All data that support the findings of this study are available from the corresponding author upon reasonable request.

Received: 20 July 2019; Accepted: 7 November 2019;
Published online: 02 December 2019

References

1. Butler, W. L., Norris, K. H., Siegelman, H. W. & Hendricks, S. B. Detection, assay, and preliminary purification of the pigment controlling photoresponsive development of plants. *Proc. Natl Acad. Sci.* **45**, 1703–1708 (1959).
2. Bae, G. & Choi, G. Decoding of light signals by plant phytochromes and their interacting proteins. *Annu. Rev. Plant Biol.* **59**, 281–311 (2008).
3. Rockwell, N. C. & Lagarias, J. C. A brief history of phytochromes. *Chemphyschem* **11**, 1172–1180 (2010).
4. Quail, P. H. Phytochrome photosensory signalling networks. *Nat. Rev. Mol. Cell Biol.* **3**, 85–93 (2002).
5. Rockwell, N. C., Su, Y.-S. & Lagarias, J. C. Phytochrome structure and signaling mechanisms. *Annu. Rev. Plant Biol.* **57**, 837–858 (2006).
6. Takala, H. et al. Signal amplification and transduction in phytochrome photosensors. *Nature* **509**, 245–248 (2014).
7. Burgie, E. S., Zhang, J. & Vierstra, R. D. Crystal structure of deinococcus phytochrome in the photoactivated state reveals a cascade of structural rearrangements during photoconversion. *Structure* **24**, 448–457 (2016).
8. Song, C. et al. 3D structures of plant phytochrome A as Pr and Pfr from solid-state NMR: implications for molecular function. *Front. Plant Sci.* **9**, 498 (2018).
9. Anders, K., Daminelli-Widany, G., Mroginski, M. A., von Stetten, D. & Essen, L.-O. Structure of the cyanobacterial phytochrome 2 photosensor implies a tryptophan switch for phytochrome signaling. *J. Biol. Chem.* **288**, 35714–35725 (2013).
10. Assafa, T. E., Anders, K., Linne, U., Essen, L.-O. & Bordignon, E. Light-driven domain mechanics of a minimal phytochrome photosensory module studied by EPR. *Structure* **26**, 1534–1545.e4 (2018).
11. Gao, R. & Stock, A. M. Biological insights from structures of two-component proteins. *Annu. Rev. Microbiol.* **63**, 133–154 (2009).
12. Yeh, K. C. & Lagarias, J. C. Eukaryotic phytochromes: light-regulated serine/threonine protein kinases with histidine kinase ancestry. *Proc. Natl Acad. Sci. USA* **95**, 13976–13981 (1998).
13. Shin, A.-Y. et al. Evidence that phytochrome functions as a protein kinase in plant light signalling. *Nat. Commun.* **7**, 11545 (2016).
14. Pham, V. N., Kathare, P. K. & Huq, E. Phytochromes and phytochrome interacting factors. *Plant Physiol.* **176**, 1025–1038 (2018).
15. Casal, J. J. Photoreceptor signaling networks in plant responses to shade. *Annu. Rev. Plant Biol.* **64**, 403–427 (2013).
16. Rausenberger, J. et al. Photoconversion and nuclear trafficking cycles determine phytochrome A's response profile to far-red light. *Cell* **146**, 813–825 (2011).

17. Leivar, P. & Monte, E. PIFs: systems integrators in plant development. *Plant Cell* **26**, 56–78 (2014).
18. Ni, M., Tepperman, J. M. & Quail, P. H. PIF3, a phytochrome-interacting factor necessary for normal photoinduced signal transduction, is a novel basic helix-loop-helix protein. *Cell* **95**, 657–667 (1998).
19. Ni, M., Tepperman, J. M. & Quail, P. H. Binding of phytochrome B to its nuclear signalling partner PIF3 is reversibly induced by light. *Nature* **400**, 781–784 (1999).
20. Martín, G. et al. Phytochrome and retrograde signalling pathways converge to antagonistically regulate a light-induced transcriptional network. *Nat. Commun.* **7**, 11431 (2016).
21. Toledo-Ortiz, G., Huq, E. & Quail, P. H. The Arabidopsis basic/helix-loop-helix transcription factor family. *Plant Cell* **15**, 1749–1770 (2003).
22. Heim, M. A. et al. The basic helix–loop–helix transcription factor family in plants: a genome-wide study of protein structure and functional diversity. *Mol. Biol. Evol.* **20**, 735–747 (2003).
23. Bailey, P. C. et al. Update on the basic helix-loop-helix transcription factor gene family in *Arabidopsis thaliana*. *Plant Cell* **15**, 2497–2502 (2003).
24. Khanna, R. et al. A novel molecular recognition motif necessary for targeting photoactivated phytochrome signaling to specific basic helix-loop-helix transcription factors. *Plant Cell* **16**, 3033–3044 (2004).
25. Shimizu-Sato, S., Huq, E., Tepperman, J. M. & Quail, P. H. A light-switchable gene promoter system. *Nat. Biotechnol.* **20**, 1041–1044 (2002).
26. Matsushita, T., Mochizuki, N. & Nagatani, A. Dimers of the N-terminal domain of phytochrome B are functional in the nucleus. *Nature* **424**, 571–574 (2003).
27. Levskaya, A., Weiner, O. D., Lim, W. A. & Voigt, C. A. Spatiotemporal control of cell signalling using a light-switchable protein interaction. *Nature* **461**, 997–1001 (2009).
28. Müller, K. et al. A red/far-red light-responsive bi-stable toggle switch to control gene expression in mammalian cells. *Nucleic Acids Res.* **41**, e77 (2013).
29. Buckley, C. E. et al. Reversible optogenetic control of subcellular protein localization in a live vertebrate embryo. *Dev. Cell* **36**, 117–126 (2016).
30. Yousefi, O. S. et al. Optogenetic control shows that kinetic proofreading regulates the activity of the T cell receptor. *eLife* **8**, e42475 (2019).
31. Huq, E. et al. Phytochrome-interacting factor 1 is a critical bHLH regulator of chlorophyll biosynthesis. *Science* **305**, 1937–1941 (2004).
32. Lee, N. & Choi, G. Phytochrome-interacting factor from Arabidopsis to liverwort. *Curr. Opin. Plant Biol.* **35**, 54–60 (2017).
33. Deisseroth, K. et al. Next-generation optical technologies for illuminating genetically targeted brain circuits. *J. Neurosci.* **26**, 10380–10386 (2006).
34. Ziegler, T. & Möglich, A. Photoreceptor engineering. *Front. Mol. Biosci.* **2**, 30 (2015).
35. Müller, K. et al. Multi-chromatic control of mammalian gene expression and signaling. *Nucleic Acids Res.* **41**, e124 (2013).
36. Müller, K., Zurbriggen, M. D. & Weber, W. Control of gene expression using a red- and far-red light-responsive bi-stable toggle switch. *Nat. Protoc.* **9**, 622–632 (2014).
37. Toettcher, J. E., Gong, D., Lim, W. A. & Weiner, O. D. Light-based feedback for controlling intracellular signaling dynamics. *Nat. Methods* **8**, 837–839 (2011).
38. Toettcher, J. E., Weiner, O. D. & Lim, W. A. Using optogenetics to interrogate the dynamic control of signal transmission by the Ras/Erk module. *Cell* **155**, 1422–1434 (2013).
39. Smith, R. W. et al. Interactions between phyB and PIF proteins alter thermal reversion reactions in vitro. *Photochem. Photobiol.* **93**, 1525–1531 (2017).
40. Burgie, E. S., Bussell, A. N., Walker, J. M., Dubiel, K. & Vierstra, R. D. Crystal structure of the photosensing module from a red/far-red light-absorbing plant phytochrome. *Proc. Natl Acad. Sci. USA* **111**, 10179–10184 (2014).
41. Castillon, A., Shen, H. & Huq, E. Phytochrome interacting factors: central players in phytochrome-mediated light signaling networks. *Trends Plant Sci.* **12**, 514–521 (2007).
42. Butler, W. L., Hendricks, S. B. & Siegelman, H. W. Action spectra of phytochrome in vitro. *Photochem. Photobiol.* **3**, 521–528 (1964).
43. Hörner, M. et al. Light-controlled affinity purification of protein complexes exemplified by the resting ZAP70 interactome. *Front. Immunol.* **10**, 226 (2019).
44. Müller, K. et al. A red light-controlled synthetic gene expression switch for plant systems. *Mol. Biosyst.* **10**, 1679–1688 (2014).
45. Leivar, P. et al. The arabidopsis phytochrome-interacting factor PIF7, together with PIF3 and PIF4, regulates responses to prolonged red light by modulating phyB levels. *Plant Cell* **20**, 337–352 (2008).
46. Monte, E. et al. The phytochrome-interacting transcription factor, PIF3, acts early, selectively, and positively in light-induced chloroplast development. *Proc. Natl Acad. Sci.* **101**, 16091–16098 (2004).
47. Kim, J. et al. Functional characterization of phytochrome interacting factor 3 in phytochrome-mediated light signal transduction. *Plant Cell* **15**, 2399–2407 (2003).
48. Penfield, S., Josse, E.-M. & Halliday, K. J. A role for an alternative splice variant of PIF6 in the control of Arabidopsis primary seed dormancy. *Plant Mol. Biol.* **73**, 89–95 (2010).
49. Ni, W. et al. PPKs mediate direct signal transfer from phytochrome photoreceptors to transcription factor PIF3. *Nat. Commun.* **8**, 15236 (2017).
50. Legris, M. et al. Phytochrome B integrates light and temperature signals in Arabidopsis. *Science* **354**, 897–900 (2016).
51. Li, F.-W. et al. Phytochrome diversity in green plants and the origin of canonical plant phytochromes. *Nat. Commun.* **6**, 7852 (2015).
52. Sakuraba, Y. et al. Phytochrome-interacting transcription factors PIF4 and PIF5 induce leaf senescence in *Arabidopsis*. *Nat. Commun.* **5**, 4636 (2014).
53. Losi, A., Gardner, K. H. & Möglich, A. Blue-light receptors for optogenetics. *Chem. Rev.* **118**, 10659–10709 (2018).
54. Hörner, M. et al. Phytochrome-based extracellular matrix with reversibly tunable mechanical properties. *Adv. Mater.* **31**, 1806727 (2019).
55. Gasser, C. et al. Engineering of a red-light-activated human cAMP/cGMP-specific phosphodiesterase. *Proc. Natl Acad. Sci. USA* **111**, 8803–8808 (2014).
56. Ryu, M.-H. et al. Engineering adenylate cyclases regulated by near-infrared window light. *Proc. Natl Acad. Sci. USA* **111**, 10167–10172 (2014).
57. Etzl, S., Lindner, R., Nelson, M. D. & Winkler, A. Structure-guided design and functional characterization of an artificial red light–regulated guanylate/adenylate cyclase for optogenetic applications. *J. Biol. Chem.* **293**, 9078–9089 (2018).
58. Stabel, R. et al. Revisiting and redesigning light-activated cyclic-mononucleotide phosphodiesterases. *J. Mol. Biol.* **431**, 3029–3045 (2019).
59. Kaberniuk, A. A., Shemetov, A. A. & Verkhusha, V. V. A bacterial phytochrome-based optogenetic system controllable with near-infrared light. *Nat. Methods* **13**, 591–597 (2016).
60. Redchuk, T. A., Omelina, E. S., Chernov, K. G. & Verkhusha, V. V. Near-infrared optogenetic pair for protein regulation and spectral multiplexing. *Nat. Chem. Biol.* **13**, 633–639 (2017).
61. Shcherbakova, D. M., Shemetov, A. A., Kaberniuk, A. A. & Verkhusha, V. V. Natural photoreceptors as a source of fluorescent proteins, biosensors, and optogenetic tools. *Annu. Rev. Biochem.* **84**, 519–550 (2015).
62. Horsten, S. et al. Mapping light-driven conformational changes within the photosensory module of plant phytochrome B. *Sci. Rep.* **6**, 34366 (2016).
63. Nagatani, A. Phytochrome: structural basis for its functions. *Curr. Opin. Plant Biol.* **13**, 565–570 (2010).
64. Kikis, E. A., Oka, Y., Hudson, M. E., Nagatani, A. & Quail, P. H. Residues clustered in the light-sensing knot of phytochrome B are necessary for conformer-specific binding to signaling partner PIF3. *PLoS Genet.* **5**, e1000352 (2009).
65. Gibson, D. G. et al. Enzymatic assembly of DNA molecules up to several hundred kilobases. *Nat. Methods* **6**, 343–345 (2009).
66. Mukougawa, K., Kanamoto, H., Kobayashi, T., Yokota, A. & Kohchi, T. Metabolic engineering to produce phytochromes with phytochromobilin, phycocyanobilin, or phycoerythrobilin chromophore in *Escherichia coli*. *FEBS Lett.* **580**, 1333–1338 (2006).
67. Beyer, H. M. et al. AQUA cloning: a versatile and simple enzyme-free cloning approach. *PLoS ONE* **10**, e0137652 (2015).
68. Panavas, T., Sanders, C. & Butt, T. R. SUMO fusion technology for enhanced protein production in prokaryotic and eukaryotic expression systems. *Methods Mol. Biol.* **497**, 303–317 (2009).
69. Gambetta, G. A. & Lagarias, J. C. Genetic engineering of phytochrome biosynthesis in bacteria. *Proc. Natl Acad. Sci.* **98**, 10566–10571 (2001).
70. Berkelman, T. R. & Lagarias, J. C. Visualization of bilin-linked peptides and proteins in polyacrylamide gels. *Anal. Biochem.* **156**, 194–201 (1986).
71. Shaner, N. C., Steinbach, P. A. & Tsien, R. Y. A guide to choosing fluorescent proteins. *Nat. Methods* **2**, 905–909 (2005).
72. Lamparter, T., Esteban, B. & Hughes, J. Phytochrome Cph1 from the cyanobacterium Synechocystis PCC6803. *Eur. J. Biochem.* **268**, 4720–4730 (2001).
73. Möglich, A. An open-source, cross-platform resource for nonlinear least-squares curve fitting. *J. Chem. Educ.* **95**, 2273–2278 (2018).
74. Baaske, J. et al. Dual-controlled optogenetic system for the rapid down-regulation of protein levels in mammalian cells. *Sci. Rep.* **8**, 15024 (2018).
75. Jacobs, J. L. & Dinman, J. D. Systematic analysis of bicistronic reporter assay data. *Nucleic Acids Res.* **32**, e160 (2004).
76. Pathak, G. P., Strickland, D., Vrana, J. D. & Tucker, C. L. Benchmarking of optical dimerizer systems. *ACS Synth. Biol.* **3**, 832–838 (2014).

Acknowledgements

We thank members of our laboratories for support and comments; Dr. J. Casal for fruitful discussion; Dr. B. Höcker for chromatography use; Dr. T. Scheibel for ultracentrifuge use; and Dr. M. Hörner and Dr. W. Weber for generously providing PhyB expression plasmids. Funding through the Deutsche Forschungsgemeinschaft (grants MO2192/7-1 to A. M., ZU259/2-1 to M.D.Z., and ES152/16 to L.-O.E.), under Germany's Excellence Strategy CEPLAS EXC2048/1 (to M.D.Z., ID 390686111), by NIH grant DP2EB024247 (to J.E.T.),

by NIH training grant T32GM007388 (to S.G.J.), and by the European Commission – Research Executive Agency (H2020 Future and Emerging Technologies (FET-Open) Project ID 801041 CyGenTiG to M.D.Z.) is appreciated. J.R.W.K. gratefully acknowledges support through the ENB program "Biological Physics."

Author contributions

D.G. designed and cloned the *At*PIF variants, expressed them and *At*PhyB, analyzed light-dependent interactions in lysate and for purified proteins, cloned the constructs for light-regulated gene expression, and analyzed data. P.F. performed and evaluated experiments on light-regulated gene expression. S.G.J. conducted and evaluated experiments on light-regulated membrane recruitment. J.R.W.K. cloned and expressed several *At*PIF variants and analyzed their interactions with *At*PhyB in lysate. L.-O.E. advised on experimental design. J.E.T. supervised experiments on light-regulated membrane recruitment. M.D.Z. conceived the project and designed and supervised research. A.M. conceived the project and designed and supervised research. D.G., P.F., M.D.Z., and A.M. wrote the manuscript with input from all authors.

Competing interests

The authors declare no competing interests.

Additional information

Supplementary information is available for this paper at https://doi.org/10.1038/s42003-019-0687-9.

Correspondence and requests for materials should be addressed to M.D.Z. or A.M.

Supplementary Information - Golonka *et al.*

Supplementary Figures

Supplementary Figure 1

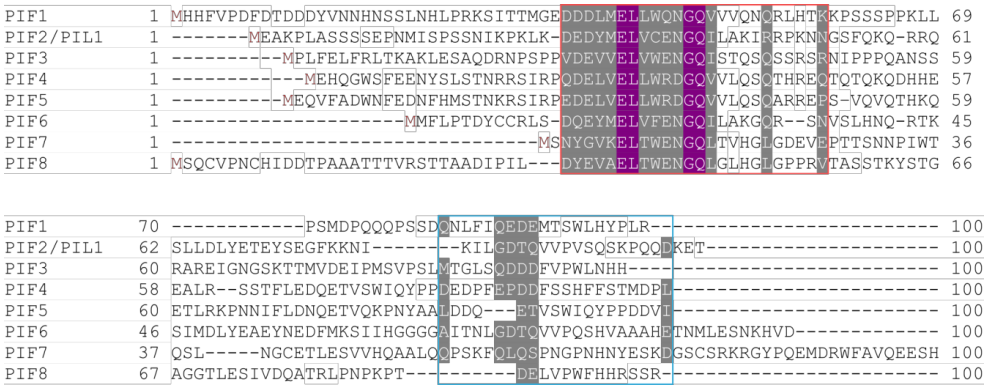

Sequence alignment of the N-terminal segments of the *A. thaliana* PIFs 1-8 according to Khanna *et al.*[1] Red color marks the N-terminal methionine; violet and gray color indicate strictly conserved and moderately conserved residues, respectively. Boxes highlight the conserved APB.A (red) and APB.B (blue) segments.

Supplementary Figure 2

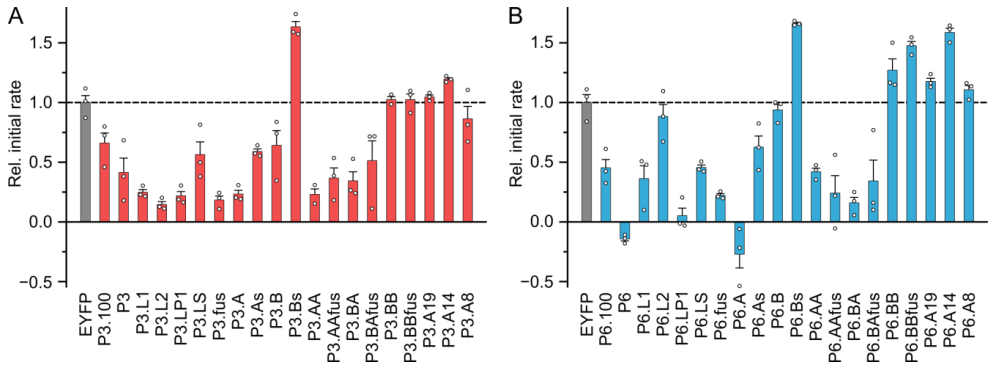

The initial rates of the recovery reaction of the *At*PhyB PCM following red-light exposure were determined in bacterial lysate in the presence of different *At*PIF variants and normalized to the reading obtained for the EYFP negative control. Data indicate mean ± SEM of *n* = 3 independent biological replicates. See Fig. 2 for details.

Supplementary Figure 3

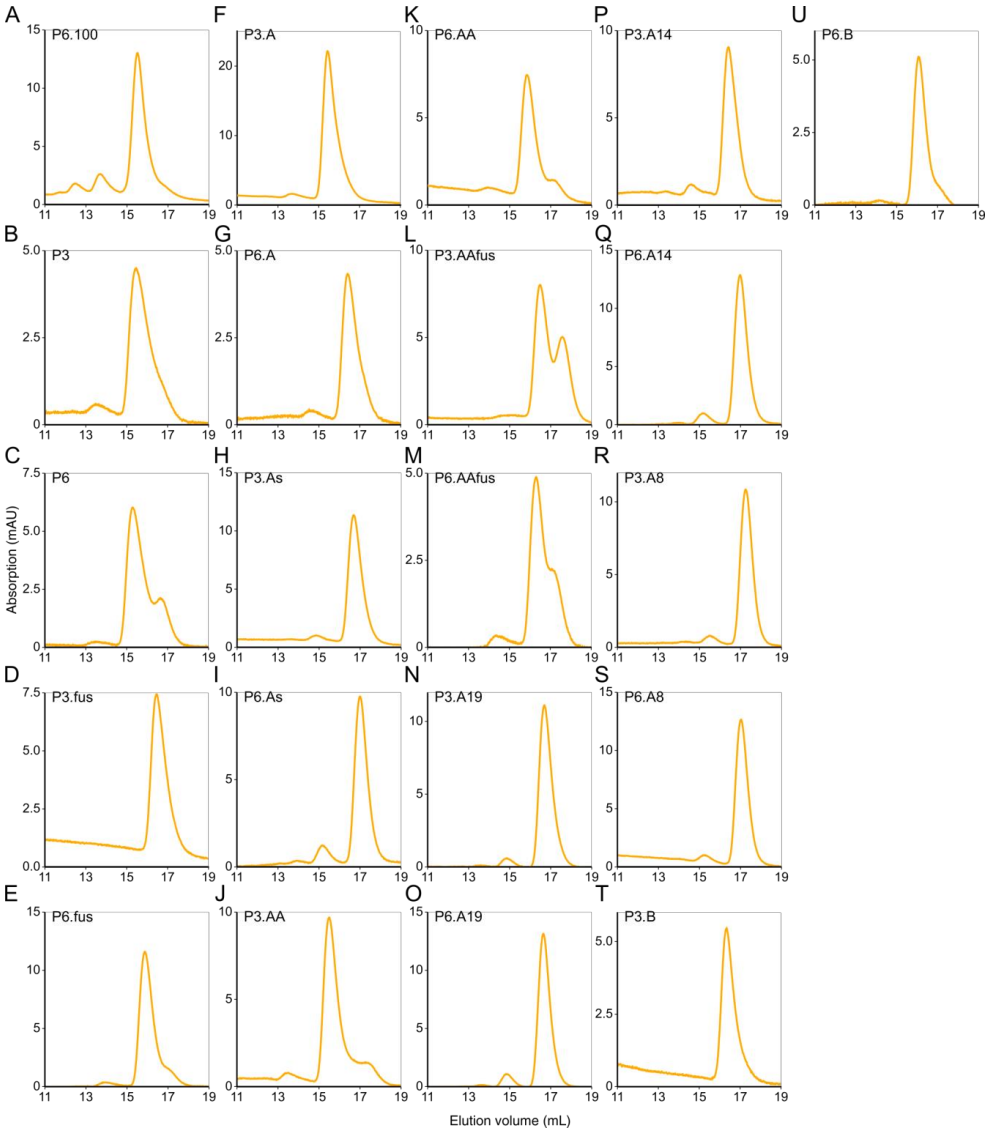

Oligomeric state of the *At*PIF variants. (A) 10 µM P6.100-EYFP were analyzed by size-exclusion chromatography, where the yellow lines represent the absorption at 513 nm. (B-U) As in (A), but for (B) P3; (C) P6; (D) P3.fus; (E); P6.fus; (F) P3.A; (G) P6.A; (H) P3.As; (I) P6.As; (J) P3.AA; (K) P6.AA; (L) P3.AAfus; (M) P6.AAfus; (N) P3.A19; (O) P6.A19; (P) P3.A14; (Q) P6.A14; (R) P3.A8; (S) P6.A8; (T) P3.B; (U) P6.B.

Supplementary Figure 4

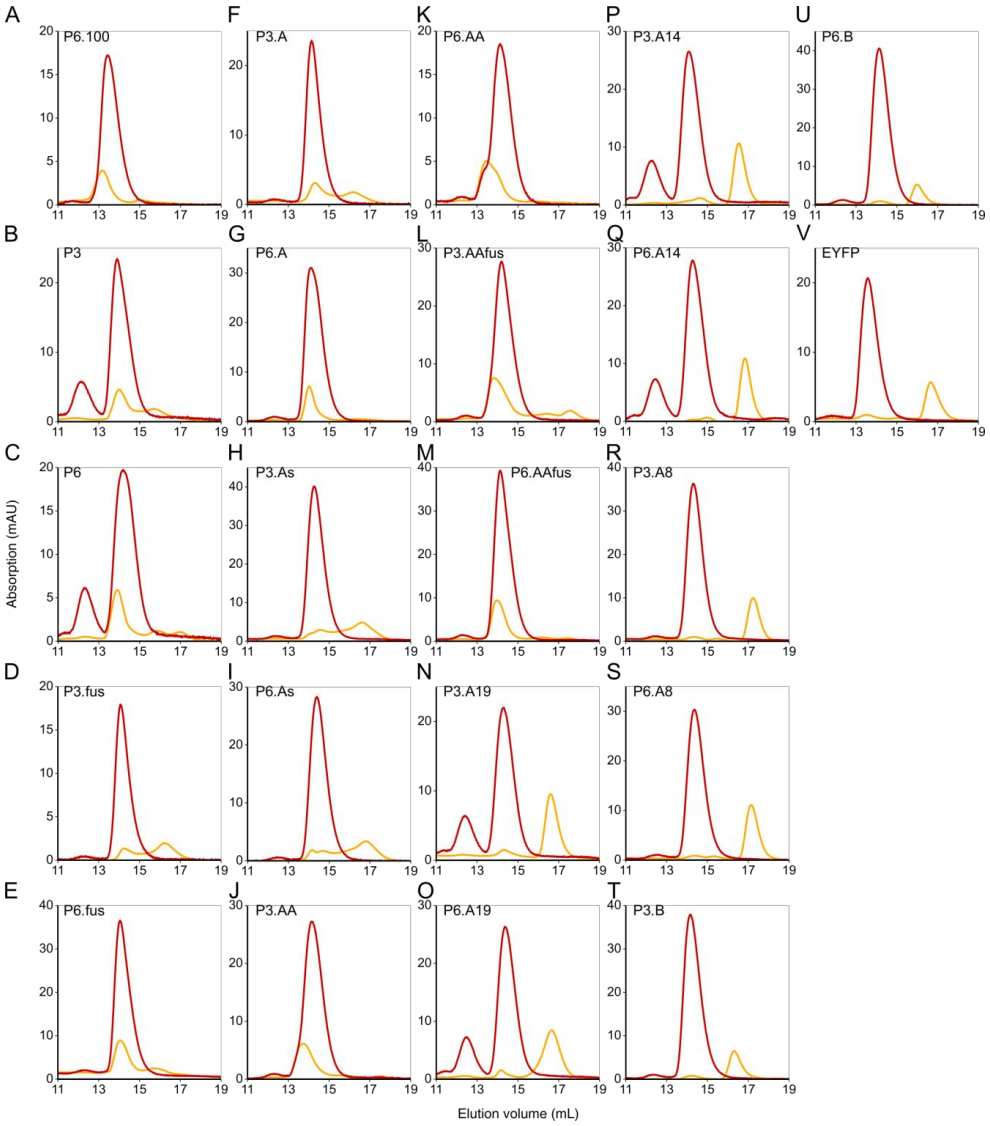

Light-dependent interactions of the *At*PIF variants with the Pfr state of the *At*PhyB PCM. (A) A mixture of 10 µM P6.100-EYFP and 50 µM *At*PhyB PCM was exposed to red light and analyzed by size-exclusion chromatography, where the yellow and red lines represent the absorption at 513 and 650 nm, respectively. (B-V) As in (A), but instead of P6.100-EYFP for (B) P3; (C) P6; (D) P3.fus; (E); P6.fus; (F) P3.A; (G) P6.A; (H) P3.As; (I) P6.As; (J) P3.AA; (K) P6.AA; (L) P3.AAfus; (M) P6.AAfus; (N) P3.A19; (O) P6.A19; (P) P3.A14; (Q) P6.A14; (R) P3.A8; (S) P6.A8; (T) P3.B; (U) P6.B; (V) EYFP. The schematics in the graphs indicate the composition of the *At*PIF variants, with variants deriving from *At*PIF3 and *At*PIF6 shown in red and blue, respectively.

Supplementary Figure 5

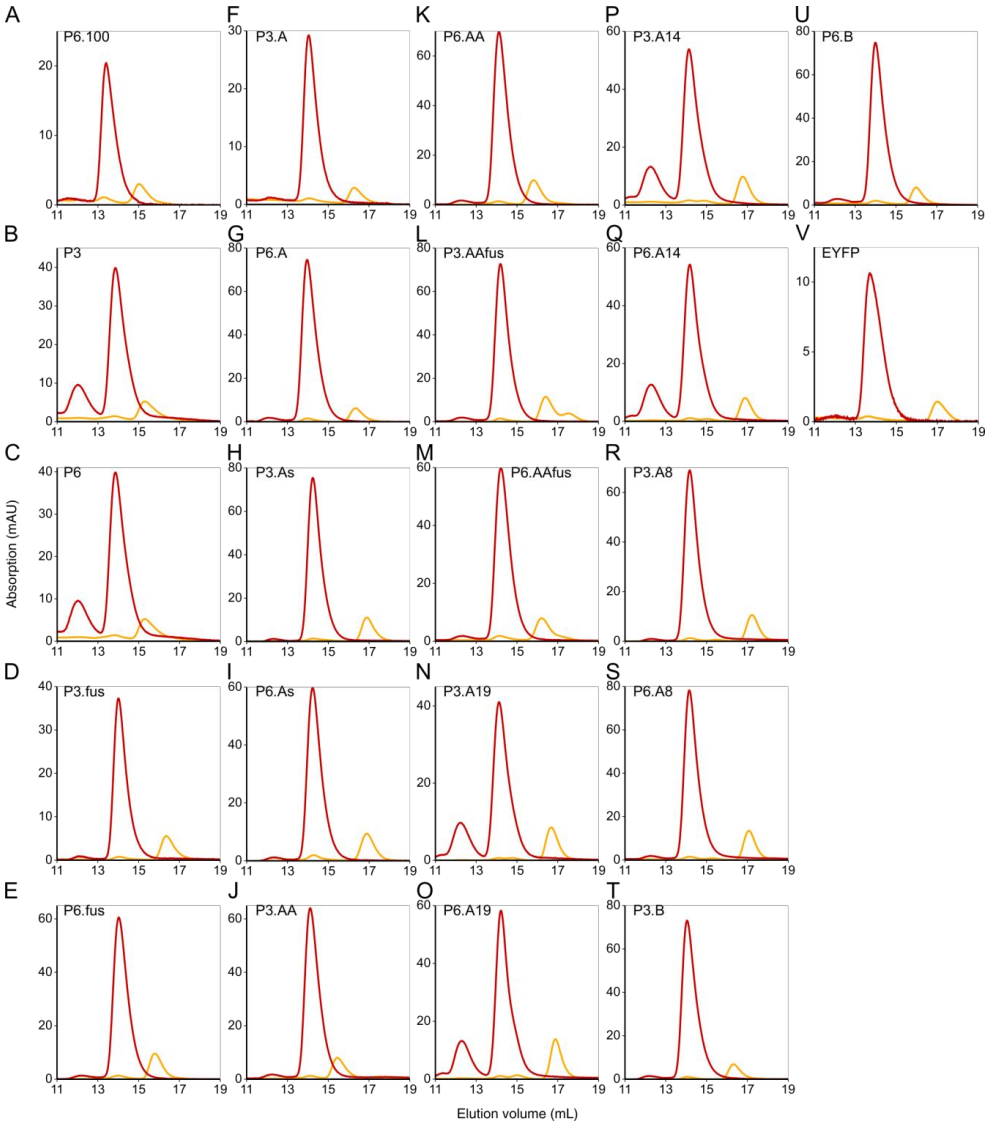

Light-dependent interactions of the *At*PIF variants with the Pr state of the *At*PhyB PCM. (A) A mixture of 10 µM P6.100-EYFP and 50 µM *At*PhyB PCM was exposed to far-red light and analyzed by size-exclusion chromatography, where the yellow and red lines represent the absorption at 513 and 650 nm, respectively. (B-V) As in (A), but instead of P6.100-EYFP for (B) P3; (C) P6; (D) P3.fus; (E); P6.fus; (F) P3.A; (G) P6.A; (H) P3.As; (I) P6.As; (J) P3.AA; (K) P6.AA; (L) P3.AAfus; (M) P6.AAfus; (N) P3.A19; (O) P6.A19; (P) P3.A14; (Q) P6.A14; (R) P3.A8; (S) P6.A8; (T) P3.B; (U) P6.B; (V) EYFP. The schematics in the graphs indicate the composition of the *At*PIF variants, with variants deriving from *At*PIF3 and *At*PIF6 shown in red and blue, respectively.

Supplementary Figure 6

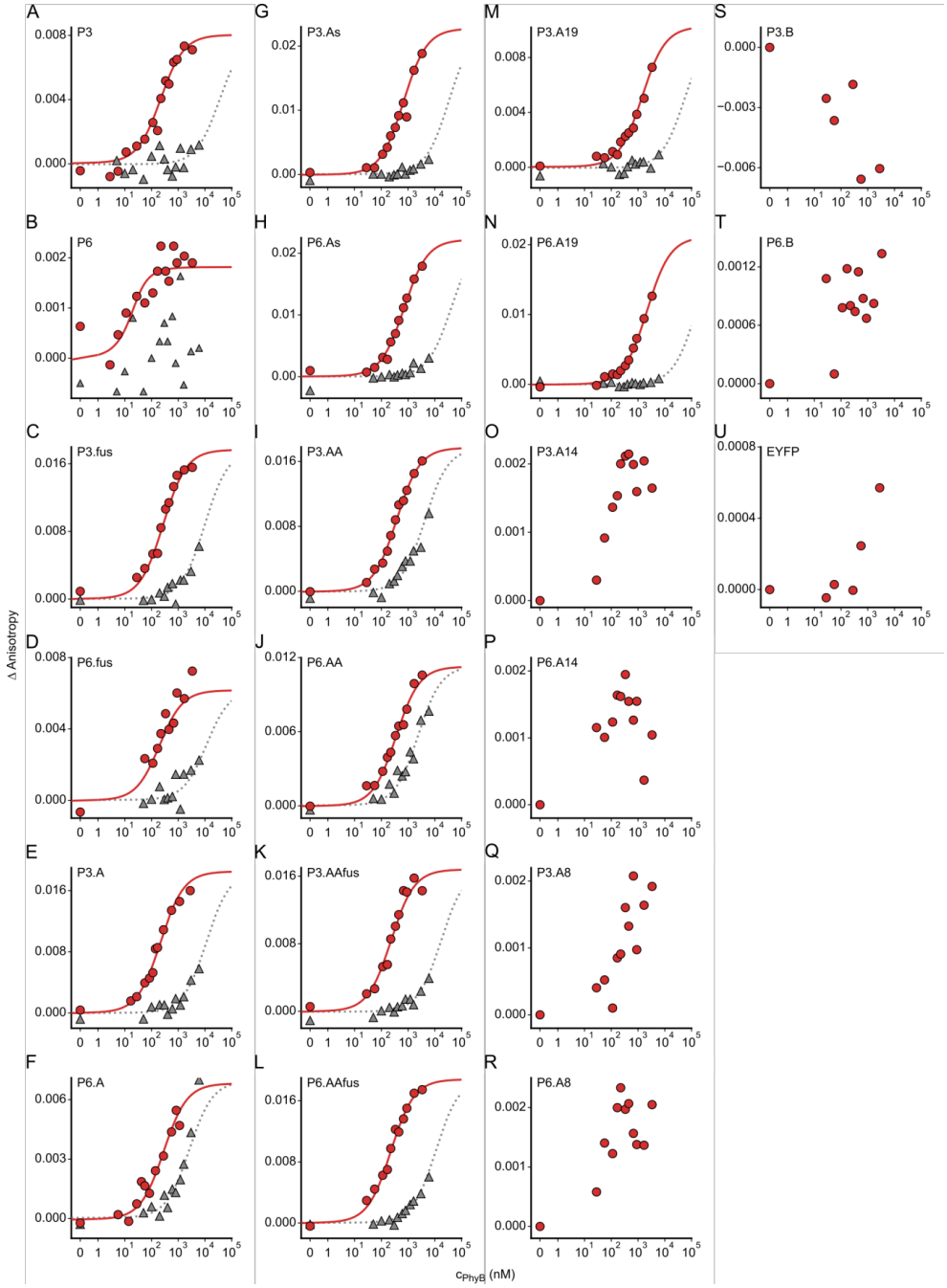

Quantitative analyses of the light-dependent protein:protein interaction between *At*PIF variants and the *At*PhyB PCM. (A) Titration of 20 nM P3-EYFP with increasing concentrations of dark-adapted

(gray) or red-light-exposed *At*PhyB PCM (red), as monitored by anisotropy of the EYFP fluorescence. Data points show averages of three biological replicates. The lines denote fits to single-site binding isotherms. (B-U) As in (A), but instead of P3-EYFP for (B) P6; (C) P3.fus; (D) P6.fus; (E) P3.A; (F) P6.A; (G) P3.As; (H) P6.As; (I) P3.AA; (J) P6.AA; (K) P3.AAfus; (L) P6.AAfus; (M) P3.A19; (N) P6.A19; (O) P3.14; (P) P6.14; (Q) P3.8; (R) P6.8; (S) P3.B; (T) P6.B; (U) EYFP.

Supplementary Figure 7

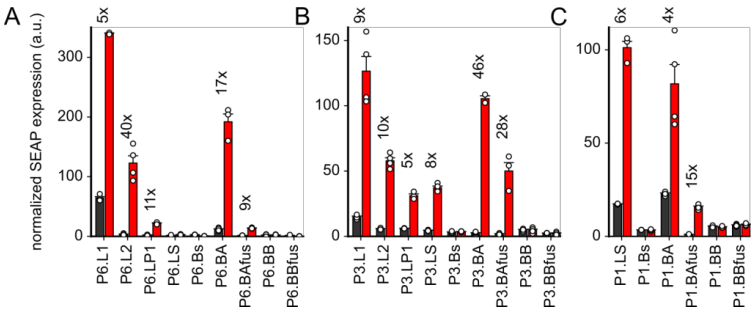

Harnessing the *At*PIF variants for the light-dependent regulation of gene expression in mammalian cells. (A) SEAP expression was determined for the diverse *At*PIF6 variants and normalized to the constitutive expression of *Gaussia* luciferase. Black and red bars denote mean normalized SEAP expression ± SEM for *n* = 4 independent biological replicates under dark conditions or red light, respectively. The numbers above the bars indicate the factor difference between dark and red-light conditions for a given *At*PIF6 variant. (B) As panel (A) but for the *At*PIF3 variants. (C) As panel (A) but for the *At*PIF1 variants.

Supplementary Figure 8

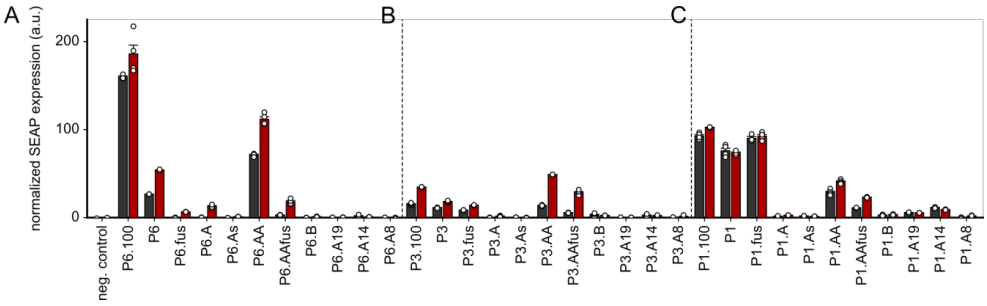

Light-dependent regulation of gene expression in mammalian cells. The experiment was conducted as described in Fig. 5 but the cells were incubated in darkness for 48 h (black bars) or for 24 h under 20 µmol m^{-2} s^{-1} 660-nm light, followed by 20 µmol m^{-2} s^{-1} 740-nm light for another 24 h (brown). (A) SEAP expression was determined for the diverse *At*PIF6 variants and normalized to the constitutive expression of *Gaussia* luciferase. Bars denote mean normalized SEAP expression ± SEM for *n* = 4 independent biological replicates. (B) As panel (A) but for the *At*PIF3 variants. (C) As panel (A) but for the *At*PIF1 variants.

Supplementary Figure 9

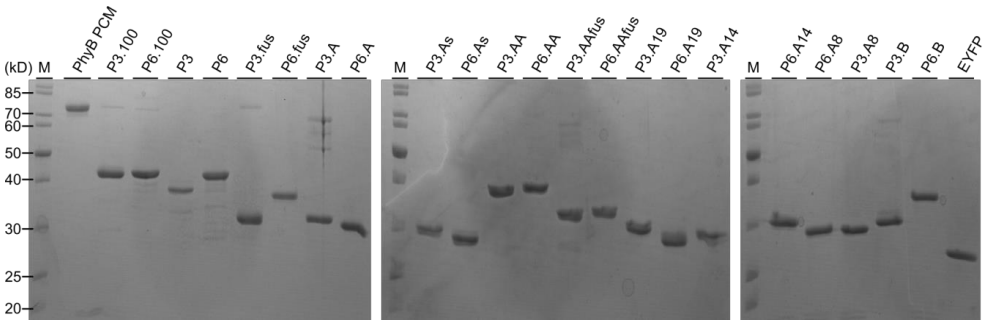

Analysis of the purified *At*PIF3/6-EYFP proteins and the *At*PhyB PCM by denaturing polyacrylamide gel electrophoresis.

Supplementary Tables

Supplementary Table 1. Amino-acid sequences of the *At*PIF variants used in this study.

Name	Sequence[a]
P1.100	MHHFVPDFDT DDDYVNNHNS SLNHLPRKSI TTMGEDDDLM ELLWQNGQVV VQNQRLHTKK PSSSPPKLLP SMDPQQQPSS DQNLFIQEDE MTSWLHYPLR
P3.100	MPLFELFRLT KAKLESAQDR NPSPPVDEVV ELVWENGQIS TQSQSSRSRN IPPPQANSSR AREIGNGSKT TMVDEIPMSV PSLMTGLSQD DDFVPWLNHH
P6.100	MMFLPTDYCC RLSDQEYMEL VFENGQILAK GQRSNVSLHN QRTKSIMDLY EAEYNEDFMK SIIHGGGGAI TNLGDTQVVP QSHVAAAHET NMLESNKHVD
P1	MDDDLMELLW QNGQVVVQNQ RLHTKKPSSS PPKLLPCMDP QQQPSSDQNL FIQEDEMTSW LHYPLR
P3	MVDEVVELVW ENGQISTQSQ SSRSRNIPPP QANSSRAREI GNGSKTTMVD EIPMSVPSLM TGLSQDDDFV PWLNHH
P6	MDQEYMELVF ENGQILAKGQ RSNVSLHNQR TKSIMDLYEA EYNEDFMKSI IHGGGGAITN LGDTQVVPQS HVAAAHETNM LESNKHVD
P3.L1	MVDEVVELVW ENGQISTQSQ SSRSRRAREI GNGSKTTMVD EIPMSVPSLM TGLSQDDDFV PWLNHH
P6.L1	MDQEYMELVF ENGQILAKGQ RSNMDLYEAE YNEDFMKSII HGGGGAITNL GDTQVVPQSH VAAAHETNML ESNKHVD
P3.L2	MVDEVVELVW ENGQISTQSQ SSRSRNIPPP QANSSRAREI GNGSKTTMTG LSQDDDFVPW LNHH
P6.L2	MDQEYMELVF ENGQILAKGQ RSNVSLHNQR TKSIMDLYEA EYNEDAITNL GDTQVVPQSH VAAAHETNML ESNKHVD
P3.LP1	MVDEVVELVW ENGQISTQSQ SSRSRKPSSS PPKLLPCMDP QQQPSSDMTG LSQDDDFVPW LNHH
P6.LP1	MDQEYMELVF ENGQILAKGQ RSNKPSSSPP KLLPCMDPQQ QPSSDAITNL GDTQVVPQSH VAAAHETNML ESNKHVD
P3.LS	MVDEVVELVW ENGQISTQSQ SSRSRDSAGS AGSAGMTGLS QDDDFVPWLN HH
P6.LS	MDQEYMELVF ENGQILAKGQ RSNDSAGSAG SAGAITNLGD TQVVPQSHVA AAHETNMLES NKHVD
P1.fus	MDDDLMELLW QNGQVVVQNQ RLHTKQNLFI QEDEMTSWLH YPLR
P3.fus	MVDEVVELVW ENGQISTQSQ SSRSRMTGLS QDDDFVPWLN HH
P6.fus	MDQEYMELVF ENGQILAKGQ RSNAITNLGD TQVVPQSHVA AAHETNMLES NKHVD
P1.A	MDDDLMELLW QNGQVVVQNQ RLHTKKPSSS PPKLLP
P3.A	MVDEVVELVW ENGQISTQSQ SSRSRNIPPP QANSSRAREI GN
P6.A	MDQEYMELVF ENGQILAKGQ RSNVSLHNQR TKSIMDLYEA
P1.B	MSMDPQQQPS SDQNLFIQED EMTSWLHYPL R
P3.B	MGSKTTMVDE IPMSVPSLMT GLSQDDDFVP WLNHH
P6.B	MEYNEDFMKS IIHGGGGAIT NLGDTQVVPQ SHVAAAHETN MLESNKHVD
P1.As	MDDDLMELLW QNGQVVVQNQ RLHTK

P3.As	MVDEVVELVW ENGQISTQSQ SSRSR
P6.As	MDQEYMELVF ENGQILAKGQ RSN
P1.Bs	MQNLFIQED EMTSWLHYPL R
P3.Bs	MMT GLSQDDDFVP WLNHH
P6.Bs	MAIT NLGDTQVVPQ SHVAAAHETN MLESNKHVD
P1.AA	MDDDLMELLW QNGQVVVQNQ RLHTKKPSSS PPKLLPCMDP QQQPSSDDDD LMELLWQNGQ VVVQNQRLHT KMTSWLHYPL R
P3.AA	MVDEVVELVW ENGQISTQSQ SSRSRNIPPP QANSSRAREI GNGSKTTMVD EIPMSVPSLV DEVVELVWEN GQISTQSQSS RSRFVPWLNH H
P6.AA	MDQEYMELVF ENGQILAKGQ RSNVSLHNQR TKSIMDLYEA EYNEDFMKSI IHGGGGDQEY MELVFENGQI LAKGQRSNTN MLESNKHVD
P1.AAfus	MDDDLMELLW QNGQVVVQNQ RLHTKDDDLM ELLWQNGQVV VQNQRLHTKM TSWLHYPLR
P3.AAfus	MVDEVVELVW ENGQISTQSQ SSRSRVDEVV ELVWENGQIS TQSQSSRSRF VPWLNHH
P6.AAfus	MDQEYMELVF ENGQILAKGQ RSNDQEYMEL VFENGQILAK GQRSNTNMLE SNKHVD
P1.BB	MQNLFIQEDE KPSSSPPKLL PCMDPQQQPS SDQNLFIQED EMTSWLHYPL R
P3.BB	MMTGLSQDDD NIPPPQANSS RAREIGNGSK TTMVDEIPMS VPSLMTGLSQ DDDFVPWLNH H
P6.BB	MAITNLGDTQ VSLHNQRTKS IMDLYEAEYN EDFMKSIIHG GGGAITNLGD TQVVPQSHVA AAHETNMLES NKHVD
P1.BBfus	MQNLFIQEDE QNLFIQEDEM TSWLHYPLR
P3.BBfus	MMTGLSQDDD MTGLSQDDDF VPWLNHH
P6.BBfus	MAITNLGDTQ AITNLGDTQV VPQSHVAAAH ETNMLESNKH VD
P1.BA	MQNLFIQEDE KPSSSPPKLL PCMDPQQQPS SDDDDLMELL WQNGQVVVQN QRLHTKMTSW LHYPLR
P3.BA	MMTGLSQDDD NIPPPQANSS RAREIGNGSK TTMVDEIPMS VPSLVDEVVE LVWENGQIST QSQSSRSRFV PWLNHH
P6.BA	MAITNLGDTQ VVPQSHVAAA HEVSLHNQRT KSIMDLYEAE YNEDFMKSII HGGGGDQEYM ELVFENGQIL AKGQRSNTNM LESNKHVD
P1.BAfus	MQNLFIQEDE DDDLMELLWQ NGQVVVQNQR LHTKMTSWLH YPLR
P3.BAfus	MMTGLSQDDD VDEVVELVWE NGQISTQSQS SRSRFVPWLN HH
P6.BAfus	MAITNLGDTQ VVPQSHVAAA HEDQEYMELV FENGQILAKG QRSNTNMLES NKHVD
P1.19	MDDDLMELLW QNGQVVVQNQ
P3.19	MVDEVVELVW ENGQISTQSQ
P6.19	MDQEYMELVF ENGQILAKGQ
P1.14	MDDDLMELLW QNGQV
P3.14	MVDEVVELVW ENGQI

P6.14	MDQEYMELVF ENGQI
P1.8	MELLWQNGQ
P3.8	MELVWENGQ
P6.8	MELVFENGQ

[a] Red color marks the N-terminal methionine; violet and gray color indicates strictly conserved and moderately conserved residues, respectively.

Supplementary Reference

1. Khanna, R. et al. A Novel Molecular Recognition Motif Necessary for Targeting Photoactivated Phytochrome Signaling to Specific Basic Helix-Loop-Helix Transcription Factors. *Plant Cell* **16**, 3033–3044 (2004).

Alternative red-light inducible split transcription factor system

Patrick Fischbach[1], David Golonka[2], Sergey Fedotov[3], Andreas Hiltbrunner[4], Andreas Möglich[2]*, Matias D. Zurbriggen[1]*

[1]Institute of Synthetic Biology, University of Düsseldorf and CEPLAS, 40225 Düsseldorf, Germany
[2]Lehrstuhl für Biochemie, Universität Bayreuth, 95447 Bayreuth, Germany
[3]?, University of Düsseldorf, Germany
[4] Institute of Biology II, Faculty of Biology, University of Freiburg, 79104 Freiburg, Germany.
*Corresponding author: Email: Andreas.Moeglich@uni-bayreuth.de ; matias.zurbriggen@uni-duesseldorf.de;
ORCID: PF: 0000-0002-2781-5264; A.M.: ; MDZ:

Abstract (181 words)

Through the last years a lot of different optogenetic tools were engineered and developed to control several cellular processes such as gene expression, protein localization and stability. One commonly used tool is the red-light induced phytochrome B based split transcription factor system. So far, this inducible tool is the only tool activated via red-light, which is a limitation for multi control of certain processes with one wavelength. Here, we present an alternative red-light inducible split transcription factor system based on phytochrome A (PhyA) and a novel screened light dependent interactor OPA. This system shows similar behavior, reversibility and sensitivity as the known PhyB based system but its fully orthogonal. As represented here, this tool is combinable with the PhyB system for an multi control of different processes via one wavelength. This approach is even separately controllable by using different red-light pulses to activate just one of the systems. As exemplified here, the novel PhyA based system is a fully inducible light switch and an expansion for the optogenetic toolbox which opens new possibilities in the multi pathway control with one wavelength.

Introduction (407 words)

Optogenetic tools are using light to regulate cellular processes in a minimally invasive manner and with a high spatiotemporal resolution. During the last years several different optogenetic switches controlled by several wavelengths has been engineered to control gene expression, protein stability and protein localization [1–4]. However, the only red-light activated and one of the commonly used optogenetic switches is based on the interaction between *Arabidopsis thaliana* phytochrome B (PhyB) and the phytochrome interaction factor 3 or 6 (PIF3, PIF6) [3,5]. Due to the ability to activate this system with red-light and actively deactivate the system with far-red light, it offered new perspectives in the optogenetic control of cellular processes. It has been reported that this system was used successfully to control protein localization and gene expression to study complex pathways, growth factors, T-cell receptors and protein:protein interactions in different organisms such as plants and mammalian cells [1–3,5–8]. Accordingly, we used this system to study the possible light dependent interaction between *Arabidopsis thaliana* phytochrome A (PhyA) and several potential interaction partners. Therefore, we could identify

one protein of unknown function (AT1G48770), from now on OPA, which is interacting with PhyA in a light dependent manner orthogonal to PhyB. PhyA is similar to PhyB, a chromoprotein that consists out of two domains. The N-terminal part includes a PAS (Per-Arnt-Sim), GAF, (cGMP-stimulated phosphodiesterase, *Anabaena* adenylate cylases, FhlA) which is binding the chromophore phytochromobilin, and a PHY (phytochrome) domain. The C-terminal part serves regulatory functions and consists of two PAS domains and a HKRD (histidine kinase-related domain) [9,10]. Upon red- light illumination PhyA is changing its conformation, due to the isomerization of the chromophore [9], and can interact with OPA. On absorption of far-red light PhyA reverts back into the inactive state, which leads to disruption of the interaction. Based on these results we aimed to construct a red-light inducible split transcription factor system with similar ON and OFF kinetics as the PhyB system but with a different light sensitivity depending on a different interaction strength between PhyA and OPA. Since PhyB-PIF interactions are the only red-light inducible system in mammalian cells so far, an additional system working orthogonal to the PhyB system offers new perspectives in regulation of pathway components and their research. Moreover, we show that an update of the optogenetic toolbox with this novel red-light inducible split transcription factor system, gives the possibility to combine two systems for the regulation and translocation of proteins with one wavelength.

Results

To analyze the light dependent interaction between *Arabidopsis thaliana* phytochrome A and several potential interactors, we designed a system similar to the known PhyB system [3] with PhyA fused to a viral trans activator VP16 and the potential interactor fused to the tetracycline repressor tetR (Fig.1a). If a light dependent interaction takes place, the trans activator comes to close proximity to the synthetic minimal promoter and induces transcription of the human placental SEAP as reporter. With this system, we screened 30 different *Arabidopsis thaliana* proteins for light dependent interaction with PhyA in mammalian cells (Fig.1b + Fig.S1a). The described system was therefore transfected into CHO-K1 cells, incubated for 24 h in dark and illuminated after supplementation of PCB (phycocyanobilin) with 20 µmol m^{-2} s^{-1} and 660 nm light for 24 h. Several potential interactors showed either no interaction (Fig1.b “PIM1b”) or light dependent interaction with a high leakiness in the dark with PhyA (Fig.1b ”FHY1”). However, one of these proteins (OPA) showed a light dependent interaction with PhyA in a similar strength in induction compared to the canonical PhyB system but with less leakiness in the dark (Fig.1b “OPA”). Based on this we started to analyze this interaction further. Since the structure of PhyA and B is quite similar, we checked for an interaction between OPA and PhyB in the same system as described before. Surprisingly, OPA showed no interaction with PhyB in a light dependent neither in a light independent manner (Fig.1c). This showed an orthogonal interaction to the PhyB system.

To optimize the PhyA system, the impact of PhyA truncations and OPA truncations were determined. Similar to the PhyB truncation (amino acids 1-650) [3], PhyA was shortened directly after the PAS-GAF-PHY domains (amino acids 1-617), what resulted in a loss of light dependent induction of SEAP expression (Fig.2b). Additionally, we truncated OPA to optimize the size of the interaction pair for further applications similar to PIF6 (amino acids 1-100). Therefore, the sequence and structure of OPA was

analyzed and showed a domain of unknown function (DUF1639; amino acids 125-176) at the C-terminus of OPA (Fig.2a). To determine if this domain is probably needed for an interaction with PhyA, we truncated OPA into two parts and analyzed the interaction as described before. Surprisingly, the N-terminus of OPA (amino acids 1-90) without the DUF1639 showed a light dependent interaction and therefore induction of SEAP expression (Fig.2b), suggesting that the domain is not needed for an interaction with PhyA. To prove, if the loss of the DUF1639 also results in a loss of orthogonality, the interaction between PhyB and the OPA truncation (amino acid 1-90) was determined. As expected, PhyB showed still no interaction with OPA (Fig.2c).

To characterize our optimized system, CHO-K1 cells were transfected as described above and incubated under increasing light intensities. SEAP expression reached full level already at a dose as low as 2.5 µmol m^{-2} s^{-1} (Fig.3a). This showed the high sensitivity of the system, which allows fully induction with a light puls of 2.5 µmol m^{-2} s^{-1} for 30 min. To evaluate the induction of SEAP expression over time we performed SEAP kinetic measurements in CHO-K1 cells. After introducing the PhyA system, CHO-K1 cells were illuminated for different time periods with 20 µmol m^{-2} s^{-1} red light and SEAP values were determined directly afterwards. Increased SEAP expression after 4 h suggest high induction of the system and constant expression over 24 h (Fig.3b). Additionally, to demonstrate the key advantage of a light inducible system, the removability from a biological system, light induced time-resolved gene-expression was tested. Therefore, the system was introduced into CHO-K1 cells and illuminated with alternating cycles of red or far-red light (660 nm; 740 nm). The high expression levels under red-light and the basal levels under far-red light illumination suggest a full reversibility of the system (Fig.3c).

To analyze the differences in interaction strength and sensitivity between the PhyB system and the PhyA system further, fluorescence anisotropy assays were done.

Discussion (~380 words)

The red/far-red light-switchable bi-stable PhyB mammalian gene expression system is so far the only red-light controllable expression system and used for several studies. Commonly it is used for gene expression control [3,11], light induced protein localization [12] and for pathway control [5]. Moreover, the PhyB based system is superior to other light-inducible systems based on other wavelengths, because of the reversibility via far-red light, the deeper penetration into tissues of the used red-light and the sensitivity [1,11]. The system is combinable with other light systems [11] but since there are no orthogonal red-light systems available, activated by the same wavelength, combinations to control different cellular processes at the same time, like with blue-light [4] are not possible. To fill this gap of additional red-light inducible systems we engineered a phytochrome A based red-light split transcription factor system, which based on the interaction with a novel screened interaction partner OPA. This new red-light inducible optogenetic tool showed a high sensitivity and reversibility upon red or far-red illumination which meets every criterion of an optimal inducible system. Due to the reduced size of OPA, the system is compact and consists out of two plasmids. Although, the system is built up similar to the PhyB system,

the sensitivity and binding affinity differs. We successfully used these differences to activate the systems separately by red-light pulsing. Moreover, we combined the two red-light inducible systems to control two cellular processes with one wavelength and with the ability to deactivate both systems simultaneously with far-red light. Nevertheless, there are other optogenetic systems existing for instance based on bacterial phytochromes, which are activated by far-red light and which are compromising endogenous biliverdin instead of supplemented PCB[13]. But, as demonstrated, the PhyA based system showed a higher sensitivity and expressions levels superior to the bacterial phytochrome system [13]. Taken together, we showed a phytochrome-based system, which can not only be used to control gene expression in a light dependent manner, it can also be used for studying light dependent interactions between phytochromes and potential interaction- or transcription factors. This demonstrates the tight linkage between basic research of light signaling pathways with the engineering of photoreceptor based optogenetic tools. Additionally, the new PhyA system shows a needed supplement for the optogenetic toolbox and important addition for the multi pathway control via one wavelength.

Material and Methods

Plasmid construction

The design and construction of the expression vectors are described in table S1, S2.

Cell culture, transfection, light induction

Chinese ovary hamster cells (CHO-K1; DSMZ, Braunschweig, Germany) were cultivated in HAMs D12 medium (PAN Biotech, Aidenbach, Germany; no.) supplemented with 10% (v/v) tetracycline-free fetal bovine serum (FBS; PAN Biotech; no. P30-3602; batch no. P080317TC) and 1.4% (v/v) streptomycin (PAN Biotech; no. P06-07100). Human embryonic kidney cells (HEK-293T; DSMZ, Braunschweig, Germany) and HeLa cells (HeLa; DSMZ, Braunschweig, Germany) were cultivated in Dulbecco´s modified Eagle´s medium (DMEM; PAN Biotech, Aidenbach, Germany; no. P04-03550) supplemented with 10% (v/v) tetracycline-free fetal bovine serum (FBS; PAN Biotech; no. P30-3602; batch no. P080317TC) and 1.4% (v/v) streptomycin (PAN Biotech; no. P06-07100). $5 \cdot 10^4$ CHO-K1, HEK-293T or HeLa cells were transfected using polyethyleneimine (PEI; Polysciences Inc. Europe, Hirschberg, Germany; no. 23966-1) as in [3]. 0.75 µg DNA were diluted in 50 µL OptiMEM (Invitrogen, Thermo Fisher Scientific) and mixed with a PEI/OptiMEM mix (2.5 µL PEI solution in 50 µL OptiMEM). The DNA-PEI mix was added to the cells after 15 min of incubation at room temperature. 4 h post transfection the medium was exchanged. If not indicated otherwise, all plasmids were transfected with PhyA system together with the reporter plasmid (pPF086; pPF034 in equal amounts (w/w). 24 h post transfection the cells were illuminated with 660-nm light for 24 h with a light intensity of 20 µmol m^{-2} s^{-1} or kept in darkness. If not indicated otherwise, experiments were done in 4 biological replicates. For illumination, custom-built LED light-boxes with LED-panels emitting 660 nm were used [4]. Exchange of media and other cell-handling was done under 522-nm, safe light, to prevent inadvertent actuation of the light-sensitive systems.

SEAP assay

The supernatant of transfected cells was transferred to 96-well round-bottom plates and to inactivate endogenous phosphatases incubated at 68°C for 1 h. Afterwards, 80 µL of the supernatant were transferred to a 96-well flat-bottom plates, and per well 100 µL SEAP buffer (20 mM homoarginine, 1 mM $MgCl_2$, 21% (v/v) diethanolamine) was added [3]. After addition of 20 µL 120 mM para-nitrophenyl phosphate, the absorption at 405 nm was measured for 1 h using a BMG Labtech CLARIOstar or a TriStar2 S LB 942 multimode plate reader (Berthold Technologies, Bad Wildbad, Germany) as in [3]. Outlier were statistically determined and excluded as described in [14].

Gaussia luciferase assay

20 µL of the supernatant of the transfected cells were transferred to a 96-well white plate and diluted in 60 µL phosphate-buffered saline (PBS; 2.68 mM KCl, 1.47 mM KH_2PO_4, 8.03 mM Na_2PO_4, 137 mM NaCl). After addition of 20 µL coelenterazine (472mM stock solution in methanol, diluted 1:1,500 in PBS; Carl Roth, Karlsruhe, Germany, no. 4094.4), the luminescence was measured for 20 min using a BMG Labtech CLARIOstar or a TriStar2 S LB 942 multimode plate reader (Berthold Technologies, Bad Wildbad, Germany).

Fluorescence anisoptropy

Statistical analysis

All data analysis was performed using Microsoft Excel or GraphPad Prism 6. Statistical outlier was determined and excluded as described in [14].

Bibliography

1. Shimizu-Sato, S., Huq, E., Tepperman, J. M. & Quail, P. H. A light-switchable gene promoter system. *Nat. Biotechnol.* **20**, 1041–4 (2002).
2. Levskaya, A., Weiner, O. D., Lim, W. A. & Voigt, C. A. Spatiotemporal control of cell signalling using a light-switchable protein interaction. *Nature* **461**, 997–1001 (2009).
3. Müller, K. *et al.* A red/far-red light-responsive bi-stable toggle switch to control gene expression in mammalian cells. *Nucleic Acids Res.* **41**, e77–e77 (2013).
4. Baaske, J. *et al.* Dual-controlled optogenetic system for the rapid down-regulation of protein levels in mammalian cells. *Sci. Rep.* **8**, 15024 (2018).
5. Toettcher, J. E., Gong, D., Lim, W. A. & Weiner, O. D. Light-based feedback for controlling intracellular signaling dynamics. *Nat. Methods* **8**, 837–9 (2011).
6. Ochoa-Fernandez, R. *et al.* Optogenetics in Plants: Red/Far-Red Light Control of Gene Expression. in *Methods in molecular biology (Clifton, N.J.)* **1408**, 125–139 (2016).
7. Yousefi, O. S. *et al.* Optogenetic control shows that kinetic proofreading regulates the activity of the T cell receptor. *Elife* **8**, (2019).
8. Baaske, J. *et al.* Dual-controlled optogenetic system for the rapid down-regulation of protein levels in mammalian cells. *Sci. Rep.* **8**, 15024 (2018).

9. Li, J., Li, G., Wang, H. & Wang Deng, X. Phytochrome Signaling Mechanisms. *Arab. B.* **9**, e0148 (2011).
10. Van Buskirk, E. K., Decker, P. V & Chen, M. Photobodies in light signaling. *Plant Physiol.* **158**, 52–60 (2012).
11. Müller, K., Engesser, R., Timmer, J., Zurbriggen, M. D. & Weber, W. Orthogonal Optogenetic Triple-Gene Control in Mammalian Cells. *ACS Synth. Biol.* **3**, 796–801 (2014).
12. Beyer, H. M. *et al.* Red Light-Regulated Reversible Nuclear Localization of Proteins in Mammalian Cells and Zebrafish. *ACS Synth. Biol.* **4**, 951–958 (2015).
13. Kaberniuk, A. A., Shemetov, A. A. & Verkhusha, V. V. A bacterial phytochrome-based optogenetic system controllable with near-infrared light. *Nat. Methods* **13**, 591–597 (2016).
14. Jacobs, J. L. & Dinman, J. D. Systematic analysis of bicistronic reporter assay data. *Nucleic Acids Res.* **32**, e160 (2004).

Acknowledgements

Author Contributions

PF, DG, SF planned and performed experiments. PF supervised SF and analyzed the data. AM, AH and MDZ were involved in the design, supervision and analysis of the experiments. PF wrote the manuscript.

Competing Financial Interest

The authors declare that they have no competing financial interest.

Figure Descriptions

Figure 1. Design, screening and orthogonality of the alternative red-light system

(a) Design and function of the used red-light split transcription factor system. *Arabidopsis thaliana* phytochrome A (PhyA) is C-terminally fused to a virus-derived transactivator domain VP16 and separated by an IRES sequence from the potential interactors or OPA fused N-terminally to the tetracycline repressor domain (tetR). On the reporter, 13 repeats of tetO are upstream of a synthetic CMV minimal promoter followed by the gene of human placental SEAP. On a second ORF, Gaussia Luciferase is under the control of the constitutive SV40 promoter as a normalization element, to normalize differences in expression level or cell amounts. Upon red-light illumination, PhyA containing the chromophore PCB, changes its conformation into its active Pfr form which allows interaction with other proteins like OPA. Due to the binding of the tetracycline repressor to the specific sequence repeats, VP16 comes to close proximity of the minimal CMV promoter, if the protein is interacting with PhyA, and recruits the transcriptional machinery to induce expression of SEAP. This interaction can be actively disrupted by illuminating with far-red light which leads PhyA changing back to its inactive Pr form and stops the expression of SEAP. **(b)** Screening of potential interactors of PhyA. CHO-K1 cells were transiently transfected with the described reporter plasmid (pPF034) and the plasmids based on the red-light split transcription factor system containing *Arabidopsis thaliana* phytochrome A (PhyA)

(pPF007) and one of the potential interactors. Additionally, the published red-light split transcription factor system was also transfected as a control. Transfected cells were kept in dark for 24 h, supplemented and incubated for 1 h with 15 µM PCB and illuminated afterwards for 24 h with 660 nm and an intensity of 20 µmol m^{-2} s^{-1} (red bars) or kept in dark (black bars). SEAP values were determined and induction folds calculated of 4 replicates. **(c)** OPA showed orthogonal interaction with PhyA. CHO-K1 cells were transfected with the reporter plasmid (pPF034) and either the PhyB system as a control or plasmids containing PhyA or PhyB together with OPA to check for a light dependent interaction (pPF013; pPF078). Transfected cells were kept in dark for 24 h, supplemented and incubated for 1 h with 15 µM PCB and illuminated afterwards for 24 h with 660 nm and an intensity of 20 µmol m^{-2} s^{-1} (red bars) or kept in dark (black bars). SEAP and Gaussia values were determined and SEAP was normalized with their Gaussia luciferase data. All experiments were done in 4 replicates and the error bars indicate standard deviation of the mean.

Figure 2. Truncation and optimization of the PhyA/OPA system

(a) Scheme of OPA truncation analysis. OPA has a C-terminal predicted domain of unknown function (amino acid 125 - 176) (DUF1679). To analyze necessity of this domain for a light dependent interaction with PhyA, OPA was truncated into two parts. The N-terminal part without the domain of unknown function and the C-terminal containing this domain. **(b)** Analysis of truncated PhyA and OPA variants. CHO-K1 cells were transfected with the reporter plasmid (pPF034) and the PhyA system as a control (pPF013) or plasmids containing the truncated versions of PhyA/OPA (pPF090; pPF086; pPF087). **(c)** Orthogonality is DUF1679 independent. CHO-K1 cells were transfected with the reporter plasmid (pPF034) and the optimized PhyA system (pPF086) or PhyB FL with OPA^{1-90} (pPF089). In **(b)** and **(c)** transfected cells were kept in dark for 24 h, supplemented and incubated for 1 h with 15 µM PCB and illuminated afterwards for 24 h with 660 nm and an intensity of 20 µmol m^{-2} s^{-1} (red bars) or kept in dark (black bars). SEAP and Gaussia values were determined and SEAP was normalized with their Gaussia luciferase data. All experiments were done in 4 replicates and the error bars indicate standard deviation of the mean. All plasmids were transfected in a molar ratio of 1:1 (w:w).

Figure 3. Characterization of the alternative system

(a) Dose-response curve for sensitivity analysis of the system. Transfected cells were illuminated with 660 nm light and an intensity of 0, 2.5, 5, 10 and 20 µmol m^{-2} s^{-1} for 24 h. Afterwards SEAP production was quantified. **(b)** Expression kinetics of the system. Transfected cells were illuminated with 660 nm and an intensity of 20 µmol m^{-2} s^{-1}. At the given timepoints (2 h, 4 h, 8 h, 24 h) the production of SEAP was determined (red line). Control cells were kept in dark for 24 h (black line). **(c)** Reversibility of the system. Transfected cells were supplemented every 24 h with fresh medium containing 15 µM PCB and illuminated with indicated wavelengths with an intensity of 20 µmol m^{-2} s^{-1}. Expression of SEAP was measured every 24 h. SEAP values were normalized by values of constantly with 660 nm illuminated cells, to correct changes in gene expression depending on growth over time. **(a-c)** CHO-K1 cells were transfected with the reporter plasmid (pPF034) and the alternative optimized PhyA system (pPF086) in a molar ratio of 1:1 (w:w). Transfected cells were kept in dark for 24 h, supplemented and incubated for

1 h with 15 µM PCB before indicated illumination conditions. All experiments were done in 4 replicates and the error bars indicate standard deviation of the mean.

Fig.1a System

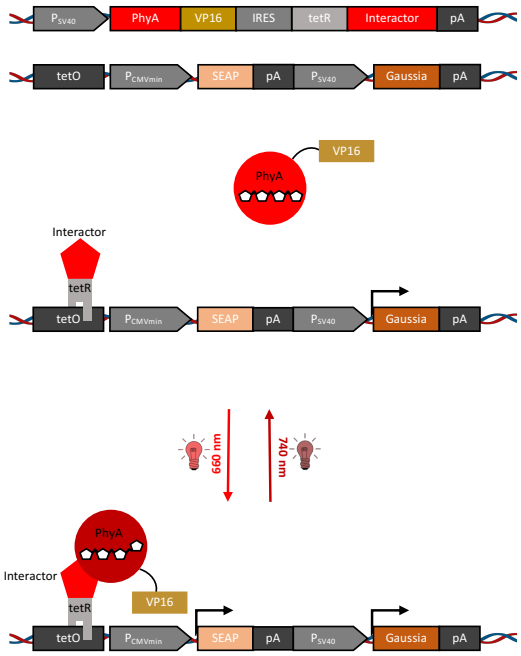

Fig.1b

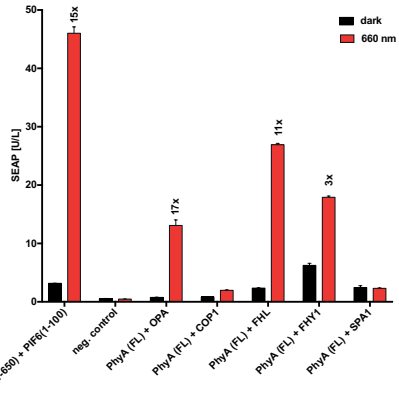

Fig.1c

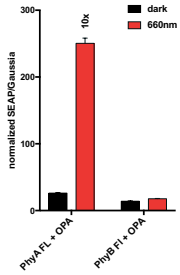

Fig.2a

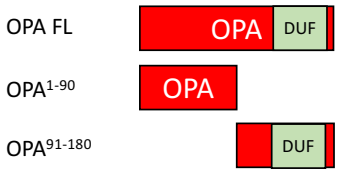

Fig.2b

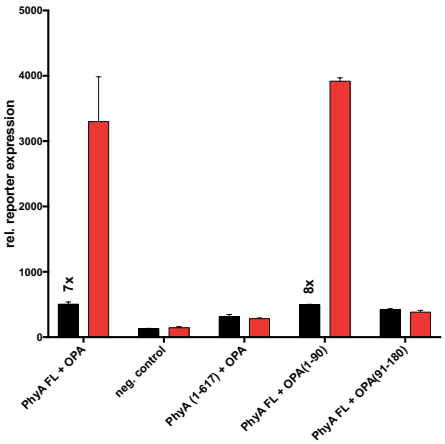

Fig.2c

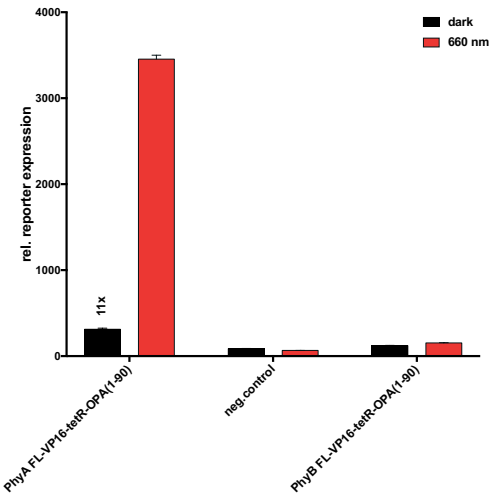

Fig.3a

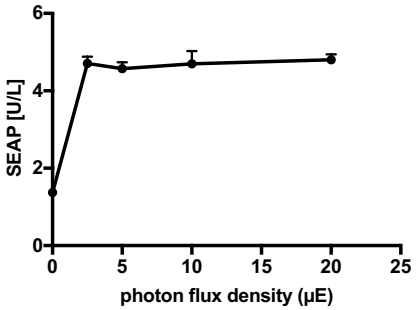

Fig.3b

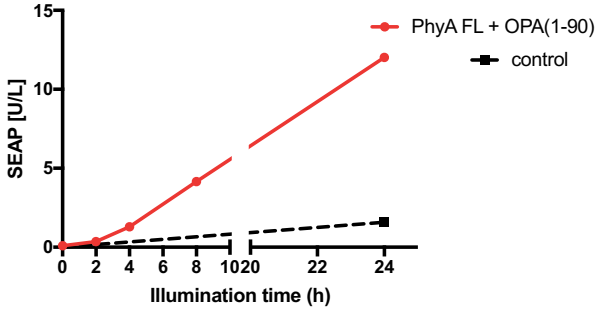

Fig.3c

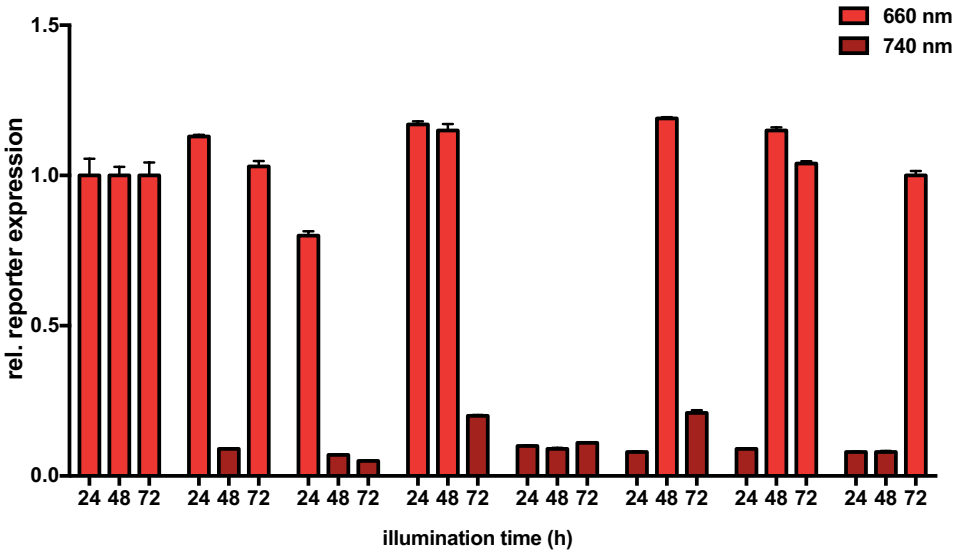

Fig.4 Fluorescence anisotropy

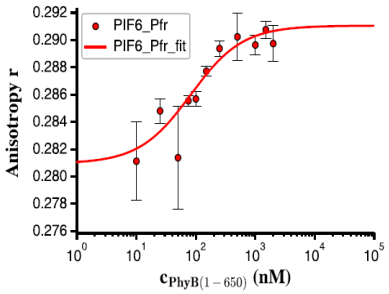

PhyB$^{1-650}$ + PIF6$^{1-100}$

$K_{D,650nm}$ = 82 nM

Error = 32 nM

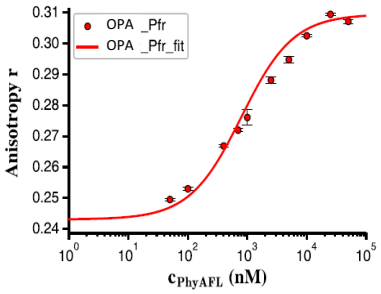

PhyA FL + OPA

$K_{D,650nm}$ = 797 nM

Error = 123 nM

Fig.S1 supplements

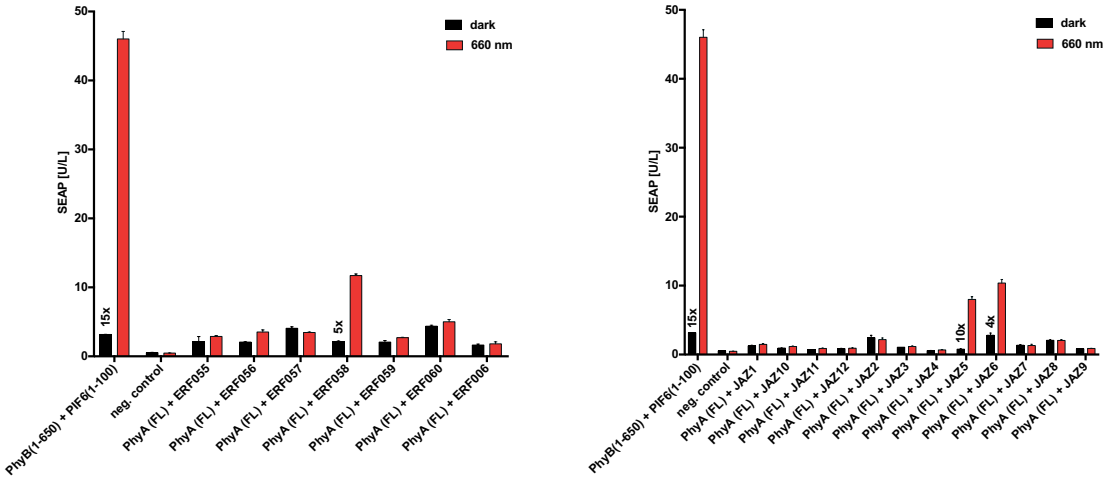

Supplements:

Supplementary Table S1: Plasmids designed and used in this study.
All plasmids were cloned using AQUA (source) or Gibson Cloning (source)

Plasmid	Description	Reference or source
pKM022	**P_{SV40}-PhyB$^{1-650}$-VP16-NLS-IRES-tetR-PIF6$^{1-100}$-pA**	
pPF001	**P_{SV40}-*SpeI*-PhyB$^{1-650}$-*EcoRV*-VP16-NLS-IRES-tetR-*BsrGI*-PIF6$^{1-100}$-*AscI*-pA** pKM022 was amplified using oligos oPF001/oPF002 to add *SpeI* and *AscI* restriction site. PhyB$^{1-650}$ was amplified from pKM022 with oPF003/oPF004 to add *EcoRV* restriction site. PIF6$^{1-100}$ was amplified from pKM022 with oPF005/oPF006 to add *BsrGI* restriction site. VP16-NLS-IRES-tetR was excised by *EcoRV* from pMZ1200. All fragments were assembled by AQUA cloning.	**This work**
pKM006	**$tetO_{13}$-P_{CMVmin}-SEAP-pA**	
pPF034	**$tetO_{13}$-P_{CMVmin}-SEAP-pA-P_{SV40}-Gaussia-pA** pKM006 was linearized using *HindIII* and *SpeI*. BGH-pA was amplified using oligos oPF007/oPF008 from pKM528. P_{SV40} was amplified using oligos oPF009/oPF010 from pKM022. Gaussia was amplified using oligos oPF047/oPF048 from pKM083. All fragments were assembled by AQUA cloning.	**This work**
pPF007	**P_{SV40}-*SpeI*-PhyA-*EcoRV*-VP16-NLS-IRES-tetR-*BsrGI*-PIF6$^{1-100}$-*AscI*-pA** pPF001 was linearized by *SpeI* and *EcoRV*. PhyA was amplified from pMZ1160 by using oligos oPF025/oPF026. Both fragments were assembled by AQUA.	**This work**
pPF013	**P_{SV40}-*SpeI*-PhyA-*EcoRV*-VP16-NLS-IRES-tetR-*BsrGI*-AAB2-*AscI*-pA** pPF007 was linearized by AscI and BsrGI. AAB2 was amplified using oligos oPF100/oPF101. Both fragments were assembled by AQUA.	**This work**
pPF086	**P_{SV40}-*SpeI*-PhyA-*EcoRV*-VP16-NLS-IRES-tetR-*BsrGI*-AAB2$^{1-90}$-*AscI*-pA** pPF007 was linearized by BsrGI and AscI. AAB2$^{1-90}$ was amplified using oligos oPF353/oPF101 from pPF013. Both fragments were assembled by AQUA.	**This work**
pPF087	**P_{SV40}-*SpeI*-PhyA-*EcoRV*-VP16-NLS-IRES-tetR-*BsrGI*-AAB2$^{91-180}$-*AscI*-pA** pPF007 was linearized by BsrGI and AscI. AAB2$^{91-180}$ was amplified using oligos oPF354/oPF100 from pPF013. Both fragments were assembled by AQUA.	**This work**

pPF078	**P_{SV40}-*SpeI*-PhyB-*EcoRV*-VP16-NLS-IRES-tetR-*BsrGI*-AAB2-*AscI*-pA** pPF009 was linearized by AsiSI and AscI. AAB2 was amplified using oligos oPF339/oPF340. Both fragments were assembled by AQUA.	**This work**
pPF090	**P_{SV40}-*SpeI*-PhyA$^{1-617}$-*EcoRV*-VP16-NLS-IRES-tetR-*BsrGI*-AAB2-*AscI*-pA** pPF013 was amplified using oligos oPF360/oPF361 and were assembled by AQUA.	**This work**
pPF089	**P_{SV40}-*SpeI*-PhyB-*EcoRV*-VP16-NLS-IRES-tetR-*BsrGI*-AAB2$^{1-90}$-*AscI*-pA** pPF009 was linearized by AsiSI and AscI. AAB2$^{1-90}$ was amplified using oligos oPF353/oPF359 from pPF013. Both fragments were assembled by AQUA.	**This work**

Supplementary Table S2: Oligonucleotides designed and used in this study.

Oligo	**Sequence (5´→ 3´)**
oPF001	TGTTCCAGATTACGCTGGCGCGCCTAAAAGCTTCGATCCAGACATGATAAGATAC ATTG
oPF002	CGGAAACCATGGTGGGACTAGTCAATTCCGATCCGGGACCTGAAATAAAAGA
oPF003	TCCCGGATCGGAATTGACTAGTCCCACCATGGTTTCCGGAGTCG
oPF004	GCACTACCAGCACTACCAGCACTATCGAATTCGATATCACCTAACTCATCAATC CCCTGTTCCC
oPF007	ACCTACAGCCCAGTGGCCTCGAGCTGCAGAAAGCTTCTTAAGCGACTGTGCCT TCTAGTTGCCAGC
oPF008	GACACACATTCCACAGCCATAGAGCCCACCGCATCCC
oPF009	GCGGTGGGCTCTATGGCTGTGGAATGTGTGTCAGTTAGGGTG
oPF010	TTCGAAGTCATGGTGGGATATCGCAATTCCGATCCGGGACCTGAAATAAAA
oPF047	TTTTATTTCAGGTCCCGGATCGGAATTGCGATATCCCACCATGGGAGTCAAAG TTCTGTTTG
oPF048	TAAATTAATTAAGCGATCGCACTAGTGCGGCCGCTTAGTCACCACCGGCCCCCTTG
oPF025	TTTGTCTTTTATTTCAGGTCCCGGATCGGAATTGACTAGTCCACCATGGATTCAG GCTCTAGGC

oPF026	GCACTACCAGCACTACCAGCACTATCGAATTCGATCTTGTTTGCTGCAGCGAGT TCCGC
oPF100	atcatgtctggatcgaagcttttaggcgcgccttaagctccattatacgaatcaatcgtcacttcttc
oPF101	ctggaggcggtggaagtggtggcggaggtagcgattgtacaatggagcctccttttgaaagatcgaaac
oPF353	ATCTTATCATGTCTGGATCGAAGCTTTTAGGCGCGCCTTAAGGTTCACTACACG CAGCTCTTCTCATC
oPF354	TGGAGGCGGTGGAAGTGGTGGCGGAGGTAGCGATTGTACAATGGGAGAAGAA ATTGAAATTGGCGTTAATAAGAG
oPF339	GGCGGTGGAAGTGGTGGCGGAGGTAGCGATGCGATCGCATGGAGCCTCCTTT TGAAAGATCGAAACG
oPF340	ATCTTATCATGTCTGGATCGAAGCTTTTAGGCGCGCCTTAAGCTCCATTATACG AATCAATCGTCACTTCTTC
oPF360	ATCTCAAAATTGATGGTATACAAGAACTAGAAGCTATCGAATTCGATAGTGCTG GTAGTGCTG
oPF361	GCACTACCAGCACTACCAGCACTATCGAATTCGATAGCTTCTAGTTCTTGTAT ACCATCAATTTTGAGATC
oPF359	GGCGGTGGAAGTGGTGGCGGAGGTAGCGATGCGATCGCTATGGAGCCTCCT TTTGAAAGATCGAAACG

Figure S1. PhyA potential interactor screening

Screening of potential interactors of PhyA. CHO-K1 cells were transiently transfected with the described reporter plasmid (pPF034) and the plasmids based on the red-light split transcription factor system containing *Arabidopsis thaliana* phytochrome A (PhyA) (pPF007) and one of the potential interactors. Additionally, the published red-light split transcription factor system was also transfected as a control. Transfected cells were kept in dark for 24 h, supplemented and incubated for 1 h with 15 µM PCB and illuminated afterwards for 24 h with 660 nm and an intensity of 20 µmol m^{-2} s^{-1} (red bars) or kept in dark (black bars). SEAP values were determined and induction folds calculated of 4 replicates. All experiments were done in 4 replicates and the error bars indicate standard deviation of the mean. All plasmid were transfected in 1:1 molar ratio (w:w).

www.nature.com/scientificreports

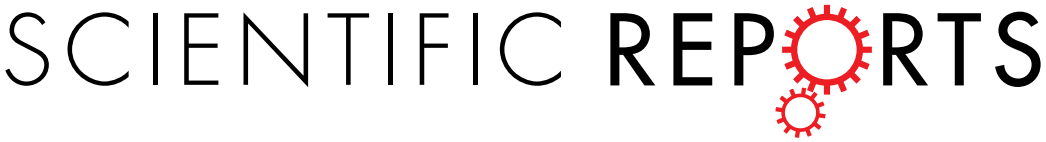

OPEN

Dual-controlled optogenetic system for the rapid down-regulation of protein levels in mammalian cells

Received: 30 April 2018
Accepted: 18 September 2018
Published online: 09 October 2018

Julia Baaske[1,2], Patrick Gonschorek[1,2,8], Raphael Engesser[2,3], Alazne Dominguez-Monedero[4], Katrin Raute[1,2,5], Patrick Fischbach[6], Konrad Müller[1,9], Elise Cachat[4], Wolfgang W. A. Schamel[1,2,7], Susana Minguet[1,2,7], Jamie A. Davies[4], Jens Timmer[2,3], Wilfried Weber[1,2] & Matias D. Zurbriggen[6]

Optogenetic switches are emerging molecular tools for studying cellular processes as they offer higher spatiotemporal and quantitative precision than classical, chemical-based switches. Light-controllable gene expression systems designed to upregulate protein expression levels meanwhile show performances superior to their chemical-based counterparts. However, systems to reduce protein levels with similar efficiency are lagging behind. Here, we present a novel two-component, blue light-responsive optogenetic OFF switch ('Blue-OFF'), which enables a rapid and quantitative down-regulation of a protein upon illumination. Blue-OFF combines the first light responsive repressor KRAB-EL222 with the protein degradation module B-LID (blue light-inducible degradation domain) to simultaneously control gene expression and protein stability with a single wavelength. Blue-OFF thus outperforms current optogenetic systems for controlling protein levels. The system is described by a mathematical model which aids in the choice of experimental conditions such as light intensity and illumination regime to obtain the desired outcome. This approach represents an advancement of dual-controlled optogenetic systems in which multiple photosensory modules operate synergistically. As exemplified here for the control of apoptosis in mammalian cell culture, the approach opens up novel perspectives in fundamental research and applications such as tissue engineering.

A common approach to study the function of a protein of interest in mammalian cells is to artificially manipulate its expression level. This approach is versatile, as it can be applied to most types of proteins, and simple, since no regulation mechanisms of the endogenous proteins need to be known or modulated.

Initially, chemical-based switches were used to manipulate expression levels by controlling transcription. Such systems are based on transcriptional activators or repressors, which alter their conformation and hence their target DNA-binding affinity upon interaction with specific small molecules. However, chemical-based switches have many limitations such as potential toxic or off-target effects of the regulatory small molecule, its poor or unpredictable diffusion through tissues and the difficulty of removing it from cells, tissues or organisms[1]. Optogenetic systems have the potential to overcome these limitations, creating great interest in implementing them in animal cell systems in culture and *in vivo*[2,3]. As optogenetic systems offer almost unlimited spatiotemporal resolution, dozens

[1]Faculty of Biology, University of Freiburg, Freiburg, Germany. [2]BIOSS - Centre for Biological Signalling Studies, University of Freiburg, Freiburg, Germany. [3]Institute of Physics, University of Freiburg, Freiburg, Germany. [4]Deanery of Biomedical Sciences, University of Edinburgh, Edinburgh, UK. [5]SGBM - Spemann Graduate School of Biology and Medicine, University of Freiburg, Freiburg, Germany. [6]Institute of Synthetic Biology, University of Düsseldorf and CEPLAS, Düsseldorf, Germany. [7]Center for Chronic Immunodeficiency, Medical Center, Faculty of Medicine, University of Freiburg, Freiburg, Germany. [8]Present address: Institute of Chemical Sciences and Engineering, School of Basic Sciences, Ecole Polytechnique Fédérale de Lausanne (EPFL), Lausanne, CH-1015, Switzerland. [9]Present address: Novartis Pharma AG, Basel, CH-4002, Switzerland. Julia Baaske and Patrick Gonschorek contributed equally. Correspondence and requests for materials should be addressed to W.W. (email: wilfried.weber@biologie.uni-freiburg.de) or M.D.Z. (email: matias.zurbriggen@uni-duesseldorf.de)

of switches have recently been implemented for the control of a wide range of intracellular processes including protein localization[4], activity[5] and stability[6,7], multi-wavelength gene-expression control[8–11] and organelle motility[12].

Optogenetic switches that control cellular protein abundance have in the last years shown much relevance and utility in biological research[2]. Most systems developed to date are based on the light-regulated induction of gene expression, some of which are reversible by illumination[8], therefore allowing high temporal and quantitative control. Systems to reduce protein levels are, however, not as established. Currently, only few systems are capable of down-regulating protein levels[6,13]. However, none of the existing systems actively represses transcription which would contribute to an efficient and quantitative reduction of protein levels. To address this limitation, we envisioned that an optogenetic system that actively represses promoter activity and simultaneously targets protein stability would result in superior reduction of cellular protein levels in terms of rate and quantitative control. For this purpose, we have developed a novel dual-controlled optogenetic system ('Blue-OFF') that combines transcriptional repression with regulation of protein stability, upon illumination with a single wavelength. The Blue-OFF system consists of two blue light-responsive protein modules: a novel, light-responsive repressor, KRAB-EL222, and the protein degradation module B-LID[6,9]. Both components utilize light-oxygen-voltage (LOV) domains, which react to blue light illumination using a flavin mononucleotide (FMN) as chromophore. Blue light illumination induces an adduct formation between FMN and a cysteine in the LOV domain, which triggers a conformational change in the protein, changing its effector function[14,15].

EL222 is a photosensitive transcription factor from the bacterium *Erythrobacter litoralis*. This transcription factor consists of a light sensitive LOV domain and a helix-turn-helix (HTH) DNA-binding domain, which can mediate light-induced transcription activation. In the dark, the LOV domain binds the HTH domain, precluding dimerization of the transcription factor and therefore no specific binding to a cognate DNA-sequence takes place. Blue light illumination disrupts the inhibitory LOV-HTH interactions and allows EL222 to homodimerize and bind specifically to the DNA sequence (C120). This interaction spontaneously reverses in the dark rendering EL222 inactive ($\tau \sim 11$ s at 37 °C)[16–18]. EL222 has already been adapted for light controllable transcriptional activation in mammalian cells by fusing it to a virus-derived transactivator domain[9]. We demonstrate for the first time its use as light-inducible transcriptional repressor by fusing it to the KRAB transrepressor domain to inhibit transcription from a constitutive promoter[19].

The B-LID module incorporates the LOV2 domain from *Avena sativa* phototropin 1 (AsLOV2). Illumination of AsLOV2 leads to an unwinding of the C-terminal Jα helix that is bound to the LOV core domain in the dark[6]. This structural change reverses spontaneously in darkness ($\tau \sim 80$ s at 22 °C)[6]. This mechanism can be exploited by integrating small peptide tags in the C-terminal Jα helix which then are structurally hidden in the dark and are only exposed upon illumination. For the development of the B-LID module, the peptide sequence RRRG was fused to the Jα helix of AsLOV2 leading to the light inducible proteasome-mediated degradation of a linked protein[6,7,15].

We present the combination of both modules in a single optogenetic system, which allows accurate control of protein production simultaneously on transcriptional and post-translational levels (Fig. 1a). This combinatorial approach enables a stronger, faster and longer-lasting reduction of cellular protein levels compared to the single modules, demonstrating the effectiveness of integrating repression on a transcriptional as well as a post-translational level. As a proof of principle, we have demonstrated the functionality of Blue-OFF with the reporter protein firefly luciferase and the mouse protein Caveolin-1 (CAV1). We show here that the Blue-OFF repression system can efficiently reduce protein expression levels, in different mammalian cell lines. Moreover, we developed a mathematical model to describe the activity of the Blue-OFF system which can hence be used for the experimental design by guiding the choice of irradiation conditions for obtaining desired repression levels. In line with these results, we further showed the applicability of the system for the optogenetic control of programmed cell death in mammalian cells by combining a drug-controlled caspase with the Blue-OFF system.

We present the first optogenetic repression system based on multiple photoreceptor modules that combines active repression with the control of protein stability and establish its use in a synergistic system. Taken together, our data highlight the advantages and strengths of this novel tool to complement the optogenetic toolbox.

Results

Design of a high-performance repression system by combining optogenetic modules. The optogenetic repressor module KRAB-EL222 was constructed by fusing a repressive KRAB domain, derived from the human *kox-1* gene[19], and two nuclear localization signals (NLS) to the N-terminus of EL222. The KRAB-EL222 module was cloned into an SV40 promoter-driven mammalian expression vector (pKM565) (Fig. 1a). As a light-regulated protein degradation system, we chose the B-LID system[6]. The functionality of both modules was assayed using a firefly luciferase (FLuc) reporter (pMZ1203), constructed to combine transcriptional and post-translational regulation (Fig. 1a): Transcriptional regulation was achieved by placing the FLuc under the control of a constitutive SV40 promoter followed by five copies of the EL222-binding sequence, $(C120)_5$, for binding of KRAB-EL222. Protein stability control was provided by fusing the B-LID degradation module C-terminally to FLuc. We first characterized the functionality of each module independently. The B-LID system was tested by replacing the EL222-KRAB module with the E-KRAB (pWW43) variant that cannot bind to $(C120)_5$. To test the KRAB-EL222 module independently, a reporter similar to pMZ1203 but lacking the RRRG degradation sequence (pMZ1210) was constructed. HEK-293T cells were transfected with the indicated plasmids in a 1:1 (w:w) ratio, incubated in the dark for 16 h, and illuminated for 8 h with 20 μmol m^{-2} s^{-1} of 460 nm light (Fig. 1b). Cells transfected with the two control plasmids showed no difference in luciferase expression between illuminated and non-illuminated cells (Fig. 1b, 'Non-regulated'). Cells transfected with only the KRAB-EL222 system showed a 50% repression in cells illuminated for 8 h, compared to those kept in the dark, demonstrating the functionality of this new photosensitive repressor. Additionally, we engineered and tested a set of variants of this module, none of which showed any better repressive behavior (Fig. S1). Cells transfected with only the B-LID

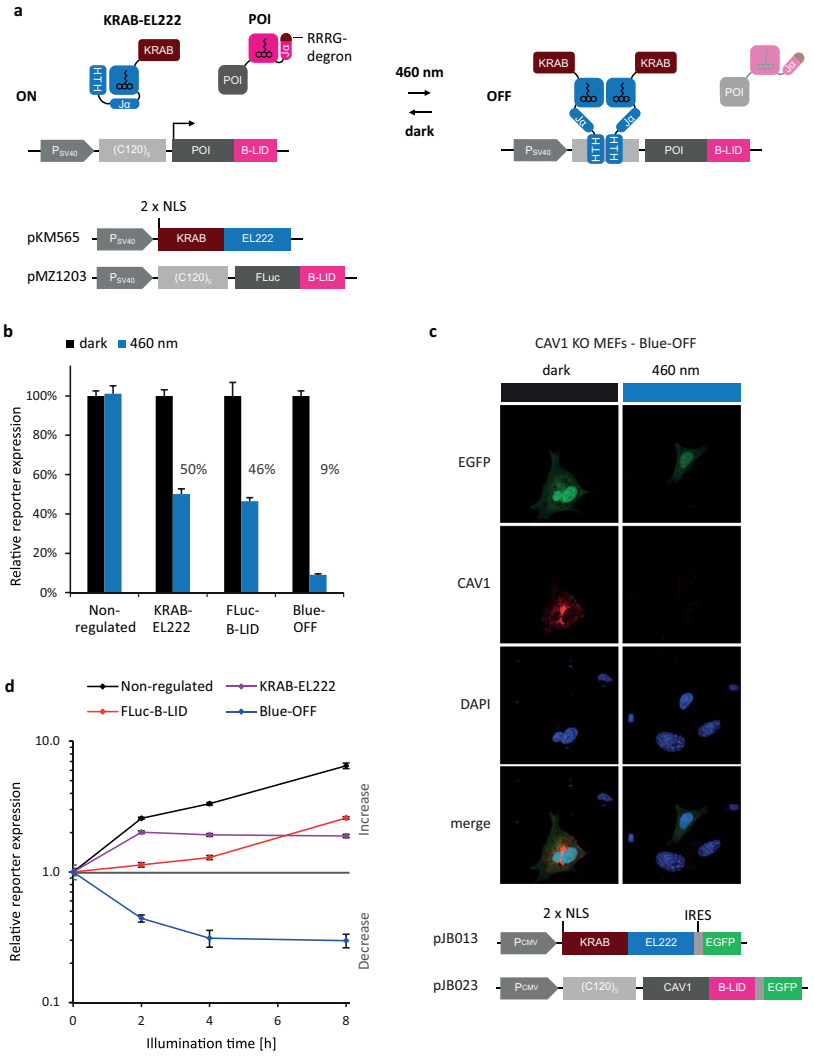

Figure 1. Design and validation of the Blue-OFF system. (**a**) Mode of function and constructs. Expression of the reporter protein FLuc-B-LID is placed under the control of a SV40 promoter followed by five copies of the EL222-binding sequence, $(C120)_5$. The photosensitive transcription factor EL222 is fused to an inhibitory KRAB domain and to two nuclear localization sequences (NLS). In the dark, KRAB-EL222 cannot bind to $(C120)_5$. Upon blue light illumination, KRAB-EL222 dimerizes and binds to $(C120)_5$ sequence inhibiting transcription. FLuc is fused to a B-LID module: in the dark the degradation peptide (RRRG) is docked to the LOV domain and thus covered. Blue light illumination exposes the peptide and leads subsequently to proteasome-mediated protein degradation. (**b**) Validation of the combined transcriptional and post-translational regulation. HEK-293T cells were transfected transiently with either no blue light-sensitive regulation module (Non-regulated: pWW43 + pMZ1210), single regulation modules (KRAB-EL222 only: pKM565 + pMZ1210; or FLuc-B-LID only: pWW43 + pMZ1203) or both modules together for the Blue-OFF system (pKM565 + pMZ1203). The cells were kept either in darkness for 24 h (black bars) or for 16 h in the dark conditions and then illuminated with 460 nm light for 8 h (blue bars). FLuc levels shown here are normalized to their dark control. (**c**) Constructs of the CAV1-Blue-OFF system. In darkness CAV1 accumulates whereas under blue light illumination active repression of transcription and degradation leads to a net decrease of CAV1 levels. CAV1 knock out (KO) primary embryonic fibroblast cells were transfected with KRAB-EL222 and CAV1-B-LID (pJB013 and pJB023,

respectively). After transfection cells were illuminated with 2 µmol m^{-2} s^{-1} of 460 nm light for 16 h. After fixation and permeabilization, cells were stained with an anti-CAV1 antibody followed by an AlexaFluor546-labelled secondary antibody and nuclei were counterstained with DAPI. Cells were imaged by confocal microscopy. (**d**) Kinetics of the blue light regulation systems. HEK-293T cells were transfected as before and incubated in darkness for 16 h. Cells were then illuminated for 0, 2, 4 and 8 h with blue light. FLuc levels were measured at the indicated time points and are represented normalized to the values obtained after 16 h darkness. In b and c, data are means of four independent replicates and error bars indicate standard deviation of the mean.

system showed 46% of the expression in non-illuminated cells. The dual-regulated system exhibited stronger repression, with only ~10% of the control levels of protein remaining. The level of down-regulation achieved is even stronger than a pure multiplicative combination of the two single modules. This result is due to nonlinearities in the system and shows a synergistic effect of the two optogenetic modules (Fig. 1b, 'Blue-OFF'). To extend the applicability of the dual-controlled Blue-OFF repression system we investigated its ability to down-regulate proteins other than reporters, e.g. Caveolin-1 (CAV1). CAV1 is the major component of endocytic caveolae plasma membrane invaginations and plays a critical role in normal tissue architecture and tumor progression[20,21]. In order to test the system, we employed the Blue-OFF system for controlling CAV1 levels (Fig. 1c). The plasmids contained EGFP as reporter to monitor transfected cells. The system was transfected in CAV1 knock-out (KO) mouse embryonic fibroblasts (MEFs). Cells were illuminated for 16 h with 2 µmol m^{-2} s^{-1} of 460 nm. CAV1 expression levels were evaluated using immunofluorescence microscopy (Figs 1c, S2). As expected, CAV1-KO cells transfected with Blue-OFF and kept in darkness showed high expression of CAV1, whereas after blue light illumination, CAV1 levels significantly decreased but not co-expressed EGFP signals.

Following these results, we set out to characterize the kinetics of repression, to gain a better insight into the contribution of transcriptional and posttranslational regulation on performance of the dual-regulated Blue-OFF system. Cells were incubated for 16 h in the dark followed by 0, 2, 4 or 8 h of illumination prior to the determination of luciferase activity (Fig. 1d). The non-regulated, blue light-insensitive control system showed ongoing protein accumulation unaffected by illumination (black line). In contrast, protein accumulation was halted by controlling only transcription using KRAB-EL222 (purple line). The repression of transcription first became apparent on the protein level 2 h after illumination, when no further increase, but a slow decrease of protein accumulation was observed. The 2 h delay is likely the result of ongoing translation from already synthesized mRNA during this time. In contrast, posttranslational control via protein degradation with the B-LID system showed a stronger and more immediate effect than transcriptional regulation (red line). The dual-regulated Blue-OFF system integrated the rapid, but temporally limited degradation effect of the B-LID system, with a delayed but persistent repressive effect of KRAB-EL222 to achieve a faster, stronger and longer-lasting repression (blue line). Furthermore, in contrast to the systems using a single optogenetic module, only the dual-controlled system achieved an absolute decrease in cellular protein levels after starting illumination. Our data demonstrates that the combination of transcriptional and posttranslational regulation in the Blue-OFF system results in a superior, light-induced down-regulation of a protein of interest.

Reversibility and versatility of the dual-controlled optogenetic Blue-OFF system. A key advantage of light as an inducer is its high temporal precision and the reversibility of its application to a given biological system[22]. To evaluate reversible control of protein expression, HEK-293T cells expressing the Blue-OFF system were kept in darkness for 12 h, followed by a cycle of 12 h blue light illumination and 12 h darkness. Blue light illumination resulted in a 90% reduction of the protein level reached in darkness. Another 12 h of darkness allowed the protein levels to recover, demonstrating that the Blue-OFF system can control protein expression in a reversible manner (Fig. 2a).

To validate versatility, the Blue-OFF system was implemented in different mammalian cell lines. To this end, we expressed the system transiently in human embryonic kidney cells (HEK-293T), human cervical cancer cells (HeLa), chinese hamster ovary cells (CHO-K1), mouse embryonic fibroblasts (NIH/3T3) and monkey fibroblast-like cells (COS-7). Cells were kept in darkness for 16 h, followed by 8 h of blue light illumination. Blue light illumination resulted in a 70% to 90% decrease of reporter protein expression among the various cell lines, suggesting a high versatility and cross-species applicability of the Blue-OFF system (Fig. 2b).

Development of a quantitative model to describe the activity of the Blue-OFF system. To further characterize the Blue-OFF system and its contributing modules, we developed a mathematical model based on ordinary differential equations (ODE) describing the time evolution of the concentrations of the involved substances. The model is parameterized using quantitative data on the time course and on the response to light intensity.

$$\frac{d[FLuc_{off}](t)}{dt} = -k_{deg,const}[FLuc_{off}] + k_{translate}[FLuc_{mRNA}] - k_{on}I(t)[FLuc_{off}] + k_{off}[FLuc_{on}] \quad (1)$$

$$\frac{d[FLuc_{on}](t)}{dt} = -k_{deg,const}[FLuc_{on}] - \frac{k_{deg,ind}[FLuc_{on}]}{K_{m,deg} + [FLuc_{on}]} + k_{on}I(t)[FLuc_{off}] - k_{off}[FLuc_{on}] \quad (2)$$

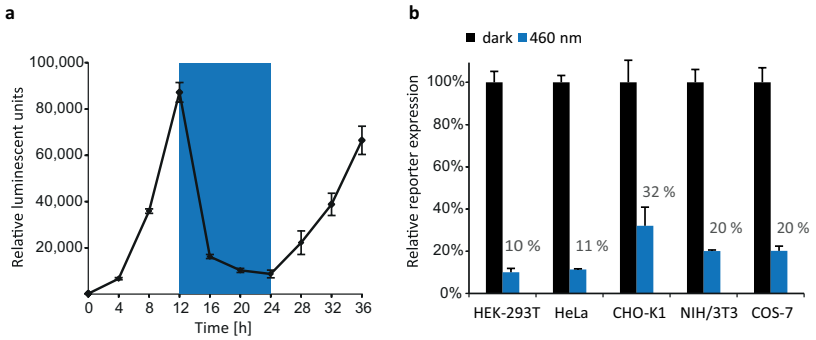

Figure 2. Reversibility and versatility of the Blue-OFF system. (**a**) HEK-293T cells were transfected with KRAB-EL222 (pKM565) and FLuc-B-LID (pMZ1203).and kept in darkness for 12 h followed by 12 h blue light illumination and again 12 h darkness. FLuc levels were measured every 2 h. (**b**) Blue-OFF characterization using different mammalian cell lines. The indicated cell lines were transfected with KRAB-EL222 and FLuc-B-LID. Cells were kept in darkness for 16 h followed by 8 h of 460 nm blue light illumination. FLuc levels were determined at the final time point. To correct for different transfection efficiencies, the expression data were normalized to co-transfected constitutively expressed Renilla luciferase (RLuc). In a and b, data are means of four independent replicates and error bars indicate standard deviation of the mean.

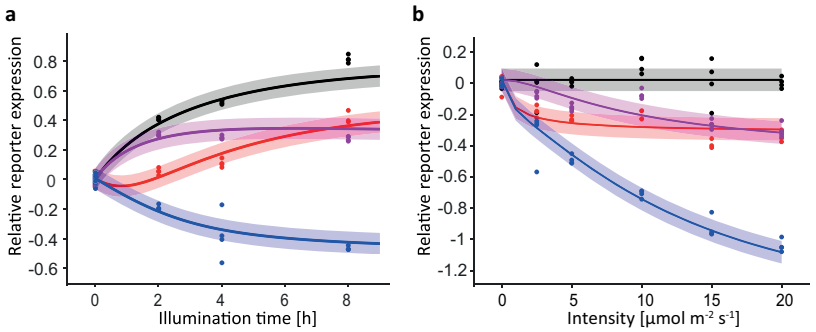

Figure 3. Quantitative characterization of the behavior of the Blue-OFF system to calibrate the mathematical model. The model was calibrated using kinetic (**a**) and intensity dose response data (**b**). For the dose response HEK-293T cells were transfected with the Blue-OFF system. The cells were kept in darkness for 16 h after transfection and subsequently illuminated for 8 h with 0, 2.5, 5, 10, 15 and 20 µmol m^{-2} s^{-1} of 460 nm light. Shown is the relative reporter expression on a logarithmic scale. The dots indicate the experimental data points and the solid lines show the model simulation for the optimal parameter set. The shaded error bands are estimated by using an error model assuming a log-normally distributed error.

$$\frac{d[KRAB_{off}](t)}{dt} = -k_{on}I(t)[KRAB_{off}] + k_{off}[KRAB_{on}] \tag{3}$$

$$\frac{d[KRAB_{on}](t)}{dt} = +k_{on}I(t)[KRAB_{off}] - k_{off}[KRAB_{on}] \tag{4}$$

$$\frac{d[FLuc_{mRNA}](t)}{dt} = \frac{k_{transcript}}{1 + k_{inh,KRAB}[KRAB_{on}]^2} - k_{deg,mRNA}[FLuc_{mRNA}] \tag{5}$$

The Blue-OFF system is based on the light-induced conformational change of two proteins. On the one hand, the FLuc-B-LID switch exists in two conformations: $FLuc_{off}$ and $FLuc_{on}$. $FLuc_{off}$ is the form present in the dark with an inactive B-LID domain which is translated from $FLuc_{mRNA}$ and degrades at the rate $k_{deg,const}$. By

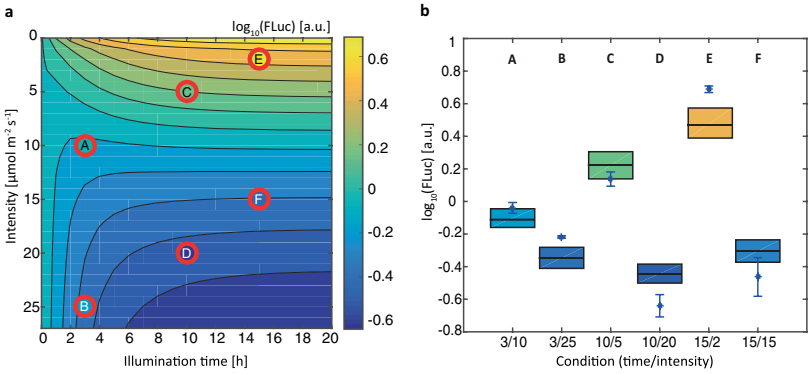

Figure 4. Model-aided prediction of protein expression levels using the Blue-OFF system. (**a**) Simulated reporter expression for different light intensities and illumination times for characterizing the system. To validate if the model can be used to determine experimental conditions to obtain a desired protein level six combinations with different intensities and illumination durations were measured and compared to the model predictions (red circles). The colored filling in the red circles indicates the experimentally determined expression levels. (**b**) The means of four determinations for each combination are denoted with blue stars and the error bars are showing the standard error of the mean. The colored boxes show the 95% prediction confidence interval calculated by analyzing the prediction profile likelihood.

illumination with blue light with the intensity I(t), the protein changes its conformation to $FLuc_{on}$ and is available for degradation via the proteasome. The parameter $K_{m,deg}$ describes saturation of the proteasome-dependent protein-degradation machinery. On the other hand, the light-inducible transcriptional repressor EL222-KRAB is in an inactive form in the dark, $KRAB_{off}$. Upon illumination with blue light the conformation is changed to $KRAB_{on}$, which represses the transcription of the $FLuc_{mRNA}$. The $FLuc_{mRNA}$ is produced with the constitutive transcription rate $k_{transcript}$ in the absence of EL222-KRAB. A detailed derivation of the model equations can be found in the Supplementary Information.

The model was calibrated by using the measured kinetics (Figs 1d and 3a) and light intensity 'dose'-response data (Fig. 3b). The parameters were estimated by maximizing the likelihood function. The resulting fit is shown in Fig. 3. The model can explain the measured data, including the high synergistic repression in the combined system. An analysis of the calibrated model suggests as reason the saturation in the process of the B-LID induced protein degradation. In cells transfected only with the B-LID system the FLuc degradation is saturated whereas for the combined system the FLuc concentration is lower therefore not reaching saturation in its degradation. To assess the uncertainties of the estimated parameters, we calculated the profile likelihood of each parameter[23]. The detailed fitting process, estimated parameter values and their 95% confidence intervals are shown in the Supplementary Information. The parameter estimation and the profile likelihood analysis were performed with the Data2Dynamics framework[24].

Implementation of the mathematical model to predict experimental outcomes. Next, we aimed to control the level of repression in a predictable manner by adjusting the illumination time and intensity using the calibrated mathematical model to predict the performance and operating range of the system. Figure 4a shows the predicted expression level of FLuc for different light intensities and illumination times. This map helps identifying the illumination conditions needed to obtain a desired reporter expression level.

Several experimental conditions were selected (A-F in Fig. 4a) and the reporter protein levels were compared to the values predicted from the mathematical model to test the applicability of the model to achieve a desired expression level by choosing the illumination time and light intensity (Fig. 4b). The uncertainties of the estimated model parameters lead to an uncertainty of the model prediction. To quantify this uncertainty in terms of prediction confidence intervals, we analyzed the prediction profiles likelihood[25] (Fig. 4b, colored boxes). The predicted expression levels (colored boxes) and the experimentally obtained expression levels (individual blue stars) show a strong correlation. These results indicate the applicability and usefulness of the model to determine conditions for experimental setups to achieve specific repression levels. Moreover, this shows the highly tunable repression levels of the Blue-OFF system by varying light intensity or illumination time.

Controlling programmed cell death using the Blue-OFF system. Finally, we set out to implement the Blue-OFF system to achieve light control over apoptosis in mammalian cells. For this purpose, we customized the tamoxifen inducible apoptosis-inducing caspase protein (Casp8-ER(T2)), previously described by Cachat *et al.*[26]. Caspase 8 is predominantly present as an inactive monomer, but upon addition of 4-hydroxytamoxifen (4-OHT) the ER(T2) domain brings about dimerization and activation, triggering apoptosis[27]. We integrated this module into the Blue-OFF system for blue-light control of caspase8 stability (Casp8-ER(T2)-Blue-OFF) (Fig. 5a).

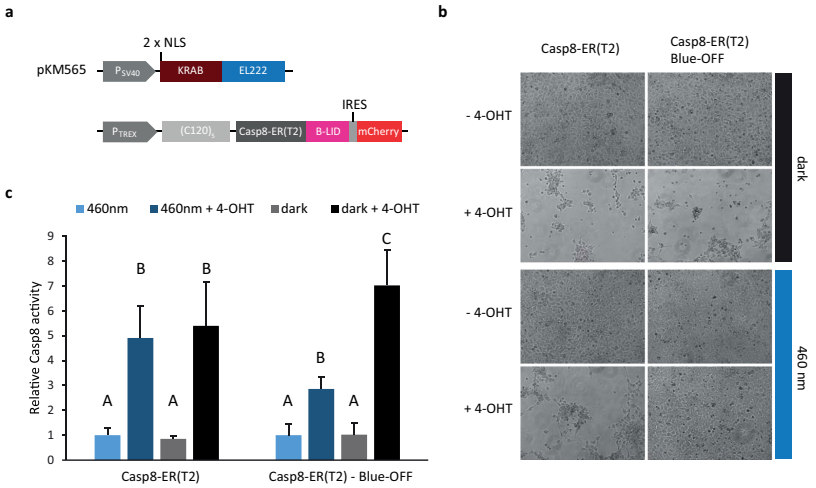

Figure 5. Application of the Blue-OFF system for the control of programmed cell death. (**a**) Constructs of the Casp8-ER(T2)-Blue-OFF system. (**b**,**c**) Optogenetic control of programmed cell death in HEK-293 cells transfected with the Casp8-ER(T2)-Blue-OFF system. (**b**) HEK-293 cells transfected with the Casp8-ER(T2) or the Casp8-ER(T2)-Blue-OFF systems form a uniform monolayer under blue light exposure or in darkness in the absence of 4-OHT. Induction of caspase 8 activity upon 4-OHT addition leads to cell death in darkness (for Casp8-ER(T2) and Casp8-ER(T2)-Blue-OFF) and under blue light exposure for Casp8-ER(T2), whereas cells transfected with the Casp8-ER(T2)-Blue-OFF system show a higher survival rate under blue-light conditions, thus building a uniform cell monolayer. (**c**) Quantification of caspase8 activity. The figure shows the caspase 8 activity of HEK-293 cells transfected with the Casp8-ER(T2) system (left) or the light-regulated Casp8-ER(T2)-Blue-OFF system (right), in the presence and absence of 4-OHT and blue light. Values are mean of three independent experiments and error bars indicate standard deviation of the mean. Statistical significance between the tested conditions for each system is indicated with uppercase letters above each bar, where "A" significantly differs from "B", "B" from "C". One-way analysis of variance (ANOVA), $P < 0.005$.

HEK-293 cells transfected with Casp8-ER(T2) showed significant apoptosis upon induction with 4-OHT both in the dark or under blue light, whereas cells transfected with the Casp8-ER(T2)-Blue-OFF system were able to grow and form a monolayer under blue light (Fig. 5b).

Subsequently, a caspase 8 activity assay was performed in order to correlate the protective effect of the dual Blue-OFF system on cell survival with reduced activity of caspase 8. After addition of 4-OHT, a 7-fold increase in caspase 8 activity was observed (Fig. 5c) in cells transfected with the Casp8-ER(T2)-Blue-OFF system when kept in the dark compared to transfected cells without addition of 4-OHT. When illuminated with blue light a 60% reduction in caspase 8 activity was observed (Fig. 5c), which is in line with the reduced cell death (Fig. 5b). As expected, blue light had no effect on caspase 8 activity in 4-OHT induced control cells transfected with Casp8-ER(T2). These results indicate that the Blue-OFF system can efficiently be used for the optogenetic control of programmed cell death in mammalian cells and opens up the possibility for the selective induction of apoptosis in specific cells by local illumination that is unachievable with diffusible drugs.

Discussion

The recent development of light-regulated synthetic molecular switches has considerably contributed to a better insight into the functions and characteristics of proteins in regulatory networks (www.optobase.org)[28]. A common function of these switches is to upregulate protein abundance in biological systems, their subcellular localization or their activity[29]. While there is a broad set of optogenetic tools available to upregulate protein expression, only few systems are available to reduce protein levels. Despite successful results in various experimental designs, these down-regulation approaches are not as efficient in terms of absolute reduction of protein levels.

To improve the efficiency of transgene expression control, transcription-translation networks have been developed. These dual approaches enable tighter control of protein expression, however until recently mainly relied on chemical switches[13,30–33].

For this purpose, we engineered a dual-controlled optogenetic switch, Blue-OFF, that confers rapid and sustained, blue light sensitive down-regulation of protein expression levels by simultaneously targeting gene repression and protein stability. The novel blue light-responsive repressor KRAB-EL222 was combined with the protein degradation module B-LID constituting a system that can be regulated upon illumination with a single wavelength.

By combining both levels of regulation the Blue-OFF system outperforms existing down-regulation systems.

Efficient down-regulation of protein expression is instrumental in answering many biological questions. Biological systems are highly dynamic, thus, reversibility is a key feature of synthetic molecular switches to better understand biological processes. Therefore, light emerges as optimal superior inducer, since it can be applied and withdrawn from biological systems in a fully reversible manner. Here, we showed how protein down-regulation by the Blue-OFF system is fully reversible. Moreover, we were able to validate the functionality of the system in different cell types, which proves its broad applicability.

To quantitatively understand the underlying processes in light-inducible gene repression and protein degradation, we developed a quantitative mathematical model that was parameterized with the experimental data. Using this model, it is possible to set the experimental parameters (light intensity and illumination regime) for tuning the Blue-OFF for desired applications. Blue-OFF can, furthermore, easily be combined with other systems by placing the target site of the repressor modules KRAB-EL222 behind any endogenous or synthetic promoter and by fusing B-LID to any protein of interest. The Blue-OFF was successfully applied for the control of programmed cell death which opens up novel perspectives for creating cellular patterns with high spatiotemporal resolution. In the frame of the current development of strategies for engineering multicellular systems, the Blue-OFF system could contribute to synthetic tissue engineering approaches and the generation of complex 3D structures.

In conclusion, we have shown that the novel Blue-OFF optogenetic approach for controlling protein levels, acting simultaneously on transcriptional and post-translational levels, leads to a fast and strong reduction of the net level of the protein of interest. In addition, a model-based quantitative characterization of the system kinetics enables the rational adjustment of parameters to achieve desired repression levels. The strong repressive effect together with the predictive properties of the system constitute a powerful and versatile tool. For the future, we envision that this system will be used to answer fundamental biological questions and boost applications such as in tissue engineering.

Methods

Plasmids. The design and the construction of the expression vectors are described in Tables S2, S3.

Cell culture and transfections. Chinese hamster ovary cells (CHO-K1) were cultivated in HTS medium (Cell Culture Technologies) supplemented with 10% tetracycline-free fetal calf serum (FCS, PAN, cat. no.: P30–3602, lot no.: P101003TC), 2 mM L-glutamine (Sigma), 100 U mL^{-1} penicillin and 0.1 mg mL^{-1} streptomycin (PAN). Mouse embryonic fibroblast cells (NIH/3T3), human embryonic kidney cells (HEK-293T), African green monkey fibroblast-like cells (COS-7), and human epithelioid cervix carcinoma cells (HeLa) were maintained in Dulbecco's modified Eagle's medium (DMEM, PAN, cat. no. P04–03550) supplemented with 10% FCS (FCS, PAN, cat. no.: P30-3306, lot no.: P140204), 100 U mL^{-1} penicillin and 0.1 mg mL^{-1} streptomycin (PAN) at 37 °C with 5% CO_2. For transfection, 30,000-75,000 cells per well of a 24-well plate were transfected using polyethylenimine (PEI, linear, MW: 25 kDa, Polyscience) as describes elsewhere[34]. Unless otherwise indicated, cells were transfected with constructs comprising the light responsive repressor KRAB-EL222 (pKM565), FLuc-B-LID (pMZ1203) and as a control CMV driven Renilla Luciferase (RLuc) at a ratio of 20:20:1 (w:w:w), respectively.

Immortalized mouse embryonic fibroblasts (MEFs) were obtained from Caveolin 1-deficient mice (B6.Cg-CAV1tm1mls/J[35]). Immortalization was induced by the simian virus 40 large T antigen (SV40-Tag). Cells were cultured in DMEM (1×) + GlutMAX™ (Gibco, cat. no.: 61965–026) supplemented with 10% fetal bovine serum (Gibco, cat. no.: 10270–106, lot no.: 42F9251K), 50 U mL^{-1} penicillin and 0.05 mg mL^{-1} streptomycin (Gibco, cat. no.: 15140–122) and 50 µM β-mercaptoethanol (Sigma). Transfections for MEFs were done using TransitX2 (Mirus, cat. no.: MIR6000). 70.000 cells were seeded in 12-well plates and transfected using 1 µg of DNA/3 µl TransitX2.

Human embryonic kidney (HEK-293) cells were maintained in DMEM (Gibco, cat. no.: 41966) supplemented with 10% fetal bovine serum (Biosera, cat. no.: FB1090/500, lot no.: 013BS145) in a humidified incubator at 37 °C and 5% CO_2. HEK-293 cells were harvested by trypsinization 24 h prior to transfection, and seeded at a density of 80.000 cells in 500 µl of complete medium per well on 24 well plates. Cells were transfected with lipofectamine 3000 (Invitrogen, cat. no.: L3000–008). Unless otherwise indicated cells were transfected with pTREX-BLID-mCherry-2A-myrcasp8-ER(T2), pKM565 or pTREX-myrCasp8-ER(T2)-IRES-mCherry. After 24 hours, the medium was replaced by fresh growth medium.

Light induction. Cells were kept in darkness or were illuminated with 460 nm light for the indicated time periods at a photon flux density of 20 µmol m^{-2} s^{-1}, unless indicated otherwise. Illumination was performed with light boxes similar to[36] with LED panels emitting at 460 nm (LED Engin, cat. no.: LZ1-10B202-0000). All cell-handling involving the blue-light inducible systems was done under 628 nm light which does not affect the light-sensitive systems described here.

Reporter gene assay. Luciferase expression was quantified by lysing cells on ice with 250 µl luciferase lysis buffer (25 mM Tris/HCl, pH 7.8, 1% Triton X-100, 15 mM $MgSO_4$, 4 mM ethylene glycol tetraacetic acid (EGTA), 1 mM DTT) per well on ice for 15 min. 80 µl lysate was transferred to Costar® 96-well flat-bottom white plates (Corning Incorporated, Germany). Firefly and Renilla luciferase luminescence was directly monitored using either a Synergy 4 multimode microplate reader (BioTek Instruments Inc., Winooski, VT) or an Infinite 200Pro microplate reader (Tecan, Switzerland) after addition of 20 µl of either firefly luciferase substrate (20 mM Tricine, 2.67 mM $MgSO_4$, 0.1 mM EDTA, 33.3 mM DTT, 0.52 mM ATP, 0.27 mM Acetyl-CoA, 5 mM NaOH, 264 µM $MgCO_3$, 0.47 mM luciferin) or Renilla luciferase substrate (472 µM coelenterazine stock solution in methanol; diluted directly before use, 1:15 in PBS).

Immunofluorescence microscopy. Cells were fixed in 4% paraformaldehyde for 15 min at room temperature and washed three times in PBS, permeabilized in 0.5% Triton X-100 for 15 min at room temperature, rewashed in PBS and blocked in PBS with1% BSA for 30 min at room temperature. Subsequently, cells were incubated overnight at 4 °C with the primary anti-Caveolin-1 antibody (1:200 in blocking buffer; BD biosciences, cat. no.: 610060). Following washing with blocking buffer, cells were incubated with AlexaFluor546-conjugated secondary goat anti-rabbit antibody (1:200 in blocking solution; Invitrogen cat. no.: A11035) for 2 h at 37 °C, rewashed and mounted on microscopy slides in ProLong Gold Antifade Mountant containing DAPI (ThermoFisher; cat. no.: P36931).

Cells were imaged with Nikon Instruments Eclipse Ni-E with a C2+ confocal laser scanner (100× Plan Apo λ oil immersion objective, NA = 1.45). DAPI, GFP and AlexaFluor546 were visualized using excitation lasers of 405, 488 and 561 nm and emission filters of 445/50, 525/50 and 660 nm LP, respectively. Image acquisition was performed with NIS-Elements AR (Nikon Instruments, version 4.20). Cells were defined as regions of interest according to their EGFP expression. Subsequently, mean fluorescence intensities of GFP and CAV1 signals were measured. Analyses were performed with Fiji[37].

Induction of apoptosis. Transfected HEK-293T cells were kept in the dark or were exposed to blue light 5 h before treatment with 1 µM 4-Hydroxytamoxifen (4-OHT, Sigma, cat. no.: H7904) to induce apoptosis. Images were acquired 48 hours after induction with 4-OHT using a Zeiss Axio Observer D1 inverted microscope with AxioCam MRm and a 20x objective.

Caspase8 activity assay. Transfected HEK-293T cells were kept in the dark or were exposed to blue light 3 h before treatment with 1 µM 4-OHT. All cells were detached 3 hours after induction with 4-OHT and centrifuged at 500 *g* for 10 min. The supernatant was discarded and cells washed with PBS. After centrifugation, cell pellet was resuspended in cold Lysis Buffer (10 mM Tris-Cl at pH 7.4, 100 mM NaCl, 2.5 mM $MgCl_2$, 0.5% NP-40, 0.5% Triton X-100) and incubated for 10 min. The cell lysate was centrifuged at 10,000 × g for 3 min. In order to quantify the Caspase8 activity, 80 µl of the resulting supernatant were mixed with 80 µl of the Caspase-Glo® 8 reagent (Promega) in 96 well flat bottom white microplates (LumitracTM 200, Greiner) for 20 min. Luminescence intensity was measured in RLU (relative luminescence units) with the BMG FLUOstar OPTIMA Microplate Reader.

Statistical analysis. One-way ANOVA with Tukey Pairwise Comparisons were performed using Minitab 17 Statistical Software (2010). Unpaired *t*-tests were performed using GraphPad Prism 6. Outliers for statistical analysis of CAV1 intensities were determined and excluded as described in[38].

References

1. Weber, W. & Fussenegger, M. Emerging biomedical applications of synthetic biology. *Nat. Rev. Genet.* **13**, 21–35 (2012).
2. Müller, K., Naumann, S., Weber, W. & Zurbriggen, M. D. Optogenetics for gene expression in mammalian cells. *Biological Chemistry* **396**, 145–152 (2015).
3. Tischer, D. & Weiner, O. D. Illuminating cell signalling with optogenetic tools. *Nat. Rev. Mol. Cell Biol.* **15**, 551–558 (2014).
4. Beyer, H. M. *et al*. Red light-regulated reversible nuclear localization of proteins in mammalian cells and zebrafish. *ACS Synth. Biol.* **4**, 951–958 (2015).
5. Wend, S. *et al.* Optogenetic Control of Protein Kinase Activity in MammalianCells. *ACS Synth. Biol.* **3**, 280–285 (2014).
6. Bonger, K. M., Rakhit, R., Payumo, A. Y., Chen, J. K. & Wandless, T. J. General method for regulating protein stability with light. *ACS Chem. Biol.* **9**, 111–115 (2014).
7. Bonger, K. M., Chen, L., Liu, C. W. & Wandless, T. J. Small-molecule displacement of a cryptic degron causes conditional protein degradation. *Nat. Chem. Biol.* **7**, 531–537 (2011).
8. Müller, K. *et al.* A red/far-red light-responsive bi-stable toggle switch to control gene expression in mammalian cells. *Nucleic Acids Res.* **41**, (2013).
9. Motta-Mena, L. B. *et al.* An optogenetic gene expression system with rapid activation and deactivation kinetics. *Nat. Chem. Biol.* **10**, 196–202 (2014).
10. Wang, X., Chen, X. & Yang, Y. Spatiotemporal control of gene expression by a light-switchable transgene system. *Nat. Methods* **9**, 266–269 (2012).
11. Yazawa, M., Sadaghiani, A. M., Hsueh, B. & Dolmetsch, R. E. Induction of protein-protein interactions in live cells using light. *Nat. Biotechnol.* **27**, 941–945 (2009).
12. van Bergeijk, P., Adrian, M., Hoogenraad, C. C. & Kapitein, L. C. Optogenetic control of organelle transport and positioning. *Nature* **518**, 111–4 (2015).
13. Pathak, G. P. *et al.* Bidirectional approaches for optogenetic regulation of gene expression in mammalian cells using Arabidopsis cryptochrome 2. *Nucleic Acids Res.* **41**, e77 (2017).
14. Herrou, J. & Crosson, S. Function, structure and mechanism of bacterial photosensory LOV proteins. *Nat. Rev. Microbiol.* **9**, 713–723 (2011).
15. Zayner, J. P. & Sosnick, T. R. Factors that control the chemistry of the LOV domain photocycle. *PLoS One* **9**, (2014).
16. Nash, A. I. *et al*. Structural basis of photosensitivity in a bacterial light-oxygen-voltage/helix-turn-helix (LOV-HTH) DNA-binding protein. *Proc. Natl. Acad. Sci.* **108**, 9449–9454 (2011).
17. Rivera-Cancel, G., Motta-Mena, L. B. & Gardner, K. H. Identification of natural and artificial DNA substrates for light-activated LOV-HTH transcription factor EL222. *Biochemistry* **51**, 10024–10034 (2012).
18. Zoltowski, B. D., Nash, A. I. & Gardner, K. H. Variations in Protein–Flavin Hydrogen Bonding in a Light, Oxygen, Voltage Domain Produce Non-Arrhenius Kinetics of Adduct Decay. *Biochemistry* **50**, 8771–8779 (2011).
19. Moosmann, P., Georgiev, O., Thiesen, H. J., Hagmann, M. & Schaffner, W. Silencing of RNA polymerases II and III-dependent transcription by the KRAB protein domain of KOX1, a Krüppel-type zinc finger factor. *Biol. Chem.* **378**, 669–677 (1997).
20. Goetz, J. G. *et al*. Biomechanical Remodeling of the Microenvironment by Stromal Caveolin-1 Favors Tumor Invasion and Metastasis. *Cell* **146**, 148–163 (2011).
21. Parton, R. G. & Simons, K. The multiple faces of caveolae. *Nature Reviews Molecular Cell Biology* **8**, 185–194 (2007).
22. Bacchus, W. & Fussenegger, M. The use of light for engineered control and reprogramming of cellular functions. *Current Opinion in Biotechnology* **23**, 695–702 (2012).

23. Raue, A. *et al*. Structural and practical identifiability analysis of partially observed dynamical models by exploiting the profile likelihood. *Bioinformatics* **25**, 1923–1929 (2009).
24. Raue, A. *et al*. Data2Dynamics: a modeling environment tailored to parameter estimation in dynamical systems: Fig. 1. *Bioinformatics* **31**, 3558–3560 (2015).
25. Kreutz, C., Raue, A. & Timmer, J. Likelihood based observability analysis and confidence intervals for predictions of dynamic models. *BMC Syst. Biol.* **6**, 120 (2012).
26. Cachat, E., Liu, W. & Davies, J. A. Synthetic self-patterning and morphogenesis in mammalian cells: a proof-of-concept step towards synthetic tissue development. *Eng. Biol.* 1–6 (2017).
27. Chu, Y., Senghaas, N., Köster, R. W., Wurst, W. & Kühn, R. Novel caspase-suicide proteins for tamoxifen-inducible apoptosis. *genesis* **46**, 530–536 (2008).
28. Kolar, K., Knobloch, C., Stork, H., Žnidarič, M. & Weber, W. OptoBase: A Web Platform for Molecular Optogenetics. *ACS Synth. Biol.* **7**, 1825–1828 (2018).
29. Ausländer, S. & Fussenegger, M. From gene switches to mammalian designer cells: Present and future prospects. *Trends in Biotechnology* **31**, 155–167 (2013).
30. Malphettes, L. & Fussenegger, M. Impact of RNA interference on gene networks. *Metab. Eng.* **8**, 672–683 (2006).
31. Malphettes, L. & Fussenegger, M. Improved transgene expression fine-tuning in mammalian cells using a novel transcription–translation network. *J. Biotechnol.* **124**, 732–746 (2006).
32. Ausländer, S., Ausländer, D., Müller, M., Wieland, M. & Fussenegger, M. Programmable single-cell mammalian biocomputers. *Nature* **487**, 123–127 (2012).
33. Deans, T. L., Cantor, C. R. & Collins, J. J. A Tunable Genetic Switch Based on RNAi and Repressor Proteins for Regulating Gene Expression in Mammalian Cells. *Cell* **130**, 363–372 (2007).
34. Müller, K. *et al*. Multi-chromatic control of mammalian gene expression and signaling. *Nucleic Acids Res.* **41**, e124 (2013).
35. Drab, M. *et al*. Loss of caveolae, vascular dysfunction, and pulmonary defects in caveolin-1 gene-disrupted mice. *Science* **293**, 2449–2452 (2001).
36. Müller, K., Zurbriggen, M. D. & Weber, W. Control of gene expression using a red- and far-red light-responsive bi-stable toggle switch. *Nat. Protoc.* **9**, 622–632 (2014).
37. Schindelin, J. *et al*. Fiji: an open-source platform for biological-image analysis. *Nat. Methods* **9**, 676–682 (2012).
38. Jacobs, J. L. & Dinman, J. D. Systematic analysis of bicistronic reporter assay data. *Nucleic Acids Res.* **32**, e160 (2004).

Acknowledgements

We thank the BIOSS toolbox imaging facility, especially Guillia Mizzon, for providing assistance for the use of the microscopes. We thank Laura Motta-Mena and Kevin Gardner for kindly providing the plasmids pGL4.23-C120-FLuc and pVP-EL222. This work was supported by funding from the Excellence Initiatives of the German Federal and State governments (DFG EXC-1028-CEPLAS, DFG EXC-294-BIOSS, DFG-SPP1926 and DFG-GSC-4-SGBM), Ministry of Culture and Science within the framework of the NRW Strategieprojekt BioSC (No. 313/323-400-00213) and the Human Frontiers Science Program (HFSP RGY0063/2017).

Author Contributions

J.B., P.G., A.D.-M., K.R., P.F., K.M. and E.C. performed research. R.E. and J.T. developed the mathematical model. W.W.A.S., S.M., J.A.D., J.T., W.W. and M.D.Z. planned the study, supervised research and/or discussed results. J.B., P.G., R.E., A.D.-M., K.R., W.W. and M.D.Z. wrote the manuscript.

Additional Information

Supplementary information accompanies this paper at https://doi.org/10.1038/s41598-018-32929-7.

Competing Interests: The authors declare no competing interests.

Publisher's note: Springer Nature remains neutral with regard to jurisdictional claims in published maps and institutional affiliations.

Supplementary Information

Dual-controlled optogenetic system for the rapid down-regulation of protein levels in mammalian cells

Julia Baaske[1,2#], Patrick Gonschorek[1,2,8,#], Raphael Engesser[2,3], Alazne Dominguez-Monedero[4], Katrin Raute[1,2,5], Patrick Fischbach[6], Konrad Müller[1,9], Elise Cachat[4], Wolfgang W.A. Schamel[1,2,7], Susana Minguet[1,2,7], Jamie A. Davies[4], Jens Timmer[2,3], Wilfried Weber[1,2*] and Matias D. Zurbriggen[6*]

[1] Faculty of Biology, University of Freiburg, Freiburg, Germany
[2] BIOSS - Centre for Biological Signalling Studies, University of Freiburg, Freiburg, Germany
[3] Institute of Physics, University of Freiburg, Freiburg, Germany
[4] Deanery of Biomedical Sciences, University of Edinburgh, Edinburgh, UK
[5] SGBM - Spemann Graduate School of Biology and Medicine, University of Freiburg, Freiburg, Germany
[6] Institute of Synthetic Biology, University of Düsseldorf and CEPLAS, Düsseldorf, Germany
[7] Center for Chronic Immunodeficiency, Medical Center, University of Freiburg, Faculty of Medicine, University of Freiburg, Freiburg, Germany.
* Corresponding author: Email: wilfried.weber@biologie.uni-freiburg.de or matias.zurbriggen@uni-duesseldorf.de

[#] Julia Baaske and Patrick Gonschorek contributed equally to this work

[8] Present address: Institute of Chemical Sciences and Engineering, School of Basic Sciences, Ecole Polytechnique Fédérale de Lausanne (EPFL), Lausanne CH-1015, Switzerland.

[9] Present address: Novartis Pharma AG, Basel CH-4002, Switzerland

Supplementary Information

Development and calibration of the mathematical model

In the following the mathematical model is derived and the calibration of the unknown model parameters by maximum likelihood estimation is described.

1. Derivation of the model equations

In order to quantitatively characterize the output of the blue OFF system we developed a mathematical model based on ordinary differential equations (ODE) describing the time evolution of the concentrations of the involved substances. Our system can be described as a biochemical reaction network. In the following we use mass action kinetics and enzyme kinetics to derive the model equations.

The system depends on the light induced conformational change of two proteins. On the one hand the protein degradation module B-LID is fused to FLuc. The resulting FLuc-B-LID is present in two conformations: $FLuc_{off}$ and $FLuc_{on}$. $FLuc_{off}$ is the present form in the dark with an inactive B-LID domain. It is translated from $FLuc_{mRNA}$ and degrades linearly with a constant rate. Under illumination with 460nm light $FLuc_{off}$ changes its conformation to $FLuc_{on}$ and is available for active degradation via the proteasome. The light induced conformational change is reversed with a constant dark reversion rate. FLuc is under the control of the P_{SV40} promoter, which produces $FLuc_{mRNA}$ at a constant rate. The FLuc protein is translated from the $FLuc_{mRNA}$ in the OFF state. This leads to the following scheme:

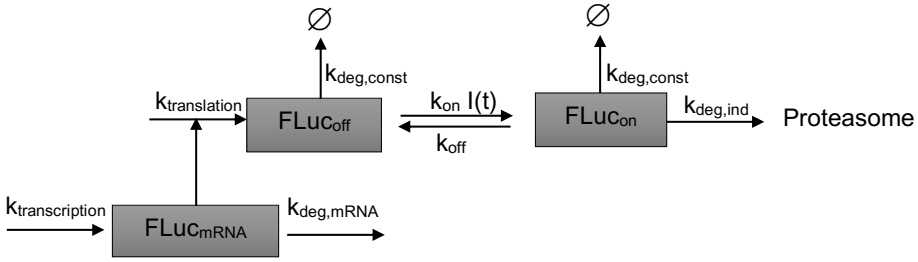

The time dependent intensity of the light is denoted with I(t). The second light-controlled process is a conformational change of the repressor KRAB-EL222. Activated KRAB-EL222 is able to bind to the $(C120)_5$ sequence and thus inhibiting the transcription of the $FLuc_{mRNA}$.

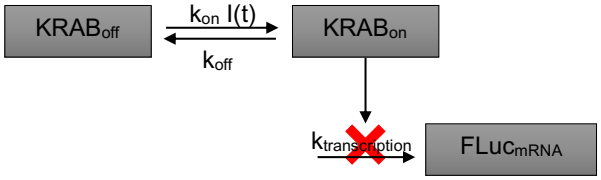

The light induced conformational changes and the dark revision rates are chosen to be the same for both processes since both use the light-oxygen-voltage (LOV) domain for sensing 460 nm light. The

total amount of EL222-KRAB is assumed to be in steady state since it is produced and degraded with a constant rate.
When translating these processes into mathematical equations using mass action kinetics and enzyme kinetics one obtains the following system of coupled and nonlinear ODEs:

(1) $\frac{d[FLuc_{off}](t)}{dt} = -k_{deg,const}[FLuc_{off}] + k_{translate}[FLuc_{mRNA}] - k_{on}I(t)[FLuc_{off}] + k_{off}[FLuc_{on}]$

(2) $\frac{d[FLuc_{on}](t)}{dt} = -k_{deg,const}[FLuc_{on}] - \frac{k_{deg,ind}[FLuc_{on}]}{K_{m,deg}+[FLuc_{on}]} + k_{on}I(t)[FLuc_{off}] - k_{off}[FLuc_{on}]$

(3) $\frac{d[KRAB_{off}](t)}{dt} = -k_{on}I(t)[KRAB_{off}] + k_{off}[KRAB_{on}]$

(4) $\frac{d[KRAB_{on}](t)}{dt} = +k_{on}I(t)[KRAB_{off}] - k_{off}[KRAB_{on}]$

(5) $\frac{d[FLuc_{mRNA}](t)}{dt} = \frac{k_{transcript}}{1+k_{inh,KRAB}[KRAB_{on}]^2} - k_{deg,mRNA}[FLuc_{mRNA}]$

The induced degradation via the proteasome in equation (2) is modelled with saturating Michaelis-Menten kinetics. The maximal degradation rate is $k_{deg,ind}$. For $FLuc_{on} = K_{m,deg}$ the half of the maximal degradation rate is reached. The repressor KRAB has multiple binding sites on the DNA. To capture cooperative binding effects we included an exponent of two in equation (5).

2. Estimation of the unknown model parameter by fitting to experimental data

2.1. Maximum likelihood approach

The mathematical model is calibrated with experimental data. To estimate the unknown model parameters, we used an approach based on the maximum likelihood. The equations (1)-(5) can be written in a vectorized form:

(6) $\frac{d}{dt}\boldsymbol{x}(t) = \boldsymbol{f}(\boldsymbol{x}, \boldsymbol{p}, \boldsymbol{u}(t))$

The vector with the internal states $\boldsymbol{x}(t) \epsilon \mathbb{R}^n$ contains the concentrations of the involved substances at the time point *t*. The function ***f*** is describing the reaction kinetics. The reactions are depending on model parameters ***p*** which are typically unknown. Additionaly, the system depends on a time dependent external input, i.e. the light intensity *I(t)*, that is described by the function ***u***(t). To obtain a unique solution of the system of ODEs one has to define an initial state $\boldsymbol{x}_0 = \boldsymbol{x}(0)$.

Usually the concentrations $\boldsymbol{x}(t)$ of the involved proteins cannot be measured directly. To map the internal states $\boldsymbol{x}(t)$ to the experimentally accessible observables $\boldsymbol{y}(t)$ we define the observation function $\boldsymbol{g}$:

(7) $y(t) = \boldsymbol{g}(\boldsymbol{x}(t), \boldsymbol{s}) + \boldsymbol{\varepsilon}(t)$

In our system, the observation parameters $\boldsymbol{s}$ are scaling parameters. $\boldsymbol{\varepsilon}(t)$ models the measurement error. A common error distribution for concentration measurements is the log-normal distribution[1]. The logarithm $\log(y_i)$ of log-normal distributed data y_i is normal distributed

(8) $\log(y_i) \sim N(\mu_j, \sigma^2)$

As error model, we assume the same variance σ^2 for all measured data points, which is estimated simultaneously with the dynamic parameters from the experimental data.
Assuming one single experiment with only one observable we can now calculate the probability of the measured data set $\boldsymbol{y}^D$ given a parameter vector $\theta = (\boldsymbol{p}, \boldsymbol{x_0}, \boldsymbol{s}, \sigma)$

(9) $L(\boldsymbol{y}^D, \boldsymbol{\theta}) = \prod_{j=i}^{N_D} \exp\left(\frac{\left(\log\left(y_j^D\right) - \log\left(g(\boldsymbol{x}(t_j), \boldsymbol{s})\right)\right)^2}{2\sigma^2}\right)$

N_D is the number of data points and t_j are the time points of measurement. When having multiple experiments with multiple observables the product of the single probabilities is giving the overall probability of the measured data

(10) $L(\boldsymbol{y}^D, \boldsymbol{\theta}) = \prod_i L_i(\boldsymbol{y}_i^D, \boldsymbol{\theta})$

$L(\boldsymbol{y}^D, \boldsymbol{\theta})$ seen as function of $\boldsymbol{\theta}$ for a given data set $\boldsymbol{y}^D$ is called likelihood function. With this, one can define the maximum likelihood estimator $\hat{\boldsymbol{\theta}}$ of the parameter set $\boldsymbol{\theta}$

(11) $\hat{\theta} = \arg\max_{\theta}(L(\boldsymbol{y}^D, \boldsymbol{\theta}))$

Instead of maximizing the likelihood *L* it is numerically advantageous to minimize

(12) $-2logL = \sum_{j=i}^{N^D}\left(\frac{\log(y_j^D) - \log\left(g(\boldsymbol{x}(t_j), \boldsymbol{s})\right)}{\sigma}\right)^2 + 2N_D \log\left(\sqrt{2\pi}\sigma\right) =: \chi^2_{mod}(\boldsymbol{\theta})$

This is just the sum of the weighted squared residuals in logarithmic space $\chi^2(\theta) = \sum_{j=i}^{N^D}\left(\frac{\log(y_j^D) - \log\left(g(\boldsymbol{x}(t_j), \boldsymbol{s})\right)}{\sigma}\right)$ with an additional term due to the error model. The optimal parameter set $\hat{\boldsymbol{\theta}}$ is then obtained by taking the minimum

(13) $\hat{\boldsymbol{\theta}} = arg\min_{\theta}(\chi^2_{mod}(\boldsymbol{\theta}))$

To assess parameter uncertainties in terms of confidence intervals one can calculate the profile likelihood[2] for each parameter θ_i

(14) $\chi^2_{PL}(\theta_i) = \min_{\theta_{i\neq j}} \chi^2_{mod}(\theta)$

The 95 % confidence interval can be calculated with

(15) $CI(\theta_i) = \{\boldsymbol{\theta} | \chi^2_{mod}(\boldsymbol{\theta}) - \chi^2_{mod}(\hat{\boldsymbol{\theta}}) < \chi^2(95\%, df = 1)\}$

where $\chi^2(95\%, df = 1)$ denotes the 95 %-quantile of a χ^2-distribution with one degree of freedom.

2.2. Scaling invariances and initial concentrations

In the following we describe the two experiments used for the calibration of the model and derive the used initial conditions.

Since EL222-KRAB is not measured, the absolute concentration of EL222-KRAB is not accessible by the model. Scaling the concentration of EL222-KRAB by a factor α can be compensated by transforming the parameters

$k_{inh,KRAB} \longrightarrow k_{inh,KRAB} \cdot \alpha^{-2}$

$\text{init\_KRAB}_{off} \longrightarrow \text{init\_KRAB}_{off} \cdot \alpha$

$\text{init\_KRAB}_{on} \longrightarrow \text{init\_KRAB}_{on} \cdot \alpha.$

The observations ***y(t)*** are invariant under these transformations. Since α is arbitrary we can set $\alpha = \text{init\_KRAB}^{-1}_{off}$ and therefore $\text{init\_KRAB}_{off} = 1$. The concentration of EL222-KRAB is then measured in multiples of the initial EL222-KRAB concentration in the OFF state.

The same argumentation is possible for the FLuc_{mRNA} therefore we can set $\text{init\_FLuc}_{mRNA} = 1$. In both experiments the cells were cultivated for 16 hours in the dark, therefore we assume that all KRAB and FLuc is in the OFF state at the start of the actual experiment. This leads to the initial concentrations:

$\text{FLuc}_{off}(0) = \text{init\_FLuc}$
$\text{FLuc}_{on}(0) = 0$
$\text{KRAB}_{off}(0) = 1$
$\text{KRAB}_{on}(0) = 0$
$\text{FLuc}_{mRNA}(0) = 1$

2.3. Implementation of the single experiments

Experiment 1: Kinetics

In this experiment the cells were cultivated for 16 hours in the dark and then illuminated with blue light with the intensity I(t) = 20 µmol m^{-2} s^{-1}. At 0, 2, 4 and 8 h after illumination the amount of FLuc was measured. As observation function, we used:

$$FLuc\_obs(t) = [FLuc_{on}](t) + [FLuc_{off}](t)$$

without a scaling factor. This means the concentration scale of FLuc is determined by this experiment.

The time course was measured for four different conditions:

(i) with the full dual-controlled system,
(ii) without light responsive KRAB,
(iii) without light responsive FLuc,
(iv) without any light responsive module.

Condition (i) is the full system as described in equation (1)-(5). To implement the conditions (ii)-(iv) following parameter transformations were used

(ii) $k_{inh,KRAB} = 0$,
(iii) $k_{deg,ind} = 0$,
(iv) $k_{inh,KRAB} = 0$ and $k_{deg,ind} = 0$.

Experiment 2: Light intensity dose response

In this experiment the system was incubated for 16 hours in the dark and then illuminated with different light intensities for 8 hours. The system was simulated for 8 hours for the different in the experiment applied light intensities. As observation function we used

$$FLuc\_obs(8\ h) = scale_{DR} \cdot ([FLuc_{on}](8\ h) + [FLuc_{off}](8\ h))$$

The experimental conditions were the same as in Experiment 1.

2.4. Fitting results

In total twelve parameters were fitted to the experimental data shown in Figure 3. The fitting and uncertainty analysis was performed with the Data2Dynamics framework[3].

The ODEs were simulated numerically with the CVODES integrator of the SUNDIALS suite[4]. As optimization algorithm to minimize $\chi^2_{mod}(\boldsymbol{\theta})$ we used a trust region algorithm implemented in the MATLAB function *lsqnonlin* with user supplied sensitivities[5].

The parameters were fitted on a logarithmic scale, this improves convergence since the parameter space is scanned over orders of magnitude and only positive parameter values are possible. To find the global optimum we performed 1000 optimization runs with randomly sampled initial parameter guesses. More than 98 % of these converged to the same lowest minimum (Supplementary Figure S3). This is a very strong indication that the global optimum was found. The parameter values of the

best fit are shown in Supplementary Table S1, the corresponding model curves describing the fitted data are shown in Figure 3. The shaded error bands are showing one standard deviation of the estimated error model, which assumes a normal error on the logarithmic scale.

The calculated likelihood profiles are shown in Supplementary Figure S4. The corresponding 95 % parameter confidence intervals are denoted in Supplementary Table S1. All parameters expect of k_{on} and k_{off} are identifiable. The light induced confirmation change k_{on} and the dark revision rate k_{off} are practical non-identifiable since the profile likelihood flattens out for high parameter values. This means, it is not possible to estimate an upper bound for the parameter values and the confirmation change can be arbitrarily fast. This result is in agreement with biological knowledge, since a confirmation change of a protein can happen within seconds and therefore on a much faster timescale than other cellular processes like gene expression (hours) or proteasome dependent protein degradation (minutes to hours). The profile likelihood can also be utilized to identify model reductions in order to obtain a fully identifiable model[6]. The analysis reveals that the ratio $K=k_{off}/k_{on}$ is identifiable. Hence, the model can be reduced by applying a steady state approximation for FLuc-B-LID and KRAB-EL222.

(16) $[FLuc_{on}](t) = I(t)K[FLuc_{off}](t)$

(17) $[KRAB_{on}](t) = I(t)K[KRAB_{off}](t)$

With this reduction the model becomes fully identifiable by the experimental data.

3. Model based description of the characteristics of the systems

With the calibrated mathematical model, it is possible to predict the performance of the system for different light intensities and durations of illumination. The heatmap in Figure 4a was obtained by simulating the calibrated system for the indicated light intensities and illumination durations and plotting the resulting reporter gene expression. This prediction can be seen as characterization of the system since it is possible to find experimental conditions to obtain a desired target gene expression.

To test the predictive power of the model, we measured the expression level of the reporter gene FLuc for different combinations of illumination duration and light intensity. Uncertainties in the parameter estimation are leading to uncertainties of the predictions. These prediction uncertainties can be calculated by evaluating the prediction profile likelihood for each prediction[7]. The resulting prediction profiles are shown in Supplementary Figure S5. The calculation was done with the doPPL plugin for the Data2dynamics software[8].

Supplementary Tables

Supplementary Table S1. Fitted parameter values obtained by the maximum likelihood estimation. σ^- and σ^+ are indicating the 95 % confidence interval obtained by the profile likelihood analysis. The corresponding likelihood profiles are shown in Supplementary Figure S4.

Parameter	**θ_{opt}**	**σ^-**	**σ^+**	**Unit**
$k_{deg,ind}$	1.226	0.8867	1.777	$h^{-1} \cdot$ RRE
$k_{deg,const}$	0.4248	0.2748	0.6692	h^{-1}
$K_{m,deg}$	0.1301	0.02259	0.2665	RRE
k_{on}	1.883	0.1286	+inf	$h^{-1} \cdot (\mu mol\ m^{-2}\ s^{-1})^{-1}$
k_{off}	22.75	0.8333	+inf	h^{-1}
$k_{translate}$	1.132	0.7497	1.724	$h^{-1} \cdot$ RRE $\cdot [FLuc_{mRNA}](0)^{-1}$
$k_{transcript}$	0.5428	0.3000	1.093	$h^{-1} \cdot [FLuc_{mRNA}](0)$
$k_{inh,KRAB}$	4.424	2.254	11.61	$[KRAB_{off}](0)^{-2}$
$k_{deg,mRNA}$	0.2539	0.1117	0.5233	h^{-1}
init_FLuc	1.010	0.9324	1.093	RRE
$scale_{DR}$	0.2196	0.2001	0.2410	1
sd_{FLuc}	0.07217	0.06493	0.08086	1

* RRE = relative reporter expression

Supplementary Table S2. Plasmids designed and used in this study.

If not indicated otherwise, all plasmids were cloned using AQUA[9]/ Gibson Cloning[10].

Plasmid	Description	Reference or source
pGL4.23-C120-FLuc	Vector encoding FLuc under the control of a minimal promoter with inserted C120.	[11]
pJB010	**P_{CMV}-CAV1-B-LID- IRES-GFP-pA** B-LID was amplified from pMZ1203 using oligos oMZ1214F/ oJB3-005R. The backbone pRR-CMV-CAV1-IRES-GFP was amplified in two fragments using primer pairs AmpF/ oJB3-006R and oJB3-007F/ AmpR. All 3 fragments were assembled using Gibson Cloning.	**this work**
pJB013	**P_{CMV}-KRAB-EL222- IRES-GFP-pA** KRAB-EL222 was amplified using oJB3-008F/ oJB3-009R from pKM565. The backbone pRR-CMV-CAV1-IRES-GFP was amplified without CAV1 in two fragments using primer pairs AmpF/ oJB3-010R and oJB3-011F/ AmpR. All 3 fragments were assembled using Gibson Cloning.	**this work**
pJB023	**P_{CMV}-$(C120)_5$-CAV1-B-LID-IRES-GFP-pA** $(C120)_5$ was amplified from pMZ1203 using oJB-064F/ oJB-058R. CAV1-B-LID was amplified from pJB010 using oJB-060F/ oJB-063R. Both fragments were fused in a PCR reaction using oligos oJB-064F/oJB-063R. The backbone pRR-CMV-CAV1-IRES-GFP was digested using BamHI/ XbaI. The C120-CAV1-B-LID fragment was assembled into digested backbone using Gibson Cloning.	**this work**
pJB036	**P_{SV40}-2x$(C120)_5$-FLuc-B-LID-pA** Amplifiy $(C120)_5$ sequence from pMZ1203 with additional SacI restriction site in overhang using oJB103/oJB104. Digest pMZ1203 and PCR product with SacI and ligate fragments.	**this work**
pJB037	**$P_{CMVtrunc}$-$(C120)_5$-FLuc-B-LID-pA** Amplify pMZ1203 with SV40 sequence using AmpF/oJB097 and oJB096/AmpR. Further amplify PCR product of oJB096/AmpR with oJB098/AmpR to completely add CMVtrunc sequence ([12]). Assemble fragments using Gibson cloning.	**this work**
pJB038	**P_{PGK}-$(C120)_5$-FLuc-B-LID-pA** Amplify PGK promoter sequence from pMSCVneo using	**this work**

	oJB099/oJB100. Amplify pMZ1203 without promoter sequence using AmpF/oJB101 and pJB102/AmpR. Assemble all fragments with Gibson cloning	
pJB039	**P_{SV40}-2x(C120)$_5$-FLuc-B-LID$_{\Delta RRRG}$-pA** Amplify pJB036 using AmpF/oMZ1253R and oMZ1252F/AmpR. Assemble fragments with Gibson cloning.	**this work**
pJB040	**$P_{CMVtrunc}$-(C120)$_5$-FLuc-B-LID$_{\Delta RRRG}$-pA** Amplify pJB037 using AmpF/oMZ1253R and oMZ1252F/AmpR. Assemble fragments with Gibson cloning.	**this work**
pJB041	**P_{PKG}-(C120)$_5$-FLuc-B-LID$_{\Delta RRRG}$-pA** Amplify pJB038 using AmpF/oMZ1253R and oMZ1252F/AmpR. Assemble fragments with Gibson cloning.	**this work**
pKM528	**$P_{EF1\alpha}$-NLS-EGFP-Med25VBD-B-LID-pA** Vector encoding PEF1a-controlled nuclear-localized EGFP-Med25VBD-B-LID	[13]
pKM565	**P_{SV40}-KRAB-EL222-pA** KRAB was amplified from pWW43 using oligos oKM455/oKM456, digested (NheI/EcoRI) and ligated (NheI/EcoRI) into pVP-EL222.	**this work**
pMSCVneo	Retroviral cloning vector containing PGK promoter.	Clontech
pMZ1203	**P_{SV40}-(C120)$_5$-FLuc-B-LID-pA** C120-FLuc was amplified from pGL4.23-C120-FLuc (oMZ1212F/oMZ1213R), B-LID was amplified from pKM528 (oMZ1214F/oMZ1215R) and both fragments were assembled into NotI and XbaI digested pMZ333.	**this work**
pMZ1210	**P_{SV40}-C120-FLuc-B-LID$_{\Delta RRRG}$-pA** Whole pMZ1203 except of the four amino acids RRRG was PCR amplified in two fragements using the two primer pairs (AmpF/oMZ1253R & oMZ1252F/AmpR) and assembled again.	**this work**
pMZ333	PSV40 driven mammalian expression vector derived from XbaI/NotI digested pSAM200 ([14]) .	[15]
pMZ-BLID-mCherry-2A-myrcasp8-ER(T2)	BLID-mCherry-2A-Myrcasp8-ER(T2) produced as gblocks (IDT) and inserted in pMZ1203 via gibson assembly	**this work**
pRR-CMV-CAV1-	**P_{CMV}-CAV1-IRES-EGFP**	[16]

IRES-GFP		
pTREX-BLID-mCherry-2A-myrcasp8-ER(T2)	BLID-mCherry-2A-myrcasp8-ER(T2) was PCR amplified (primers: pMZ-BLID F and pMZ-BLID R) and cloned into a pTREX backbone (primers: pTREX F and pTREX R) via gibson assembly	**this work**
pTREX-myrCasp8-ER(T2)-IRES-mCherry	myristoylated caspase 8 fused to the mutant ligand binding domain of the estrogen receptor (primers: attB1-myrCasp8 and attB2-ER(T2)) inserted into pTREx-DEST-IRES-mCherry through Gateway® recombination	[17]
pVP-EL222	**P_{SV40}-NLS-VP16-EL222-pA**	[11]
pWW43	**P_{SV40}-E-KRAB-pA**	[18]

Supplementary Table S3. Oligonucleotides designed and used in this study.

Primer	Sequence
AmpF	5' - GCTCCTTCGGTCCTCCGATCG - 3'
AmpR	5' - ACTTCTGACAACGATCGGAGGACC - 3'
oJB-058R	5' - CCCTCGGAGTCTACGTATTTGCCCCCAGACATGGTGGCTTTACCAACAGTACCG- 3'
oJB-060F	5' - ATGTCTGGGGGCAAATACGTAG- 3'
oJB-063R	5' - GAATTCGAAGCTTGAGCTCGAGGCCTGCAGGGATCCTTAGCCGCGGCGGCGGGCGGCCTCGTCGATG- 3'
oJB-064F	5' - GCTGTTTTGACCTCCATAGAAGACACCGACTCTAGAAGCTACCTGAGCTCGCTAGCCTCGAG- 3'
oJB-096	5' - CATTAGTTCATAGCCCATATATGGAGTTCCGCGTTACATAACTTACGGTAAATGGCCCGCCTGCCCTCG AGGAACTGGAAAACC- 3'
oJB-097	5' - ATTACTATTAATAACTAGTCAATAATCAATGTAGCTAGCTTATCGATGATAAGCTGTC- 3'
oJB-098	5' –ACATTGATTATTGACTAGTTATTAATAGTAATCAATTACGGGGTCATTAGTTCATAGCCCATATATGGAG TTC-3'
oJB-099	5' - TGTTTGACAGCTTATCATCGATAAGCTAGCTTGGGTAGGGGAGGCGCTTTTCC- 3'
oJB-100	5' - GTTAACTTTCTGGTTTTCCAGTTCCTCGAGGGCGAAAGGCCCGGAGATGAGGAAG- 3'
oJB-101	5' - AGCTAGCTTATCGATGATAAGCTGTC- 3'
oJB-102	5' - CCCTCGAGGAACTGGAAAACC- 3'
oJB-103	5' - GATCGAATTGCGGCCGC- 3'
oJB-104	5' - ATCGAGGAGCTCCTTCCATTATATACCCTCTAGTGTCTAAGC- 3'
oJB3-005R	5' - TTAGCCGCGGCGGCGGGCGGCCTCGTCGATG - 3'
oJB3-006R	5' - GTAGTAGCCAAAAAGGCGCCGGCGCCGCTAGCTATCTCTTTCTGCGTGCTGATGC - 3'
oJB3-007F	5' - CATCGACGAGGCCGCCCGCCGCCGCGGCTAAGGATCCCTGCAGGCCTC - 3'
oJB3-008F	5' - CTCCATAGAAGACACCGACTCTAGAAGCATGGATCCAAAAAAGAAGAGAAAGGTAGATCC - 3'
oJB3-009R	5' - GCTTGAGCTCGAGGCCTGCAGGGATCCTCAGATTCCGGCTTCGACGGC - 3'
oJB3-010R	5' - CATGCTTCTAGAGTCGGTGTCTTC - 3'
oJB3-011F	5' - TGAGGATCCCTGCAGGCC - 3'
oKM455	5' - TCCAGGCACATGCGTCCGCGTGCTAGCCCCACCATGGATCCAAAAAAGAAGAGAAAGGTAGATC - 3'
oKM456	5' - CAAGTCGAATTCCCAGAGATCATTCCTTGCCATTC - 3'
oMZ1212F	5' - TGTCTTTTATTTCAGGTCCCGGATCGAATTGCGGCCGCTACCTGAGCTCGCTAGCCTCGAG - 3'
oMZ1213R	5' - GTAGTAGCCAAAAAGGCGCCGGCGCCGCTAGCCACGGCGATCTTGCCGCC - 3'
oMZ1214F	5' - GCTAGCGGCGCCGGCGCC - 3'
oMZ1215R	5' - GGATCGAAGCTTGGGCTGCAGGTCGACTCTAGATTAGCCGCGGCGGCGG - 3'
oMZ1252F	5' - CATCGACGAGGCCGCCTAATCTAGAGTCGACCTGCAGCCC - 3'
oMZ1253R	5' - GGTCGACTCTAGATTAGGCGGCCTCGTCGATGTTC - 3'
pTREX F	5' - GCAGCCCAAGCTTCTACCCAGCTTTCTTGTACAAAGTGGTTGATGG- 3'
pTREX R	5' - TTCCAGTTCCTCGAGGGAAGCCTGCTTTTTTGTACAAACTTGTTGATGG- 3'
pMZ-BLID F	5' - TACAAAAAAGCAGGCTTCCCTCGAGGAACTGGAAAACC- 3'
pMZ-BLID R	5' - GCTGGGTAGAAGCTTGGGCTGCAGGTCGACTCTA- 3'
attB1-myrCasp8-	5' - GGGGACAAGTTTGTACAAAAAAGCAGGCTTCACCATGGGGAGTAGCAAGAGC- 3'
attB2-ER(T2)	5' - GGGGACCACTTTGTACAAGAAAGCTGGGTCTAAGCTGTGGCAGGGAAACC- 3'

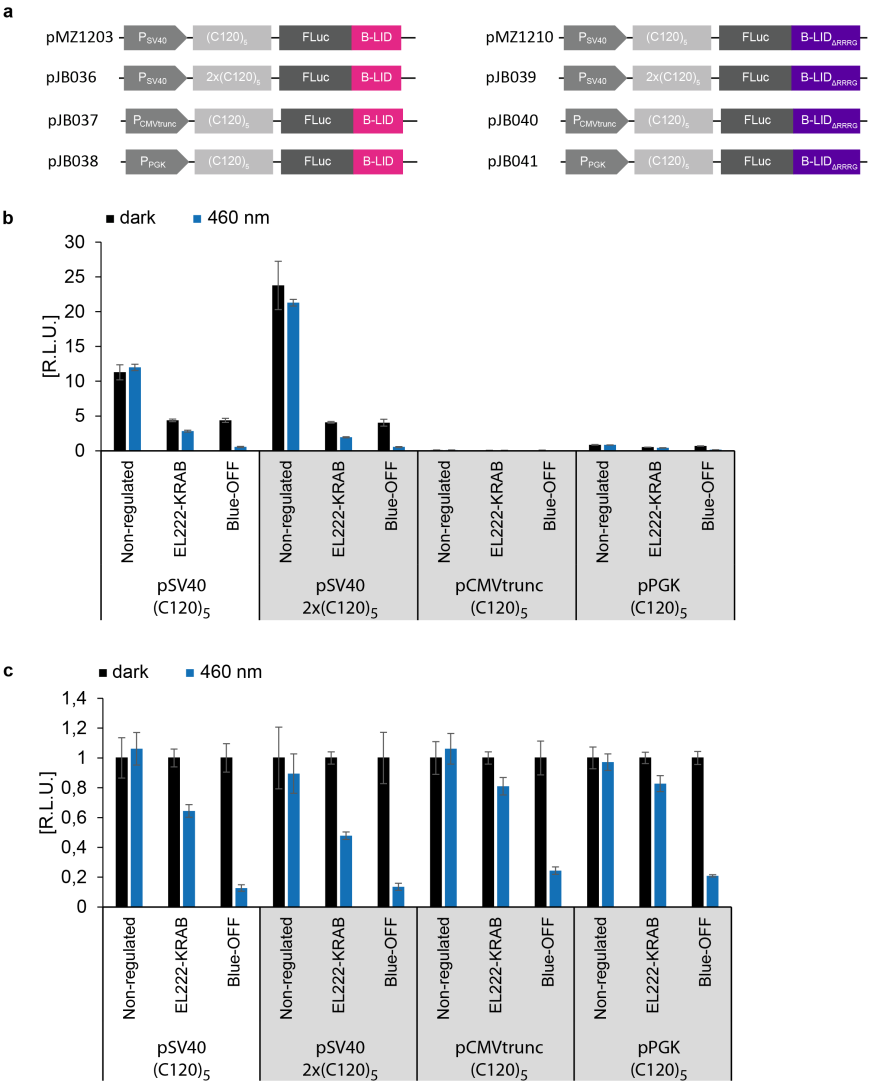

Supplement Figure S1. Evaluation of repression efficiency of a set of engineered EL222-KRAB/promoter modules as single and dual regulation systems (Blue-OFF). **(a)** Constructs of different variants of the promoter module of the reporter plasmids: i) system displayed in the main text containing a single EL222 binding sequence, $(C120)_5$ (pMZ1203 and pMZ1210) or ii) two repeats thereof, $2x(C120)_5$, downstream of a P_{SV40} promoter (pJB036 and pJB039); and two different promoter versions: iii) a truncated version of the pCMV, pCMVtrunc (pJB037 and pJB040), and iv) the phosphoglycerate kinase promoter, pPGK (pJB38 and pJB041). **(b)** and **(c)** Cells were transfected

with KRAB-EL222 (pKM565) and the respective reporter plasmids, kept for 16 hours in darkness after transfection and subsequently placed in darkness or 20 µmol m^{-2} s^{-1} 460 nm light for 8 h before lysis. **(b)** Firefly luciferase luminescence normalized to Renilla luciferase luminescence (relative luminescence units, R.L.U.). The 'non-regulated' samples have no blue light responsive repression or degradation module, i.e. pWW43 with either pMZ1210/pJB039/pJB040/pJB041. 'EL222-KRAB' depicts the EL222-KRAB module as single regulation system (pKM565 with either pMZ1210/pJB039/pJB040/pJB041), 'Blue-OFF' describes the complete dual system with both light-responsive modules: pKM565 (blue-light repression, EL222-KRAB) and either pMZ1203/pJB036/pJB037/pJB038 (blue-light degradation, B-LID). **(c)** blue light data from (b) normalized to dark controls. None of the engineered variants (grey shade) based on either two repeats of the EL222 binding site, a truncated version of the pCMV or the pPGK promoters showed improved performance in comparison to the promoter P_{SV40}-$(C120)_5$ which was used throughout the work.

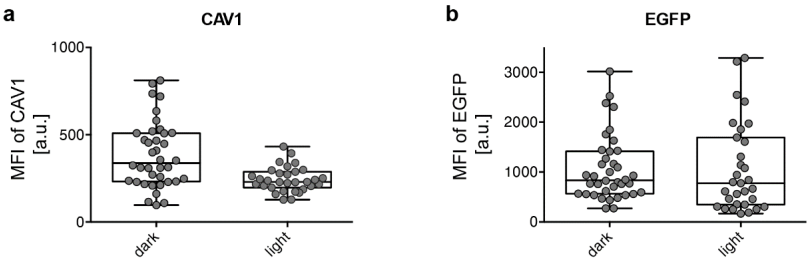

Supplement Figure S2. Statistical quantification of CAV1 downregulation in MEF cells **(a)** Mean fluorescent intensities (MFI) of CAV1 staining of transfected cells after 16 h in darkness (n= 38) or under 2 µmol m^{-2} s^{-1} of 460 nm light (n=31). Unpaired t-test shows significant difference (P = 0.0001) **(b)** Mean fluorescent intensities of GFP co-expression in analysed cells (P = 0.4752)

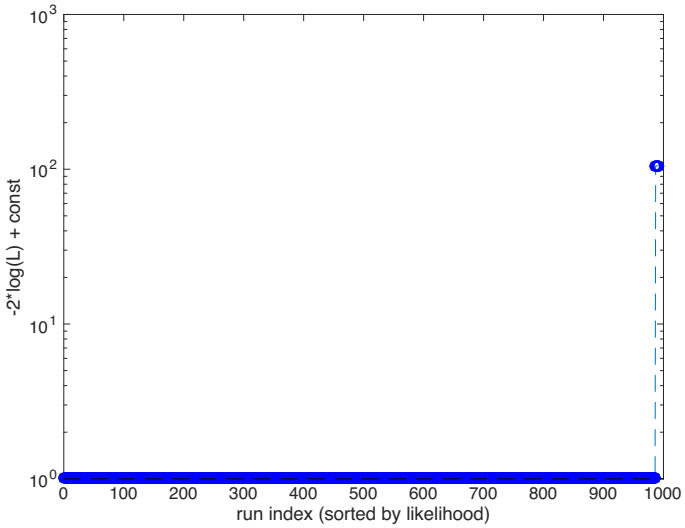

Supplement Figure S3. Multiple optimization runs with random initial parameter guesses sorted by their –2 log(L) value. The steps are indicating local minima. More than 98 % converged to the same optimum.

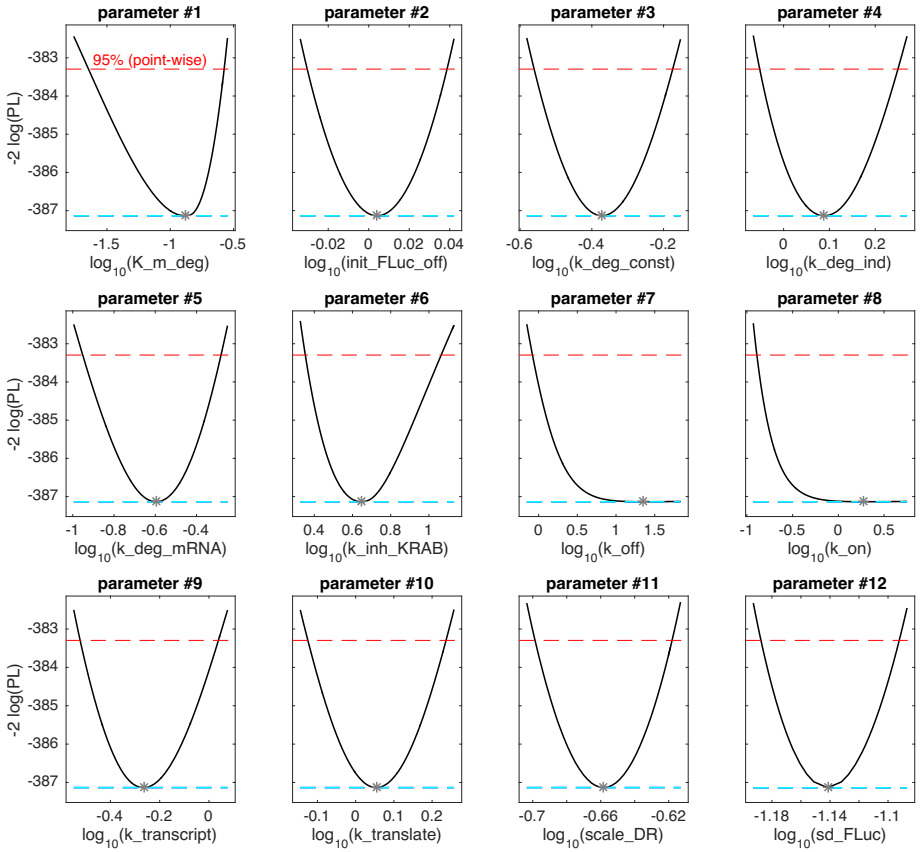

Supplement Figure S4. Profile likelihood of the estimated parameters. The solid lines indicate the profile likelihood; the optimal parameter set is marked with a grey star. The red dashed line marks the 95 % confidence level. The parameter axis is on a logarithmic scale.

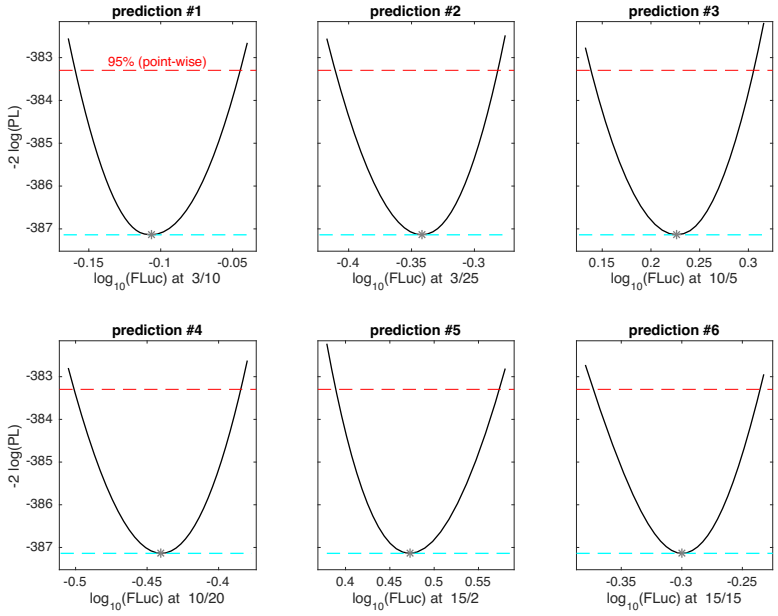

Supplement Figure S5. Prediction profile likelihood for the measured points in Figure 4. The solid lines indicate the prediction profile likelihood, the prediction for the optimal parameter set is marked with a grey star. The red dashed line marks the 95 % confidence level.

Supplementary References

[1] C. Kreutz, M. M. Bartolome Rodriguez, T. Maiwald, M. Seidl, H. E. Blum, L. Mohr, J. Timmer, *Bioinformatics* **2007**, *23*, 2747–2753.

[2] A. Raue, C. Kreutz, T. Maiwald, J. Bachmann, M. Schilling, U. Klingm??ller, J. Timmer, *Bioinformatics* **2009**, *25*, 1923–1929.

[3] A. Raue, B. Steiert, M. Schelker, C. Kreutz, T. Maiwald, H. Hass, J. Vanlier, C. Tönsing, L. Adlung, R. Engesser, et al., *Bioinformatics* **2015**, *31*, 3558–3560.

[4] A. C. Hindmarsh, P. N. Brown, K. E. Grant, S. L. Lee, R. Serban, D. E. Shumaker, C. S. Woodward, *ACM Trans. Math. Softw.* **2005**, *31*, 363–396.

[5] T. Coleman, Y. Li, *SIAM J. Optim.* **1996**, *6*, 418–445.

[6] T. Maiwald, H. Hass 1☯, B. Steiert 1☯, J. Vanlier, R. Engesser, A. Raue, F. Kipkeew, H. H. Bock, D. Kaschek, C. Kreutz, et al., **n.d.**, DOI 10.1371/journal.pone.0162366.

[7] C. Kreutz, A. Raue, J. Timmer, *BMC Syst. Biol.* **2012**, *6*, 120.

[8] H. Hass, C. Kreutz, J. Timmer, D. Kaschek, *Bioinformatics* **2016**, *32*, 1204–1210.

[9] H. M. Beyer, P. Gonschorek, S. L. Samodelov, M. Meier, W. Weber, M. D. Zurbriggen, *PLoS One* **2015**, *10*, e0137652.

[10] D. G. Gibson, L. Young, R.-Y. Chuang, J. C. Venter, C. A. Hutchison, H. O. Smith, C. A. H. Iii, N. America, *Nat. Methods* **2009**, *6*, 343–345.

[11] L. B. Motta-Mena, A. Reade, M. J. Mallory, S. Glantz, O. D. Weiner, K. W. Lynch, K. H. Gardner, *Nat. Chem. Biol.* **2014**, *10*, 196–202.

[12] S. Kainrath, M. Stadler, E. Reichhart, M. Distel, H. Janovjak, *Angew. Chemie Int. Ed.* **2017**, *56*, 4608–4611.

[13] K. Müller, M. D. Zurbriggen, W. Weber, *Biotechnol. Bioeng.* **2015**, *112*, 1483–1487.

[14] M. Fussenegger, S. Moser, X. Mazur, J. E. Bailey, *Biotechnol. Prog.* **1997**, *13*, 733–740.

[15] S. Juillot, H. M. Beyer, J. Madl, W. Weber, M. D. Zurbriggen, W. Römer, *Mol. BioSyst.* **2016**, *12*, 345–349.

[16] R. Strippoli, J. Loureiro, V. Moreno, I. Benedicto, M. L. Pérez Lozano, O. Barreiro, T. Pellinen, S. Minguet, M. Foronda, M. T. Osteso, et al., *EMBO Mol. Med.* **2014**, *7*, 102–123.

[17] E. Cachat, W. Liu, J. A. Davies, *Eng. Biol.* **2017**, 1–6.

[18] W. Weber, C. Fux, M. Daoud-el Baba, B. Keller, C. C. Weber, B. P. Kramer, C. Heinzen, D. Aubel, J. E. Bailey, M. Fussenegger, *Nat. Biotechnol.* **2002**, *20*, 901–907.

Optogenetic downregulation of protein levels to control programmed cell death in mammalian cells with a dual blue-light switch.

Patrick Fischbach[1], Patrick Gonschorek[2,3], Julia Baaske[2], Jamie A. Davies[4], Wilfried Weber[2,5], Matias D. Zurbriggen[1,6]

[1]Institute of Synthetic Biology, University of Düsseldorf, Germany

[2]Faculty of Biology, University of Freiburg, Germany

[3]Present address: Institute of Chemical Sciences and Engineering, School of Basic Sciences, Ecole Polytechnique Fédérale de Lausanne (EPFL), Lausanne, Switzerland

[4]Deanery of Biomedical Sciences, University of Edinburgh, Edinburgh, UK

[5]Signalling Research Centres BIOSS and CIBSS, University of Freiburg, Germany

[6]CEPLAS - Cluster of Excellence on Plant Sciences, Düsseldorf, Germany

[#]Corresponding author: MDZ matias.zurbriggen@uni-duesseldorf.de

Abstract:

Optogenetic approaches facilitate the study of signaling and metabolic pathways in animal cell systems. In the past 10 years, a plethora of light-regulated switches for the targeted control over the induction of gene expression, subcellular localization of proteins, membrane receptor activity, and other cellular processes have been developed and successfully implemented. However, only a few tools have been engineered towards the quantitative and spatio-temporally resolved downregulation of proteins. Here we present a protocol for reversible and rapid blue light-induced reduction of protein levels in mammalian cells. By implementing a dual-regulated optogenetic switch (Blue-OFF), both repression of gene expression and degradation of the target protein are triggered simultaneously. We apply this system for the blue light-mediated control of programmed cell death. HEK-293T cells are transfected with the pro-apoptotic proteins PUMA and BID integrated into the Blue-OFF system. Overexpression of these proteins leads to programmed cell death, which can be prevented by irradiation with blue light. This experimental approach is very straightforward, requires just simple hardware and therefore can be easily implemented in state-of-the art equipped mammalian cell culture labs. The system can be used for targeted cell signalling studies and biotechnological applications.

Key Words: Optogenetics; protein down-regulation; blue-light degron; blue-light gene repression; Blue-OFF; dual optogenetic switch; optogenetic apoptosis control.

1. Introduction:

The development of synthetic switches for the targeted manipulation of protein levels in animal cells has facilitated the study of signaling and metabolic pathways ***(1–6)***. A common approach is to control the expression or stability of a protein of interest with chemically-induced switches. These normally consist of engineered activators or repressors, the binding of which to synthetic promoters is regulated by the presence of a chemical. For protein degradation, chemically regulated degrons have been developed ***(7)***. However, chemically-based switches have limitations such as toxicity, irregular spatially controlled distribution by diffusion in cell culture or tissues, and limited reversibility ***(7–10)***. To overcome these limitations, light has begun to be used as an inducer, and numerous optogenetic switches have been developed recently ***(1, 2, 11)***. However, only a few are designed for the targeted downregulation or destabilization of a protein ***(11, 12)*** still leading to substantial residual protein levels due to constant protein neo-synthesis. Here, we present a protocol for the application of an optogenetic tool that combines blue light inducible repression of transcription and the simultaneous degradation of the target

protein in animal cells ***(13)***. We show its applicability to control apoptosis upon reduction of the levels of two pro-apoptotic proteins in mammalian cells.

Molecular layout and mechanism of the Blue-OFF system

The dual system designed for the simultaneous transcriptional repression and degradation of a protein of interest (POI) consists of two switches ***(13)***: i) the photosensitive transcription factor EL222 from *Erythrobacter litoralis* fused to the KRAB transrepressor domain ***(14–17)*** (pKM565) to inhibit transcription of the POI from a target promoter (Fig. 1); ii) the POI, in this case either the pro-apoptotic proteins PUMA or BID (pPF088, pPF092), fused to the B-LID module which mediates the proteasomal degradation upon illumination with blue-light ***(11)***. The B-LID module incorporates the LOV2 domain of *Avena sativa* phototropin I (*As*LOV2). It contains a Jα helix which is bound to the core domain of LOV2 in the dark, but unwinds after illumination with blue light exposing a C-terminally fused RRRG degron (Fig. 1). The pro-apoptotic proteins PUMA and BID are targets of the transcription factor p53 keeping the balance of cell cycle arrest and cell death upon DNA damage or other cell death insults ***(18–20)***. Overexpression of those proteins leads to cell death. In this work we show the applicability of the Blue-OFF system for the regulation of apoptosis by reducing the levels pro-apoptotic proteins constitutively expressed from a transfected plasmid in HEK293-T cells. The POI-B-LID module is cloned under the control of a synthetic promoter comprising five copies of the DNA target sequence of EL222-KRAB, namely $(C120)_5$, placed downstream of a constitutive promoter (Fig. 1). Upon illumination with 460 nm light, EL222-KRAB homodimerizes and binds via its helix-turn-helix (HTH) DNA-binding domains to the C120 sequences repressing

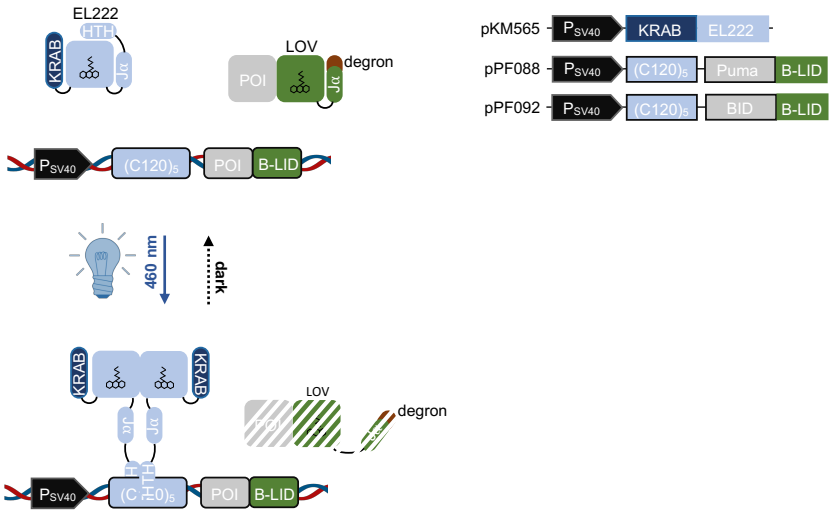

transcription. Simultaneously, the LOV2 domain of the B-LID module exposes the RRRG degron leading to degradation of the POI***(13)***.

Fig. 1. Molecular design and mode of function of the Blue-OFF system for blue light-regulated downregulation of the levels of a POI. The pro-apoptotic proteins Puma and BID are fused to the B-LID system, and placed under the control of a constitutive SV40 promoter (pPF088, pPF092). The promoter sequence is followed by five copies of the EL222-binding sequence ($C120_5$). The photosensory transcription factor EL222 is fused to the inhibitory KRAB domain (pKM565). In the dark, the KRAB-EL222 fusion is not bound to the target sequence on the DNA and the B-LID system is inactive leading to accumulation of the POI. Upon blue light illumination, the Jα helix unwinds, exposing the docked degradation peptide (RRRG) which leads to proteasome mediated protein degradation. Simultaneously, the EL222 transcription factor dimerizes and binds to the $C120_5$ sequence inhibiting transcription via the fused KRAB repressor domain. Adapted from Baaske *et al.*, 2018.

Application and experimental considerations

This dual-controlled optogenetic switch shows highly efficient and rapid blue-light induced down-regulation of protein expression and stability. These characteristics can be used to knock down essential genes in a cell, tissue or organism to study the effect of losing a given protein in an otherwise wild type context. We have previously shown a quantitative characterization of the system and its ability to control a synthetic caspase-based switch to induce programmed cell death ***(13)***. Here, we describe a protocol to demonstrate further the applicability of the system by regulating the levels of ectopically overexpressed pro-apoptotic proteins such as PUMA or BID**.**

Blue light illumination can have toxic effects on cells. However, the intensity- and time-doses needed for full activation of the Blue-OFF system (20 µmol m^{-2} s^{-1} for 8 h or 10 µmol m^{-2} s^{-1} for 24 h) have no negative effect on the cells ***(13)***. It is worth considering when designing an experiment that higher doses might have a negative influence on growth and health. The system represses transcriptional activity and targets the protein for degradation, however it has no effect over the mRNA, meaning that there might be remaining expression from previously synthesized messengers. An advantage of the Blue-OFF switch is that there is no need of extra addition of FMN, the chromophore of the LOV domains, to the growth media ***(21)***. As the photoreceptors are activated also by daylight or room light, all work should be done under green or red safe light.

Experimental design

In this protocol, HEK-293T cells are transfected with plasmids encoding the pro-apoptotic proteins PUMA and BID engineered into the Blue-OFF system (pPF088, pPF092, pKM565). As a negative control, the plasmids encoding for the pro-apoptotic proteins fused to B-LID without the RRRG degron (pMZ1427, pTB505) under the control of a constitutive promoter were transfected. The light treatments were performed in closed LED-boxes, with a wavelength of 460 nm and an intensity of 10 µmol m^{-2} s^{-1} for 24 h as described below. Control cells are kept in dark for the same incubation period. Transfections for microscopy are done in

duplicates. After 24 h of treatment, the cells can be directly observed under the microscope or be fixed for long-term storage.

2 Materials:

2.1 Reagents, consumables and kits

1) Plasmids (Fig. 1):
    a. pMZ1203: P_{SV40}-$C120_5$-Firefly-B-LID-pA
    b. pMZ1427: P_{SV40}-RFP-2A-Puma-B-LIDΔRRRG
    c. pTB505: P_{SV40}-RFP-2A-BID-B-LIDΔRRRG
    d. pPF088:P_{SV40}-$C120_5$-Puma-B-LID-pA
    e. pPF092: P_{SV40}-$C120_5$-BID-B-LID-pA
2) Top10 chemically competent cells (Life Technologies, cat.no.C4040-10)
3) M&N NucleoBond Xtra Midi Kit (M&N, cat no. 740410.10)
4) Ampicillin (Roth, cat.no. K029.2)
5) LB agar (Roth, cat.no. X969.3)
6) LB medium (Roth, cat.no. 6673.4)
7) HEK-293T cells (DSMZ, ACC-305)
8) DMEM (PAN Biotech, cat.no. P04-03550)
9) FBS (PAN Biotech, cat.no. P30-3602)
10) Penicillin-streptomycin (PAN Biotech, cat.no. P06-07100)
11) Trypsin-EDTA (PAN Biotech, cat.no. P10-023500)
12) CASY ton buffer (OLS, cat.no. 5651808)
13) Opti-MEM (Life Technologies, cat.no. 22600-134)
14) Polyethyleneimine (PEI) linear molecular weight (MW) 25 kDa (Polyscience, cat.no. 23966-1)
15) DMSO (Sigma, cat.no. D8418)
16) Filter bottle Top 500 mL 0.2 µM Membrane (VWR, cat no. 514-0340)
17) CASY cups (OLS, cat.no. 5651794)
18) Cell culture dishes (100 mm; Corning, cat.no. 430167)
19) Cell culture plates (24 well; Corning, cat.no. 3524)
20) Glass cover slides (VWR, cat.no. 631-0150)
21) Microscopy slides (VWR, cat.no. 631-1551)
22) Paraformaldehyde (PFA) (Alfa Aesar, cat.no. J61899)
23) PBS
24) Mowiol (Roth, cat.no. 0713)
25) Dabco (Roth, cat.no. 0718)

2.2 Reagent setup

2.2.1 Plasmid DNA preparation

Prepare LB agar plates by mixing LB agar (40 g/L) with H_2O according to manufacturer´s instructions and autoclave it. Add 100 µg ml^{-1} ampicillin (from a 100 mg ml^{-1} stock solution in H_2O, sterile filtered) to the cooled-down LB agar and pour it in 100 mm Petri dishes and let it solidify. The plates can be stored at 4°C for one month. Transform chemically competent *Escherichia coli* TOP10 cells according to Beyer et al., 2015a ***(22)*** and plate 10 and 50 µL on LB agar plates supplemented with ampicillin. Incubate at 37°C for 24 h. Inoculate 120 mL of autoclaved LB medium supplemented with 100 µg ml^{-1} ampicillin with a single colony by using a sterile pipette tip, and incubate at 37°C for 24 h at 150 rpm (Innova 44, New Brunswick). Centrifuge 100 mL of the overnight culture and isolate the DNA with the NucleoBond Xtra Midi kit according to the manufacturer´s instructions. Determine the DNA concentration with a spectrophotometer.

2.2.2 PEI solution (1 mg ml^{-1})

Dissolve 200 mg of PEI in 160 mL H_2O in a glass beaker and stir it. For faster dissolution heat it up to 50 °C. Adjust the pH to 7 with HCl until it is completely dissolved and fill in with ddH_2O to 200 mL. Filter the PEI solution through a 0.2-µm filter in a cell culture hood and divide it into 1 mL aliquots. The aliquots can be stored at -80 °C for at least one year.

2.2.3 PBS solution (10x)

Dissolve 26.82 mM KCl, 14.7 mM KH_2PO_4, 80.34 mM $Na_2HPO_4 \cdot 2H_2O$ and 1.37 M NaCl in 1 L ddH_2O. Dilute the PBS to 1x, sterile filter and aliquot it in 50 mL Falcon tubes.

2.2.4 Mowiol-DABCO-solution

Mix 6 g of glycerol with 2.4 g Mowiol in a 50 mL Falcon tube, incubate 30 min and mix it by vortexing every 10 min. Afterwards add 6 mL H_2O and stir it for 2 h. Add 12 mL Tris-HCl 0.2 M pH 8.5 and heat at 53 °C in a water bath until dissolution (approximately 2 h). Stir every 30 min with a magnetic stirring bar. Then, centrifuge the solution for 20 min at 5000 *g*, transfer the supernatant to a fresh tube and add 25 mg DABCO for each mL solution, and stir until complete dissolution. Prepare 500 µL aliquots and freeze them at -20 °C.

2.3 Equipment

1) Spectrophotometer (Eppendorf Biospectrometer basic cat no. 6135000904)
2) Tissue culture hood (Thermo Scientific, HeraSafe S2020 1.8 cat no. 104222784)
3) Tissue culture incubators (Thermo Scientific, HeraCell vios 250i)

4) CASY cell counter and analyzer (OLS, CasyTT, cat no. 5651736)
5) Spectroradiometer (Avatec, Avaspec-2048)
6) LED band deco Flex RGB plug and light set (Prisma Leuchten, cat.no. 2200-090P)
7) LED Boxes (LEDs: Roithner LED450-series)
8) Confocal microscope (Nikon Eclipse Ti + C2+ confocal upgrade)

2.4 Equipment setup

2.4.1 Safe-light

Stick the LED band to the internal surface/walls of the cell culture hood. The safe-light (green or red) can be turned on from the outside via remote control. If required, additional LED stripes can be installed all over the room. Cover all ambient light sources such as windows and/or doors with curtains or black adhesive vinyl foil to achieve full darkness.

2.4.2 LED boxes

LED boxes were constructed and used as described in Müller et al., 2014 and Ochoa-Fernandez et al., 2016 ***(8, 23)***. In brief, we use custom-made light boxes built out of PVC (20 cm x 20 cm 20 cm) and equipped with an LED panel. The light boxes are additionally equipped with fans for gas exchange. Irradiation wavelength and intensity control is achieved with an Arduino microcontroller installed in the aluminum LED panel with a USB port for programming irradiation time and pulsing. In this protocol, boxes containing blue LEDs (460 nm) were used.

3 Methods:

3.1 Seeding of HEK-293T cells • Estimated duration 1 h (mid-day or afternoon of day 1)

1.) Start with a HEK-293T 80-90% confluent cell culture in 100-mm petri-dishes with 10 mL DMEM supplemented with 10% (V/V) FBS and 1,4% (V/V) penicillin-streptomycin! **Critical step:** Healthy cells are essential (viability and morphology)! (*see* **Note 1**)
2.) For collecting the cells, remove the culture medium, add 2 mL of trypsin-EDTA solution and incubate at 37°C for 5 min.
3.) During the incubation time prepare a 15 mL tube with 8 mL fresh DMEM medium supplemented with 10% (vol/vol) FBS and 1,4% (vol/vol) penicillin-streptomycin (to get a final total volume of 10 mL). Cells of a maximum of 3 plates can be pooled in one tube to speed up the process. In this case use only 4 mL fresh DMEM medium.
4.) Wash away the cells from the plate by rinsing the trypsin-EDTA cell suspension 2 – 3 times, and pipet the suspension up and down to resuspend the cells. Transfer the cell suspension into the 15 mL tube with DMEM (prepared in step 3 above) and sediment

the cells by centrifugation (3 min, 300 *g*, RT). Discard the supernatant and resuspend the cells in 10 mL fresh DMEM supplemented with 10% (V/V) FBS and 1,4% (V/V) penicillin-streptomycin. Determine the cell concentration with the CASY cell counting system or with a Neubauer cell-counting chamber.

5.) Seed HEK-293T cells in 10 wells of each of two 24-well plates at a density of 40,000 – 50,000 cells per well in 500 µL DMEM supplemented with 10% (V/V) FBS and 1,4% (V/V) penicillin-streptomycin. Incubate the cells for 24 h at 37 °C with 5 % CO_2 in an incubator.

3.2 Transfection of HEK-293T cells • Estimated duration: 1,5 h in the morning and 30 min in the afternoon (day 2)

1) Inspect the seeded cells under the microscope. They should be uniformly and evenly distributed. The confluency should be *ca.* 30 – 50%.
2) For transfection, prepare a premix of DNA/PEI. For each well of a 24-well plate mix a total of 0.75 µg of plasmid DNA in 50 µL of Opti-MEM, and 2.5 µL of 1 mg ml^{-1} PEI solution in 50 µL of Opti-MEM.
   Therefore, 5 different DNA mixes need to be prepared in Opti-MEM in a total volume of 250 µLas follows (*see* **Note 2**):
   1. Mix 1: (the negative control) pMZ1203 = 1.875 and pKM565 = 1.875 µg.
   2. Mix 2: (Blue-OFF controlled Puma) pPF088 = 1.875 µg and pKM565 = 1.875 µg.
   3. Mix 3: (Blue-OFF controlled BID) pPF092 = 1.875 µg and pKM565 = 1.875 µ.
   4. Mix 4: (unregulated Puma) pMZ1427 = 3.75 µg.
   5. Mix 5: (unregulated BID) pTB505 = 3.75 µg.
3) In an additional 15 mL tube, prepare the PEI mix as follows: add 96 µL of 1 mg ml^{-1} PEI solution to 1,829 µL Opti-MEM (Calculate a 10% excess, in case of pipetting deviation/mistakes).
4) To produce the DNA-PEI complexes, add 250 µL of the PEI mix in two separate steps to the DNA mixes 1 – 5, and mix the tubes by vortexing for 10 s after each addition of the PEI mix. Incubate the tubes at RT for 10 min.
5) Add 100 µL of the transfection mix dropwise to each well of the plate seeded in 3.1. step 5. Transfect with each transfection mix 2 wells on the 24-well plate that will be kept in darkness (as control), and 2 wells on the 24-well plate that will be illuminated. Finally, distribute the added transfection mix evenly by gently moving the plates in '8-shape- or up-down/left-right movements', and then incubate them in a CO_2 incubator at 37°C, 5% CO_2.

6) Four to five hours after transfection, replace the culture medium carefully in both 24-well plates with 0.5 mL of prewarmed DMEM supplemented with 10% (V/V) FBS and 1,4% (V/V) penicillin-streptomycin per well (*see* **Note 3**).
! Critical Step: Incubation with PEI for more than five hours might lead to decreased cell viability. **IMPORTANT: From now on every step should be carried out in the absence of blue/room light, i.e. 'darkness'. Use green (530 nm) or red (660 nm) safe-light to avoid activation of the system.** Illuminate one 24-well plate directly after changing the medium with 460 nm light with 10 µmol m^{-2} s^{-1} intensity and keep the other plate in 'darkness' for 16 h at 5% CO_2 and 37°C (*see* **Note 4**).

3.3 Fixating cells for long term storage • Estimated duration: 1 h (day 3)

1.) After illumination aspirate the medium of the wells with the transfected cells. Wash the cells once with 500 µL PBS and add 200 µL PFA (**!** TOXIC, check manufacturer´s guidelines for proper handling) (*see* **Note 5**).
2.) Incubate the cells covered with PFA for 10 min on ice, and additional 10 min at RT.
3.) Remove the PFA (use a waste tube and dispose it according to the toxic waste handling guidelines of your lab).
4.) Add 500 µL PBS. The cells are now fixated and the following steps can be carried in normal room light.
5.) Prepare microscopy slides and add 8 µL Mowiol/Dabco to the microscopy slide.
6.) Use forceps to transfer the glass slides (remove carefully the excess liquid from the glass slide with a tissue paper) with cells upside down on the Mowiol/Dabco droplet on the microscopy slide. After 30 min incubation at 37 °C the slides can be stored for more than one month at 4°C (*see* **Note 6**).

3.4 Analysis of apoptosis • Estimated duration: 0,5 h (day 3)

1) Check for cell growth under the microscope. Observe the formation of a confluent monolayer (if it does form).
2) Perform quantification and statistics accordingly/as needed.

3.5 Optional! Quantitative monitoring of rapid downregulation of protein level. To analyze the rapid downregulation of protein levels in a quantitative manner, one can use reporter genes, e.g. luciferases, phosphatases or fluorophores, instead of pro-apoptotic proteins ***(13)***.

4 Blue light-control over programmed cell death by regulating the levels of pro-apoptotic proteins

The above-described protocol was implemented for the optogenetic regulation of programmed cell death via the control of the levels of pro-apoptotic proteins. HEK-293T cells were transfected with the Blue-OFF optogenetic switch engineered to control PUMA or BID. Incubation of the cells in the dark led to a high cell death rate, in contrast to control cells transfected with pMZ1203 (Blue-OFF controlling FLuc) which formed a uniform monolayer (Fig. 2). Cells transfected with the systems showed as expected a higher survival rate (uniform monolayer) when illuminated with blue light. The results open up novel perspectives for the targeted regulation of programmed cell death in animal cells with applications in fundamental research such as the study of apoptotic and carcinogenic cellular mechanisms ***(24, 25)***. Additionally, the high spatiotemporal resolution of the system might be of advantage for the establishment of cellular patterns in tissue engineering approaches.

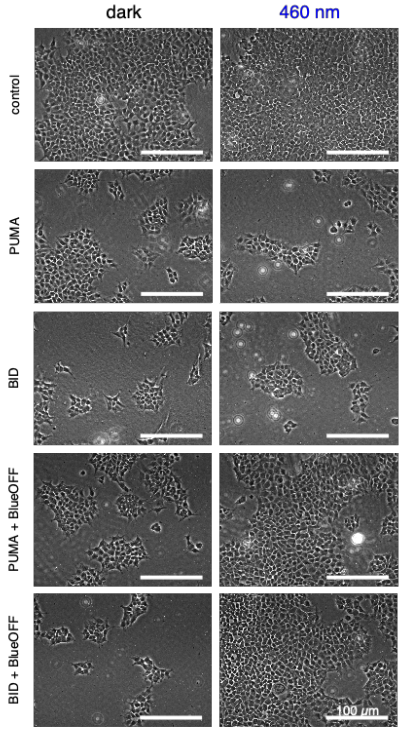

Fig. 2. Control of programmed cell death. Representative results of HEK-293T cells transfected with control (pMZ1203) forming a uniform monolayer in darkness and under blue illumination. Constitutive expression of PUMA or BID (pMZ1427; pTB505) in darkness and blue light, and of PUMA-Blue-OFF and BID-Blue-OFF (pPF088 + pKM565; pPF092 + pKM565) in darkness leads to increased cell death. In contrast to this, cells transfected with PUMA-Blue-OFF or BID-Blue-OFF show a higher survival rate, observed as a uniform monolayer, upon blue light illumination.

Notes

1. Healthy cells are essential (viability and morphology)! Low cell viability leads to low expression levels. Ideally cells should be neither too young (passage number < 5) nor too old (passage number > 30) for best expression results.

2. For high transfection efficiencies it is recommended to use RNA-free, super-coiled DNA. For best results we use the NucleoBond Xtra MIDI Kit for DNA-preparations.

3. Incubation with PEI for more than five hours might lead to decreased cell viability. However, very short incubation times with PEI decrease transfection efficiency. Additionally, the PEI solution has to be kept at pH=7, this is essential for high transfection efficiency.

4. The system is very light-sensitive. After transfection, every step should be carried out in the absence of blue/room light, i.e. always in 'darkness'. Use green (530 nm) or red (660 nm) safe-light to avoid activation of the system.

5. PFA is toxic! All work with PFA should be performed following the manufacturer´s guidelines for proper handling. Use gloves and dispose of the liquid waste and all consumables/material which had contact with PFA under the toxic waste instructions of your institute.

6. Fixed cells can be stored for at least one month at 4°C. Expressed fluorescent proteins are still detectable with a fluorescence microscope.

Acknowledgments

We thank J. Andres, L. Koch and T. Blomeier for experimental support and fruitful discussions, and R. Wurm, M. Gerads and J. Müller for valuable experimental support. This work was supported by the German Research Foundation (DFG) (grant ZU259/2-1 to MDZ and under Germany´s Excellence Strategy CEPLAS – EXC-2048/1 – Project ID 390686111 to MDZ, BIOSS – EXC-294 and CIBSS – EXC-2189 – Project ID 390939984 to WW) and the European Commission – Research Executive Agency (H2020 Future and Emerging Technologies (FET-Open) Project ID 801041 CyGenTiG to JAD and MDZ).

Author Contributions

PF designed the system and performed the experiments, analyzed the data and wrote the protocol. PG and JB designed the system. JD designed experiments and analyzed the data.

WW designed the system and experiments, and analyzed the data. MDZ designed the system and experiments, analyzed the data and wrote the protocol.

References:

1. Wend S, Wagner HJ, Müller K, et al (2014) Optogenetic Control of Protein Kinase Activity in Mammalian Cells. ACS Synth Biol 3:280–285
2. Beyer HM, Juillot S, Herbst K, et al (2015) Red Light-Regulated Reversible Nuclear Localization of Proteins in Mammalian Cells and Zebrafish. ACS Synth Biol 4:951–958
3. Toettcher JE, Gong D, Lim WA, et al (2011) Light-based feedback for controlling intracellular signaling dynamics. Nat Methods 8:837–9
4. Levskaya A, Weiner OD, Lim WA, et al (2009) Spatiotemporal control of cell signalling using a light-switchable protein interaction. Nature 461:997–1001
5. Andres J, Blomeier T, and Zurbriggen MD (2019) Synthetic Switches and Regulatory Circuits in Plants. Plant Physiol 179:862–884
6. Kolar K, Knobloch C, Stork H, et al (2018) OptoBase: A Web Platform for Molecular Optogenetics. ACS Synth Biol 7:1825–1828
7. Bonger KM, Chen L, Liu CW, et al (2011) Small-molecule displacement of a cryptic degron causes conditional protein degradation. Nat Chem Biol 7:531–537
8. Müller K, Zurbriggen MD, and Weber W (2014) Control of gene expression using a red- and far-red light–responsive bi-stable toggle switch. Nat Protoc 9:622–632
9. Frey AD, Rimann M, Bailey JE, et al (2001) Novel pristinamycin-responsive expression systems for plant cells. Biotechnol Bioeng 74:154–63
10. Gossen M and Bujard H (1992) Tight control of gene expression in mammalian cells by tetracycline-responsive promoters. Proc Natl Acad Sci 89:5547–5551
11. Bonger KM, Rakhit R, Payumo AY, et al (2014) General Method for Regulating Protein Stability with Light. ACS Chem Biol 9:111–115
12. Pathak GP, Spiltoir JI, Höglund C, et al (2017) Bidirectional approaches for optogenetic regulation of gene expression in mammalian cells using Arabidopsis cryptochrome 2. Nucleic Acids Res 45:e167–e167
13. Baaske J, Gonschorek P, Engesser R, et al (2018) Dual-controlled optogenetic system for the rapid down-regulation of protein levels in mammalian cells. Sci Rep 8:15024
14. Nash AI, McNulty R, Shillito ME, et al (2011) Structural basis of photosensitivity in a bacterial light-oxygen-voltage/helix-turn-helix (LOV-HTH) DNA-binding protein. Proc Natl Acad Sci 108:9449–9454
15. Rivera-Cancel G, Motta-Mena LB, and Gardner KH (2012) Identification of Natural and Artificial DNA Substrates for Light-Activated LOV–HTH Transcription Factor EL222. Biochemistry 51:10024–10034
16. Moosmann P, Georgiev O, Thiesen HJ, et al (1997) Silencing of RNA polymerases II and III-dependent transcription by the KRAB protein domain of KOX1, a Krüppel-type

zinc finger factor. Biol Chem 378:669–77

17. Motta-Mena LB, Reade A, Mallory MJ, et al (2014) An optogenetic gene expression system with rapid activation and deactivation kinetics. Nat Chem Biol 10:196–202
18. Nakano K and Vousden KH (2001) PUMA, a novel proapoptotic gene, is induced by p53. Mol Cell 7:683–94
19. Sax JK, Fei P, Murphy ME, et al (2002) BID regulation by p53 contributes to chemosensitivity. Nat Cell Biol 4:842–849
20. Deng J (2017) How to unleash mitochondrial apoptotic blockades to kill cancers? Acta Pharm Sin B 7:18–26
21. Müller K, Engesser R, Metzger S, et al (2013) A red/far-red light-responsive bi-stable toggle switch to control gene expression in mammalian cells. Nucleic Acids Res 41:e77–e77
22. Beyer HM, Gonschorek P, Samodelov SL, et al (2015) AQUA Cloning: A Versatile and Simple Enzyme-Free Cloning Approach. PLoS One 10:e0137652
23. Ochoa-Fernandez R, Samodelov SL, Brandl SM, et al (2016) Optogenetics in Plants: Red/Far-Red Light Control of Gene Expression, In: Methods in molecular biology (Clifton, N.J.), pp. 125–139
24. Lee JH, Soung YH, Lee JW, et al (2004) Inactivating mutation of the pro-apoptotic geneBID in gastric cancer. J Pathol 202:439–445
25. Giotopoulou N, Valiakou V, Papanikolaou V, et al (2015) Ras suppressor-1 promotes apoptosis in breast cancer cells by inhibiting PINCH-1 and activating p53-upregulated-modulator of apoptosis (PUMA); verification from metastatic breast cancer human samples. Clin Exp Metastasis 32:255–265

Fast and reversible blue light activated CRISPR/Cas13b mediated mRNA knockout (BLACKout)

Patrick Fischbach[1], Tim Blomeier[1], Matias D. Zurbriggen[1]*

[1]Institute of Synthetic Biology, University of Düsseldorf and CEPLAS, Düsseldorf, Germany

*Corresponding author: Email: matias.zurbriggen@uni-duesseldorf.de

ORCID: PF: 0000-0002-2781-5264; TB: ; MDZ:

Abstract (201 words)

The CRISPR/Cas toolbox offers a lot of efficient tools for genomic modifications, gene control or recently also regulation of mRNA. Especially, the regulation of mRNA levels is mostly based on inducible RNAi or CRISPR/Cas systems which are efficient but not reversible and with a low spatiotemporal resolution. Optogenetic control of a CRISPR/Cas system resulting in regulation of mRNA levels are still missing. Here, we present a novel blue light activated, CRISPR/Cas13b mediated mRNA knock-out (BLACKout) which allows a blue-light induced decrease of mRNA levels in a reversible and with high spatiotemporal precision. The BLACKout system combines the blue-light inducible split transcription factor system, based on a LOV2 domain and an ePDZ domain, with the recently published type VI Cas-effector enzyme Cas13b. This approach shows an advancement of mRNA regulation and temporary protein knock-down and novel application possibilities in fundamental research and splicing variants analysis. This system, as a supportive tool of the recently published Blue-Off, works synergistically with other optogenetic tools, which results in a complete knock-out of the protein of interest. Additionally, the system can knock down endogenous mRNAs which opens completely new perspectives in studying essential genes and cancer research.

Introduction (628 words)

Common approaches to control and regulate RNA levels are often based on the interference of translation of mRNA by RNA interference (RNAi), CRISPR/Cas9 mediated interference or knock-down on miRNAs as well as mRNA [1,2]. In contrast to RNAi, CRISPR/Cas9 systems showed more extensively applications. In addition to RNA and DNA interference as well as knock-down, transcriptional regulation and *in vivo* applicability, CRISPR/Cas9 has the feature for direct genome editing with a high specificity [3,4]. However, spatiotemporal resolution and reversibility are big limitations of those tools. Clustered regularly interspaced short palindromic repeats (CRISPR) – Cas9 system introduces advances in synthetic biology, gene therapy and gene modification in almost every model organism. Together with a specific single guide RNA (sgRNA) the CRISPR-Cas9 system is able to cleave double stranded DNA by inducing a double strand break. This CRISPR-Cas9 systems require a short protospacer adjacent motif (PAM) [5]. Over the last years, a lot of different Cas-variants from different microorganisms were identified to overcome limitations like the size for *in vivo* applications, or recognition of RNA instead of DNA [6,7]. Moreover, those CRISPR/Cas9 system were optimized for usage as an inducible split variant or in a light dependent manner for a higher spatiotemporal control of gene expression or double stranded

DNA cleavage [8,9]. CRISPR proteins capable of engaging with RNA in a RNA-dependent manner – known as Cas13 effectors – have also been discovered and optimized as tools [5]. Those engineered type VI CRISPR effectors can be used to efficiently knock down endogenous RNAs in human cells and manipulate alternative splicing [10,11]. Additionally, fusion proteins of type VI catalytically inactive PspCas13 with an adenosine deaminase showed a functional RNA guided RNA editing by replacing an adenosine by inosine (REPAIR) [11]. In contrast to the default CRISPR-Cas9 systems, those Cas13 effectors do not need a PAM sequence at the editing site [11]. Nevertheless, until now there are quite a few light dependent RNA cleavage or modification tools known [12]. Especially, tools to control mRNA level or mRNA editing directly with a high spatiotemporal resolution in reversible manner are still missing. For this purpose, we constructed an optogenetic tool to control mRNA level, based on the blue-light inducible split transcription factor system and the *Prevotella sp.* derived Cas13b effector (PspCas13b) [11,13]. The blue light activated Cas13b induced mRNA knockout (BLACKout) system consists of the *Avena sativa* LOV2 domain fused to Gal4 DNA binding domain and an ePDZ domain fused to a virus-derived transactivator VP16. Additionally, on another construct PspCas13b is downstream of a synthetic minimal CMV promoter. Upstream of this minimal promoter the GAL4 target sequence is inserted. Upon blue light illumination, the Jα helix of the LOV2 domain unwinds, exposes the hidden tag which leads to an interaction with the ePDZ domain. Due to this interaction, the transactivator is in close proximity to the minimal promoter and recruit´s transcriptional machinery. With this blue-light system we control the expression of PspCas13b which allows us indirectly to regulate mRNA levels with high spatiotemporal resolution by cleaving them via a customizable gRNA. Furthermore, we combined this tool with the recently published Blue-Off system to get an even higher reversible blue light induced knock down of our gene of interest [14]. As proof of principle, we demonstrated the quantitative cleavage of a reporter gene and an additional knockdown of GFP in mammalian cells. Furthermore, we showed a blue light induced G2 cell cycle arrest by knocking down endogenous CDK1. All together this is a novel upgrade for the optogenetic toolbox.

Results (1206 words)

Design of light inducible RNA guided mRNA cleavage

The inducible Cas13b vector was constructed by cloning PspCas13b [11] downstream of five repeats of GAL4 UAS and fused to a NES sequence (pTBPF001). As light inducible split transcription factor system we chose the *Avena sativa* LOV2-ePDZ system [13]. For the RNA guidance two different gRNAs were designed as described in [11,15]. All gRNAs were cloned into an U6 promoter-driven mammalian expression vector [11] (pTBPF002; pTBPF003). To assay the functionality of the system, firefly luciferase (FLuc) was constitutively expressed under the control of the SV40 promoter (pTBPF015) (Fig1a). We first characterized the functionality of the gRNAs with constitutive expressed PspCas13b (pC0046) (Fig.1b). The indicated plasmids were transfected in HEK-293T cells in a 1:1:1 or 1:1:1:1 (w:w:w:w) ratio and incubated 24 h in dark. Afterwards, the cells were illuminated for 24 h with 10 µmol m^{-2} s^{-1} of 460 nm light. As a transfection and expression control constitutive expressed FLuc was transfected alone. Cells transfected with constitutive PspCas13b and the designed gRNAs showed less than 10 % or 50 % expression compared to the constitutive control (Fig.1b) indicating the functionality of the gRNAs. To test for an additive effect of the gRNAs, we transfected HEK-293T cells with both designed gRNAs and

constitutively expressed Cas13b but an additive effect failed to appear (Fig.1b). Cells transfected with the BLACKout system showed decreased expression down to 21.2 % with gRNA1 and 19.3 % expression with gRNA2 after 24 h illumination with 10 µmol m^{-2} s^{-1} 460 nm light compared to the cells kept in dark (Fig.1c). Since already translated protein and expression of mRNA is still on going, the decrease of expression due to mRNA cleavage suggests to be highly efficient.

To show the applicability on other reporters, BLACKout was used to knock down PGK-driven eGFP expression. Therefore, HEK-293T cells were transfected with PGK-eGFP (pTBPF018) and additionally for normalization of transfection and expression, SV40-mCherry (pTBPF014). As described above, two different gRNAs against eGFP were designed, tested and demonstrated high functionality against eGFP with no off-target behavior for mCherry (Fig. S1). To demonstrate the blue-light induced eGFP knockdown cells were transfected with the BLACKout system and illuminated for 48 h with 10 µmol m^{-2} s^{-1} of 460 nm. As expected, cells transfected with the BLACKout system and kept in darkness showed high expression of eGFP (Fig.2b). Cells illuminated with blue light showed highly decreased eGFP expression with both designed gRNAs (Fig.2).

Following all these results we characterized the reversibility, kinetics of cleavage and the dose response to get better insights into the system. Therefore, cells transfected with the BLACKout system and constitutively expressed FLuc were kept in dark for 24 h and followed by 0, 2, 4 ,8 or 24 h illumination with 10 µmol m^{-2} s^{-1} and 460 nm to analyze FLuc activity (Fig.3a). As expected, the control cells showed firefly reporter accumulation. Also, cells transfected with the BLACKout system and gRNA1 showed within the first 2 h accumulation of firefly before a decrease in protein level was observable (Fig.3a). This delay is likely the result of the needed time for transcription and translation of Cas13b which takes place beforehand of the cleavage. Anyway, after the delay the protein level decreased down to 80 % with gRNA1 and 80 % with gRNA2 (Fig.3a). For dose response experiments, cells were incubated 24 h in dark followed by 24 h illumination with 0, 2.5, 5, 10, 15, 20 µmol m^{-2} s^{-1} and 460 nm. As expected, increasing light intensities resulted in higher decrease of FLuc expression with each of the gRNAs (Fig.3b) showing the sensitivity of the system and demonstrating the needed blue-light intensity of 10 µmol m^{-2} s^{-1} to reach the maximum degradation of mRNA (Fig.3b). To validate the reversibility of the system, HEK-293T cells were transfected with the BLACKout system and kept in darkness for 16 h, followed by a cycle of 12 h blue light (10 µmol m^{-2} s^{-1}) and again 40 h in darkness. Cells illuminated for 12 h showed decreased FLuc expression down to 60 % compared to expression levels after 16 h in darkness. The recovering of expression of FLuc after the second period in darkness demonstrated the reversibility of the system in darkness (Fig.3c). Taken all together, these results demonstrate that the BLACKout system is able to down-regulate the expression of a protein of interest via a customizable gRNA in a rapid light dependent manner.

Complete blue light induced protein knock-down by combining BLACKout with the Blue-Off system

The recently published dual-controlled optogenetic system for down-regulation of protein levels showed a blue-light decreased protein level down to 10 % in HEK-293T cells [14]. The left 10 % are likely still

transcribed mRNAs which are resulting in protein expression. To demonstrate the functionality also in combination with other optogenetic tools, the both systems were combined to reach a complete light-induced protein knockout. Therefore, the Blue-Off system together with the BLACKout system were transfected into HEK-293T cells and incubated for 24 h in dark, followed by 24 h illumination with 10 µmol m^{-2} s^{-1} and 460 nm. As expected, blue light illumination resulted in more than 99 % decrease of FLuc expression level (Fig.4). Due to the reversibility, both systems can be activated by one wavelength and recover in dark, which shows a completely novel possibility to knockout proteins for a certain time period.

Blue light induced endogenous cell cycle control

The control of the cell cycle and the arrest of cells in the same cell cycle phase is particular difficult and often needed in mitosis research. However, one key protein involved in the cell cycle checkpoints is the cyclin-dependent kinase 1 (CDK1) (Source). Loss or mutation of CDK1 leads to a cell cycle arrest in the G2-phase before DNA-replication (Source). For control of the cell cycle, chemicals and mutant strains were used which are often not reversible or toxic for the cells. To overcome this limitation and to give a tight light dependent control of the cell cycle, we aimed to target CDK1 in HEK-293T with our BLACKout system to arrest the cells in the G2-phase. Towards this aim, we designed two gRNAs targeting the endogenous mRNA of CDK1. As described before, we tested via constitutive Cas13b expression the functionality of the gRNAs. Therefore, HEK-293T cells were transfected and analyzed under the microscope after 48 h in darkness. As expected, transfected cells with Cas13b and gRNA demonstrated less confluent growth compared to the not transfected cells, suggesting an arrest in cell cycle (Fig. 5). Next, HEK-293T cells were transfected with the functional gRNAs and the BLACKout system to control the cell cycle by light. Therefore, transfected cells were illuminated directly after transfection with 10 µmol m^{-2} s^{-1} at 460 nm blue-light for 48 h. As demonstrated before with constitutive Cas13b, cells transfected with BLACKout and gRNAs showed less uniform growth compared to the cells kept in dark or the not transfected control cells (Fig.6). These results indicate the first endogenous control of cell cycle via CDK1 knock down with blue-light and opens novel perspectives in manipulating endogenous protein level and cancer research.

Discussion (399 words)

Common approaches to control RNA level and alternative splicing are based on RNAi and riboswitches [17–20]. These tools are successfully used to study signal pathways, as possible therapeutic in cancer therapy and for cell cycle regulation [20,21]. Nevertheless, most of them are either expressed constitutively or induced by chemicals like tetracycline or doxycycline, which shows a limitation for spatiotemporal control and reversibility [22,23]. To overcome those limitations, a broad set of optogenetic tools were engineered. Most of those optogenetic tools are available to upregulate protein expression, regulate protein localization and recently also gene repression and protein stability [13,14,24–29]. However, there is almost no optogenetic regulation of mRNA level and the combination of gene repression and protein stability to control mRNA [12]. For this purpose, we engineered a blue light activated Cas13b mediated mRNA knockout (BLACKout), for a reversible mRNA knockdown to regulate mRNA level. The recently published CRISPR/Cas type VI effector PspCas13b was combined with the blue light inducible split

transcription factor system based on GAL4 and the engineered LOV2 domain of *Avena sativa.* The combination of an optogenetic tool outperforms the possibility to control mRNA level by a customizable gRNA and blue light. Here we successfully demonstrated, how light induced mRNA cleavage by BLACKout leads to missing proteins in a reversible manner. Additionally, we showed the functionality with knockdowns of different reporter proteins. Moreover, we successfully combined the BLACKout system with the recently published Blue-Off system for a complete knockdown of the gene of interest via one wavelength [14] by targeting gene expression, mRNA and protein stability at the same time. Furthermore, we could demonstrate the first reversible light induced endogenous knock down to control the cell cycle of human embryonic kidney cells. Taken together the BLACKout system is a versatile and easy customizable tool for regulating mRNA level of given proteins. This opens novel perspectives in essential gene studies and cancer research. Vogel et al., 2017 [12] published a site directed RNA editing via UV light. This system is depending on UV light which is toxic to mammalian cells and it showed no reversibility. Superior to this system, we demonstrated a reversible, nontoxic control of Cas13 mediated mRNA cleavage applicable for overexpressed and endogenous proteins. For the future, we envision an application of the system in *in vivo* studies to answer fundamental biological questions, advantages in cancer research and control of alternative splicing variants.

Material and methods

Plasmid construction

The design and construction of the expression vectors are described in table S1, S2.

Cell culture, transfection, light induction

Human embryonic kidney cells (HEK-293T; DSMZ, Braunschweig, Germany) were cultivated in Dulbecco´s modified Eagle´s medium (DMEM, PAN Biotech, Aidenbach, Germany; no. P04-03550) supplemented with 10% (v/v) tetracycline-free fetal bovine serum (FBS; PAN Biotech; no. P30-3602; batch no. P080317TC) and 1.4% (v/v) streptomycin (PAN Biotech; no. P06-07100). $5 \cdot 10^4$ HEK-293T cells were transfected using polyethyleneimine (PEI; Polysciences Inc. Europe, Hirschberg, Germany; no. 23966-1) as in [29]. 0.75 µg DNA were diluted in 50 µL OptiMEM (Invitrogen, Thermo Fisher Scientific) and mixed with a PEI/OptiMEM mix (2.5 µL PEI solution in 50 µL OptiMEM). The DNA-PEI mix was added to the cells after 15 min of incubation at room temperature. 4 h post transfection the medium was exchanged. If not indicated otherwise, all plasmids were transfected with BLACKout system compromising the LOV2 based blue light system (pKM516), inducible Cas13b (pTBPF001) and a sequence specific gRNA plasmid (pTBPF003, pTBPF004) in equal amounts (w/w). 24 h post transfection the cells were illuminated with 460-nm light for the indicated periods of time with a light intensity of 10 µmol m^{-2} s^{-1} or kept in darkness. If not indicated otherwise, experiments were done in 4 biological replicates. For illumination, custom-built LED light-boxes with LED-panels emitting 460 nm were used [29]. Exchange of media and other cell-handling was done under 522-nm, safe light, to prevent inadvertent actuation of the light-sensitive systems.

Firefly luciferase assay

To quantify luciferase expression, cells were lysed on ice with 200 µL luciferase lysis buffer (25 mM Tris/HCl, pH 7.8, 1% Triton X-100, 15 mM MgSO4, 4 mM ethylene glycol tetraacetic acid (EGTA), 1 mM DTT) on each well, incubated for 15 min on ice. After resuspending, the lysate was transferred to a 96-well white plate (Corning Incorporated, Germany, no.) and supplemented with 20 µL firefly luciferase substrate (20 mM Tricine, 2.67 mM MgSO4, 0.1 mM EDTA, 33.3 mM DTT, 0.52 mM ATP, 0.27 mM Acetyl-CoA, 5 mM NaOH, 264 µM MgCO3, 0.47 mM luciferin). Luminescence was monitored using a Centro XS LB 960 plate reader (Berthold).

Fluorescence microscopy

Transfected cells were fixated in 200 µL 4% paraformaldehyde and incubated for 10 min on ice and another 10 min at room temperature. Afterwards cell containing cover slides were washed with PBS, mounted on microscopy slides with 8 µL Mowiol/Dabco solution and incubated for 30 min at 37°C. Fluorescence was imaged by using a Nikon confocal microscope. GFP and mCherry were visualized using excitation laser of 488, 525 nm and emission filter of 525/50 and 660 nm.

Statistical analysis

All data analysis was performed using Microsoft Excel or GraphPad Prism 6. Statistical outlier was determined and excluded as described in [30].

References

1. Chang, H. *et al.* CRISPR/cas9, a novel genomic tool to knock down microRNA in vitro and in vivo. *Sci. Rep.* **6**, 22312 (2016).
2. Unniyampurath, U., Pilankatta, R. & Krishnan, M. N. RNA Interference in the Age of CRISPR: Will CRISPR Interfere with RNAi? *Int. J. Mol. Sci.* **17**, 291 (2016).
3. Tabebordbar, M. *et al.* In vivo gene editing in dystrophic mouse muscle and muscle stem cells. *Science* **351**, 407–411 (2016).
4. Ousterout, D. G. *et al.* Multiplex CRISPR/Cas9-based genome editing for correction of dystrophin mutations that cause Duchenne muscular dystrophy. *Nat. Commun.* **6**, 6244 (2015).
5. Brooks, A. K. & Gaj, T. Innovations in CRISPR technology. *Curr. Opin. Biotechnol.* **52**, 95–101 (2018).
6. Fellmann, C., Gowen, B. G., Lin, P.-C., Doudna, J. A. & Corn, J. E. Cornerstones of CRISPR–Cas in drug discovery and therapy. *Nat. Rev. Drug Discov.* **16**, 89–100 (2017).
7. Strutt, S. C., Torrez, R. M., Kaya, E., Negrete, O. A. & Doudna, J. A. RNA-dependent RNA targeting by CRISPR-Cas9. *Elife* **7**, (2018).
8. Polstein, L. R. & Gersbach, C. A. A light-inducible CRISPR-Cas9 system for control of endogenous gene activation. *Nat. Chem. Biol.* **11**, 198–200 (2015).
9. Nihongaki, Y., Kawano, F., Nakajima, T. & Sato, M. Photoactivatable CRISPR-Cas9 for optogenetic genome editing. *Nat. Biotechnol.* **33**, 755–760 (2015).
10. Konermann, S. *et al.* Transcriptome Engineering with RNA-Targeting Type VI-D CRISPR Effectors. *Cell* **173**, 665-676.e14 (2018).
11. Cox, D. B. T. *et al.* RNA editing with CRISPR-Cas13. *Science (80-.).* **358**, 1019–1027 (2017).

12. Vogel, P., Hanswillemenke, A. & Stafforst, T. Switching Protein Localization by Site-Directed RNA Editing under Control of Light. *ACS Synth. Biol.* **6**, 1642–1649 (2017).
13. Müller, K., Engesser, R., Timmer, J., Zurbriggen, M. D. & Weber, W. Orthogonal Optogenetic Triple-Gene Control in Mammalian Cells. *ACS Synth. Biol.* **3**, 796–801 (2014).
14. Baaske, J. *et al.* Dual-controlled optogenetic system for the rapid down-regulation of protein levels in mammalian cells. *Sci. Rep.* **8**, 15024 (2018).
15. Takara bio. How to design sgRNA sequences. Available at: https://www.takarabio.com/learning-centers/gene-function/gene-editing/gene-editing-tools-and-information/how-to-design-sgrna-sequences. (Accessed: 13th June 2019)
16. Fu, J. L., Kanno, T., Liang, S.-C., Matzke, A. J. M. & Matzke, M. GFP Loss-of-Function Mutations in Arabidopsis thaliana. *G3 (Bethesda).* **5**, 1849–55 (2015).
17. Vogel, M., Weigand, J. E., Kluge, B., Grez, M. & Suess, B. A small, portable RNA device for the control of exon skipping in mammalian cells. *Nucleic Acids Res.* **46**, e48–e48 (2018).
18. Dery, K. J. *et al.* Alternative splicing as a therapeutic target for human diseases. *Methods Mol. Biol.* **555**, 127–44 (2009).
19. Celotto, A. M. & Graveley, B. R. Exon-specific RNAi: a tool for dissecting the functional relevance of alternative splicing. *RNA* **8**, 718–24 (2002).
20. Dillon, C. P. *et al.* RNAI AS AN EXPERIMENTAL AND THERAPEUTIC TOOL TO STUDY AND REGULATE PHYSIOLOGICAL AND DISEASE PROCESSES. *Annu. Rev. Physiol.* **67**, 147–173 (2005).
21. Sierant, M., Piotrzkowska, D. & Nawrot, B. RNAi mediated silencing of cyclin-dependent kinases of G1 phase slows down the cell-cycle progression and reduces apoptosis. *Acta Neurobiol. Exp. (Wars).* **75**, 36–47 (2015).
22. Peacock, R. W. S., Sullivan, K. A. & Wang, C. L. Tetracycline-Regulated Expression Implemented through Transcriptional Activation Combined with Proximal and Distal Repression. *ACS Synth. Biol.* **1**, 156–162 (2012).
23. Gossen, M. & Bujard, H. Tight control of gene expression in mammalian cells by tetracycline-responsive promoters. *Proc. Natl. Acad. Sci.* **89**, 5547–5551 (1992).
24. Pathak, G. P. *et al.* Bidirectional approaches for optogenetic regulation of gene expression in mammalian cells using Arabidopsis cryptochrome 2. *Nucleic Acids Res.* **45**, e167–e167 (2017).
25. Nash, A. I. *et al.* Structural basis of photosensitivity in a bacterial light-oxygen-voltage/helix-turn-helix (LOV-HTH) DNA-binding protein. *Proc. Natl. Acad. Sci.* **108**, 9449–9454 (2011).
26. Motta-Mena, L. B. *et al.* An optogenetic gene expression system with rapid activation and deactivation kinetics. *Nat. Chem. Biol.* **10**, 196–202 (2014).
27. Beyer, H. M. *et al.* Red Light-Regulated Reversible Nuclear Localization of Proteins in Mammalian Cells and Zebrafish. *ACS Synth. Biol.* **4**, 951–958 (2015).
28. Wend, S. *et al.* Optogenetic Control of Protein Kinase Activity in Mammalian Cells. *ACS Synth. Biol.* **3**, 280–285 (2014).
29. Müller, K. *et al.* A red/far-red light-responsive bi-stable toggle switch to control gene expression in mammalian cells. *Nucleic Acids Res.* **41**, e77–e77 (2013).
30. Jacobs, J. L. & Dinman, J. D. Systematic analysis of bicistronic reporter assay data. *Nucleic*

Acids Res. **32**, e160 (2004).

Acknowledgements

Author Contributions

PF and TB planned and performed experiments and analyzed the data. MDZ were involved in the design, supervision and analysis of the experiments. PF and TB wrote the manuscript.

Competing Financial Interest

The authors declare that they have no competing financial interest.

Figure Descriptions

Figure 1. Design and validation of BLACKout system

(a) Function and description of the system. The photosensitive LOV2 peptide, containing a specific tag on the Jα helix, is fused to the GAL4 DNA binding domain and separated by an IRES from the ePDZ-VP16 fusion. Five repeats of the specific GAL4 DNA sequence followed by a TATA box are upstream of Cas13b. An U6-promoter driven gRNA vector contains a gRNA specific for the gene of interest. Upon blue light illumination, the Jα helix of the LOV2 domain unwinds and exposes the specific tag, which leads to an interaction with the ePDZ-VP16 fusion. Due to binding to the specific GAL4 sequence on the DNA near the TATA box, VP16 is in close proximity and can recruit the transcriptional machinery. The resulting Cas13b protein, guided by the specific gRNA, is cleaving the mRNA of interest. **(b)** Functionality of the designed gRNAs. HEK-293T cells were transfected transiently with constitutively expressed FLuc (pTBPF011), constitutively expressed Cas13b (pC046) and specifically designed gRNAs against FLuc mRNA (gRNA1, gRNA2 (pTBPF003, pTBPF004)). Cells were kept in dark for 24 h post transfection and afterwards illuminated for 24 h with a photon flux density of 10 µmol m^{-2} s^{-1} and 460 nm (blue bars) or kept in dark (black bars). Firefly was determined in relative luminescence units (RLUs). **(c)** Validation of the BLACKout system. HEK-293T cells were transfected with the constitutively expressed FLuc, the BLACKout system (pTBPF001, pKM516) and either one specific gRNA or both together and kept in dark for 24 h. Cells were illuminated as before for 24 h with 460 nm light (blue bars) or kept in dark (black bars). FLuc levels were normalized to their dark control. The errors bars in (b) and (c) indicate standard deviation of the mean.

Figure 2. Blue light induced GFP mRNA knockdown

In darkness GFP accumulates similar to mCherry signal in transfected cells. Upon blue light illumination the GFP level decreases in cells transfected with BLACKout system and either gRNA1 or gRNA2. HEK-293T cells were transfected with PGK-GFP (pTBPF018), SV40-mCherry (pTBPF014), the BLACKout system (pTBPF001, pKM516) and either gRNA1 or gRNA2 (pTBPF005, pTBPF006). After transfection

cells were kept in dark for 24 h and illuminated for 48 h with 10 µmol m^{-2} s^{-1} and 460 nm light. Afterwards cells were fixed and imaged by confocal microscopy.

Figure 3. Reversibility and characterization of the BLACKout system

(a) mRNA kinetic of the BLACKout system. HEK-293T cells were transfected as described above with BLACKout system (pTBPF001, pKM516) and kept in dark for 24 h. Afterwards cells were for illuminated with 460 nm blue light with photon flux density of 10 µmol m^{-2} s^{-1} and FLuc expression levels were measured at the given timepoints. Expression data were normalized to FLuc expression level of cells kept in dark. **(b)** Reversibility of the BLACKout system. HEK-293T cells were transfected with the BLACKout system (pTBPF001, pKM516) and either a specific gRNA1 or gRNA2 (pTBPF003, pTBPF004) and kept in dark for 12 h. Afterwards cells were illuminated for 12 h with blue light and again 12 h of darkness. FLuc expression levels were measured at the given timepoints and normalized by values of constitutive expressed FLuc at the same timepoint. **(c)** Dose response of the BLACKout system. HEK-293T cells were transfected as described above with BLACKout system (pTBPF001, pKM516) and kept in dark for 24h. Afterwards cells were illuminated with the given blue light intensity (0, 2.5, 5, 10, 15, 20 µmol m^{-2} s^{-1}) for 24 h. Expression date were normalized to FLuc expression levels of cells kept in dark. The error bars in **(a), (b), (c)** indicate standard deviation of the mean for four independent replicates.

Figure 4. Complete knockdown by combining BLACKout with Blue-Off system

HEK-293T cells were transfected with BLACKout system (pTBPF001, pKM516), Firefly-B-LID and either gRNA1 and gRNA2 (pTBPF003, pTBPF004) and the EL222-KRAB repressor. Cells were kept in dark for 24 h followed by illumination for 24 h with 10 µmol m^{-2} s^{-1} and 460 nm light. Firefly expression level were normalized to the dark control. The error bars indicate standard deviation of the mean for four independent replicates.

Figure 5. Blue light induced cell cycle arrest

HEK-293T cells were transfected with constitutive Cas13b plasmid and/or gRNA1 or 2 and kept in dark for 48 h. Cells transfected with Cas13b and one gRNA showed less growth compared with the un-transfected cells which demonstrated a uniform monolayer. Cells were fixated, DAPI stained and analyzed by confocal microscopy.

Figure S1. Functionality of the gRNAs targeting GFP

In darkness GFP accumulates similar to mCherry signal in transfected cells. Constitutive Cas13b and gRNA transfected cells showed decreased GFP signal under both conditions. HEK-293T cells were transfected with PGK-GFP (pTBPF018), SV40-mCherry (pTBPF014), constitutive Cas13b (pC046) and either gRNA1 or gRNA2 (pTBPF005, pTBPF006). After transfection cells were kept in dark for 24 h and illuminated for 48 h with 10 µmol m^{-2} s^{-1} and 460 nm light. Afterwards cells were fixated and imaged by confocal microscopy.

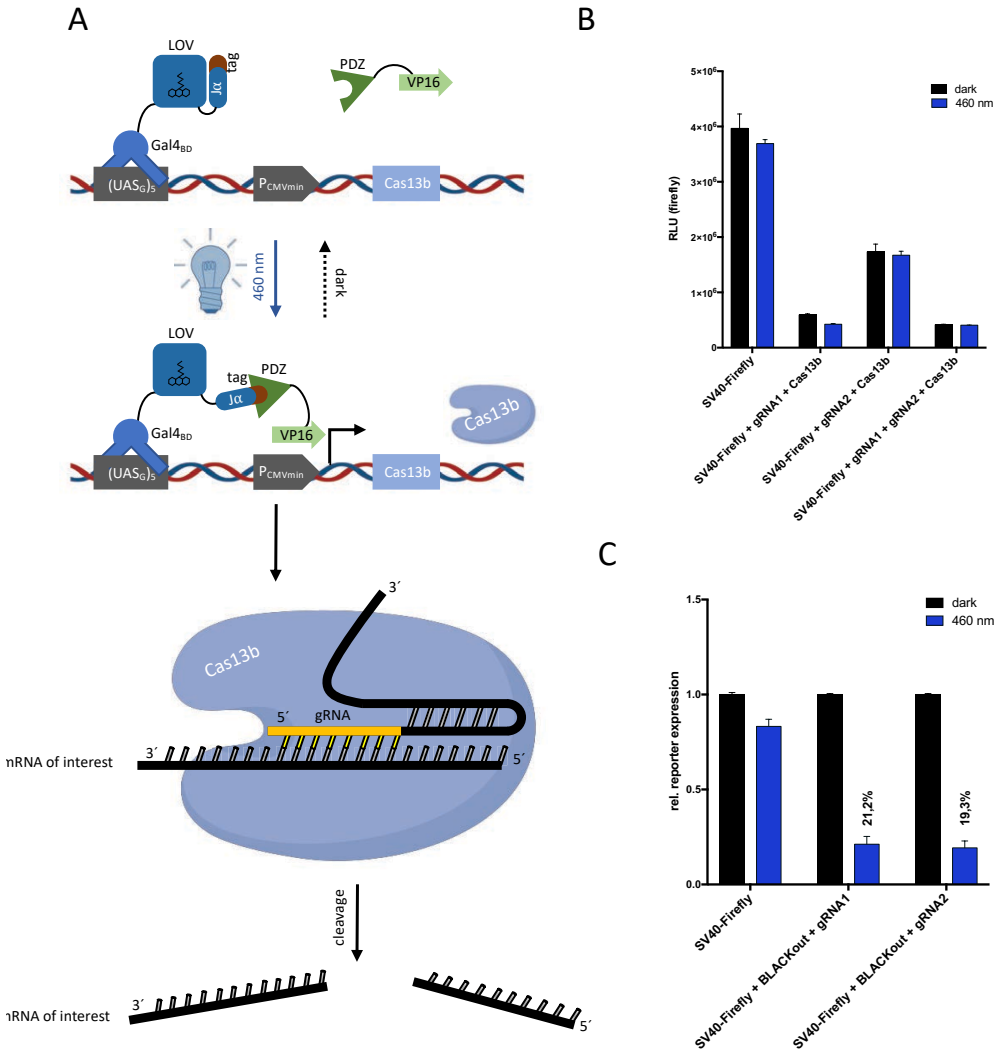
A
LOV
tag
Jα
PDZ
VP16
Gal4BD
(UASG)5
PCMVmin
Cas13b
460 nm
dark
LOV
tag
PDZ
Jα
Gal4BD
VP16
Cas13b
(UASG)5
PCMVmin
Cas13b
3´
Cas13b
5´
gRNA
nRNA of interest
3´
5´
cleavage
nRNA of interest
3´
5´
B
dark
460 nm
RLU (firefly)
5×10^6
4×10^6
3×10^6
2×10^6
1×10^6
0
SV40-Firefly
SV40-Firefly + gRNA1 + Cas13b
SV40-Firefly + gRNA2 + Cas13b
SV40-Firefly + gRNA1 + gRNA2 + Cas13b
C
dark
460 nm
rel. reporter expression
1.5
1.0
0.5
0.0
21.2%
19.3%
SV40-Firefly
SV40-Firefly + BLACKout + gRNA1
SV40-Firefly + BLACKout + gRNA2

Fig.2

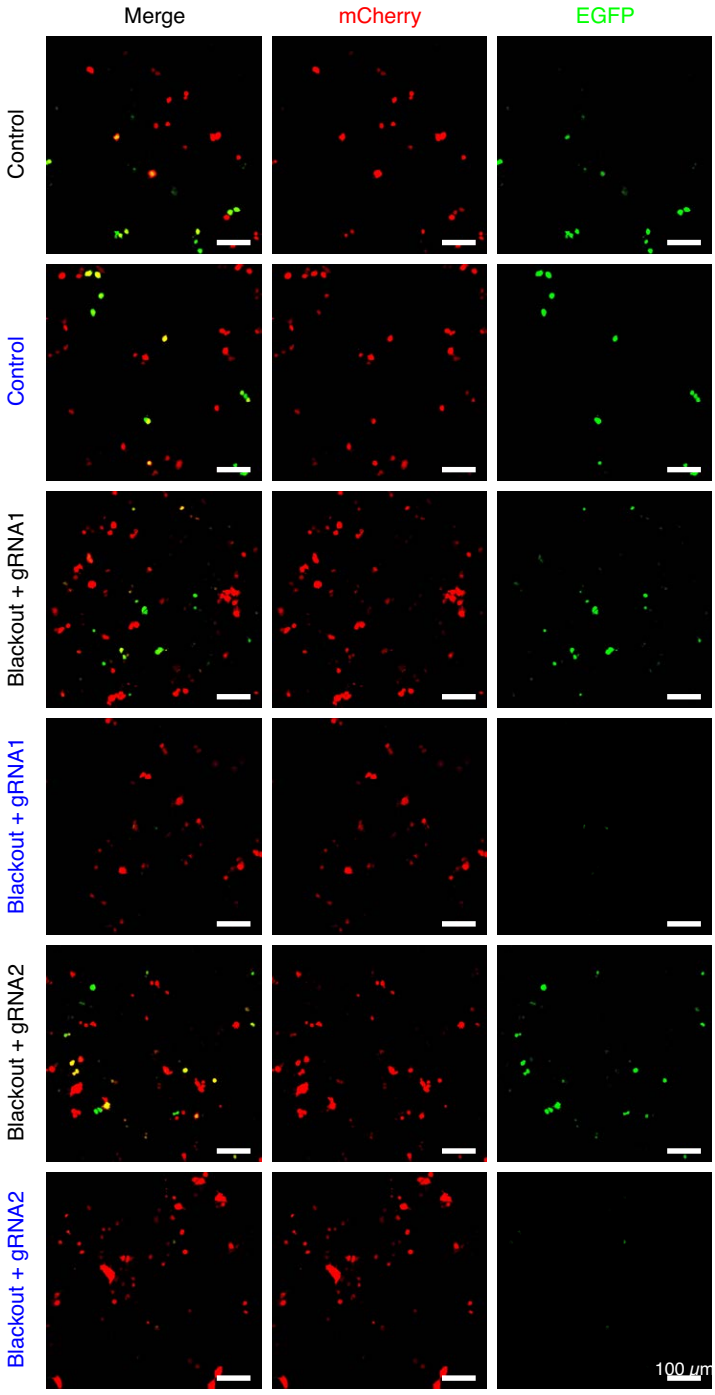
Merge
mCherry
EGFP
Control
Control
Blackout + gRNA1
Blackout + gRNA1
Blackout + gRNA2
Blackout + gRNA2
100 μm

Fig.3

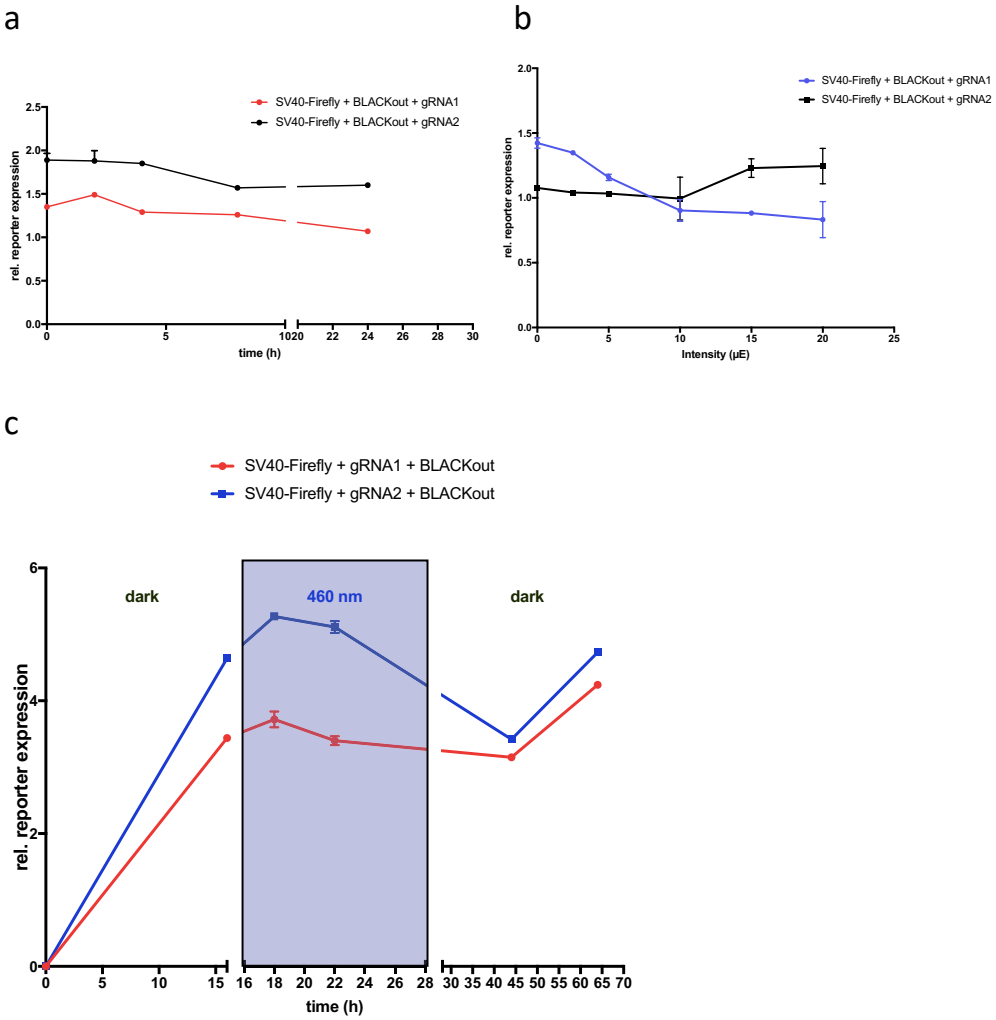
a
SV40-Firefly + BLACKout + gRNA1
SV40-Firefly + BLACKout + gRNA2
rel. reporter expression
time (h)
b
SV40-Firefly + BLACKout + gRNA1
SV40-Firefly + BLACKout + gRNA2
rel. reporter expression
Intensity (µE)
c
SV40-Firefly + gRNA1 + BLACKout
SV40-Firefly + gRNA2 + BLACKout
dark
460 nm
dark
rel. reporter expression
time (h)

Fig.4

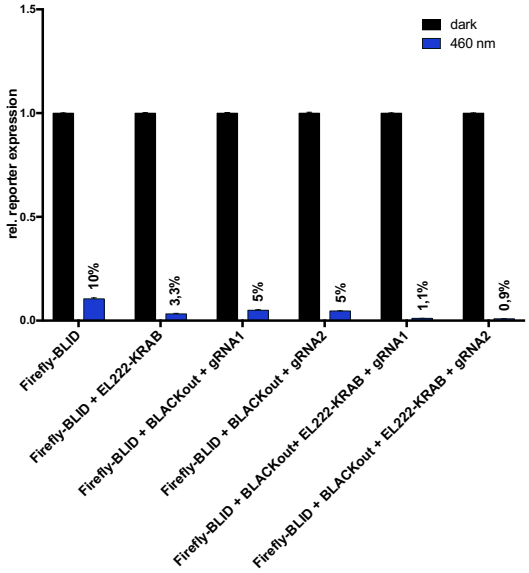
dark
460 nm
rel. reporter expression
1.5
1.0
0.5
0.0
10%
3,3%
5%
5%
1,1%
0,9%
Firefly-BLID
Firefly-BLID + EL222-KRAB
Firefly-BLID + BLACKout + gRNA1
Firefly-BLID + BLACKout + gRNA2
Firefly-BLID + BLACKout+ EL222-KRAB + gRNA1
Firefly-BLID + BLACKout + EL222-KRAB + gRNA2

Fig.5

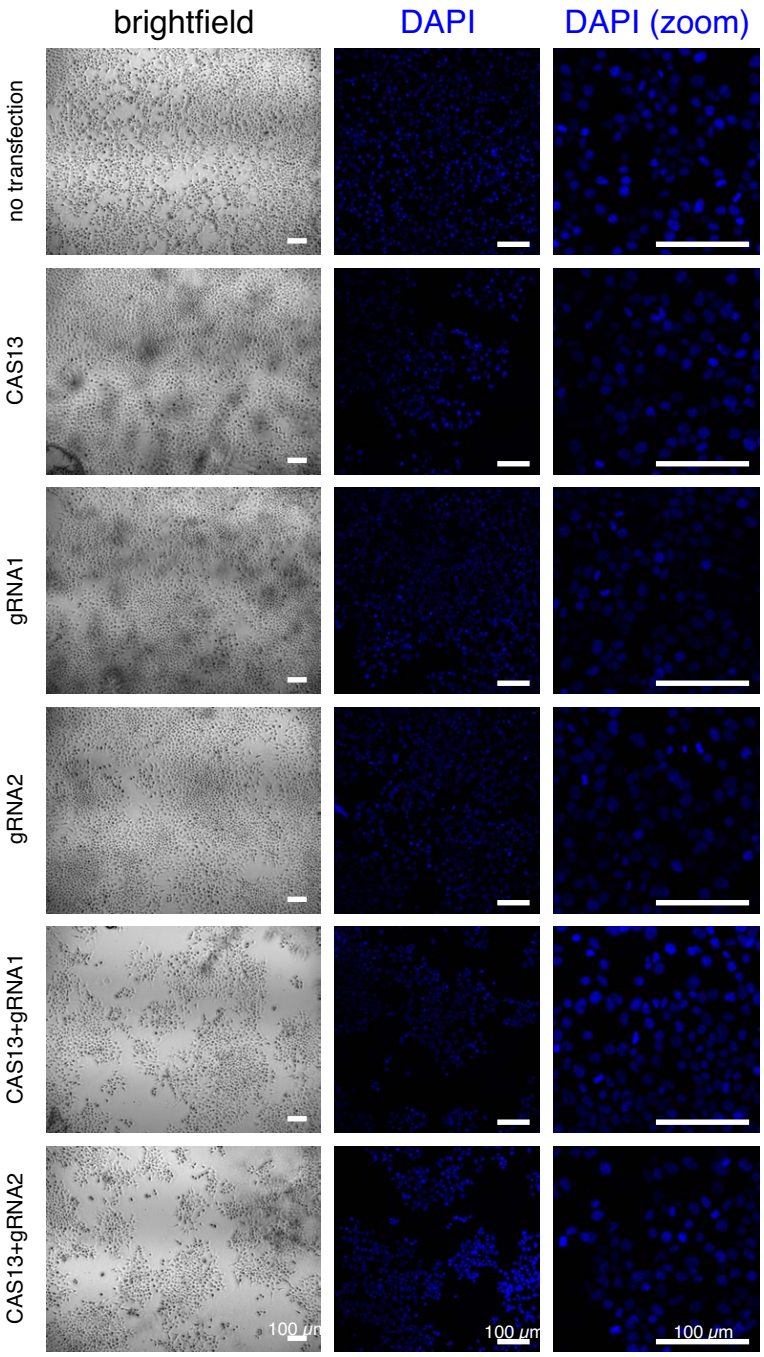
brightfield
DAPI
DAPI (zoom)
no transfection
CAS13
gRNA1
gRNA2
CAS13+gRNA1
CAS13+gRNA2
100 µm
100 µm
100 µm

Fig.S1

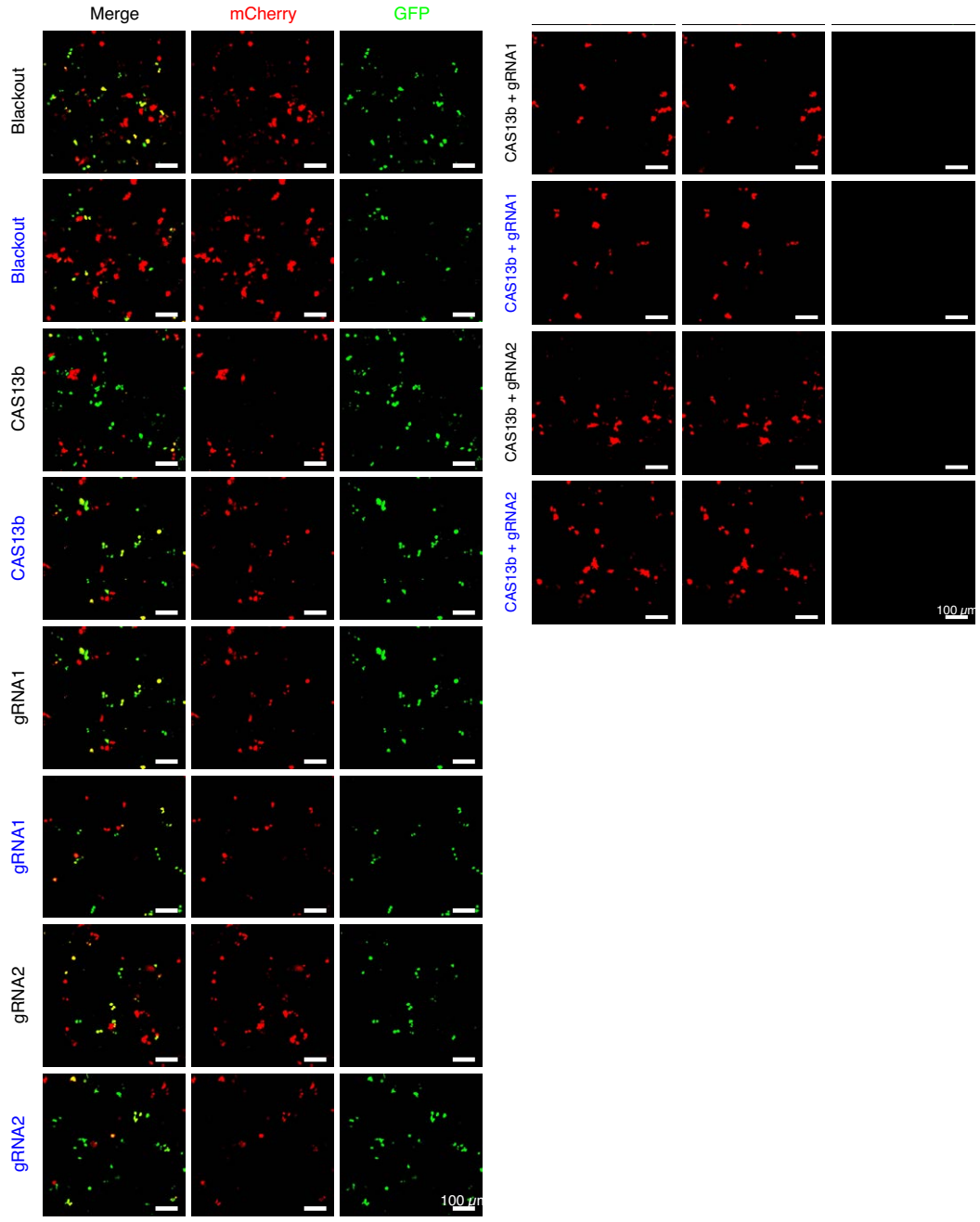
Merge
mCherry
GFP
Blackout
Blackout
CAS13b
CAS13b
gRNA1
gRNA1
gRNA2
gRNA2
CAS13b + gRNA1
CAS13b + gRNA1
CAS13b + gRNA2
CAS13b + gRNA2
100 μm
100 μm

Supplements:

Supplementary Table S1: Plasmids designed and used in this study.
All plasmids were cloned using AQUA [1] or Gibson Cloning [2].

Plasmid	Description	Reference or source
pKM516	**P_{SV40}-Gal4BD-LOV2-tag-IRES-ePDZ-VP16-pA**	[3]
pC0046	**$P_{EF1\alpha}$-PspCas13b-NES-HA-pA**	[4]
pTBPF001	**5xGal4UAS-TATA-PspCas13b-NES-HA-pA** PspCas13b-NES-HA was amplified from pC0046 using oligos oTBPF001/oTBPF002. The backbone was amplified using oligos oTBPF003/oTBPF004. Both fragments were assembled via AQUA cloning.	**This work**
pC0043	**P_{U6}-*BbsI*-PspCas13bDR-pA**	[4]
pTBPF015	**P_{SV40}-Firefly-pA** Firefly was amplified using oligos oTBPF036/oTBPF037. pTBPF008 was linearized with *XhoI/BamHI.* Both fragments were assembled via AQUA cloning.	**This work**
pTBPF003	**P_{U6}-gRNA1(firefly)-PspCas13bDR-pA** pC0043 was linearized by using BbsI restriction enzyme and assembled with oTBPF009 via AQUA cloning.	**This work**
pTBPF004	**P_{U6}-gRNA2(firefly)-PspCas13bDR-pA** pC0043 was linearized by using BbsI restriction enzyme and assembled with oTBPF010 via AQUA cloning.	**This work**
pTBPF018	**P_{PGK}-eGFP-pA** P_{PGK} was amplified using oTBPF041/oTBPF042. The backbone was linearized by *NheI/XhoI.* Both fragments were assembled using AQUA cloning.	**This work**
pTBPF005	**P_{U6}-gRNA1(eGFP)-PspCas13bDR-pA** pC0043 was linearized by using BbsI restriction enzyme and assembled with oTBPF011 via AQUA cloning.	**This work**
pTBPF006	**P_{U6}-gRNA2(eGFP)-PspCas13bDR-pA** pC0043 was linearized by using BbsI restriction enzyme and assembled with oTBPF012 via AQUA cloning.	**This work**
pC0053	**P_{CMV}-dPspCas13b-NES-ADAR2DD-pA**	[4]
pTBPF007	**5xGal4UAS-TATA-dPspCas13b-NES-ADAR2DD-pA** dPspCas13b-NES-ADAR2DD was amplified from pC0053 using oligos oTBPF025/oTBPF026. The backbone was amplified using oligos oTBPF003/oTBPF004. Both fragments were assembled via AQUA cloning.	**This work**

pTBPF008	**P_{SV40}-eGFP^{G67S}-pA** Mutation was inserted via site directed mutagenesis using oligos oTBPF027/oTBPF028.	**This work**
pTBPF009	**P_{U6}-gRNA(eGFP^{G67S})-PspCas13bDR-pA** pC0043 was linearized by using BbsI restriction enzyme and assembled with oTBPF029 via AQUA cloning.	**This work**
pTBPF014	**P_{SV40}-mCherry-pA** mCherry was amplified using oTBPF034/oTBPF035. pTBPF008 was linearized with *NotI/XbaI*. Both fragments were assembled via AQUA cloning	**This work**

pC0043-PspCas13b crRNA backbone was a gift from Feng Zhang (Addgene plasmid # 103854 ; http://n2t.net/addgene:103854 ; RRID:Addgene_103854)

pC0046-EF1a-PspCas13b-NES-HIV was a gift from Feng Zhang (Addgene plasmid # 103862 ; http://n2t.net/addgene:103862 ; RRID:Addgene_103862)

pC0053-CMV-dPspCas13b-GS-ADAR2DD(E488Q)-delta-984-1090 was a gift from Feng Zhang (Addgene plasmid # 103869 ; http://n2t.net/addgene:103869 ; RRID:Addgene_103869)

Supplementary Table S2: Oligonucleotides designed and used in this study.

Oligo	Sequence (5´→3´)
oTBPF001	CGTTCGAGATCTGCGATCTAAGTAAGCTTGGCCACCATGAACATCCCCGC TCTGGTGGAAAAC
oTBPF002	CTCCCATTCATAAGTTCCATAGGATGGGCGGCCGCTTAGGCATAGTCGGGGA CATCATATGG
oTBPF003	GCGGCCGCCCATCCTATGG
oTBPF004	GGTGGCCAAGCTTACTTAGATCGCAG
oTBPF036	CATGTTTGACAGCTTATCATCGATAAGCTAGCTTGGATCCCTGTGGAATGTGTG TCAGTTAGGGTG
oTBPF037	TTACCAGTTAACTTTCTGGTTTTCCAGTTCCTCGAGAGCTTTTTGCAAAAGCCTA GGCCTCC
oTBPF009	ATAGCCCCTCAAAACTGGACCTTCCACAACGAGGTGGACATTACCTACGCCGAG TACTTCGGTGTTTCGTCCTTTCCACAAGATATATAA
oTBPF010	ATAGCCCCTCAAAACTGGACCTTCCACAACCACGGTAAAACCATGACCGAGAAG GAGATCGGTGTTTCGTCCTTTCCACAAGATATATAA
oTBPF041	TTCTCATGTTTGACAGCTTATCATCGATAAGCTAGCTTGGGGTTGCGCCTTTTCC AAGGC
oTBPF042	TTACCAGTTAACTTTCTGGTTTTCCAGTTCCTCGAGCTGGGGAGAGAGGTCGG TGATTC

oTBPF011	ATAGCCCCTCAAAACTGGACCTTCCACAACCTGGACGGCGACGTAAACGGCCAC AAGTTCGGTGTTTCGTCCTTTCCACAAGATATATAA
oTBPF012	ATAGCCCCTCAAAACTGGACCTTCCACAACACCCAGTCCAAGCTGAGCAAAGAC C CCAACCGGTGTTTCGTCCTTTCCACAAGATATATA
oTBPF025	CGTTCGAGATCTGCGATCTAAGTAAGCTTGGCCACCATGAACATCCCCGCTC TGGTGGAAAAC
oTBPF026	CTCCCATTCATAAGTTCCATAGGATGGGCGGCCGCTTAAACGGGCCCTCTAG GCTCGAG
oTBPF027	CCCTGACCTACAGCGTGCAGTG
oTBPF028	CACTGCACGCTGTAGGTCAGGG
oTBPF029	ATAGCCCCTCAAAACTGGACCTTCCACAACTGCCCTGGCCCACCCTCGTGACCA CCCTGACCTACGGCGTGCAGTGGGTGTTTCGTCCTTTCCACAAGATATATAA
oTBPF034	TTTTGTCTTTTATTTCAGGTCCCGGATCGAATTGCGGCCGCATGGTGAGCAAGG GCGAGGAGG
oTBPF035	CTGGATCGAAGCTTGGGCTGCAGGTCGACTTCTAGACTACTTGTACAGCTCG TCCATGCCG

Supplementary Table S3: guide RNAs designed and used in this study.

gRNA	**Sequence (5´→ 3´)**
Firefly 1	GAGGTGGACATTACCTACGCCGAGTACTTC
Firefly 2	CACGGTAAAACCATGACCGAGAAGGAGATC
GFP 1	CTGGACGGCGACGTAAACGGCCACAAGTTC
GFP 2	ACCCAGTCCAAGCTGAGCAAAGACCCCAAC
GFP^{G67S}	TGCCCTGGCCCACCCTCGTGACCACCCTGACCTACGGCGTGCAGTG